MRC Cancer Unit

Defining the pro-tumour impact of the evolving stromal microenvironment

Sarah Elizabeth Davidson

Jesus College Cambridge

This dissertation is submitted for the degree of Doctor of Philosophy

September 2019

Declaration

This dissertation is the result of my own work and includes nothing which is the outcome of work done in collaboration except as specified in the following section or in the text.

It is not substantially the same as any that I have submitted, or, is being concurrently submitted for a degree or diploma or other qualification at the University of Cambridge or any other University or similar institution except as declared in the Preface and specified in the text. I further state that no substantial part of my dissertation has already been submitted, or, is being concurrently submitted for any such degree, diploma or other qualification at the University of Cambridge or any other University of similar institution except as declared in the Preface and specified in the text.

This dissertation does not exceed 60,000 words

Defining the pro-tumour impact of the evolving stromal microenvironment

Sarah Elizabeth Davidson

Much like normal tissues, tumours require a supporting microenvironment for growth and survival, known as the tumour stroma. However, tumours represent a dynamic and turbulent environment, in which factors such as hypoxia, fibrosis, nutrient deprivation and the local cytokine milieu continually fluctuate as the tumour grows and develops. These factors influence stromal phenotypes and create heterogeneity, which can confound our understanding of their role within the microenvironment. In particular, cancer associated fibroblasts (CAFs) represent a diverse population of cells, which cannot be identified by one universal marker. CAFs promote tumour growth and dissemination by secreting growth factors, stimulating angiogenesis, aiding the development of tumour-promoting inflammation and remodelling the extra-cellular matrix (ECM). However, recent investigations have shown these functions belong to defined populations that differ between tumour types.

This project aimed to investigate stromal heterogeneity across melanoma development, with a specific focus on the CAF compartment. Whilst conventional techniques such as IF and flow cytometry showed varied expression of fibroblast markers, they lacked the resolution to discern functional subsets. Thus, we employed single cell RNA sequencing (scRNAseq) to profile CAF populations at different stages of tumour development. To avoid bias, CAFs were isolated from the B16-F10 melanoma model using a ‘negative selection’ approach. Our data revealed the presence of 3 functionally distinct fibroblast populations, termed ‘immune’, ‘desmoplastic’ and ‘contractile’, which expressed genes involved in immune cross talk, matrix remodelling and stress fibre contraction respectively. Furthermore, these populations are dynamic, changing in prevalence as the tumour grows. While ‘immune’ and ‘desmoplastic’ populations were present from early stages, ‘contractile’ CAFs were more abundant at later time points. Owing to their unique marker profiles, we were able to identify these populations within the tumour stoma and validate their temporal nature.

Subsequent investigation into the contribution of these subsets to tumour growth, revealed that ‘immune’ CAFs promoted accumulation of suppressive macrophages by production of C3 and its cleavage product C3a. Significantly, inhibition of the C3a/C3aR axis reduced the number of macrophages and decreased tumour volume. This reduction in tumour growth was accompanied by increased CD8 T-cell infiltration, implying that ‘immune’ CAFs may inhibit adaptive anti-tumour immunity through controlling the myeloid compartment. The interaction between C3 producing CAFs and C3aR expressing macrophages was conserved in different murine tumours and human cancer. Thus, ‘immune’ CAFs and C3a signalling may represent therapeutic targets in multiple cancer types. Overall, our data highlights the complexity of stromal phenotypes and microenvironment interactions, which likely reflects the convoluted climate of the developing tumour.

Assistance and Collaborations

ScRNAseq studies

Single cell sequencing studies were performed in collaboration with the Teichmann Lab (Wellcome Sanger Institute). Mice were injected with tumour cells by Dr. Angela Riedel. Non-immune stromal and immune populations were isolated by Dr. Riedel and Dr. Bidesh Mahata for scRNAseq (Chapters 3, 4 and 5). Together, Dr. Riedel and I generated cDNA from stromal cells, and immune populations were processed by Dr. Mahata. Purification, library preparation and sequencing were performed by Sanger core facilities. Alignment and quality control for the pilot study and time course, was completed by Dr. Gozde Kar and Dr. Mirjana Efremova respectively. Once count data was generated, I performed downstream bioinformatic analysis of pilot data. Initial clustering of sequenced cells from time course data was conducted by Dr. Efremova, while I characterised fibroblasts populations (Chapter 4) and immune subsets were analysed in collaboration (Chapter 5). I performed all validation and unless specified in the text, I produced all featured plots.

Mouse work

Animals were housed at the Ares facility (Babraham), where staff were responsible for mouse husbandry. I induced tumours by orthotopic injection of tumour cells and collected tissue samples. Ares Technicians performed drug dosing, irradiation, intravenous infusions and tumour measurements.

Acknowledgements

First and foremost, I would like to thank Dr. Jaqueline Shields for the opportunity to work on this project and her supervision throughout my PhD. Thank you for all the scientific discussions, as well as your patience and personal support over the last 4 years. To the Shields lab, you are kind, generous and constantly make me laugh. Yet, most of all, you are fantastic scientists. Luisa, Angi and Hafsa, thank you for always taking the time to teach me new techniques and for your advice and encouragement. James, Jen, Jake, Carlo, Corrado and Will thank you for making the lab such a fun place to work. I am grateful for all your scientific contributions and support throughout this project, without you I would not have succeeded.

To all member of the Hutch, past and present, I greatly appreciate all your help throughout my PhD. Francis and Emma, thank you for bringing much entertainment to 2.19 and for always being available for pub trips. To the Hutch core staff, I am extremely grateful for all your hard work, without which we could not function. In addition, I would like to thank Reiner and the CIMR flow team for their continuous support. You have gone above and beyond to help with experimental design and ensure sorts were completed. To the Ares staff, thank you for all your help with our animal experiments. In particular, to everyone in E23 and Quarantine, your assistance and support has been invaluable.

I would also like to thank Dr. Sarah Teichmann for providing the expertise and platforms integral for this project, and for her continual guidance. Furthermore, I am immensely appreciative of all the help received from members of the Teichmann lab and Sanger core facilities. I would like to thank Ricardo for walking us through plate processing and Bidesh for isolating and processing immune populations, as well as his contributions to the scientific discussions surrounding this project. In particular, I would like to thank Gozde and Mirjana for all their help processing and analysing the sequencing data produced. Your knowledge and assistance were fundamental to this project and enabled me to learn and perform bioinformatic analysis. In addition, I would like to thank Mirjana for her scientific contributions to this project; it has been a pleasure working with you.

Finally, Oscar, Mum, Dad and James, for everything you have done you will never know how grateful I am. Simply, thank you for always being there.

List of Abbreviations

4-HT: 4-Hydroxy Tamoxifen

APCs: Antigen Presenting Cells

ARG1: Arginase

αSMA: α-Smooth Muscle Actin

BFA: Brefeldin-A

BSA: Bovine Serum Albumin

CAFs: Cancer Associated Fibroblasts

CCL2: Chemokine Ligand 2

CCL22: C-C motif Chemokine Ligand 22

CDCs: Classical Dendritic cell

CTLA-4: Cytotoxic T lymphocyte Antigen-4

CXCL12: C-X-C motif chemokine 12

DAPI: 4',6-diamidino-2-phenylindole

Dcs: Dendritic Cells

DE: Differentially Expressed

DMEM: Dulbecco's Modified Eagle medium

DMSO: Dimethyl Sulfoxide

DPT: Diffusion Pseudo-Time

ECM: Extracellular Matrix

EDTA: Ethylenediaminetetraacetic acid

EdU: 5-ethynyl-2´-deoxyuridine

EGF: Epithelial Growth Factor

EMT: Epithelial Mesenchymal Transition

endMT: Endothelial to Mesenchymal Transition

ER: Oestrogen Receptor

ERCC: External RNA Control Consortium

FACS: Flow Activated Cell Sorting

FAK: Focal Adhesion Kinase

FAP: Fibroblast Activation Protein

FBS: Foetal Bovine Serum

FGF: Fibroblast Growth Factor

FOXP3: Forkhead Box P3

FPKM: Fragment Per Kilobase of transcripts per Million

FSP1: Fibroblast-Specific Protein-1

GO: Gene Ontology

HA: Hyaluronan

HGF: Hepatocyte Growth Factor

HLA: Human Leukocyte Antigen

IDO: indoleamine 2,3-dioxygenase

IFNγ: Interferon γ

IL: Interleukin

IP: Intraperitoneal

IV: Intravenous

KEGG: Kyoto Encyclopaedia of Genes and Genomes

LAG3: Lymphocyte Activation Gene 3 protein

LDH: Lactate Dehydrogenase

LN: lymph node

LOX: Lysyl Oxidase

MCAM: Melanoma Cell Adhesion Molecule

MDSC: Myeloid Derived Suppressor Cell

MHC: Major Histocompatibility Complex

migDC: migratory DC

MMP: Matrix Metalloproteinases

MP: Mononuclear Phagocytes

MSC: Mesenchymal Stem Cell

mt: Mitochondrial

NETs: Neutrophil Extracellular Traps

NG2: Neural Glial antigen 2

NK: Natural Killer

NKG2D: Natural Killer Group 2 member D

NO: Nitric Oxide

NSCLC: Non-Small Cell Lung Cancer

OCT: Optimal Cutting Temperature

OX40L: OX-40 Ligand

PCA: Principal Component Analysis

PCs: Principle Components (PCs)

PD1: Programmed Cell Death Protein 1

PDAC: Pancreatic Adenocarcinoma

pDC: plasmacytoid DCs

PDGFRα: Platelet Derived Growth Factor Receptor α

PDGFRβ: Platelet Derived Growth Factor Receptor β

PDK1: Pyruvate Dehydrogenase Kinase

PDL1: Programmed Cell Death Ligand-1

PDL2: Programmed Cell Death Ligand-2

PDPN: Podoplanin

PGE2: Prostaglandin E2

Ph: Phagocytes

PSCs: Pancreatic Stellate Cells

ROS: Reactive Oxygen Species

scRNAseq: Single cell RNA Sequencing

SPADE: Spanning-tree Progression Analysis of Density-normalised Events

SPARC: Secreted Protein Acidic And Cysteine Rich

TCR: T-Cell Receptor

TGFβ: Transforming Growth Factor β

Th: T-helper

TIM3: T-cell immunoglobulin domain and mucin domain protein 3

TLR: Toll-Like Receptor

TNFα: Tumour Necrosis Factor α

TPM: Transcript Per Million

T-regs: T-regulatory

tSNE: T-distributed Stochastic Neighbourhood Embedding

uPA: urokinase-type plasminogen activator

VEGFA: Vascular Endothelial Growth Factor A

Contents

1 Introduction 1
1.1 The tumour microenvironment 2
1.1.1 Immune cells 3
1.1.2 Endothelial Cells 9
1.1.3 The Extracellular Matrix 9
1.1.4 Fibroblasts 10
1.2 The role of CAFs in the TME 12
1.2.1 Regulation of the immune compartment 12
1.2.2 CAFs and Angiogenesis 13
1.2.3 CAFs are involved in matrix remodelling, and promote tumour invasion and metastasis 13
1.2.4 CAFs and treatment resistance 14
1.3 CAFs are derived from multiple origins 15
1.3.1 Tissue resident fibroblasts adopt a ‘CAF’ phenotype 16
1.3.2 Tumour cells as a source of CAFs 17
1.3.3 Endothelial cells as a source of CAFs 17
1.3.4 Pericytes as a source of CAFs 17
1.3.5 CAFs derived from recruited bone marrow cells 18
1.4 Targeting CAFs for anti-tumour therapy 19
1.5 CAFs are a heterogeneous population of cells 19
1.5.1 Heterogeneity of normal fibroblasts 20
1.5.2 Heterogeneity of CAFs 20
1.5.3 Heterogeneity clouds our understanding of CAF function in tumour development. 22
1.6 Malignant Melanoma 23
1.6.1 The Melanoma Microenvironment 24

1.6.2 Melanoma Mouse Models 25
1.7 Project Aims 29
2 Materials and Methods 31
2.1 Mouse Models 32
2.1.1 B16-F10 injectable model 32
2.1.2 BRAFV600E PTEN-/- model 32
2.1.3 E0771 orthotopic breast model 33
2.1.4 Bone marrow chimeras 33
2.1.5 KPC model of PDAC 33
2.2 Tissue Processing 34
2.3 Flow cytometry 34
2.3.1 Detection of intracellular cytokines by flow cytometry 37
2.3.2 Analysis of flow cytometry data by SPADE analysis 37
2.4 Immunofluorescence 37
2.5 In vivo assays 40
2.5.1 EdU Histology 40
2.5.2 EdU Flow cytometry 40
2.5.3 C3a and C3aR inhibition 41
2.6 Isolating CAF populations from B16-F10 melanoma for in vitro culture 42
2.7 Statistical analysis 42
2.8 Single cell RNA sequencing 43
2.8.1 Isolating stromal cells 43
2.8.2 Isolating immune cells 43
2.8.3 cDNA preparation and sequencing 43
2.9 Bioinformatic analysis 44
2.9.1 Alignment and quality control 44
2.9.2 Analysis with Seurat 45

2.9.3 Gene Ontology analysis 45
2.9.4 Cell Cycle analysis 45
2.9.5 Publicly available data 46
3 Devising an approach to investigate CAF heterogeneity 47
3.1 Introduction 48
3.2 Results 49
3.2.1 Exploring CAF heterogeneity in the $BRAF^{V600E}$ $PTEN^{-/-}$ melanoma model 49
3.2.2 Employing single cell RNA sequencing to explore CAF heterogeneity. 62
3.3 Summary 77
4 Identification and validation of CAF populations in the developing melanoma microenvironment 81
4.1 Introduction 82
4.2 Results 83
4.2.1 Applying single cell technologies to profile stromal cells across tumour development 83
4.2.2 CAFs cluster into 3 phenotypically distinct populations 86
4.2.3 The CAF compartment is a dynamic niche, changing and adapting as the tumour progresses 96
4.2.4 Identifying CAF populations in the tumour microenvironment and validating their functional signatures 103
4.3 Summary 119
5 Investigating the functional significance of CAF populations in melanoma and their conservation in other cancer types 125
5.1 Introduction 126
5.2 Results 127
5.2.1 Characterising the Immune Compartment 127

5.2.2 Examining the role of ‘immune’ CAF1 fibroblasts in the development of an immunosuppressive microenvironment 138
5.2.3 Investigating whether fibroblasts derived from different origins form functionally distinct populations 149
5.2.4 Investigation of ‘immune’, ‘desmoplastic’ and ‘contractile’ CAF populations in other murine cancer models and human cancers 151
5.3 Summary 171
6 Discussion 177
6.1 Functionally distinct CAF populations were identified in melanoma 178
6.2 CAF populations across different types of Cancer 185
6.3 Local environmental factors may impact the composition of the CAF compartment and population dynamics as the tumour develops 187
6.4 The interplay between tumour biology the surrounding tissue in shaping CAF heterogeneity 192
6.5 The complement pathway as a therapeutic target 195
6.6 Conclusions and future directions 197
References 201

1

Introduction

1.1 *The tumour microenvironment*

Tumours are not merely an isolated collection of proliferating cells. Instead, they grow in the context of a host tissue, which contains a heterogeneous population of local and recruited cells. Known as the tumour stroma, these populations include immune, fibroblasts and both blood and lymphatic endothelial cells (Fig. 1.1). However, malignant cells manipulate this surrounding environment to create a supportive niche for their growth and survival. The role of different stromal components in tumour maintenance, growth, progression and metastasis are discussed below [1]. Importantly, tumour and stromal populations exist in an interactive network, which together determine tumour fate [2–4].

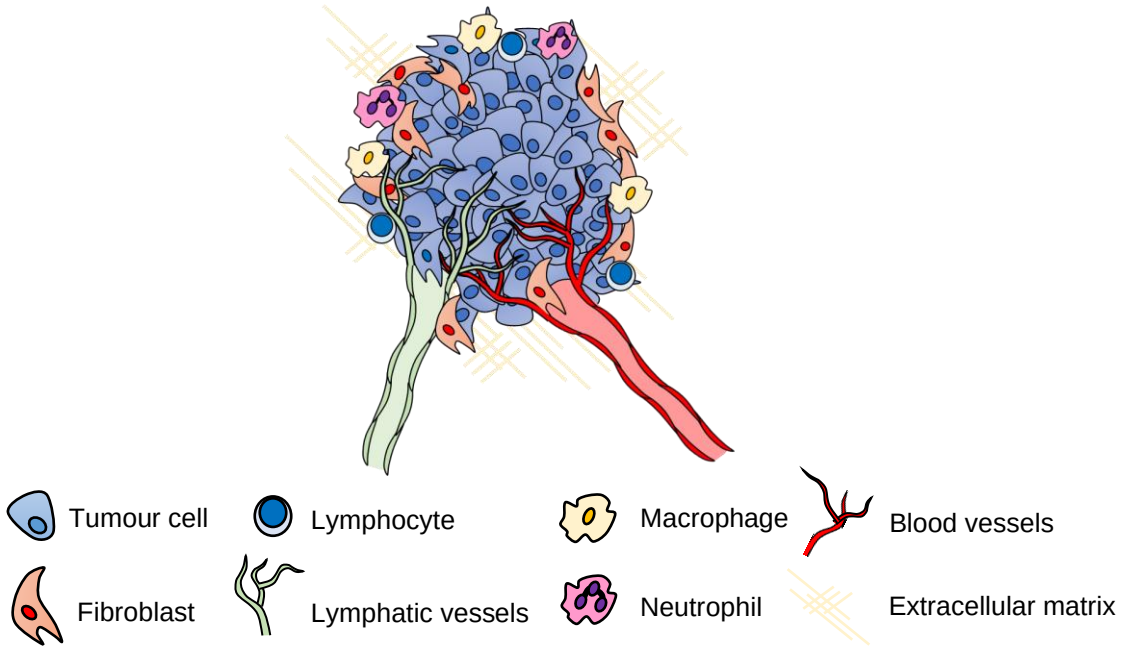

Fig. 1.1 The tumour microenvironment

The tumour microenvironment encompasses a supporting niche of ‘normal’ cells. These include both blood and lymphatic endothelial cells, fibroblasts and an assortment of immune cells such as macrophages neutrophils and lymphocytes

1.1.1 *Immune cells*

The involvement of inflammatory cells in cancer was first proposed by Virchow in 1863, who identified cancer as a consequence of chronic inflammation [5]. While the tumour supporting role of immune infiltrates is well documented, these cells also have the ability to detect and destroy malignant cells [6]. The balance of immune activation and suppression can ultimately determine tumour outcome [7].

1.1.1.1 *Cytotoxic T-cells*

During pathogenic infection, CD8+ T-cells identify and destroy host cells containing intracellular bacteria or viruses. This interaction is mediated by the presentation of foreign antigen, by Major Histocompatibility Complex (MHC) I, on the surface of infected cells. T-cells recognise these specific antigens via their T-Cell Receptor (TCR), bind and lyse infected cells [8]. Owing to genetic mutations, induced by DNA damage, carcinogens or inadequate DNA repair, tumours have the capacity to produce unique antigens specific to malignant cells [9,10]. The ability of CD8 lymphocytes to recognise tumour antigens and destroy malignant cells, was demonstrated in sarcoma models [11,12]. Thus, the presence of CD8 T-cells is correlated with better prognosis and survival in a number of solid tumours [13–17].

However, tumour infiltrating lymphocytes are often functionally impaired or 'exhausted', displaying reduced proliferation and production of Interferon γ (IFNγ) and Tumour Necrosis Factor α (TNFα) [18–25]. T-cell exhaustion was first observed in murine models of chronic viral infection, where activated T-cells lost anti-viral functions [26]. It is characterised by expression of inhibitory receptors, such as Programmed Cell Death Protein 1 (PD-1), Lymphocyte Activation Gene 3 protein (LAG-3), T-cell Immunoglobulin domain and Mucin domain protein 3 (TIM-3), and cytotoxic T lymphocyte antigen-4 (CTLA-4) [27–32]. These markers are upregulated by tumour resident lymphocytes, whose dysfunction promotes tumour immune escape[18–21,23].

Indeed, immune mediated tumour repression largely relies on recruiting and maintaining durable CD8 T-cell responses [13]. However, dysfunction is promoted by the development of an immunosuppressive tumour microenvironment. This includes

expression of immune checkpoint molecules, such as Programmed Cell Death Ligand-1 (PDL1) and PDL2, by tumour and stromal cells [33–36]. These ligands engage the PD1 receptor which directly dampen lymphocyte function [37–39]. Consequently, expression of both molecules is correlated with poor prognosis in multiple cancer types [40–44]. In addition, the establishment of a suppressive cytokine milieu, also contributes to the inhibition of T-cell function. This includes high abundance of immunosuppressive factors Transforming Growth Factor β (TGFβ) and Prostaglandin E2 (PGE2) [45,46], as well as depletion of the lymphocyte metabolite tryptophan by the enzyme indoleamine 2,3-dioxygenase (IDO) [47]. These mechanisms are driven by both malignant and stromal cells, including other immune populations [48]. Indeed, tumour infiltrating leukocytes have the ability to both promote and inhibit T-cell function, which in turn impacts tumour survival.

1.1.1.2 ***CD4 T cells***

The CD4+ T-cell lineage can be further divided into discrete effector populations based on their functional properties. T-helper (Th) cells primarily consist of Th1 and Th2 subsets, which aid specific arms of the immune response via secretion of soluble factors. Th1 cells produce IFNγ and Interleukin-2 (IL2) and promote lysis of intracellular pathogens through heightened CD8 T-cell activity [49]. On the other hand, Th2 populations produce cytokines such as IL4 and IL13, which are associated with allergic inflammation and anti-helminth immunity [50]. In cancer, cytokine signatures associated with Th1 cells have been correlated with better prognosis, while the presence of Th2 cells was linked with reduced survival and tumour induction [51–54]. Favourable outcomes associated with Th1 populations may be due to their role in promoting activity and survival of CD8+ cytotoxic T-cells [55]. Furthermore, indirect priming of CD8 lymphocytes, through Th1 stimulation of Antigen Presenting Cells (APCs), has also been suggested [56]. This hypothesis is supported by the reduced ability of Th1 cells to enhance CD8 tumour cell lysis, upon MHCII depletion *in vivo*. However a direct effect on APCs has not been shown [57].

T-regulatory (T-regs) represent another CD4 subset and are defined by expression of the transcription factor Forkhead Box P3 (FOXP3) [58]. These cells play a critical role in self-tolerance, demonstrated by the onset of severe autoimmunity upon their depletion[59–61]. Although the mechanisms through which T-regs supress immune function are complex, they centre around reducing contact between APCs and T-cells, as well as directly supressing lymphocyte proliferation and cytokine secretion [62–65]. Expression of the checkpoint inhibitor CTLA-4 plays a critical role in this process, aided by the production of regulatory cytokine IL10 and inhibitory factor adenosine [66–70]. These cells are common in solid tumours [71–76], where they contribute to the development of an immunosuppressive microenvironment. This was illustrated by the restoration of anti-tumour immunity upon their removal [77–79]. Thus, increased T-reg infiltration is associated with poor prognosis, particularly when combined with reduced numbers of cytotoxic lymphocytes [75,80–82]. To promote immune escape, tumour cells are thought to actively recruit T-regs or induce their differentiation, through production of C-C motif Chemokine Ligand 22 (CCL22) and PGE2 respectively [75,83].

1.1.1.3 ***Macrophages***

Macrophages are a dominant tumour resident immune population and are generally associated with poor prognosis [84–86]. These cells are either derived from embryonic tissue resident populations or recruited bone marrow monocytes, which differentiate upon arrival [87]. However, recruitment of Ly6C+ monocytes has been the major focus of the field, of which Colony Stimulating Factor 1 (CSF1) and Chemokine Ligand 2 (CCL2) are key mediators [88–92]. Historically, macrophage phenotypes have been divided into M1 and M2 polarisation states, first described in chronic inflammation. Here, M1 macrophages display proinflammatory functions, such as antigen presentation and secretion of IL-12, Nitric Oxide (NO) and Reactive Oxygen Species (ROS). Alternatively, M2 cells are associated with tissue regeneration and angiogenesis [93]. Owing to similar functional properties, tumour resident macrophages are often categorised as M2 polarised. However, this paradigm may be too simplistic to describe macrophages in the tumour microenvironment, as they often display features consistent with both states. Currently, these cells are considered as a collection of populations, defined by their specific functions in tumour development [87].

Irrespective of nomenclature, infiltrating macrophages potently support tumour development. This includes promotion of angiogenesis, invasion and metastasis, via CSF1/ Epithelial Growth Factor (EGF) paracrine signalling and secretion of Secreted Protein Acidic And Cysteine Rich (SPARC) and TGFβ [88,94–97]. In addition, macrophages play a key role in the suppression of T-cell functions, inhibiting proliferation in ex-vivo assays [87,89,98,99]. This may be driven by NO production and breakdown of arginine by the enzyme arginase (ARG1), which is required for T-cell function [89,100]. Furthermore, macrophages express PDL1 and recruit T-reg populations via secretion of CCL22 [101] [75].

1.1.1.4 ***MDSCs***

Myeloid Derived Suppressor Cells (MDSCs) are described as immature myeloid cells that induce immune tolerance [102]. Similar to macrophages, MDSCs supress cytotoxic T-cell functions by production of arginine and promote T-reg induction via Il10 and TGFβ secretion [103–109]. These cells are divided into CD11b+ Ly6C+ Monocytic (M-MDSCs) or CD11b+ Ly6G+ polymorphonuclear (PMN-MDSCs). However, markers commonly used to identify these populations are also expressed by other myeloid cells [102]. Thus, reported MDSC functions may be attributable to other myeloid subtypes, leading to considerable controversy surrounding their presence and influence in the tumour microenvironment. Consequently, many now consider MDSCs as a phenotypic state, rather than a distinct cell type, which describes multiple suppressive myeloid populations [110].

1.1.1.5 ***Neutrophils***

Neutrophils are the most abundant cells in the blood stream and rapidly respond to pathogenic infection. These cells utilise four main mechanism to destroy foreign bodies, including phagocytosis, degranulation and release of ROS and Neutrophil Extracellular Traps (NETs) [111]. However, in a malignant setting, neutrophils both aid and inhibit tumour growth. For example, neutrophils promote angiogenesis[112,113], increase tumour cell proliferation and invasion[114,115] and are implicated in T-cell

suppression via the PDL1/PD1 axis [116,117]. Thus, these cells are associated with poor prognosis in renal carcinoma[118], melanoma[119], colorectal[120], oesophageal[121] and non-small cell lung cancer (NSCLC)[122]. Furthermore, NET production is positively associated with tumour metastasis [123]. Here, NETs are formed by neutrophil release of DNA and chromatin, which acts as a 'sticky' mesh, capturing circulating tumour cells[124]. In a breast cancer model, DNase digestion of NETs, reduced the number of metastatic lesions [125]. Conversely, neutrophils have also been reported to inhibit tumour growth by promoting CD8 T-cell activity, colrelatingd with better prognosis in human colorectal cancer [126]. Due to the dichotomy between pro- and anti-tumour neutrophil functions, similar to macrophages, 'N1' and 'N2' polaristiaion states have been proposed, which are dictated by the surrounding microenvironment [127].

1.1.1.6 ***Dendritic Cells***

By delivering and presenting antigen to T-cells, dendritic cells (DCs) are key orchestrators of the adaptive response. DCs can be separated into two classical populations, (CDC1 and CDC2), as well as plasmacytoid DCs (pDCs). In the context of malignancy, CDC1 cells have drawn particular attention, owing to their ability to cross-present antigen to CD8 T-cells [128]. The importance of this population for the development of anti-tumour cytotoxic immunity was demonstrated upon their depletion in Baft3-/- mice [129]. However, the ability of DCs to initiate lymphocyte activation is dampened by the immunosuppressive microenvironment. This is mediated through suppression of cross-presentation as well as increased expression of T-cell inhibitory ligands PDL1 and TIM3 [130–132].

1.1.1.7 ***NK Cells***

Natural Killer (NK) cells are part of the innate immune system that recognise and lyse infected host cells, through a series of activating and inhibitory receptors [133]. This population has the ability to detect and kill malignant cells, which upregulate ligands for activating receptors [134–136]. Thus, the presence of NK cells is correlated with improved survival [137,138]. However, tumour cells can evade detection by upregulating

ligands for inhibitory receptors, such as non-classical MHCI molecule Human Leukocyte Antigen (HLA) G [139,140], as well as shedding ligands that bind the activating receptor Natural Killer Group 2 Member D (NKG2D) [141].

1.1.1.8 *Immunotherapy*

Considering the power of a coordinated immune response against malignant growth, restoring anti-tumour immunity is a key focus for therapeutic intervention. As CD8 T-cells are the cornerstone of immune mediated tumour lysis, the most successful treatments have concentrated on re-activating their cytotoxic properties [142]. In particular, blocking inhibitory signals via immune checkpoint interactions have shown significant efficacy. Known as checkpoint inhibitors, these are largely composed of antibodies against PD1 and CTLA4 and improve outcome for patients with melanoma [143,144], NSCLC [145–147], renal [148], urothelial [149] and head neck cancer [150]. However, not all patients in these studies respond to therapy, with response rates ranging between 15-30%. Understanding why some cancers respond to immunotherapy and others do not, remains a key unanswered question and is the subject of an expanding area of research [151].

As current immunotherapies target T-cell activity, it is thought that failure to elicit T-cell responses in the tumour microenvironment, underlie poor efficacy. This may reflect the availability of tumour specific antigens for T-cell activation. Indeed, higher mutational burden has been linked to production of tumour antigens, increased CD8 T-cell infiltration and improved responses to immune checkpoint inhibitors [152–154]. However, reduced susceptibility to therapy may also be mediated by inhibition of lymphocyte recruitment or exclusion from the tumour compartment [155,156]. Furthermore, tumour resident lymphocytes express a variety of inhibitory molecules, which may compensate for the inhibition of a single axis [22,23]. Finally, the ability of other immune populations, discussed above, in preventing T-cell recruitment and function, likely contribute to poor responses.

While some patients do not respond to checkpoint inhibitors in the first instance, others acquire resistance after initial benefit [157]. This may be driven by therapy-induced immuno-editing, in which anti-tumour immunity removes immunogenic malignant cells,

allowing colonisation by those that have developed mechanisms to evade or dampen the immune response [157]. In both cases, a second generation of immunotherapies are currently being investigated, which aim to tackle these problems. This includes combinational approaches to improve T-cell infiltration and function, targeting multiple pathways and different populations simultaneously[158]. Furthermore, uncovering biomarkers that predict efficacy of current therapies will aid their application [159].

1.1.2 *Endothelial Cells*

The tumour endothelium is comprised of both blood and lymphatic vessels. Development of a blood vasculature is essential, providing oxygen and nutrients for the growing malignant compartment. While tumours orchestrate angiogenesis through production of factors such as Vascular Endothelial Growth Factor A (VEGFA), these vessels are more permeable and promote intravasation and metastasis [160–163]. In addition, as the point of entry for most leukocyte populations, endothelial cells play an important role in immune recruitment. Under inflammatory conditions the vasculature becomes activated, upregulates adhesion molecules and traps circulating immune cells. Blood endothelium also regulates immune phenotypes and can present antigen to local leukocytes [164–170]. However, angiogenic factors in the TME prevent endothelial activation, reduce expression of adhesion molecules and promote immune exclusion [171–173]. Thus, the tumour vasculature actively contributes to tumour immune escape. Similar to blood endothelium, the lymphatic system is expanded in the tumour stroma and supports metastasis. However, lymphatics also provide a crucial link to tumour draining lymph nodes, in which immune responses are orchestrated [174,175].

1.1.3 *The Extracellular Matrix*

The extracellular matrix (ECM) is cell extrinsic network of fibrillar proteins and proteoglycans. As well as providing structural support to tissue, it has a critical role in cell signalling and tissue homeostasis [176]. ECM remodelling is a prominent characteristic of the tumour microenvironment, known as the ‘desmoplastic reaction’ [177]. This process involves increased deposition of collagens, fibronectin and

proteoglycans, as well changes in their bio-mechanical properties. Here, alignment of collagen fibres and cross-linking, mediated by the enzyme Lysyl Oxidase (LOX), increases matrix stiffness [178,179]. Stiffening is sensed by tumour cells, resulting in increased cytoskeletal tension and focal adhesion maturation, which in turn, promotes tumour invasion and metastasis [180,181]. Indeed, reducing cytoskeletal tension in breast cancer cells suppressed their malignant behaviour [181].

Interestingly, the synthesis of a fibrotic matrix also impacts the tumour immune response. To begin with, dense collagen matrices act as a physical barrier to infiltrating T-cells, preventing tumour cell contact. When this constraint was relieved, by collagen digestion, lymphocytes were able to interact with malignant cells [182,183]. Furthermore, matrix components can regulate immune recruitment and influence their phenotype. For example, cleavage products of Collagen-1 and Elastin, as well as Hyaluronan (HA), act as chemotactic stimuli for myeloid cells [183–185], while Tenascin-C and Heparan Sulphate activate macrophages to produce inflammatory cytokines and induce DC maturation [186,187]. This highlights how different components of the tumour microenvironment interact and cooperate to augment tumour development. Thus, regulation of one compartment may have a manifold of indirect consequences.

1.1.4 ***Fibroblasts***

Fibroblasts are spindle shaped, mesenchymal cells that reside in local connective tissue. In the absence of pathology, these cells are described as quiescent but become ‘activated’ upon initiation of tissue remodelling. Activated cells, known as myofibroblasts, display prominent stress fibres and are defined by their expression of α-Smooth Muscle Actin (αSMA) [188]. During wound healing, myofibroblasts induce extracellular matrix (ECM) remodelling by synthesising matrix proteins and producing remodelling enzymes. Once the wound is resolved, these cells undergo programmed cell death [188,189]. In cancer, fibroblasts are a crucial stromal component. Known as Cancer Associated Fibroblasts (CAFs), they resemble activated myofibroblasts and express many similar markers, such as Fibroblast-Specific Protein-1 (FSP-1), Fibroblast Activation Protein (FAP), the Platelet Derived Growth Factor Receptors α (PDGFRα) and β (PDGFRβ), Podoplannin (PDPN), THY-1 and αSMA [190,191].

Furthermore, CAFs are distinct from normal fibroblasts, displaying enhanced proliferation and a discrete proteome profile [192–194]. CAFs possess many pro-tumour functions and are involved in the development of numerous 'hallmarks of cancer'. This includes, production of growth factors that stimulate tumour growth, development of angiogenesis, ECM remodelling, invasion and metastasis and regulation of immune infiltrates (Fig. 1.2) [195–198]. As this project particularly focuses on CAFs, their role in TME is discussed in detail below.

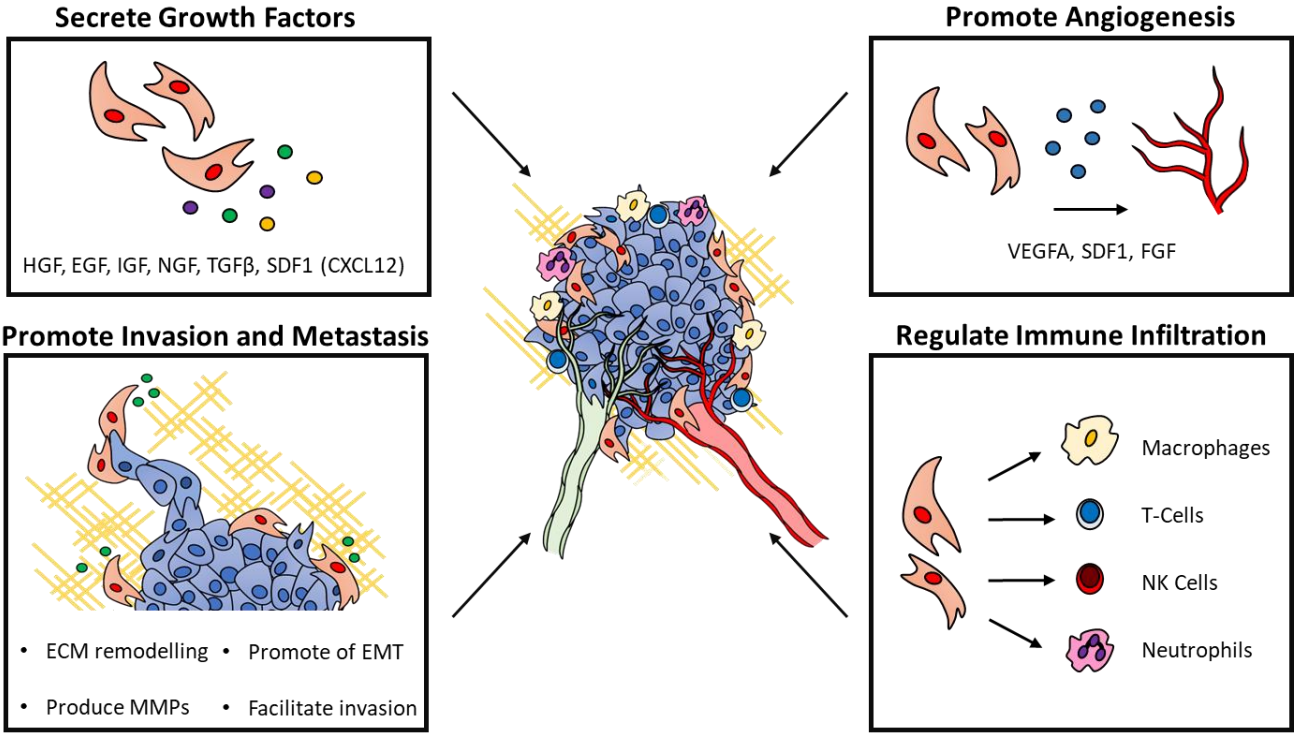

Fig. 1.2 CAFs promote tumour growth and development

CAFs have numerous pro-tumour functions: By secreting growth factors CAFs can directly enhance tumour cell proliferation and survival. They also promote angiogenesis and are the primary source of ECM proteins within the tumour, which they remodel to facilitate tumour cell invasion and metastasis. Finally, CAFs regulate immune infiltrates by attracting certain immune populations, as well as altering their phenotypes.

1.2 *The role of CAFs in the TME*

1.2.1 *Regulation of the immune compartment*

Pioneering work by Erez *et al* showed CAFs possess a pro-inflammatory signature, implying these cells were involved in the development of tumour associated inflammation [199]. Since this study, CAFs have been shown to recruit and regulate immune cells from both the innate and adaptive systems, as well as promote immune suppression [198].

Promotion of T-cell dysfunction is a key mechanism through which CAFs aid tumour immune escape [198]. This is largely driven, indirectly, through recruitment and modulation of suppressive myeloid cells, such as monocytes, macrophages, MDSCs and neutrophils [200–203]. CAF secreted CCL2 is the most documented mediator of this process, driving myeloid recruitment in models of lymphoma, breast and Hepatic cancer [201,202,204,205]. In addition, CAFs induce tumour supporting and immunosuppressive properties in macrophages and MDSCs, through secretion of C-X-C motif chemokine 12 (CXCL12) and IL6 [206,207]. As DCs are essential for the activation of cytotoxic T-cells, their modulation by the fibroblast compartment is a key mechanism of immune evasion. CAFs supress DC function through downregulation of costimulatory molecules and increased expression of regulatory cytokines IL10 and TGFβ [208], via production of tryptophan metabolite kynurenine bytryptophan 2,3-dioxygenase (TOD2). Furthermore, secretion of Thymic Stromal Lymphopoietin (TSLP) polarised DCs towards induction of Th2 responses, which promote tumour development [53,209].

Attenuation of CAF derived factors that modulate the myeloid compartment, such as Chitinase 3 Like 1 (Chi3L1) and CCL2, increased T-cell infiltration and reduced tumour growth [200,202]. However, CAFs have also been shown to directly supress T-cell activity through sampling and presentation of antigen to CD8 T-cells. With negative co-stimulation via PD-L2 and Fas Ligand (FASL), this induced antigen-dependent T cell dysfunction [35]. Moreover, CAFs reduced T-cell proliferation and production of IFNγ, in addition to promoting expression of dysfunction markers [210–213]. Production of PGE2,

NO and expression of PDL1 were implicated in this process. As well as regulating cytotoxic lymphocytes, tumour fibroblasts also attract and retain immunosuppressive T-reg populations via expression of CXCL12, OX-40 Ligand (OX-40L), PDL2 and Junctional Adhesion Molecule 2 (JAM2) [214,215]. Furthermore, CAFs promote tumour immune escape via mechanisms that are independent of lymphocyte activity. These involve inhibition of NK cell lysis by secretion of PGE2 and IDO or degradation of activating ligands on the tumour cell surface [216–218].

1.2.2 *CAFs and Angiogenesis*

As previously discussed, the development of a tumour vasculature is a crucial element for the maintenance of malignant growth. It is thought that CAFs aid this process, by secreting a number of pro-angiogenic factors. VEGF is a potent inducer of angiogenesis and is secreted by tumour cells themselves [219]. However, VEGF is also secreted by CAFs, upon treatment with tumour conditioned media, or by a hypoxic environment [220,221]. Furthermore, CAFs in gastric cancer enhanced production of VEGF in neighbouring tumour cells by stimulation with galectin-1. Other CAF secreted factors, thought to be involved in angiogenesis, include Fibroblast Growth Factor (FGF) and CXCL12 [196,222].

1.2.3 *CAFs are involved in matrix remodelling, and promote tumour invasion and metastasis*

In normal tissue, fibroblasts are responsible for maintaining homeostasis of the surrounding ECM and play an important role in its pathological transformation in cancer [197]. This is facilitated by production of ECM remodelling enzymes such as matrix metalloproteinases (MMPs) and LOX [223–228]. Furthermore, ovarian cancer cells induce expression of urokinase-type plasminogen activator (uPA) in resident fibroblasts, which converts plasminogen to the fibrin degrading protein plasmin, as well as activating MMPs [229]. In addition to enzymatic modifications, fibroblasts physically alter the ECM, contracting and stiffening matrix fibres, via their cytoskeletal

machinery [230]. It is now becoming clear that CAF ECM remodelling induces Epithelial Mesenchymal Transition (EMT) and promotes invasion and metastasis. This was evidenced by the development of a mesenchymal phenotype in epithelial cells seeded in a CAF synthesized matrix [231]. In addition, their ability to align fibronectin fibres or sculpt 'tracks' within the ECM, directs tumour cell migration [232,233]. CAFs also actively lead malignant cells through these passages, enabling metastasis [233]. As well as ECM remodelling, CAFs have been shown to promote EMT and tumour cell invasion by secreting soluble factors such as IL11, TGFβ, Hepatocyte Growth Factor (HGF), CXCL12, osteopontin (OPN), FGF and IL6 [196,234–238]. Furthermore, CAF derived exosomes activated the planar cell polarity (PCP) pathway in breast cancer cells, which established a polarized morphology and enhanced motility and metastasis [239,240].

1.2.4 *CAFs and treatment resistance*

CAF remodelling of the tumour microenvironment also contributes to therapeutic resistance via a number of different mechanisms. To begin with, CAF derived soluble factors aid resistance to chemo-therapeutic agents, as well as targeted therapies. For example, the efficacy of chemotherapies, such as gemcitabine and cis-platin, are ameliorated by CAF Interleukin 1 Receptor Associated Kinase 4 (IRAK4) signalling and secretion of IL6 [241,242]. Interestingly, chemotherapy was also reported to induce DNA damage in tumour resident fibroblasts, leading to the release of WNT16B and subsequent induction of tumour EMT [243]. Thus, the non-specific nature of chemotherapy can impact its ability to reduce tumour growth. However, CAFs also promote resistance to targeted therapies by re-activating inhibited signalling pathways. For example, secretion of HGF induced resistance to EGFR inhibitors by activation of downstream MET. Furthermore, ECM remodelling activated Focal Adhesion kinase (FAK) signalling, which conferred resistance to BRAF inhibitors [244,245]. Interestingly, CAFs also contribute to the poor efficacy of immunotherapies in a number of tumours types. Here, CAFs constrain T-cells to outlying stromal regions through production of factors such as TGFβ and CXCL12. Targeting both secreted factors and the PD1/PDL1 axis enabled both T-cell infiltration and anti-tumour

cytotoxicity [246–248]. As such, the contribution of CAFs to cancer therapy and the underlying mechanisms involved, is an actively growing field of research.

1.3 *CAFs are derived from multiple origins*

Despite the numerous ways in which CAFs promote tumour growth and metastasis, their cellular origin is unclear and many sources have been suggested. These include transformation of tissue resident fibroblasts, tumour cells that undergo EMT, endothelial cells that undergo an EMT-like process, termed endothelial to mesenchymal transition (EndMT), pericytes and recruited mesenchymal cells from the bone marrow (Fig. 1.3).

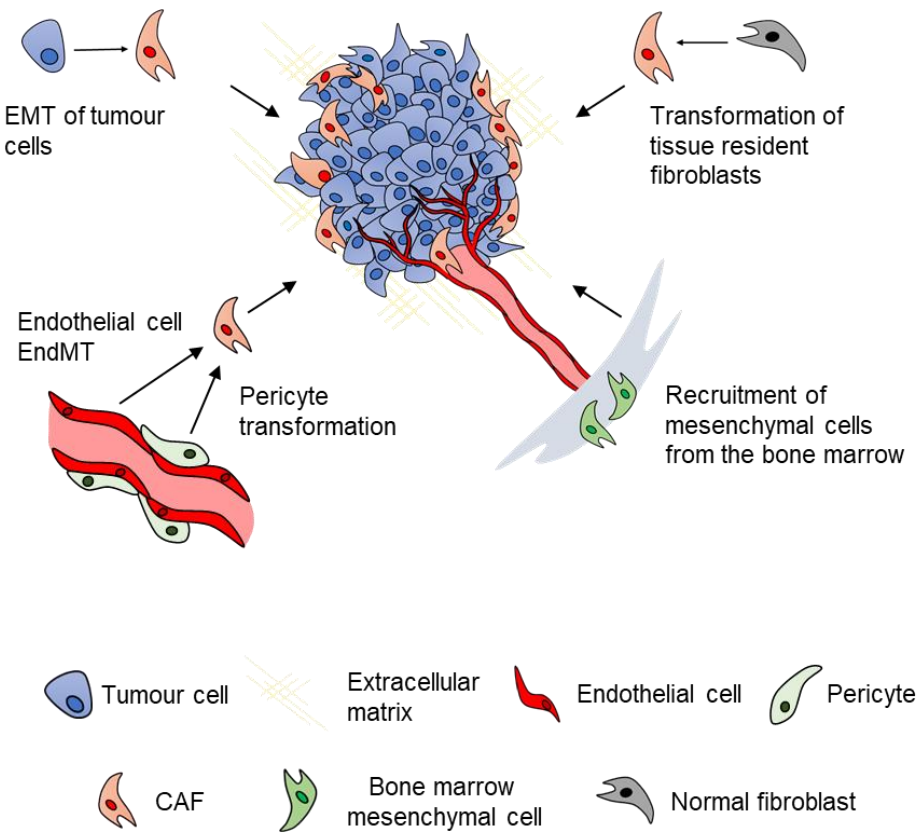

Fig. 1.3 CAFs are derived from multiple origins

The source of tumour resident fibroblasts is the basis of much debate. These include transformation of tissue resident fibroblasts, tumour cells that undergo epithelial to mesenchymal transition (EMT), endothelial cells that undergo an EMT-like process termed endothelial to mesenchymal transition (EndMT), pericytes and recruited mesenchymal cells from the bone marrow.

1.3.1 *Tissue resident fibroblasts adopt a 'CAF' phenotype*

It has been proposed that tumour secreted factors may transform 'normal' resident fibroblasts into tumour promoting CAFs. This is evidenced by the adoption of CAF-like features by normal fibroblasts when exposed to tumour derived factors, such as upregulation of ECM remodelling enzymes and pro-inflammatory cytokines [249]. Furthermore, mammary fibroblasts, that have undergone serial isolation and co-transplantation with tumour cells, upregulated αSMA and promoted tumour growth [250]. This suggests that tumours may engineer local fibroblasts to support their growth and progression.

Interestingly, isolated CAFs retained the ability to promote tumourigenesis across several passages, implying that these fibroblasts may be genetically or epigenetically altered [196]. Although this study did not detect genetic alterations, others have described loss of heterozygosity, as well as mutations in p53 and PTEN [251,252]. Thus, it has been suggested that genetic changes may lie behind the transformation of normal fibroblasts. However, whether CAFs are genetically altered is a controversial topic, as opposing evidence has shown that these cells do not possess genetic mutations or chromosomal abnormalities [253,254]. Epigenetic modifications, on the other hand, have been extensively reported and may contribute to the transformation of normal fibroblasts. CAFs display alterations in micro-RNA (mi-RNA) expression, as well as histone methylation profiles, compared to normal fibroblasts [255–261]. In particular, downregulation of miR-31 and miR-214 in CAFs, compared to normal fibroblasts, enables these cells to support tumour invasiveness and metastasis [255,256]. Furthermore, by targeting signalling pathways such as TGFβ, IL6 and HGF, the CAF miRNA repertoire can have a profound effect on their interactions with tumour cells [262]. Similarly, histone methylation may also alter fibroblast susceptibility to soluble cues in the local TME and affect communication between compartments. For example, hypermethylation of SMAD3 may render CAFs less responsive to TGFβ signalling. Furthermore, hypermethylation of SHP-1 causes constitutive activation of the JAK/STAT pathway and enhances ability of CAFs to promote tumour invasiveness [263].

1.3.2 *Tumour cells as a source of CAFs*

The development of a mesenchymal phenotype during EMT, led to the proposal that CAFs are derived from tumour cells. Although EMT is a well characterized process in embryogenesis, it is less common in adult tissue and is only described in pathological conditions. Interestingly, in a model of kidney fibrosis, renal epithelial cells were shown to undergo EMT to generate fibroblast-like cells [264]. Furthermore, cells from breast cancer biopsies displayed a fibroblast morphology and expressed αSMA and Vimentin, while retaining epithelial traits such as keratin expression. These cells possessed an unstable karyotype and displayed the same X-chromosome inactivation pattern, observed in tumour cells from the original biopsy [265]. Although this suggests tumour cells gain mesenchymal properties, whether these cells transition to a true 'fibroblast phenotype' is unclear. Owing to a lack of lineage tracing experiments, there is no direct evidence that fibroblasts in the TME are derived from malignant origins.

1.3.3 *Endothelial cells as a source of CAFs*

In addition, it has been suggested that CAFs may be derived from endothelial cells that undergo EndMT. There are many parallels between EndMT and EMT, as in both processes, cells lose cell-cell junctions and gain an invasive and migratory phenotype. Furthermore, like EMT, EndMT is largely described as a developmental phenomenon. Here, endothelial cells of the developing heart acquire a mesenchymal phenotype and begin forming the valves and septa [266]. Recently, EndMT has also been observed during cardiac fibrosis in adult hearts and murine cancer models [267,268]. Here, endothelial cells were labelled with the Lac-Z enzyme, which colocalised with expression of CAF markers FSP-1 and αSMA.

1.3.4 *Pericytes as a source of CAFs*

Pericytes are mural cells that reside on the surface of blood endothelium and regulate vasculature homeostasis [269]. Lineage tracing in kidney and liver fibrosis suggested

pericytes detach from vessels, forming myofibroblast populations [270,271]. However, these studies relied on colocalization between fibroblast markers and fluorescent proteins, under the control of pericyte related genes. Thus, it is possible that fibrosis may promote expression of these genes in fibroblast populations, inducing expression of fluorescent proteins. To avoid this problem, tamoxifen inducible Lac-Z expression was activated in pericyte populations during embryonic kidney development. This labelled a proportion of resident adult pericytes, which upon initiation of fibrosis, significantly contributed to the myofibroblast pool [272]. A similar phenomenon was observed in response to PDGFβ signalling in various tumour models, suggesting pericytes contribute to the CAF compartment in malignant settings [273].

1.3.5 *CAFs derived from recruited bone marrow cells*

Finally, two elegant studies, in which mice receive bone marrow transplants containing labelled cells, showed that between 20-40% of αSMA$^+$ fibroblasts in pancreatic cancer, originated from the bone marrow [274,275]. While the identity of these bone marrow derived mesenchymal cells remains elusive, it is possible they represent recruited Mesenchymal Stem Cells (MSCs). MSCs are extremely plastic, differentiating into adipocytes, chondrocytes, osteoblasts, smooth muscle cells, neurons and cells of the visceral mesoderm [276]. This inherent plasticity, as well their morphological resemblance to fibroblasts *in vitro*, suggests that MSCs may act as a source of bone marrow derived CAFs [277]. However, it is difficult to distinguish between MSCs and bone marrow derived fibroblasts, as they share many of the same markers and properties. Nevertheless, Quante *et al.* demonstrated that αSMA$^+$ fibroblasts, in a model of gastric cancer, were generated by a pool of self-renewing bone marrow mesenchymal cells [278]. This cycling population was able to differentiate into chondrocytes, osteoblasts and adipocytes *in vitro,* a property used to identify MSCs. This suggests that a pool of bone marrow MSCs exist in the tumour microenvironment, whose purpose is to generate fibroblasts that aid in tumour development. However, a large amount of uncertainty still surrounds the true identity of marrow derived mesenchymal cells in the tumour microenvironment

1.4 *Targeting CAFs for anti-tumour therapy*

The tumour promoting functions of CAFs render these cells attractive therapeutic candidates. Therapies aiming to deplete fibroblasts from the tumour microenvironment, have mostly targeted these cells based on their expression of FAP. These include anti-FAP antibodies, which are internalised to deliver a mitotic inhibitor, as well as a FAP targeting immunotoxin [279,280]. Other strategies aimed to induce immune killing of FAP+ cells, by administration of DNA vaccines or adoptive transfer of specific Chimeric Antigen Receptor (CAR) T-cells [281–283]. Interestingly, all pre-clinical studies showed reduced tumour growth. However, FAP expression is not restricted to fibroblasts at the tumour site, leading to systemic toxicity upon depletion of FAP^+ cells [284]. Indeed, most CAF markers are expressed by their normal counter parts in a wide variety of tissues. Thus, targeting CAFs in the TME, based on marker expression, is likely to have numerous side-effects.

Other approaches have focussed on targeting the tumour promoting properties of CAFs or inhibiting their activation. For example, anti-fibrotic agents such as Pirfenidone and TGFβ antagonists, were administered to reduce CAF matrix production. This has promising effects, improving responses to chemotherapy and increasing anti-tumour immunity [183,285]. Furthermore, inhibition of fibroblast activation in Pancreatic Ductal Adenocarcinoma (PDAC), by treatment with an agonist for the Vitamin D Receptor, reduced ECM deposition. This, restored a functional vasculature and enhanced the efficacy of gemcitabine chemotherapy [286].

1.5 *CAFs are a heterogeneous population of cells*

Despite the emergence of CAFs as key players in tumour development, their roles are diverse and complex. This multifaceted nature may be explained by the existence of numerous CAF populations within the tumour stroma. CAFs, as well as their normal counter parts, are extremely heterogenous and cannot be uniformly identified by a single marker [287]. Thus, determining fibroblast sub populations and whether they have specific functions in the tumour microenvironment, is a growing focus.

1.5.1 *Heterogeneity of normal fibroblasts*

Fibroblasts are largely characterised by their ability to adhere to plastic and distinct spindle morphology. However, a large volume of work in the 80's and 90's showed subpopulations could be defined based on morphology, rates of proliferation, presence of lipid droplets, ability to produce pro-fibrotic growth factors and cell surface markers [288]. At the turn of the century, developments in microarray analysis enabled a much broader investigation of the fibroblast heterogeneity. This revealed that fibroblasts from different anatomical locations displayed specific transcriptional signatures, such as genes encoding ECM components and growth factors [289]. These distinct expression profiles persisted *in vitro*, suggesting they may be cell autonomous [289,290]. In addition, fibroblast heterogeneity within the same tissue is also evident. In particular, dermal fibroblasts from the upper papillary and lower reticular dermis, are both morphologically and phenotypically distinct [291]. While papillary fibroblasts are spindle shaped and proliferative, reticular fibroblasts display a flattened morphology, decreased growth kinetics and increased expression of αSMA [292,293]. This suggests that under normal physiological conditions, these distinct fibroblasts sub-sets may perform specific functions to maintain tissue homeostasis.

1.5.2 *Heterogeneity of CAFs*

Fibroblast heterogeneity in a malignant setting, has mostly been identified based on differential expression of surface markers. For example, in models of pancreatic and breast cancer, fibroblasts could be divided into either PDGFRβ^{+}/ Neural Glial Antigen 2 (NG2)$^{+}$/ αSMA^{+}, or FSP-1^{+} cells [294]. Recently, it has become clear that differences between populations extend beyond marker repertoire, with reports of specific functional characteristics. A common theme, emerging across different models of cancer, is the existence of distinct immune-regulating populations. Using markers CD29, FSP1, FAP, αSMA, PDGFRβ and Caveolin1, to sort cells, four different CAF populations were identified in breast tumours. Here, one subset was uniquely able to induce T-reg differentiation and promote immune suppression [214]. Moreover, in PDAC, a population defined by its low expression of αSMA, was shown to upregulate the pro-

inflammatory cytokine IL6. An *in vitro* culture system, used to maintain these population phenotypes, revealed expression of additional factors involved in immune cross-talk specific to this subset [295]. Outside of immune regulation, another IL6 secreting population was identified in breast and lung cancer, where it promoted tumour formation and reduced the efficacy of chemotherapy [296]. Furthermore, regulation of resistance to targeted therapies, was also attributed to a specific fibroblast population. Here, a Melanoma Cell Adhesion Molecule $(MCAM)^{+}$ subset, which controlled the expression of the Oestrogen Receptor (ER), mediated tamoxifen resistance[297].

However, these early studies predefined populations based on marker expression, which may mask the true extent of heterogeneity. In the last few years advancements in single cell RNA sequencing (scRNAseq) have enabled vast and unbiased profiling of cancer associated populations. This has begun to reveal fibroblast subsets with unique transcriptional signatures and functional properties in lung, breast, PDAC and head and neck cancer [298–301]. Interestingly, the key features of identified populations varied across tumour type, likely reflecting their unique microenvironment and intrinsic tissue specificity. For example, as well as the previously identified 'immune regulating' CAF population in PDAC, distinct matrix producing and antigen presenting populations were also observed. While a similar 'desmoplastic' population was present in a murine breast model, these tumours also contained a subset involved in 'vasculature support'. By examining expression of a unique set of surface markers, this study showed that this population expanded at later time points.

While the development of single cell sequencing has advanced our knowledge of different CAF populations, there are several limitations within the current literature. As fibroblasts were not the focus of many such investigations, few of these studies have addressed the influence of identified populations on tumour development. Although function is implied based on their transcriptional profile, whether they promote or constrain malignant growth is rarely addressed experimentally. Similarly, the prevalence of identified populations at different stages of tumour development has only been explored based on surface markers. Comprehensive transcriptional profiling of the fibroblast compartment across tumour development, at the single cell level, is yet to be performed. This would enable the examination of both the dynamics of fibroblast populations, as well as changes in fibroblast phenotype in individual

populations across time. Finally, variation in population characteristics across different tumour types, suggests heterogeneity is tissue specific. Thus, further sequencing is required to identify the unique composition of the CAF compartment in other types of cancer.

1.5.3 *Heterogeneity clouds our understanding of CAF function in tumour development.*

The diverse expression of CAF markers may undermine our current understating of their role in tumour development. Historically, many studies have relied on single marker approaches to distinguish and characterise CAFs from the tumour stroma. Given the discovery of functionally distinct populations, these results may only pertain to a subset of cells and bias our perceptions of CAF function. Moreover, CAFs recruited from different tissues may also contribute to fibroblast diversity. For example, in a model of breast cancer, bone marrow derived fibroblasts formed a population possessing unique functional properties [302]. This raises the question of whether CAF phenotype is predetermined by their tissue of origin or is dependent on local cues. As previously discussed, transcriptional profiles of normal fibroblasts were influenced by anatomical location. Thus, in addition to diverse CAF sources, tissue specific programming of resident fibroblasts may also influence the composition of the CAF compartment.

Uncovering the functional properties of different populations and unique markers for their identification, is critical for therapeutic targeting. This is particularly pertinent for therapies aiming to remove CAFs from the tumour stroma. Targeting a single marker may only deplete a subset of cells, which could impact the outcome of treatment. This is illustrated by the contrasting results of two depletion studies in murine models of PDAC. Here, eliminating FAP+ CAFs reduced tumour growth, while removing αSMA+ cells led to increased tumour invasion and reduced survival [248,303]. Thus, it is critical to unearth the role of different populations during tumour development. Furthermore, the discovery of markers that identify functional subsets will improve the application of therapies targeting specific fibroblast properties.

1.6 *Malignant Melanoma*

Malignant melanoma is one of the most common types of cancer and is associated with poor clinical outcome. In 2019 melanoma represented the 3rd and 5th most prevalent cancer in US males and females respectively, and its incidence is increasing [304,305]. Although diagnosis at stage 1 is associated with almost 100% chance of survival, this rapidly declines as the cancer progresses, leaving only a 19% chance of survival if diagnosed at stage 4 [305]. Melanoma itself is caused by aberrant growth and dissemination of skin melanocytes. The early stages of this disease, known as the radial growth phase (RGP), are characterised by proliferation of melanocytes which form a 'nevus' and loss of contact with surrounding keratinocytes [306]. This is followed by the vertical growth phase (VGP), in which malignant melanocytes invade the basement membrane, before metastasising to lymph nodes, lungs, liver or brain [306,307]. While melanoma broadly follows this pattern of growth and invasion, it also represents a heterogenous disease, varying in anatomic location, histological appearance and genetic landscape [308].

Despite its prevalence and lethality, therapeutic options for melanoma patients are limited. As chemotherapy has little effect and is mostly used as a palliative treatment [309–311], the field has largely focussed on developing therapies targeting specific melanoma mutations. The presence of the BRAF V600E mutation in over 50% of cases, lead to the development of BRAF inhibitors [312]. However, within 7 months, the disease continued to progress in almost half of the patients treated [313], likely through acquired resistance [314]. Although clinical trials for MEK inhibitors are ongoing in RAS driven melanoma, at present no targeted therapies are available for patients that lack BRAF mutations [310]. Thus, the emergence of immunotherapies represented a breakthrough in melanoma treatment. Checkpoint inhibitors, such as antibodies targeting CTLA4 (Ipilimumab) and PD1 (Nivolumab and Pembrolizumab) have shown significant efficacy in this disease [144,315]. However, survival rates of roughly 30% are still low, leaving a significant clinical unmet need. Although the combination of CTLA4 and PD1 inhibitors has improved outcome, a large proportion of patients still do not respond [316]. The underlying mechanisms governing patient response to immunotherapies in melanoma are currently unclear but likely reflect those previously

discussed [151]. Thus, the discovery of predicative biomarkers or novel mechanisms of resistance, could significantly improve their effects.

1.6.1 *The Melanoma Microenvironment*

The melanoma microenvironment encompasses many of the common pathological features of cancer, described above. To begin with, malignant melanomas produce melanoma specific antigens, thus, are capable of orchestrating a functional anti-cancer immune response and contain clonally expanded T-cells [317,318]. However, these cells often display markers of T-cell dysfunction [23], which may be induced by expression of immunomodulating ligands such as PDL1 and PDL2 on tumour and stromal cells [319]. This is supported by studies showing PDL1 as a prognostic marker for melanoma progression [320]. Immunosuppressive populations such as MDSC's macrophages and T-regs, are also enriched in melanoma and may contribute towards loss of T-cell activity [321–324]. Indeed, T-reg populations isolated from melanoma patients were shown to recognise melanoma antigens and possess immunosuppressive properties [323,324]. Furthermore, a subset of MDSCs ($CD14^+$ $HLA\text{-}DR^{low}$) that possess a high immuno-suppressive capacity, were present in patients with metastatic melanoma but not their healthy counterparts [325]. The presence of tumour infiltrating lymphocytes likely explains the success of immunotherapies for melanoma treatment, while the multiple mechanisms of immune regulation may provide additional targets to improve their efficacy. Interestingly, as well as supressing anti-tumour immunity, innate immune cells regulate the melanoma vasculature. TAMs are recruited by MCP-1, whose inhibition reduced vessel formation and growth [321,326]. Once recruited, TAMs promote angiogenesis by secreting IL8, as well as enhancing VEGFA production by melanoma cells [327,328]. MDSCs were also identified as a source of IL8 and VEGFA in the melanoma microenvironment and may play a role in vessel maintenance [329].

Owing to their location at the epidermal/dermal junction, malignant melanoma cells likely interact with resident dermal fibroblasts. Interestingly, at early stages of melanoma development, dermal fibroblasts have been shown to inhibit and restrain tumour growth [330]. As the tumour grows and develops, the fibroblast compartment

expands and CAFs acquire pro-tumour properties, however, the underlying mechanisms are poorly understood [331,332]. This was demonstrated by elegant experiments performed in 3D collagen matrices. Here, in response to melanoma secreted factors, fibroblasts surrounded and invaded the primary tumour, as well produced ECM and soluble factors [333]. Indeed, desmoplasia and ECM remodelling is a common feature of malignant melanoma. In particular, expression of matrix proteins Osteopontin, SPARC and TNC increase at later stages of tumour development and are prognostic markers, predicting metastasis [334–338]. In addition to synthesis of matrix components, CAFs also promote melanoma metastasis by production of remodelling enzymes MMP1, MMP2 and MMP13 [339–341]. However, one of the most pertinent roles of fibroblasts in the melanoma microenvironment is their ability to promote treatment resistance. Here, resistance to chemotherapy was induced by production of IL6 and IL8, while HGF secretion reduced the efficacy of BRAF inhibitors [332,342].

Thus, the melanoma microenvironment represents a rich source of potential therapeutic targets. Furthermore, owing to their role in treatment resistance and immunosuppression, targeting stromal populations and innate immune cells may overcome resistance to current therapeutic strategies.

1.6.2 *Melanoma Mouse Models*

Mouse models of melanoma are important research tools, enabling investigation of the processes driving malignancy and metastasis. Furthermore, they provide a platform to test new therapies and interrogate mechanisms of treatment resistance. Murine models of this disease can be classified into three main categories: syngeneic, genetically engineered and xenograft.

1.6.2.1 *Syngeneic Models*

Syngeneic models are generated using murine melanoma cell lines, which are subcutaneously injected into the strain of mice from which they were initially isolated. Derived from a spontaneous murine melanoma, the B16 cell lines are one of the most

commonly used. These lines were generated by *in vivo* passaging of the parent F-0 population and possess different metastatic potential. This describes a cyclic process in which cancer cells are isolated from metastatic lesions, expanded *in vitro* and re-injected to form tumours. Each 'passage' selects cells with a higher metastatic potential, thus, cells from the 10th 'passage' (B16-F10) are potently metastatic. [343,344]. A key advantage of this model is the ease at which it can be genetically modified, enabling investigations into role of specific factors during malignancy, by knocking out or over expression genes of interest. This can also be achieved in the host tissue, through implantation of tumour cells in genetically modified mice. Although similar studies can be performed in genetic models, it is complicated by the need to interbreed different strains.

Considering the potential of immunotherapies in melanoma treatment, another advantage of syngeneic models is that tumours are established in immune competent mice. Indeed, the B16 model is commonly used to investigate methods aiming to enhance anti-tumour immunity, including the original CTLA4 and PD1 inhibition studies [345,346]. However, owing to their low expression of MHCI, the ability of B16 tumours to induce an adaptive immune response has been questioned [347,348]. Despite these concerns, B16 expression of melanoma associated antigens TRP2 and gp100 is sufficient for T-cell recognition and activation [349]. Furthermore, the success of immune checkpoint inhibitors in this model indicates anti-tumour immunity against B16 cells can be induced [345,346].

While the B16 model may be suitable for the study of melanoma associated inflammation and immunotherapies, it does not harbour activating mutations in the BRAF gene, which represents the most common mutation in human melanoma. Similarly, PTEN expression is frequently lost in the human disease yet was expressed by B16 cells [350]. Such differences in the genetic landscape of this model precludes it from studies investigating mutational driven changes in signalling cascades, therapies targeting these pathways and associated resistance. In addition, changes in underlying mutations could alter both cell autonomous and paracrine signalling, which may cause extensive differences in tumour biology. Finally, the rapid growth of B16 tumours does not re-capitulate the human disease. This is particularly pertinent when studying the microenvironment, which may be affected by this stark difference in latency.

1.6.2.2 ***Genetic models***

Many of the concerns regarding the suitability of the B16 model to study melanoma development and treatment, can be addressed using genetically engineered mouse models. A range of strains are available that encompasses different mutations found in the human disease, accommodating the genetic heterogeneity associated with melanoma. Furthermore, these models typically display longer latency than their syngeneic counterparts.

Genetic manipulation of BRAF

A metastatic model incorporating the most common mutation associated with melanoma, , $BRAF^{V600E}$, was developed by Dankort *et al* [351]. Using the Cre-ER system, under control of the tyrosinase promoter, this model enables conditional induction of $BRAF^{V600E}$ and expression of functionally null PTEN upon application of tamoxifen, specifically in melanocytes. Interestingly, while expression of mutated BRAF alone was sufficient to form benign lesions, these lesions did not progress to malignant melanoma. However, in combination with PTEN silencing, mice developed skin lesions that extensively infiltrate the dermis after 25 days. These lesions show histological signs of malignancy, including enlarged nuclei, prominent chromatin and abnormal mitosis. This reflects the human setting, in which the combination of BRAF and PTEN mutations correlates with progression [352,353]. Furthermore, pigmented cells were observed in draining lymph nodes and secondary lesions were present in lungs of $BRAF^{V600E}$ PTEN $^{-/-}$ mice, suggesting this model accurately recapitulates the development of human metastatic melanoma.

Genetic manipulation of RAS

The second most common mutation in melanoma is $NRAS^{Q61R}$, leading to constitutive activation of NRAS. Interestingly, despite accounting for almost 80% of melanomas, NRAS and BRAF mutations appear to be mutually exclusive [354,355]. Introduction of the activating $NRAS^{Q61K}$ mutation in mouse melanocytes triggered melanoma formation. However, deletion of P16INK4a and P14ARF, in combination with NRAS activation, augmented this process and enabled metastasis [356]. P16INK4 and P14ARF are tumour suppressor genes, inhibiting cell cycle progression through the Rb and p53

pathways respectively [357,358]. Both genes map to the CDKN2A locus, which is also commonly mutated in the human melanoma [359]. Although knocking out CDKN2A does not induce murine melanoma, deletion of this gene corporates with both NRAS and BRAF to promote malignancy [358,360,361].

Overall, genetically engineered models preserve interactions and corporation between common melanoma mutations, such as BRAF/PTEN and RAS/CDKN2A, and provide a platform for further interrogation. Consequently, these models are highly suitable for screening of inhibitors targeting dysfunctional proteins, as well as the mechanisms of drug resistance [362]. However, how well these models recapitulate both the immune and non-immune microenvironment has not been reported. In addition, differences in the location of mouse and human melanocytes may reduce the utility of these models to study metastasis. Mouse melanocytes are situated within hair follicles and in the dermis, while human melanocytes are found at the epidermal-dermal junction. As human melanoma is characterised by dermal invasion, this limits the faithfulness of murine models to recapitulate this process. Furthermore, position of mouse melanocytes protects them from UV radiation. Thus, WT mice do not develop melanoma upon UV exposure, a major contributor to the human disease [363]. However, expression of the hepatocyte growth factor/scatter factor (HGF/SF) transgene has been shown to redistribute mouse melanocytes at the dermal-epidermal junction. This renders melanocytes susceptible to UV radiation and better portrays invasion and metastasis [364,365].

1.6.2.3 ***Xenograft models***

Variability between species has prompted the use of xenograft models in which human melanoma cells are grafted into immunocompromised mice. However, long term *in vitro* culture of cell lines effects their biology and physiological properties [366]. To combat these issues, patient-derived tumour xenografts (PDTX) are now commonly used in pre-clinical studies. Engrafting tumours from a range of patients enables the development of mouse colonies which accurately recapitulates melanoma genetic heterogeneity [366]. Indeed, these models have predicted melanoma treatment responses in the clinic. Thus, PDTX lines which develop in parallel with the patient's

disease may be used to guide their specific therapeutic strategy [367]. While PDTX models are useful to examine drug responses, establishing these models is difficult and time consuming, with a limited success rate [366]. Furthermore, they are not receptive to genetic manipulation, limiting their use for basic research [368]. However, most importantly, these models lack a competent immune system. Not only does this preclude them from studies investigating tumour immunity and immunotherapies but will affect soluble cues and cell signalling within the local microenvironment.

Overall, the heterogenous nature of human melanoma will never be recapitulated by a single mouse model. Indeed, each model has a unique set of advantages and disadvantages that render them suitable for investigating particular aspects of melanoma biology.

1.7 *Project Aims*

Hypothesis: Functionally distinct CAF populations are present in malignant melanoma, change as the tumour develops and influence tumour progression.

In the struggle to improve melanoma therapies, CAFs represent a wealth of potential targets. Furthermore, CAFs closely interact with immune populations and were shown to be involved in resistance to immunotherapies [248]. Thus, studying CAF function during melanoma development may uncover novel therapeutic targets, as well as the mechanisms underlying response to checkpoint inhibitors. However, as previously discussed, fibroblasts are a heterogenous population, in which different subsets possess unique functions and express an array of markers. Furthermore, while some phenotypes are conserved, CAF populations fluctuate across different cancer types. Currently, the composition of subsets that make up the fibroblast compartment in melanoma has not been investigated. Therefore, delineation of fibroblast heterogeneity is vital to elucidate their contribution to malignant growth.

In addition, there has been limited investigation into the development of CAF phenotypes across tumour evolution. This is particularly interesting, as discussed earlier, evidence shows that normal dermal fibroblasts actively inhibit tumour growth

[189,369]. Thus, it is important to understand the mechanisms leading to the acquisition of a pro-tumour phenotype. Stromal cells must adapt to the environmental pressures of the growing malignant compartment. For example, factors such as nutrient deprivation, hypoxia and fibrosis all arise as the tumour evolves. Differential exposure to these factors over the course of tumour development, in combination with changes in tumour cell signalling, may impact CAF phenotype and function. As mentioned above, the impact of this unstable environment on individual CAF populations remains to be explored at the transcriptional level.

Thus, the overall aim of this project was to identify CAF sub-sets and elucidate their roles in melanoma development. The caveats of conventional techniques, such as IF and flow cytometry, were experienced first-hand upon initial exploration of CAF heterogeneity in murine models. These approaches lacked the resolution to uncover the true extend of fibroblast diversity and introduced marker-based bias. Thus, a 'negative selection' approach was combined with scRNAseq technology, to profile the CAF compartment of B16-F10 melanoma at high resolution. This was initially tested on a single time point, to ensure unique CAF populations could be identified and their transcriptional signatures could be validated. This method was then applied to sequence CAFs from different stages of tumour development. Thus, for the first time, this project provides fibroblast transcriptomics, at single cell resolution, across time. Our results revealed functionally and temporally distinct populations. Finally, the impact of these subsets on malignant growth, their conservation in other cancer types and translation to human tumours were investigated.

2

Materials and Methods

2.1 *Mouse Models*

Animals were housed in accordance with UK regulations and experiments were performed under project licence 80/2574 and P8837835. Tumour induction, culling and sample collection was carried out by myself or other members of the Shields lab. Intraperitoneal (IP) dosing of drugs, intravenous (IV) transfusions, tail vein bleeds, irradiation and tumour measurements were performed by animal Technicians at the Ares facility (Babraham, Cambridge).

2.1.1 *B16-F10 injectable model*

C57BL/6 derived B16-F10 melanoma cells were purchased from American Type Culture Collection (ATCC) and cultured in Dulbecco's Modified Eagle medium (DMEM, Life Technologies), supplemented with 4.5 g/L of glucose and glutamine, pyruvate, 1% Penstrep and 10% Foetal Bovine Serum (FBS). mCherry expression was induced by Dr. Angela Reidel and selection was maintained by adding 8µg/ml of blasticidin to the media. $2.5x10^5$ B16-F10 melanoma cells in 50µl of Phosphate-Buffered Saline (PBS) were subcutaneously injected into the mouse shoulder. Sham controls were created by injecting 50µl of PBS using the same method. Animals were sacrificed at various time points.

2.1.2 **BRAFV600E PTEN-/- model**

The inducible melanoma model C57BL/6 B6.Cg-Braftm1Mmcm Ptentm1Hwu Tg(Tyr-cre/ERT2)13Bos/BosJ ($BRAF^{V600E}$ $PTEN^{-/-}$) was purchased from Jackson laboratories. For time course experiments, 25mg/ml 4-Hydroxy Tamoxifen (4-HT) (Sigma) was applied to the mouse shoulder and tumours were collected at 11, 14 and 24 days post induction. However, carrier mice also develop spontaneous tumours, which were also isolated and analysed.

2.1.3 *E0771 orthotopic breast model*

The C57BL/6 E0771 breast cancer cell line were purchased from CH3 BioSystems and cultured in RPMI 1640 (Sigma), supplemented with 1% Penstrep, 10% FBS and 10mM 4-(2-hydroxyethyl)-1-piperazineethanesulfonic acid (HEPES, Gibco). 2.5 $x10^5$ cells in 50µl of PBS were injected into the 4th inguinal mammary fat pad of C57BL/6 mice. Again, sham controls were created by injecting 50µl of PBS into fat pads. Tumours were collected after 8 and 16 days of tumour development and the fat pad was collected from non-tumour bearing mice.

2.1.4 *Bone marrow chimeras*

The bone marrow of Wilde Type (WT) C57BL/6 mice was depleted by exposing mice to two doses of 5 Gray radiation. Bone marrow was harvested from the femurs and tibias of CAG-EGFP mice, in which GFP is ubiquitously expressed. Here, muscle and flesh were removed, and bones were flushed with PBS using a 25 gage needle to extract marrow. $20x10^5$ GFP^+ bone marrow cells were injected IV into WT irradiated mice. After 1 month, blood from chimeric mice was tested for bone marrow reconstitution. Once reconstituted, B16-F10 melanoma cells were injected according to section 2.1.1.

2.1.5 *KPC model of PDAC*

PDAC tumours from the LSL-KrasG12D/+;LSL-Trp53R172H/+; Pdx-1-Cre (KPC) were donated by Dr. Tobias Janowitz (CRUK Cambridge institute department of Oncology). Tumours were cut in half and either processed for flow cytometry (section 2.2 and 2.3) or snap frozen for histology (Section 2.4). For flow cytometry experiments pancreatic tissue from non-carriers was used as a control. However, not enough tissue was available for histology, thus, the pancreases from WT C57BL/6 mice was isolated and used instead.

2.2 *Tissue Processing*

All tumours were mechanically dissociated and digested in 1mg/ml collagenase D (Roche), 1mg/ml collagenase A (Roche) and 0.4mg/ml DNase (Roche) in PBS, at 37^{O}C. B16-F10 and E0771 tumours were digested for 1.5-2hs, whereas the more fibrotic PDAC and BRAF^{V600E} PTEN$^{-/-}$ tumours were digested for 3hs. Brachial lymph nodes were isolated, mechanically dissociated and digested with collagenases. Here, 1mg/ml collagenase A (Roche) and 0.4mg/ml DNase in PBS, were added for 30 mins at 37^{O}C, followed by Collagenase D (final concentration of 1mg/ml) for a further 30 mins. Ethylenediaminetetraacetic acid (EDTA) was added to all samples to neutralise collagenase activity (final concentration of 5mM) and digested tissues were passed through 70µm filters (Flacon) ready for staining. Blood samples were incubated using 5ml of red blood cell lysis buffer (150mM NH_4Cl, 1mM $KHCO_3$, 0.1mM EDTA in dH_2O) at RT for 5mins. This was neutralised using 45ml of PBS and centrifuged at 300g for 5 mins to remove debris.

2.3 *Flow cytometry*

Samples were incubated with a Live Dead fixable fluorescent viability stain (Life Technologies) for 20mins, diluted 1:1000 in PBS, to label dead cells. Fluorescently conjugated primary antibodies were diluted in FACS Buffer (0.5% Bovine Serum Albumin (BSA) in PBS)) according to Table 1 and incubated with cells for 20mins at 4^{o}C. If analysing immune cell populations, surface antibodies were diluted in a 50/50 mix of FACS buffer and 2.4G2 FC Blocker (hybridoma supernatant generated in-house). Fluorescently conjugated secondary antibodies and streptavidin were diluted 1:300 in FACS buffer and added with primary antibodies or in a further 30min secondary step. If required, cells were fixed and permeabilized, for 1h at RT, using the FOXP3 permeabilization kit (Biolegend) according to manufactures instructions. Antibodies against intracellular targets were diluted in 1x perm buffer (FOXP3 permeabilization kit) for a further 30mins. Samples were run on the BD LSR III Fortessa system and analysed using FlowJo Version 10.

Target	*Conjugation*	*Species*	*Company*	*Clone*	*Dilution*
CAF markers					
PDPN	PE, APC	Syrian Hamster	Biolegend	8.1.1	1:300
PDPN	Biotin	Goat	R&D Systems	8.1.1	1:100
FAP	Purified	Sheep	R&D Systems	polyclonal	1:50
αSMA	488, eFluor570	Mouse	Thermo Fisher	1A4	1:200
PDGFRα	Biotin, PE, PECy7	Rat	Biolegend	APA5	1:300
PDGFRβ	Biotin	Rat	Biolegend	APB5	1:300
Thy1	Purified	Rat	eBioscience	G7	1:100
Thy1	APCCy7	Rat	Biolegend	30-H12	1:300
CD34	APC	Armenian Hamster	Biolegend	MEC 14.7	1:200
CD34	660	Rat	Biolegend	RAM34	1:300
Immune markers					
CD45	BV785, FITC, APCCy7	Rat	Biolegend	30-F11	1:300
CD31	PE-Cy7	Rat	eBioscience	390	1:300
CD31	Biotin	Rat	eBioscience	MEC13-.3	1:300
CD3e	488, PE	Armenian Hamster	Biolegend	145-2C1	1:300
NK1.1	PE	Mouse	Biolegend	PK136	1:300
CD4	PE-Cy7	Rat	eBioscience	GK1.5	1:300
CD8a	BV785, 780, PE	Rat	eBioscience	53-6.7	1:300

FOXP3	PerCp Cy5.5	Rat	eBioscience	FJK-16	1:300
Lag3	Biotin	Rat	Biolegend	C9B7W	1:300
PDL1	PE-Cy7, APC	Rat	Biolegend	10F.9G2	1:300
PD1	APC	Rat	Biolegend	RMP1-30	1:300
IL-7Ra	APC	Rat	Biolegend	A7R34	1:300
B220	488	Rat	Biolegend	RA3-6B2	1:300
CD11b	647, PECy7	Rat	Biolegend	M1/70	1:300
CD11c	PE-Cy7	Armenian Hamster	Biolegend	N418	1:300
Ly6C	FITC	Rat	BD Pharmogen	AL-21	1:300
Ly6G	PE-Cy7	Rat	Biolegend	1A8	1:300
F4/80	FITC, APC-eFluor780	Rat	eBioscience	BM8	1:300
ARG1	APC	Rat	eBioscience	A1exF5	1:300
Other					
Ki67	PECY7	Rat	Biolegend	16A8	1:100
CXCL12	PE	Mouse	R&D Systems	MAB350	1:100
C3	PE	Rat	Novus	11H9	1:750

Table 1 Antibodies used in flow cytometry

2.3.1 *Detection of intracellular cytokines by flow cytometry*

To detect intracellular cytokines Brefeldin-A (BFA, Biolegend) was added to the tissue digestion mix (1:1000). After processing to a single cell suspension, samples were further incubated with BFA in media (1:1000 in DMEM 10% FBS) at 37◦C. Samples were incubated with BFA for a total time of 4hs yet the length of digestion and media incubation varied depending on the tissue digested.

2.3.2 *Analysis of flow cytometry data by SPADE analysis*

Spanning-tree progression analysis of density-normalised events (SPADE)[370,371] was performed using the cytobank online tool (www.cytobank.org). Trees were generated using flow cytometry data, in which doublets, dead, immune ($CD45^+$) and endothelial ($CD31^+$) cells were removed. Samples were down-sampled by 10% and 100 nodes were specified for each tree. Clustering was performed on CAF markers PDPN, FAP, Thy1 and PDGFRα. A more detailed description of SPADE analysis can be found in (section 3.2.1.3).

2.4 *Immunofluorescence*

Tissues were embedded in Optimal Cutting Temperature (OCT) medium (VWR), snap frozen on dry ice and stored at -80ºC. 10µm sections were cut using the Leica cryostat CM1900. Sections were air dried and fixed in either acetone (Fluka)/ methanol (Fisher) (1:1) at -20ºC for 2mins, or 4% PFA at RT for 10 mins. PFA fixation was followed by permeabilization using PBS 0.2% Triton-X (Fisher) for 10 mins at RT. Sections were blocked using 10% chicken serum 2% BSA in PBS (Blocking Buffer) for 1h at RT. Primary antibodies were diluted in blocking buffer according to Table 2 and added to sections overnight at 4ºC. After washing 3x 5mins in PBS 0.1% Tween, sections were incubated with secondary antibodies or fluorescently labelled streptavidin, diluted 1:300 in blocking buffer, for 1-2hs at RT. To visualise FAP staining, an extra amplification step was required. Here, samples were incubated with a biotin labelled

anti-sheep antibody (Novex, diluted 1:100), after application of primary antibodies. This was detected by addition of fluorescently labelled streptavidin (diluted 1:100).

Sections were washed 3x 5 mins in PBS 0.1% tween and 1µg/ml of 4',6-diamidino-2-phenylindole (DAPI) was added for 10mins to visualise the nucleus. Slides were mounted using liquid mountant ProLong Gold (Thermo) and sealed with nail varnish. High power 63x imaging was performed using the Zeiss 880 confocal microscope. To visualise larger regions or ECM components tile scans, in which consecutive images are stitched together, or tiled z-stacks were used respectively. Whole sections were imaged at 20x using either the Zeiss 880 or Zeiss Axioscan-z1 systems. All images were processed using Zen lite or Zen black software.

Target	Species	Company	Clone	Dilution
PDPN	Syrian Hamster	Biolegend	8.1.1	1:100
αSMA	Rabbit	abcam	Polyclonal	1:50
FAP	Sheep	R&D Systems	Polyclonal	1:20
PDGFRα	Goat	R&D Systems	Polyclonal	1:50
Thy1	Rat/Biotin	Abcam	G7	1:100
CD34	Rat	eBioscience	RAM34	1:50
CD34 488	Rat	eBioscience	RAM34	1:20
F4/80	Rat	AbDserotech	A3-1	1:100
F4/80 488	Rat	AbDserotech	A3-1	1:20
CXCR4	Rat	R & D Systems	247506	1:50

CSFR1	Sheep	R & D Systems	Polyclonal	1:50
CXCL12 PE	Mouse	R & D Systems	MAB350	1:50
CSF1	Rabbit	ABGENT	Polyclonal	1:50
NG2	Rabbit	abcam	Polyclonal	1:50
CD31	Rat	Biolegend	MEC13.3	1:100
C3aR	Rabbit	Invitrogen	Polyclonal	1:25
Ly6C APC	Rat	BD Pharmogen	AL-21	1:20
CD11b biotin	Rat	Biolegend	M1/70	1:100
GLUT1	Rabbit	Abcam	EPR3915	1:100
LDHA	Rabbit	Abcam	Polyclonal	1:100
HIF1α	Rabbit	Abcam	EPR1687	1:30
CA9	Goat	R & D Systems	AF2344	1:100
Collagen-1	Rabbit	AbD Serotec	Polyclonal	1:100
Periostin	Rabbit	Novus	Polyclonal	1:100
Tenacin-C	Rat	R & D Systems	578	1:100
TRP2	Goat	Santa Cruz	D-18	1:100

Table 2 Antibodies used in IF imaging

2.5 *In vivo assays*

2.5.1 *EdU Histology*

B16 melanomas were established in WT C57BL/6 mice, according to section 2.1.1. IP injections of 500μg/ml of 5-ethynyl-2´-deoxyuridine (EdU, Thermo) were performed every 24hs for the 4 days prior to culling. Tumours were collected after 11 days and snap frozen in OCT medium and sectioned according to section (2.4). Sections were fixed at -20ºC, in a mixture of acetone and methanol (50:50). After fixation, the EdU Click-it Alexa Fluor 647 imaging kit (Invitrogen) was used to visualise incorporated EdU. The Click-it reaction cocktail was made according to

Table **3** and incubated with sections for 30 mins RT. After washing with PBS (3x 5mins), sections were blocked and immuno stained as described in (section 2.4)

Reaction components	Volumes added
1X Click-iT reaction buffer *	860 µL
CuSO4	40 µL
Alexa Fluor azide	2.5 µL
Reaction buffer additive	100 µL
Total volume	1ml

Table 3 Click-iT reaction cocktail for histology

Volumes of components added to the Click-iT reaction cocktail used for histology. All components were added in the order given and the cocktail was used within 15 mins.*10x Click-iT reaction buffer stock solution was made by diluting reaction buffer 1:10 in dH_20. This was further diluted 1:10 in dH_20 to make a 1x working solution.

2.5.2 *EdU Flow cytometry*

B16-F10 melanomas were established as previously described and IP injections of 500μg/ml of EdU (Thermo) were performed every 24hs for the 2 days prior to culling.

Tumours were collected at day 5 and day 11 and skin was collected from non-tumour bearing mice. Tumours were processed according to section 2.2 and incubated with a viability dye and stained for surface markers as described in section 2.3. As PE and PECy7 fluorophores are quenched by the Click-iT reaction, antibodies conjugated to these colours were only used after this step was performed. Cells were fixed with 4% PFA for 15 mins at RT, followed by permeabilization with saponin buffer (EdU flow cytometry kit, Invitrogen) for a further 15 mins. Saponin buffer was diluted 1:10 in dH_20 from the stock solution provided. Samples were then incubated with the Click-iT cocktail using reagents from the EdU Click-iT Alexa Fluor 488 imaging kit (Invitrogen) made according to Table 4, for 30 mins at RT. After washing with Saponin buffer, antibodies against intracellular targets were added, diluted according to Table 1 in FACs buffer.

Reaction components	Volumes added
PBS	860 µL
CuSO4	40 µL
Alexa Fluor azide	2.5 µL
Reaction buffer additive	100 µL
Total volume	1ml

Table 4 Click-iT reaction cocktail for flow cytometry

All components were added in the order given and the cocktail was used within 15 mins.*10x Click-iT reaction buffer stock solution was made by diluting reaction buffer 1:10 in dH_20. This was further diluted 1:10 in dH_20 to make a 1x working solution.

2.5.3 *C3a and C3aR inhibition*

B16-F10 melanomas were established in WT C57BL/6 mice as described in section 2.1.1 and allowed to develop for 5 days before treatment. For C3a neutralisation, mice were treated with 10µg/ml anti-C3a (HyCult Biotech, clone: 3/11) or IgG2a control (BioXCell, clone 2A3) in 200µl of PBS. To inhibit C3aR signalling, mice were treated with 100µg of the small molecule SB290157 (Sigma) diluted in 200µl of PBS 5% Dimethyl Sulfoxide (DMSO) or vehicle control. Inhibitors were injected IP at day 5, day 7 and day 9. Mice were sacrificed either 24hs after the first injection (day 6) or at day 11 and tumours were isolated. Blood was collected at both time points by cardiac

puncture and stored in capped EDTA tubes. A second time course was performed using the antagonist SB290157 in which mice were treated at either day 4 and day 6 or day 8 and day 10. Tumours were allowed to develop until day 11, at which time mice were sacrificed and samples collected. Tumour volumes were taken daily and calculated using the formula $(\pi/6)(\text{shortest length}*\text{longest length})^2$. Data points from all animals were included unless tumours failed to form following technical issues with injection of cells.

2.6 *Isolating CAF populations from B16-F10 melanoma for in vitro culture*

To isolate CAF populations B16-F10 tumours were established in B6.FVB-Tg(Acta2-DsRed)1Rkl/J mice (aSMA-DsRed, Jackson Laboratories), according to section 2.1.1. Tumours were processed according to section 2.2 and stained with a viability dye and primary antibodies as previously described. Immune and endothelial cells were excluded based on CD45 and CD31 expression and CAFs were selected based on combined expression of Thy1, PDGFRα and PDGFRβ. CAFs were identified based on CD34 and αSMA expression and isolated by FACS using the BD influx flow cytometry system. Roughly 20,000 cells per population were collected in RPMI 1640 media (10% FBS and 1% Penstrep) and were plated in a 24 well plate. Media was changed every 2 days and cells were split once 70% confluent. To assess expression αSMA throughout *in vitro* culture, images were taken using the Evos fluorescent microscope system at 10X. After 2 weeks, CAF composition was evaluated by flow cytometry. Here cells were dissociated from plastic by incubation for 10 mins with accutase (Biolegend) at 37^{o}C and stained according to section 2.3.

2.7 *Statistical analysis*

To evaluate statistical significance between two samples a T-test was performed. For multiple comparisons, a one way or two way ANOVA was employed with a Tukey post-hoc test. The Sidak post-hoc test was also used when analysing two way ANOVAs, depending on the number of conditions in each group. All analysis was performed

using GraphPad Prism 7.0. P values < 0.05 were considered significant, giving a 95% confidence level.

2.8 *Single cell RNA sequencing*

2.8.1 *Isolating stromal cells*

WT or mCherry$^+$ B16-F10 melanoma cells were injected into CAG-EGFP mice. Mice were sacrificed 5, 8 and 11 days post injection and tumours and lymph nodes were collected. In addition, skin samples were collected from non-tumour bearing mice. Tissues were processed as described in section 2.2 and samples were incubated with a viability stain and primary antibodies according to section 2.3. Cells were index sorted using the BD influx flow cytometer system, excluding GFP$^-$ tumour cells and CD45$^+$ immune cells. Stromal populations were divided into CD31$^+$ endothelial cells or CD31$^-$ fibroblasts. These cells were sorted into a 96 well plate containing 2µl of Lysis Buffer (1:20 solution of RNase Inhibitor, Clontech in 0.2% Triton X-100, Sigma) and frozen at -80 degrees.

2.8.2 *Isolating immune cells*

WT B16-F10 melanoma cells were injected into WT C57BL/6 mice and sacrificed after 5, 8 and 11 days. Tumours and lymph nodes were collected, processed and stained as previously described. Similar to stromal cells, cells were index sorted using the BD influx flow cytometer directly into Lysis Buffer. Immune cells were selected using CD45 and separated into different populations based on expression of CD3e, CD4, CD8, CD11b, CD11c and B220.

2.8.3 *cDNA preparation and sequencing*

Reverse transcription (RT) and cDNA pre-amplification were performed according to the SmartSeq2 protocol [372]. Oligo-dT primers, dNTPs (Thermo) and external RNA control consortium (ERCC) RNA Spike-Ins (final dilution 1:50,000,000, Ambion) were

added to lysates. Primers were then annealed to poly(A) tails, capturing mRNA transcripts. RT transcription and template switching PCR was performed to create single strand cDNA copies of the original transcript, followed by PCR amplification using 50U of SMARTScribe™ Reverse Transcriptase (Clontech). PCR purification using AMPure XP beads (Beckman Coulter) and tagmentation using Nextera XT DNA Sample Preparation Kit (Illumina), were performed by Sanger-EBI core facilities. cDNA libraries were sequenced using the Illumina HiSeq 2500 with an average depth of 1 Million reads/cell (paired-end 100-bp reads).

2.9 *Bioinformatic analysis*

2.9.1 *Alignment and quality control*

2.9.1.1 *Pilot study (3.2.2)*

Alignment and quantification was performed Dr. Gozde Kar (Teichmann Lab). For each cell, reads were aligned using Genomic Short-read Nucleotide Alignment Program (GSNAP) with default parameters. Mapped reads were counted using htseq-count (http://www-huber.embl.de/users/anders/HTSeq/) and normalized with size factors using the R package DEseq2. Cells were excluded if less than 100,000 mapped reads were detected or mitochondrial (mt) expression was >5%. Genes were also removed if expressed in < 3 cells.

2.9.1.2 *Time course (4.2.1)*

For these studies alignment and quality control was performed by Dr. Mirjana Efermova (Teichmann Lab). Briefly, data was quantified using Salmon[64] (version 0.8.2), to generate Transcript Per Million (TPM) values. ERCC spike ins were removed and TPM values were scaled so that the total number summed one million. Cells with less than 1500 detected genes and greater than 20% mitochondrial genes were excluded, as well as genes that were expressed in less than 3 cells.

2.9.2 *Analysis with Seurat*

Downstream analysis was performed using Seurat (version 2.3.4) [361]. Data was log transformed and scaled using the 'ScaleData' function. Variable genes were calculated using the 'FindVariableGenes' function and used for principal component analysis (PCA). For each data set the most significant principle components (PCs) were selected using the a PCElbow which compares the standard deviation of all PCs. Clusters were assigned using the 'FindClusters' function, which was performed using significant PCs. The same PCs were used in tSNE analysis and clusters were projected onto tSNE plots. Differentially expressed genes (DE genes) were generated using the 'FindMarkers' function based on the Wilcoxon rank sum test. Genes expressed in <10% of cells in a cluster, or with a pvalue of >0.05 were excluded. Populations were subsetted using 'SubsetData', re-scaled and variable genes were re-calculated. Subsequent analysis was performed as described above. Cell cycle phase induced a large amount of variability in T cell subsets. Thus, this was regressed out during data scaling, based on cell cycle scores produced by cyclone (section 2.9.4).

2.9.3 *Gene Ontology analysis*

Gene Ontology (GO) terms relating to each cluster were calculated using gProfileR. Significantly upregulated genes (pvalue < 0.05) for each population were matched to the Kyoto Encyclopaedia of Genes and Genomes (KEGG) terms, using moderate hierarchical filtering.

2.9.4 *Cell Cycle analysis*

Cell cycle phase was assigned using the R package Cyclone [373]. This package uses a training data set, in which the cell cycle phase is known, to generate a list of marker pairs for each phase. Marker genes pairs for a specific phase are determined by higher

expression of the first gene compared to than the second. This first gene must, however, be lower than the second in all other phases. These marker pairs are tested on the new data set and the proportion of markers for which the above is true are calculated. This generates a score for each stage across all cells, which are used to assign a phase.

2.9.4.1 *Pseudo-time*

Pseudo-time analysis was performed using the R package Destiny [374,375] and diffusion maps were created using significant PCs calculated in section 2.9.2. Diffusion Pseudo-Time (DPT) probabilities were computed for all cells using the 'DPT' function. DPT probabilities for the first or 'tip' cell, in the diffusion map, were ordered to create a trajectory and superimposed. A more detailed description of destiny and DPT can be found in section (0).

2.9.5 *Publicly available data*

Publicly available data sets were downloaded from Gene Expression Omnibus (GEO) using the accession numbers listed in Table 5. Raw counts were used to analyse bulk RNA sequencing data and differentially expressed genes were calculated using DeSeq2. However, heatmaps were generated using normalised Fragment Per Kilobase of transcripts per Million (FPKM), provided in GEO. Single cell data was analysed as described above.

Cancer type	**Data Type**	**Species/model**	**GEO accession no.**
Breast	ScRNAseq	Mouse/ MMTV-PyMT	GSE81954
PDAC	Bulk RNASeq	Mouse/ KPC	GSE42605
PDAC	ScRNASeq	Mouse/ KPC	GSE129455
Melanoma	ScRNASeq	Human	GSE72056
Head and Neck Cancer	ScRNASeq	Human	GSE103322
Colorectal cancer	ScRNASeq	Human	GSE81861

Table 5 Publicly available data analysed

3

Devising an approach to investigate CAF heterogeneity

3.1 *Introduction*

Delineating CAF heterogeneity is critical to elucidating the mechanisms by which they contribute to tumour development. However, as previously discussed, the extent of fibroblast diversity in melanoma remains unclear. Thus, this chapter aimed to develop an approach to uncover the composition of the fibroblast compartment in two murine models of melanoma. Initially, conventional methods such as confocal imaging and flow cytometry were utilised, revealing divergent expression of typical CAF markers. Furthermore, the novel clustering algorithm SPADE was employed to visualise multi-dimensional flow cytometry data. The combination of IF, flow cytometry and SPADE enabled profiling of CAF populations across development of $BRAF^{V600E}$ $PTEN^{-/-}$ tumours.

In addition, this chapter describes the application of scRNAseq technology to investigate fibroblasts isolated from B16-F10 melanoma, using a negative selection approach. This system uncovered distinct transcriptional differences between CAF populations, which were validated *in vivo*. Furthermore, these results highlighted the influence of compartmentalised environmental factors on CAF phenotype. The proficiency and constraints of both conventional and non-conventional approaches to identify and characterise CAF populations are discussed.

3.2 *Results*

3.2.1 *Exploring CAF heterogeneity in the BRAF^{V600E} PTEN$^{-/-}$ melanoma model*

To begin exploring the extent of CAF heterogeneity in melanoma, we first profiled the fibroblast compartment of the BRAF^{V600E} PTEN$^{-/-}$ murine model using conventional approaches, such as imaging and flow cytometry [351]. As previously discussed, this model accurately recapitulates the development of human metastatic melanoma and is a valuable tool to explore the evolution of the CAF compartment, from early lesions to advanced tumours. We collected tumours after 11 and 24 days, post 4-HT induction (performed by Dr. Angela Riedel), as well as skin from induced non-carriers (NC). In addition, a proportion of these transgenic mice develop spontaneous tumours, a phenomenon previously described [376]. These tumours were reported to harbour BRAFV600E mutations and PTEN loss, indicating that their development may be driven by 'leaky' Cre-activity. Thus, spontaneous tumours were also collected and analysed.

3.2.1.1 *Extensive fibroblast compartments expand as the tumours develop*

To characterise the CAF compartment across tumour development, we initially examined expression of 4 typical markers, PDPN, FAP, THY1 and PDGFRα, by flow cytometry and IF staining. Histological analysis revealed BRAF^{V600E} PTEN$^{-/-}$ tumours were fibrotic and fibroblast rich. At day 11, epidermis was significantly thickened, and small lesions present. Although PDPN could be detected outside of normal lymphatic staining in these early lesions, together with FAP and THY1, the fibroblast compartment became dramatically more fibrotic by day 24 (Fig. 3.1 and Fig. 3.2). The greatest fibroblast content was observed in spontaneous tumours, which also displayed a large fibrillar network of collagen. Thus, it appears that CAFs constitute a significant stromal population in this model, which expands in parallel with malignant cells. Staining with just 4 CAF markers was sufficient to reveal significant

heterogeneity (Fig. 3.3). Both $PDPN^{+}FAP^{+}$(Fig 3a), $PDPN^{+}$ $THY1^{+}$ (Fig 3b) and single labelled cells were observed. However, using IF limited the number of markers that could be examined in tandem, making it difficult to resolve specific populations. Thus, flow cytometry was used to examine expression of all 4 markers simultaneously at the single cell level.

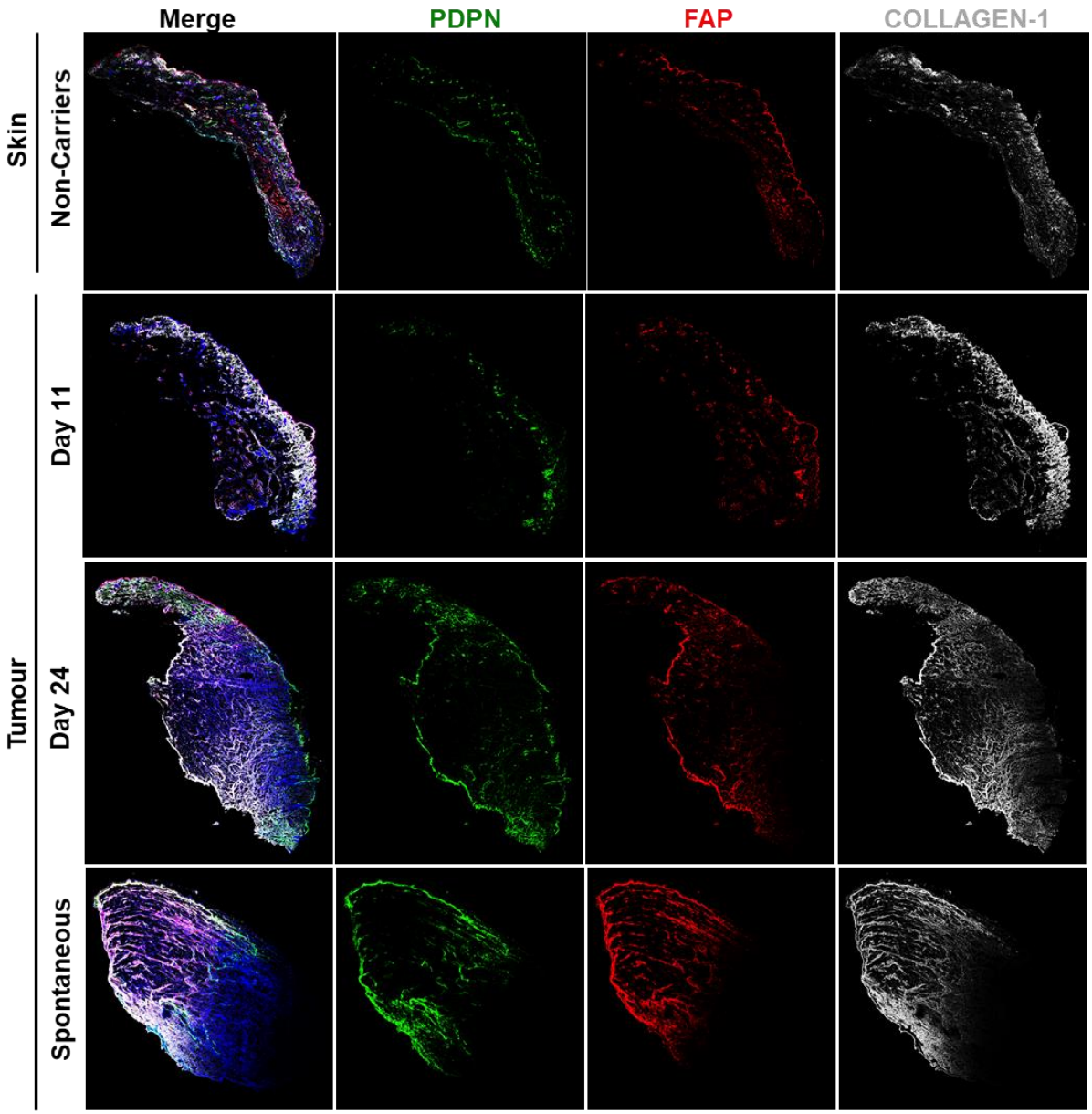

Fig. 3.1 Confocal imaging of CAF markers in BRAFV^{600E}PTEN$^{-/-}$ at different stages of tumour development

20x tile scans of 4-HT treated skin from Non-Carriers, induced tumours collected at day 11 and day 24, as well as spontaneous tumours. Sections were stained for PDPN (green), FAP (red), Collagen-1 (grey) and DAPI (blue). Images are representative of n=2 tumours/time point.

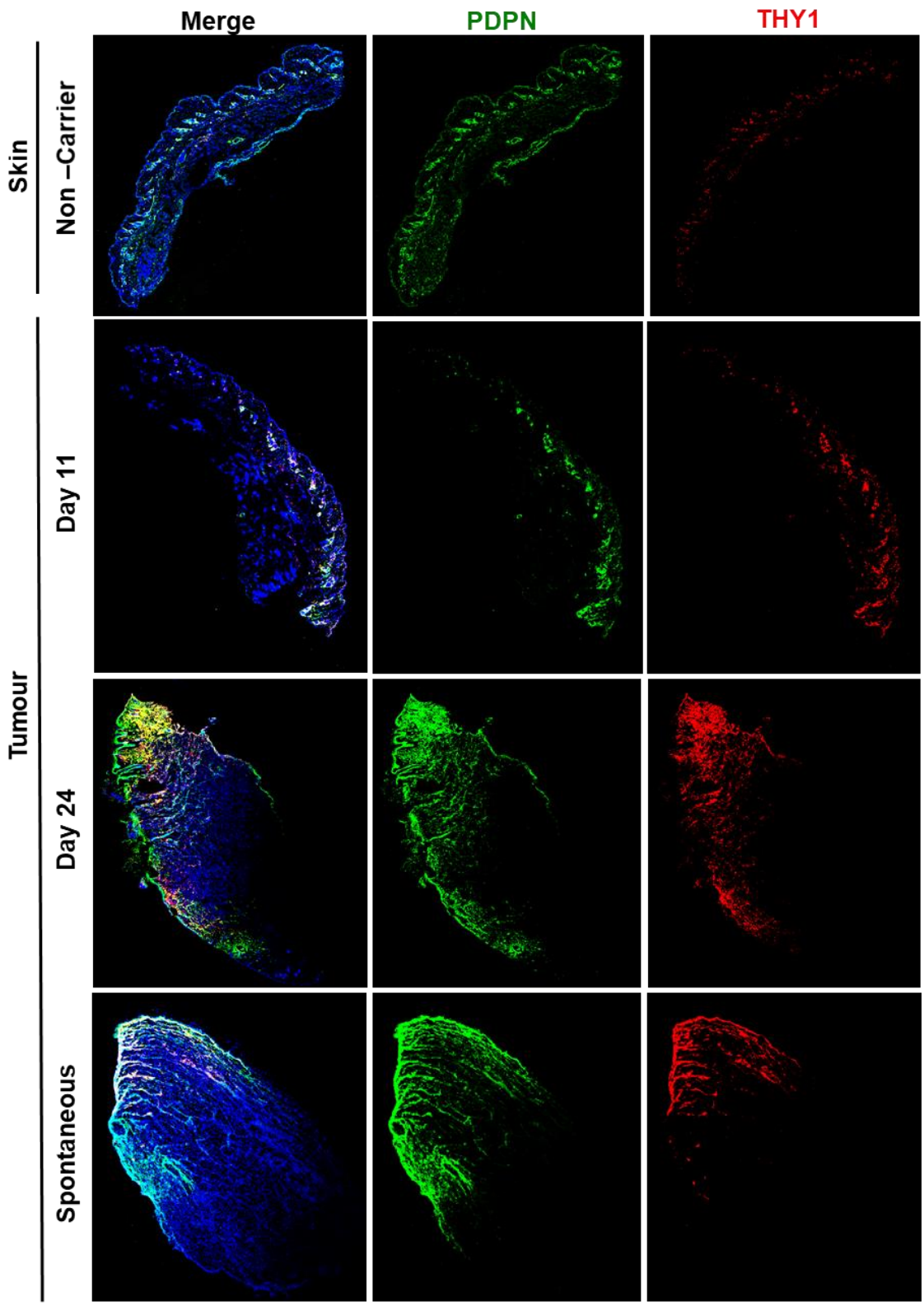

Fig. 3.2 Confocal imaging of CAF markers in BRAFV^{600E}PTEN$^{-/-}$ at different stages of tumour development

20x tile scans of 4-HT treated skin from Non-Carriers, induced tumours collected at day 11 and day 24, as well as spontaneous tumours. Sections were stained for PDPN (green), THY1 (red), and DAPI (blue). Images are representative of n=2 tumours/time point.

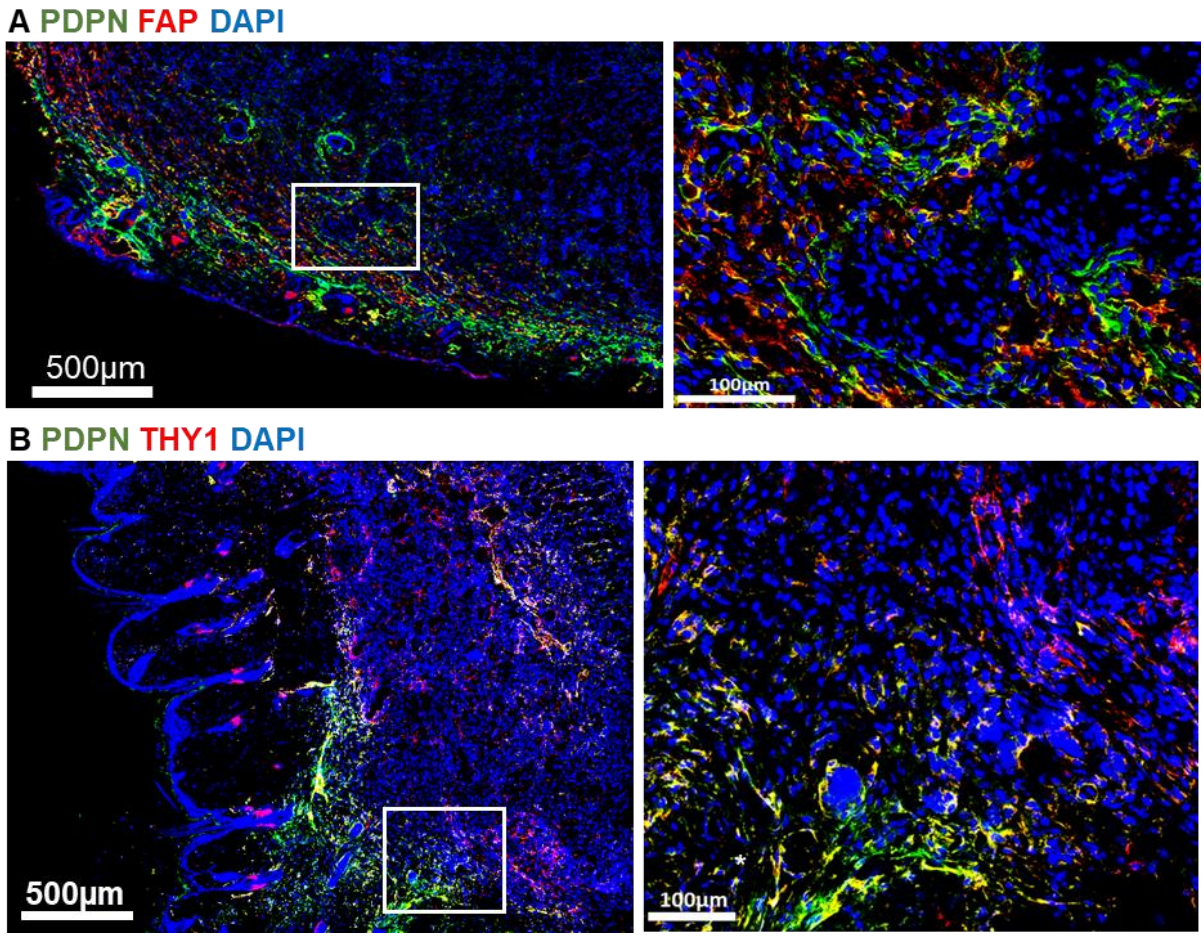

Fig. 3.3 Expression of CAF markers within BRAF^{V600E}PTEN$^{-/-}$ tumours is heterogeneous

Representative confocal tile scans of spontaneous tumours showing heterogeneous populations of fibroblasts in the tumour microenvironment. Single positive PDPN (green) or FAP (red) fibroblasts are present, as well as cells expressing both markers (A). Similarly, PDPN (green) and THY1 (red) single positive and double positive cells were observed (B). Regions of interest are shown inset and scale is indicated.

3.2.1.2 ***Flow cytometry revealed further CAF heterogeneity***

To remove immune and endothelial cells from our analysis, we examined populations that were CD45 and CD31 negative respectively (Fig. 3.4 A). However, we lacked a robust tumour cell marker for this system and were unable to exclude these cells from this data. Nevertheless, expression of CAF markers investigated (FAP, THY1, PDPN and PDGFRα) are rarely seen in the malignant melanoma compartment, thus, positive cells likely represent fibroblasts. Consistent with IF imaging, CAF marker expression, determined by flow cytometry, was heterogenous. Within populations gated on each of the fibroblast marker tested, positive and negative subsets of other markers were observed (Fig. 3.4 B). However, as only two markers at a time could be compared using conventional plots, extrapolation of different populations remained challenging. Thus, we explored alternative methods to analyse this data.

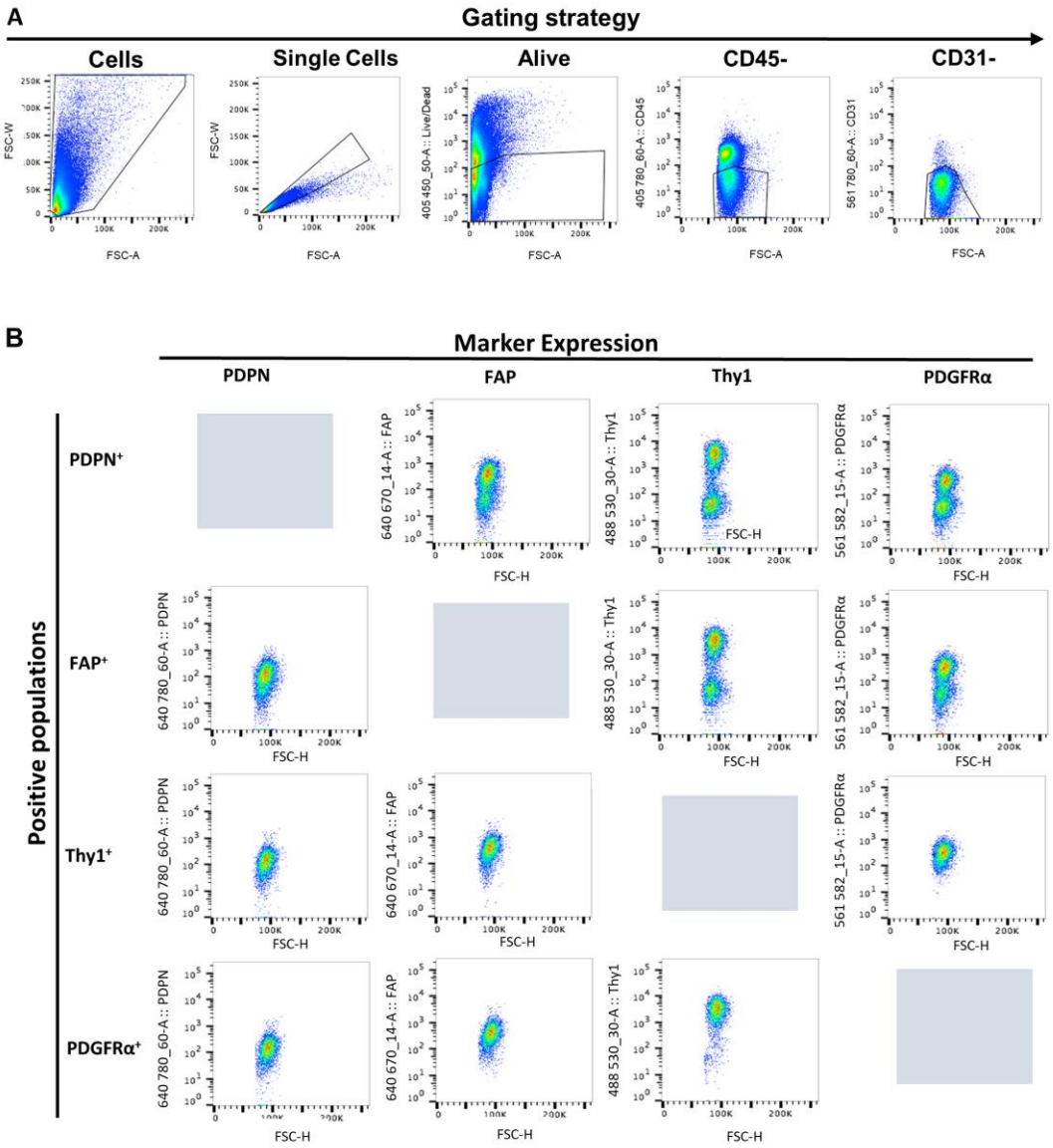

Fig. 3.4 Flow cytometry reveals heterogeneous expression of CAF markers

(A) Gating strategy, removing doublets, dead cells, CD45+ (immune) and CD31+ (endothelial) cells. Within the $CD45^-/CD31^-$ fraction of the tumour CAFs were gated on individual expression of PDPN, FAP, THY1 or PDGFRα. (B) Shows expression of PDPN, FAP, THY1 and PDGFRα within populations selected to be either $PDPN^+$, FAP^+, $THY1^+$ or $PDGFRα^+$. Plots represent 1 of 5 tumours.

3.2.1.3 *SPADE analysis of flow cytometry data*

One method to visualise multi-dimensional flow cytometry samples is the algorithm SPADE, which clusters cells into tree-like structures based on marker expression. Initially, SPADE organises cells into a cloud, whose dimensions are defined by combined expression of selected markers. Dense regions of this cloud correspond to large populations and are 'down-sampled', preventing masking of rare subsets. The down-sampled data is then clustered into a set number of groups or 'nodes'. Here, each cell is partnered with its nearest neighbour. The process is then repeated to group these pairs with similar pairs, continuing until the number of nodes reaches a predetermined limit.

These nodes are then arranged into a tree-like structure, where similar nodes are grouped together. Once the tree has been constructed, the data is 'up-sampled', which involves allocating each cell from the original data to a specific node. The size of the node is changed, relative to the number of cells that it represents. Trees can then be coloured based on the expression of a specific marker of interest, making it easy to visualise nodes that strongly express a particular protein [370,371]. This enabled us to look at the expression and abundance of all CAF markers tested simultaneously, something that could not be achieved by conventional analysis.

3.2.1.4 *SPADE analysis shows two distinct populations of CAFs are present within the BRAF tumours*

To test the SPADE algorithm, we applied it to flow cytometry data collected from spontaneous $BRAF^{V600E}$ $PTEN^{-/-}$ tumours from two different mice. SPADE analysis was performed on CD31- CD45- cells and samples were clustered based on expression of PDPN, FAP, THY1 and PDGFRα. The size of each node is proportional to the number of cells it represents, i.e. the bigger the node, the bigger the population. Trees were coloured based on the percentage of cells each node contains, as well as the expression of each individual CAF marker. To compare the distribution of markers, nodes positive for each protein have been highlighted and overlaid on trees that are coloured by percent total (Fig. 3.5).

A large proportion of the trees did not express any of CAF markers tested (denoted by blue nodes), most likely representing the tumour cells themselves. Similar to our previous findings, expression of CAF markers overlapped, yet also displayed unique expression patterns. Two distinct populations were observed; the first expressed all four markers, while the second only expressed PDPN and FAP. Furthermore, smaller populations, that express a single marker, or a combination of two or three markers e.g. THY1 and PDGFRα, were also present. However, these were not consistent, with the size and marker combination of sub-populations differing between the two animals.

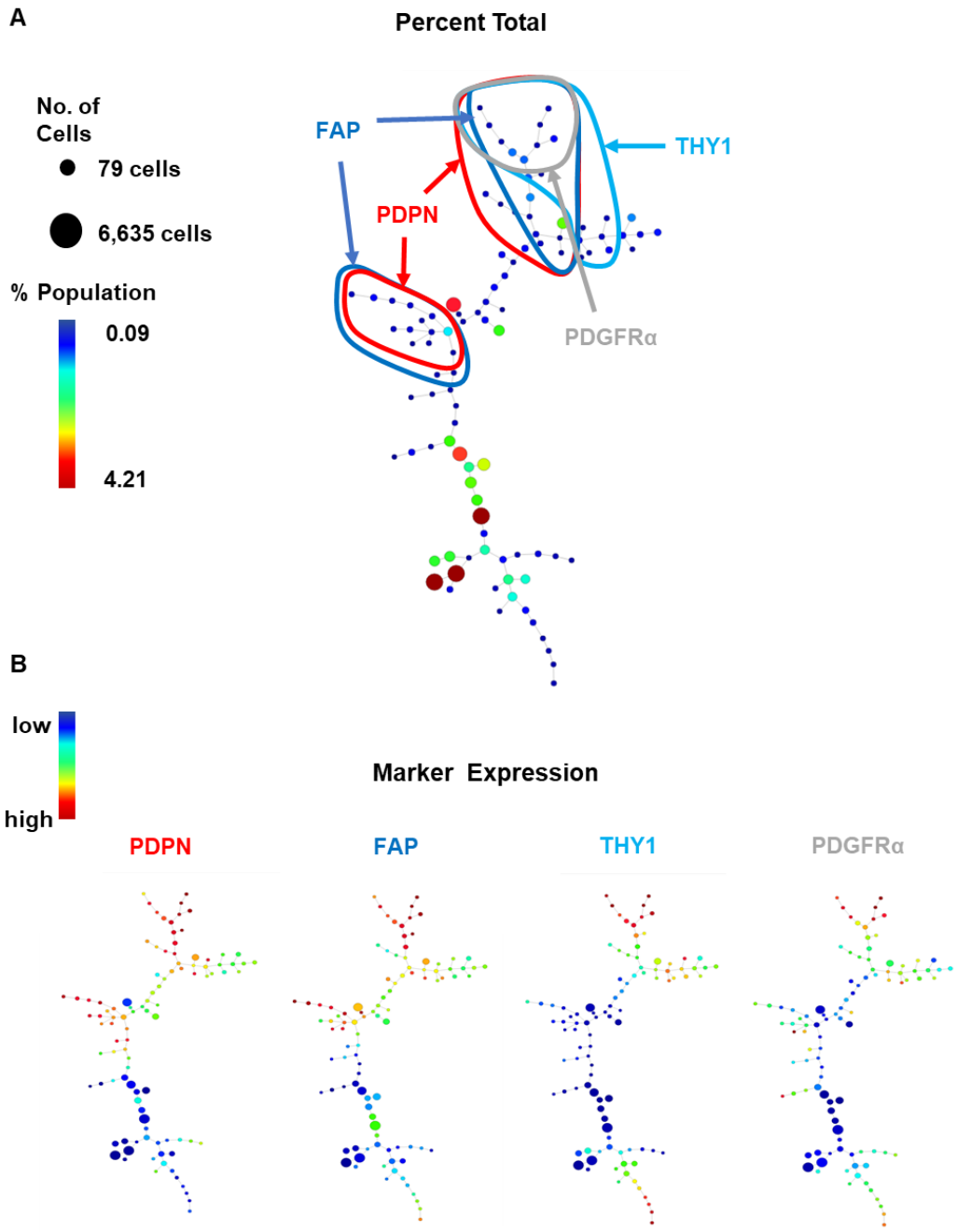

Fig. 3.5 Visualising CAF populations using SPADE in mouse 1

SPADE analysis performed on FACS data from 3 $BRAF^{V600E}PTEN^{-/-}$ spontaneous tumours from a single mouse. Cells were gated to exclude doublets, dead and $CD45^{+}/CD31^{+}$ cells. SPADE clustering was performed on remaining cells, based on expression of PDPN, FAP, THY1 and PDGFRα. A single spade tree was produced, where each node represents a cluster of cells which share similar expression profiles for the four CAF markers. The size of the node is proportional to the number of cells it represents. (A) The SPADE tree has been coloured based on the percentage of the total number of cells each node represents. Thus, large red nodes indicate dominant populations, while small blue nodes indicate rarer subsets. (B) The same tree was also coloured according to expression of markers PDPN, FAP, THY1 and PDGFRα. Here, red indicates high expression and blue represents low expression, while node size still represents the prevalence of the population. To show the expression pattern of each marker in tandem, coloured lines were added to (A), indicating nodes that highly express PDPN (red), FAP (dark blue), THY1 (light blue) and PDGFRα (Grey).

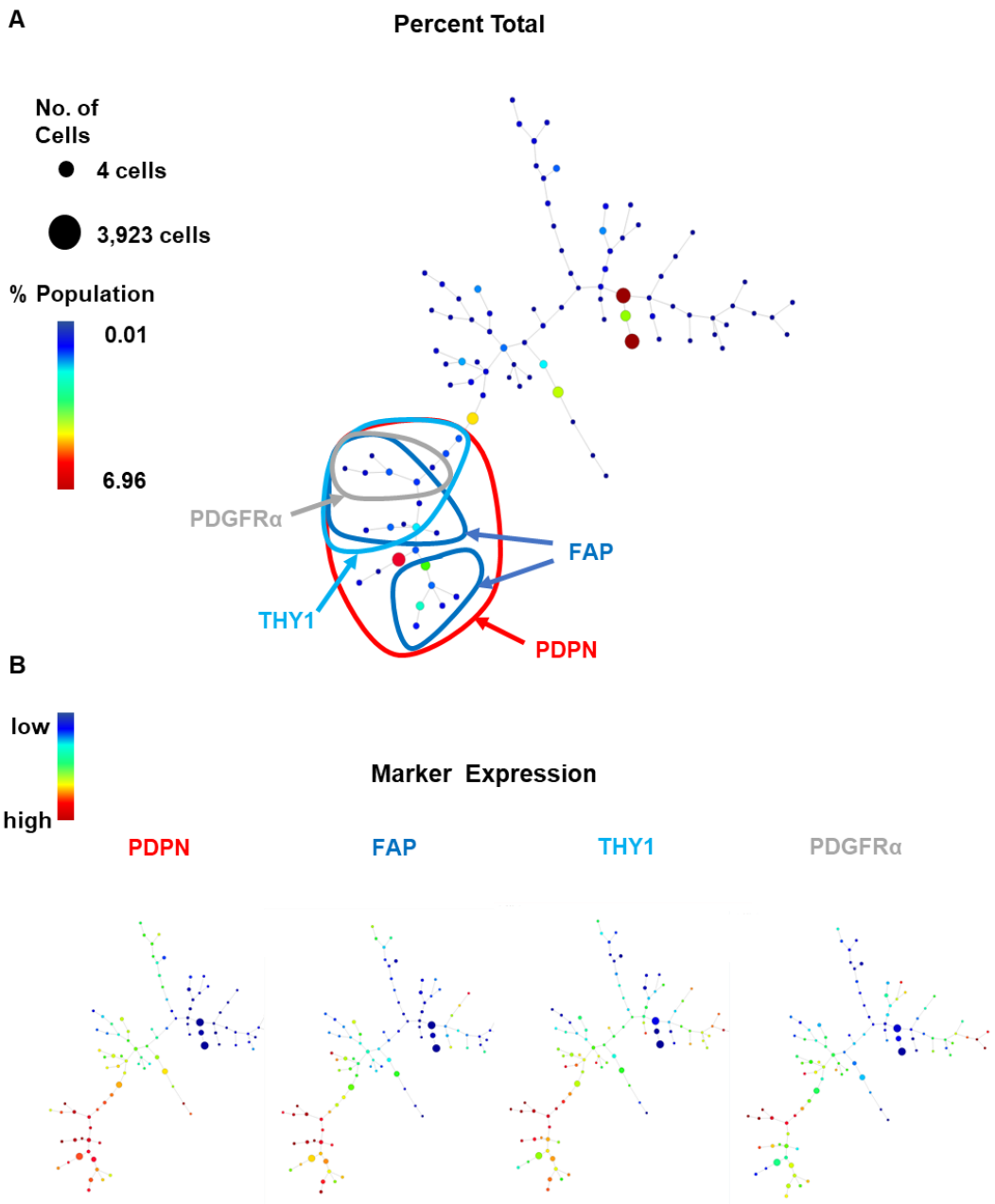

Fig. 3.6 Visualising CAF populations using SPADE in mouse 2

SPADE analysis was also performed on FACS data from 2 $BRAF^{V600E}PTEN^{-/-}$ spontaneous tumours form a different mouse. Cells were gated to exclude doublets, dead and $CD45^{+}/CD31^{+}$ cells. SPADE clustering was performed on remaining cells, based on expression of PDPN, FAP, THY1 and PDGFRα. A single spade tree was produced, where each node represents a cluster of cells which share similar expression profiles for the four CAF markers. The size of the node is proportional to the number of cells it represents. (A) The SPADE tree has been coloured based on the percentage of the total number of cells each node represents. Thus, large red nodes indicate dominant populations, while small blue nodes indicate rarer subsets. (B) The same tree was also coloured according to expression of markers PDPN, FAP, THY1 and PDGFRα. Here, red indicates high expression and blue represents low expression, while node size still represents the prevalence of the population. To show the expression pattern of each marker in tandem, coloured lines were added to (A), indicating nodes that highly express PDPN (red), FAP (dark blue), THY1 (light blue) and PDGFRα (Grey).

3.2.1.5 *SPADE analysis showed distinct CAF populations are present in normal skin through to advanced tumours*

To investigate whether these populations are present in normal skin, or change as the tumour develops, we applied the SPADE algorithm to data collected from different stages of tumour development, as well as spontaneous tumours which tended to present as late established lesions. Tumours from the same time point were grouped together and a representative SPADE plot for each stage produced. For simplicity, a single tree coloured according to the percentage of the total population is shown, in which expression of each CAF marker is indicated by coloured lines (Fig. 3.7).

Interestingly, with the marker combination tested, two distinct fibroblast populations ($PDPN^+FAP^+THY1^+PDGFR\alpha^+$ and $PDPN^+ FAP^+$) dominated at all stages of tumour evolution, as well as normal skin (Fig. 3.7). This suggests that tissue resident fibroblasts may shape the identity of CAF populations within the tumour. Furthermore, in the more advanced spontaneous tumours, these populations formed two separate tree branches, indicating that existing populations further diverge as the tumour progresses (Fig. 3.7 D).

In addition, the clustering algorithm was performed on individual samples to provide a unique SPADE tree for each mouse. This highlighted the heterogeneity existing between tumours at the same stage and normal skin. Despite this considerable diversity between mice, the two main fibroblast populations previously described could still be discerned. However, significant differences in marker overlap and smaller sub-populations were evident (data not shown).

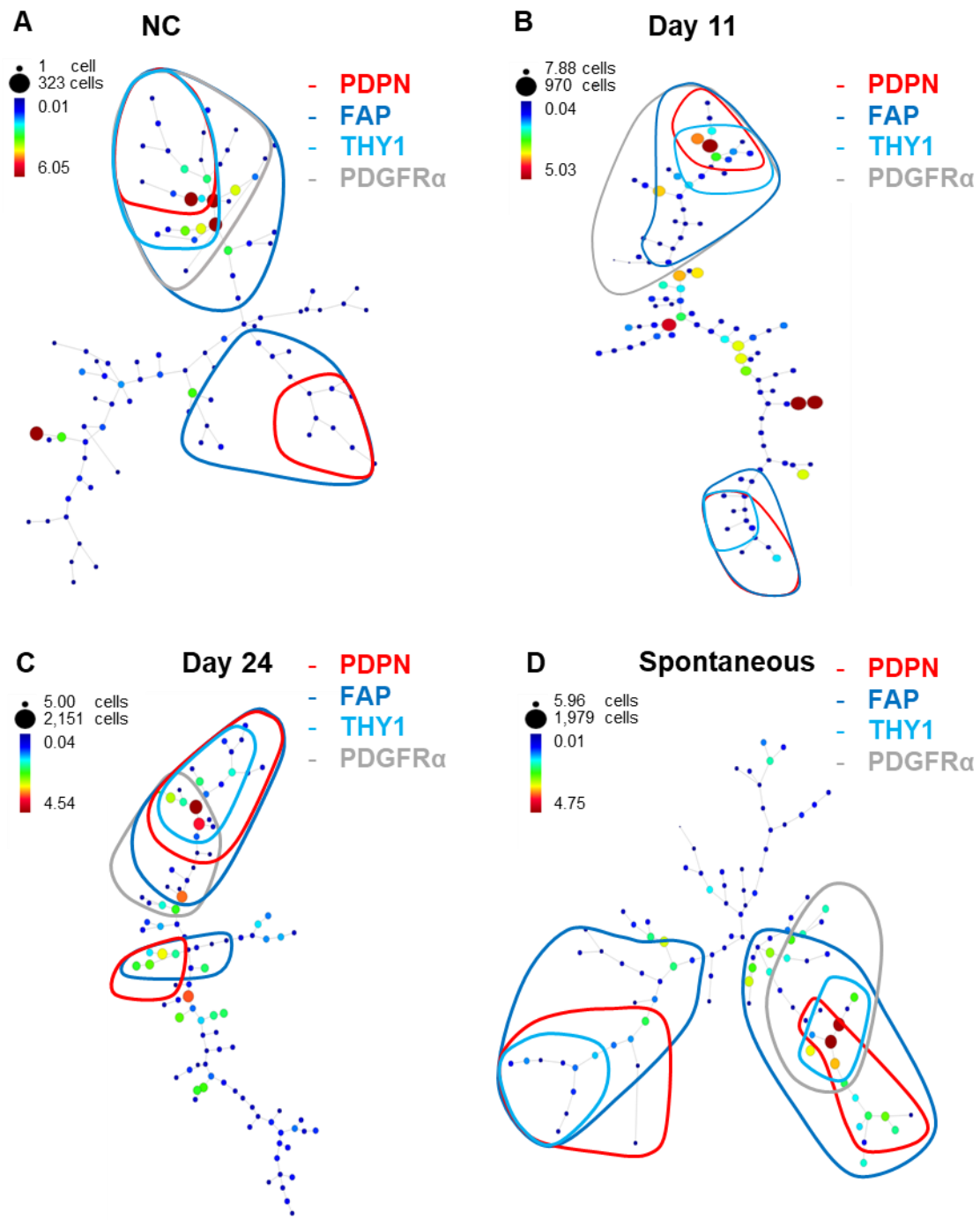

Fig. 3.7 SPADE analysis of CAF populations at different points in tumour development

Cells were gated to exclude doublets, dead cells and $CD45^{+}/CD31^{+}$ cells. Tumours from each time point were grouped together and SPADE analysis was performed on each group to producing a single tree. Cells were clustered based on their expression of PDPN, FAP, THY1 and PDGFRα. The size and colour of the node is proportional to the number of cells it represents. Coloured lines indicate the nodes that highly express PDPN (red), FAP (dark blue), THY1 (light blue) and PDGFRα (Grey). Trees represent skin from non-carriers (NC), n=5 mice (A), induced day11 tumours, n=2 mice (B), induced day24 tumours, n=6 mice (C) and spontaneous tumours, n=3 mice (D).

Thus, using just 4 CAF markers the presence of different fibroblast populations was confirmed within the stroma of $BRAF^{V600E}$ $PTEN^{-/-}$ melanomas. Interestingly, these populations were observed in normal skin through to more advanced, collagen rich tumours. This begins to highlight the limitations associated with use of a single markers to study fibroblasts within the tumour. However, the use of 4 markers is likely insufficient to identify the complete extent of CAF heterogeneity. Furthermore, marker expression may be unrelated to function and could introduce significant bias, preventing the identification of true phenotypically distinct populations. Thus, we decided to move away from marker-based approaches to identify CAF subsets, instead focussing on defining these cells by function.

3.2.2 *Employing single cell RNA sequencing to explore CAF heterogeneity*

ScRNAseq offers the opportunity investigate fibroblast phenotypes and functional differences at high resolution. To avoid relying on expression of fibroblast markers to identify CAFs, we designed a negative selection approach in which tumour and other stromal populations were removed. However, as we could not reliably identify tumour cells in the $BRAF^{V600E}$ $PTEN^{-/-}$ model, based on surface marker expression, the B16-F10 orthotopic melanoma model was adopted. Using this model, $mCherry^{+}$ B16 melanoma cells were injected into the shoulder of CAG-EGFP mice, which constitutively express GFP. This enabled exclusion of tumour cells (GFP^{-} $mCherry^{+}$), as well as immune and endothelial cells ($CD45^{+}$ $CD31^{+}$) by FACS (Fig. 3.8). Theoretically, this approach enables a completely unbiased analysis of heterogeneity within the non-immune, non-endothelial compartment i.e. predominantly fibroblasts, at the single cell level.

To test the feasibility of this approach, $mCherry^{-}GFP^{+}CD45^{-}CD31^{-}$ cells were index sorted from two established (day11) tumours into a 96 well plate, in which each well contained a single cell. In collaboration with Dr Sarah Teichmann's group (EBI-Sanger Institute), these cells were processed and sequenced. Tumour induction, processing and sorting was performed by Dr Angela Riedel (Shields Lab), as well as plate processing and pre-amplification steps, with the aid of members of the Teichmann

Lab. PCR purification and sequencing was performed by EBI-Sanger core facilities. In this pilot study, alignment and quality control was performed by Dr. Gozde Kar. I performed subsequent analysis, including clustering, tSNE, calculating DE genes and GO term analysis.

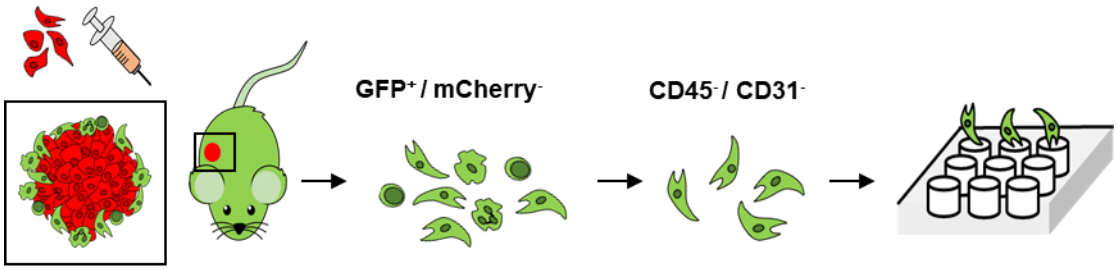

Fig. 3.8 A negative selection approach was used to isolate fibroblasts from B16-F10 melanoma for scRNAseq.

(A) Schematic of negative selection approach to isolate fibroblasts from B16-F10 melanomas. mCherry+ B16 melanoma cells were injected into CAG-EGFP mice, in which GFP is ubiquitously expressed by all host cells. After 11 days CAFs were isolated from tumours by FACS sorting. Here, tumour, immune and endothelial cells were excluded based on mCherry, CD45 and CD31 expression, respectively.

3.2.2.1 ***Removing keratinocyte contamination***

Quality control excluded cells in which number of exon mapped reads was < 100,000 or that contained >5% mt genes (Fig. 3.9 A). Similar to principle component analysis (PCA), tSNE plots are a form of dimensional reduction, where cells with similar transcriptional profiles are grouped together. This showed a clear separation between two populations (Fig. 3.9 B). While cluster 1 was enriched for fibroblast markers, cluster 2 expressed the epithelial marker *EpCam* and keratins *Krt5*, *Krt17*, *Krt14* (Fig. 3.9 C and D). This indicated that cluster 1 likely represents keratinocyte contamination. Although unexpected, these keratinocytes acted as a useful internal control, ensuring fibroblast populations could be separated from contaminating cell types.

3.2.2.2 ***CAFs formed 3 transcriptionally distinct clusters***

Once keratinocytes were removed, cells were re-clustered revealing 3 distinct CAF populations (Fig. 3.10 A). Recapitulating our earlier findings, from the $BRAF^{V600E}$ $PTEN^{-/-}$ model, CAF marker expression was heterogenous across these clusters. This emphasises the drawbacks of using single marker-based approaches to isolate fibroblasts (Fig. 3.10 B). Most importantly, however, these 3 clusters appeared transcriptionally distinct, implying that they may have unique characteristics (Fig. 3.10 C).

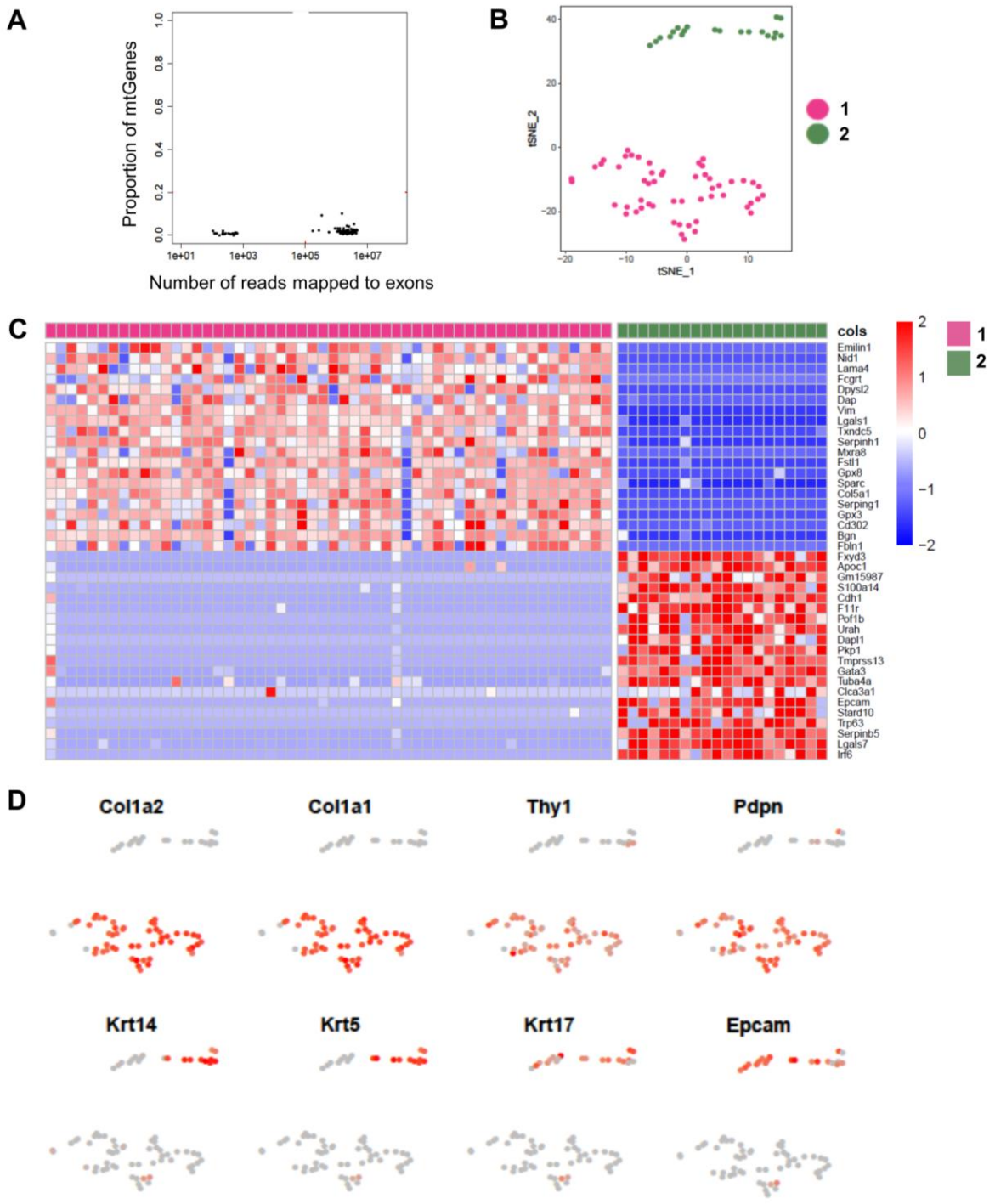

Fig. 3.9 Using scRNAseq to isolate fibroblasts from B16-F10 melanomas

(A) Plot produced by Dr. Gozde Kar, displaying the proportion of mitochondrial genes against the number of mapped exon reads, after quality control. (B) tSNE plot displays 74 successfully sequenced cells, where each dot represents a single cell. Cells formed two distinct clusters. (C) Heatmap displaying top 20 upregulated genes within each cluster. Z-score is displayed. Cluster 1 expressed epithelial markers and keratins indicating they may represent contaminating keratinocytes, while cluster 0 expressed typical fibroblast markers. (D) tSNE plots coloured according to the expression of typical fibroblast markers (top) and keratinocytes (bottom). Red indicates high expression and grey indicates low expression.

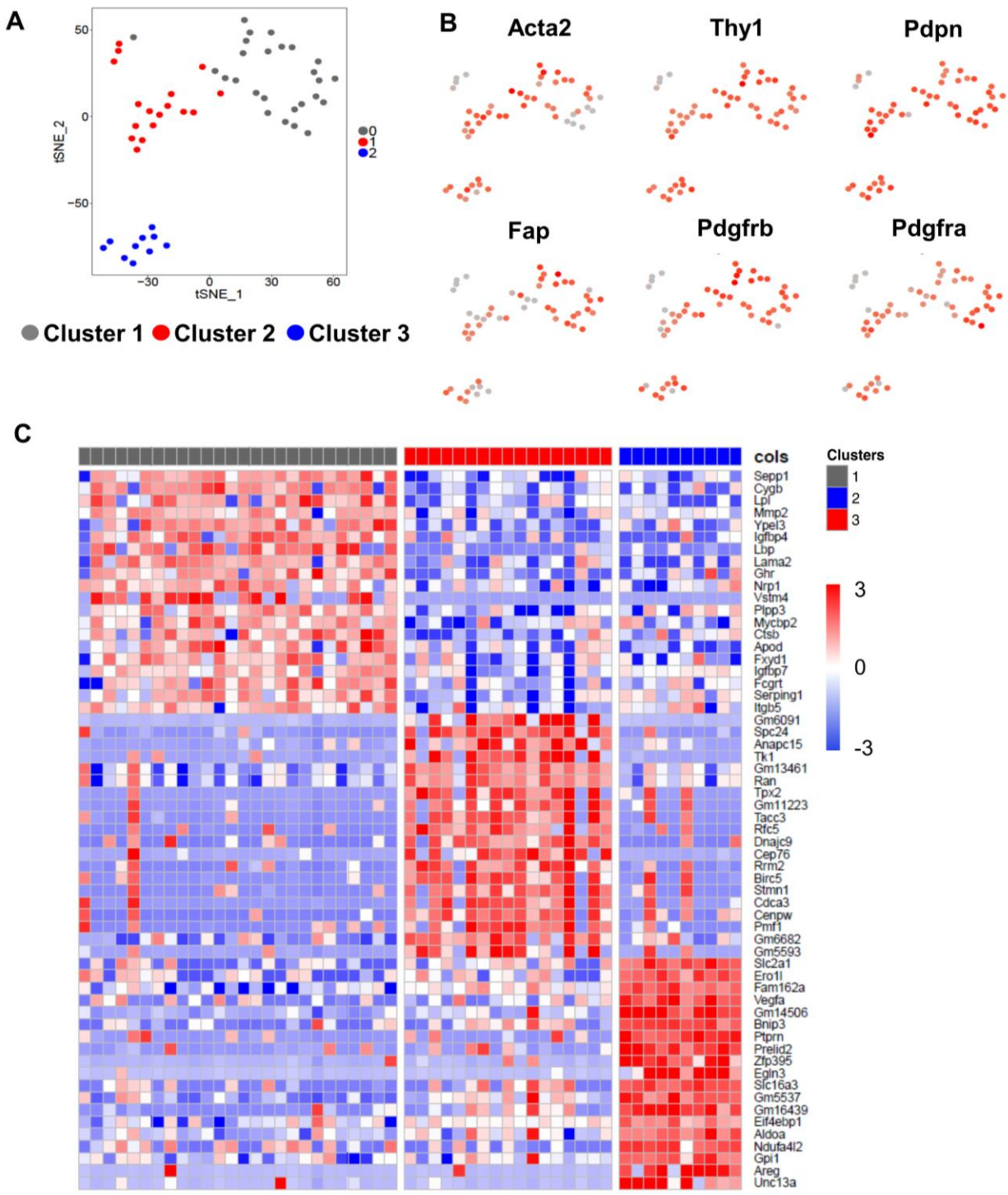

Fig. 3.10 scRNAseq revealed 3 transcriptionally distinct CAF populations

(A) tSNE plot displaying 53 successfully sequenced CAFs, in which each dot represents a single cell. CAFs clustered into 3 distinct groups. (B) Typical CAF markers were heterogeneously expressed across sub-populations. tSNE plots show expression of individual CAF markers, red indicates high expression and grey indicates low expression. (C) Each cluster is transcriptionally distinct. Heatmap displaying the top 30 upregulated, differentially expressed genes across the three clusters. Z-scores are displayed, red indicates high expression and blue indicates low expression.

3.2.2.3 *Each cluster contained unique functional signatures.*

To ascertain whether the 3 clusters possessed distinct phenotypes, GO analysis was performed on differentially expressed genes within each group. The top upregulated GO terms (Fig. 3.11 to Fig. 3.13) were unique to each cluster, demonstrating potential functional distinctions. While Cluster 1 highly expressed genes involved in ECM remodelling and immune regulation, Cluster 2 upregulated genes related to the cell cycle. Cluster 3, on the other hand, expressed metabolic enzymes involved in glycolysis/gluconeogenesis.

3.2.2.4 *Hypoxia may induce increased expression of glycolytic enzymes in Cluster 3*

The metabolic signature associated with Cluster 3 included high expression of glycolytic enzymes, as well as the *Ldha*. This gene encodes part of the Lactate Dehydrogenase (LDH) complex, which converts pyruvate to lactate (Fig. 3.14 A). Under physiological conditions, the glycolysis product Pyruvate enters mitochondria and the tricarboxylic acid (TCA) cycle, fuelling the electron transport chain and ATP production. Pyruvate can be precluded from entering the TCA cycle, by upregulation of the enzyme Pyruvate Dehydrogenase Kinase (PDK1). This causes pyruvate to build up in the cytosol, where it is metabolised to lactate, by LDH, and secreted from the cell (Fig. 3.14 B). Upregulation of glycolytic enzymes, *Ldha*, and *Pdk1* (Fig. 3.14 C) imply cluster 3 may be metabolically distinct, relying more heavily on glycolysis than oxidative phosphorylation.

By increasing expression of glycolytic genes, HIF1 may function as a key driver of this metabolic switch [377]. Interestingly, other known targets of HIF1 were upregulated in cluster 3, including the mitophagy inducer *Bnip3* and the angiogenesis factor *Vegfa* (Fig. 3.14 C). In tumour cells, perturbed cellular signalling can inhibit HIF1 regulators, enabling its transcriptional activity under normoxic conditions [378,379]. However, unlike tumour cells, the genomic stability of CAFs largely remains intact, meaning that mutational driven changes in protein function are unlikely to activate HIF1 in these cells [251,380,381]. As HIF1 is primarily activated in non-malignant cells by low oxygen

concentrations, this glycolytic population may reside in a hypoxic microenvironment. Thus, to investigate whether our model contained hypoxic regions, we stained for the associated marker Carbonic Anhydrase 9 (CA9). Interestingly, extensive areas of CA9 staining were detected throughout B16 tumours and were located in regions devoid of blood vessels, indicating our melanoma model is poorly perfused (Fig. 3.14 D).

The discovery of extensive hypoxia in this model prompted the examination of hypoxia as a driving force for HIF1 induced metabolic changes, in the fibroblast compartment. IF staining revealed nuclear localised HIF1 in CAFs, identified by PDPN expression, residing in or adjacent to hypoxic regions (Fig. 3.15. A). To see if these 'hypoxic' CAFs were also more glycolytic, tumour sections were stained for GLUT1 and LDHA (Fig. 3.15 B and C), as both are direct targets of HIF1 and their expression is associated with increased glycolysis. Remarkably, GLUT1 and LDHA expression was higher in CAFs located next to hypoxic areas, in comparison with those situated further away. This suggests that proximity to hypoxic regions may regulate HIF1 activation and glucose metabolism in tumour resident fibroblasts.

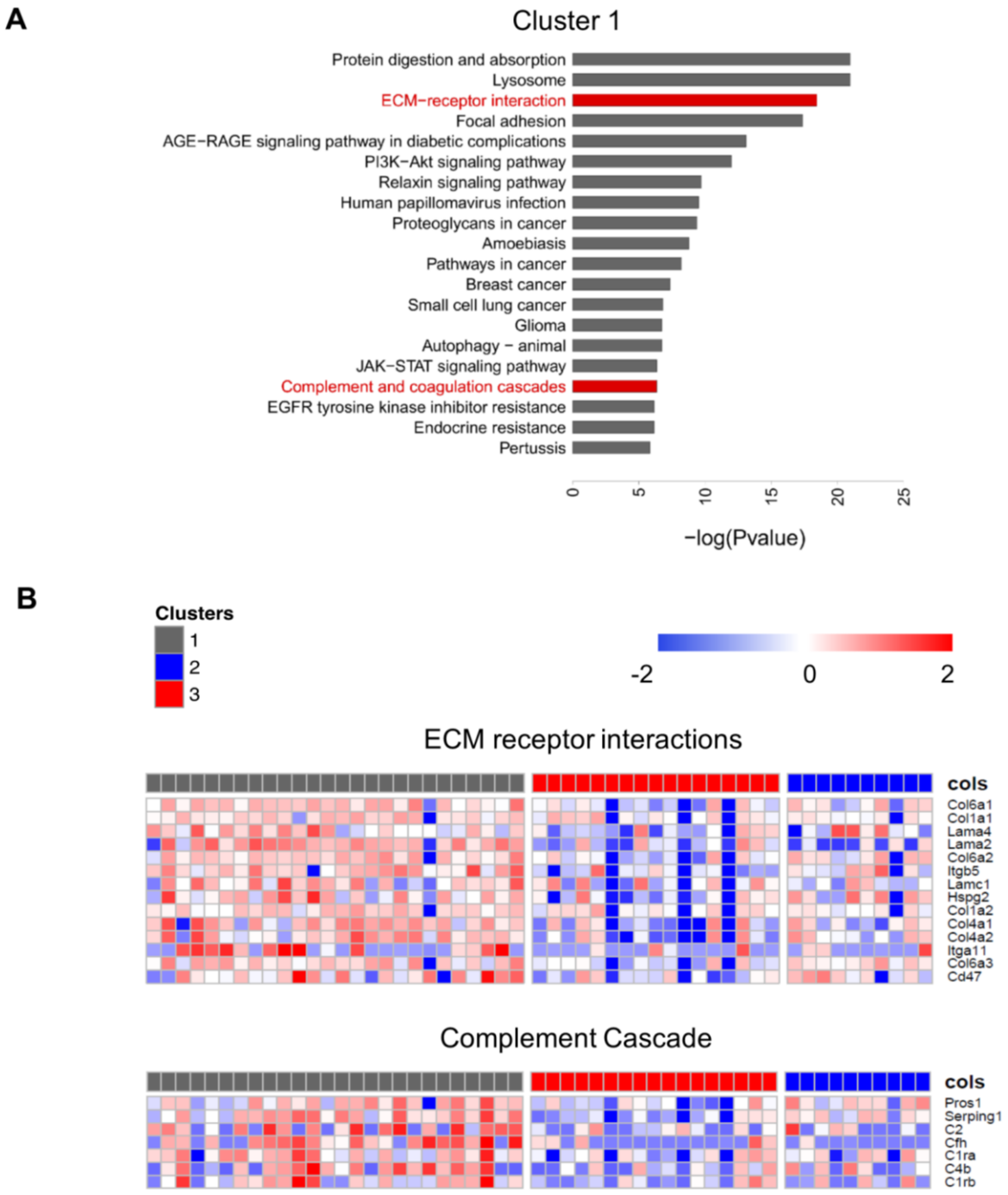

Fig. 3.11 GO analysis reveals functional phenotypes of Cluster 1

(A) GO analysis was performed on the significantly upregulated ($p < 0.05$) genes for each cluster. Plots show the top 20 pathways and the -log(p values) associated with Cluster 1. (B) Heatmaps show the z score expression of genes in selected pathways of interest. Red indicates high expression, blue indicates low expression.

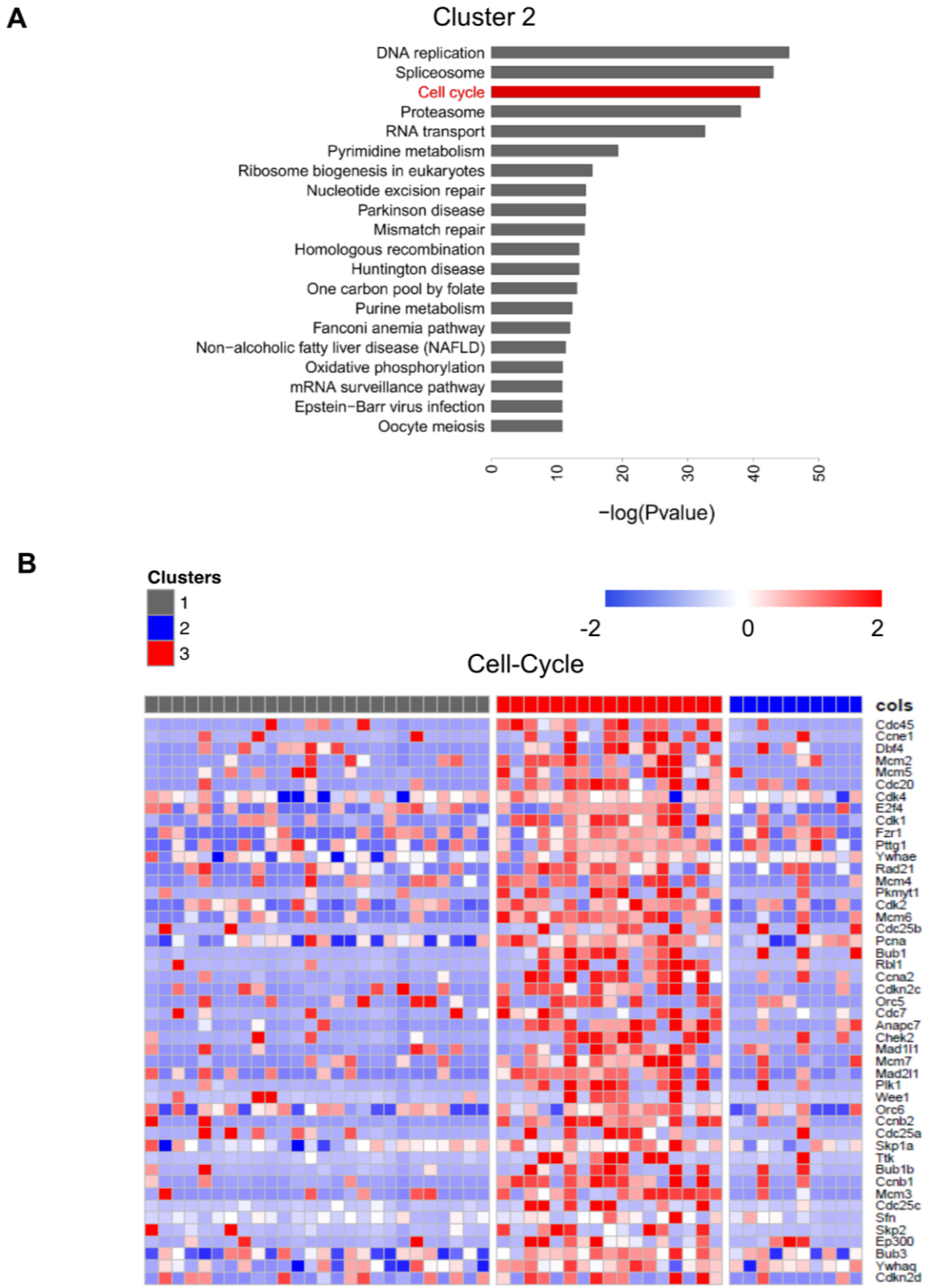

Fig. 3.12 GO analysis reveals functional phenotypes of Cluster 2

(A) GO analysis was performed on the significantly upregulated ($p < 0.05$) genes for each cluster. Plots show the top 20 pathways and the -log(p values) associated with Cluster 2. (B) Heatmaps show the z score expression of genes in selected pathways of interest. Red indicates high expression, blue indicates low expression.

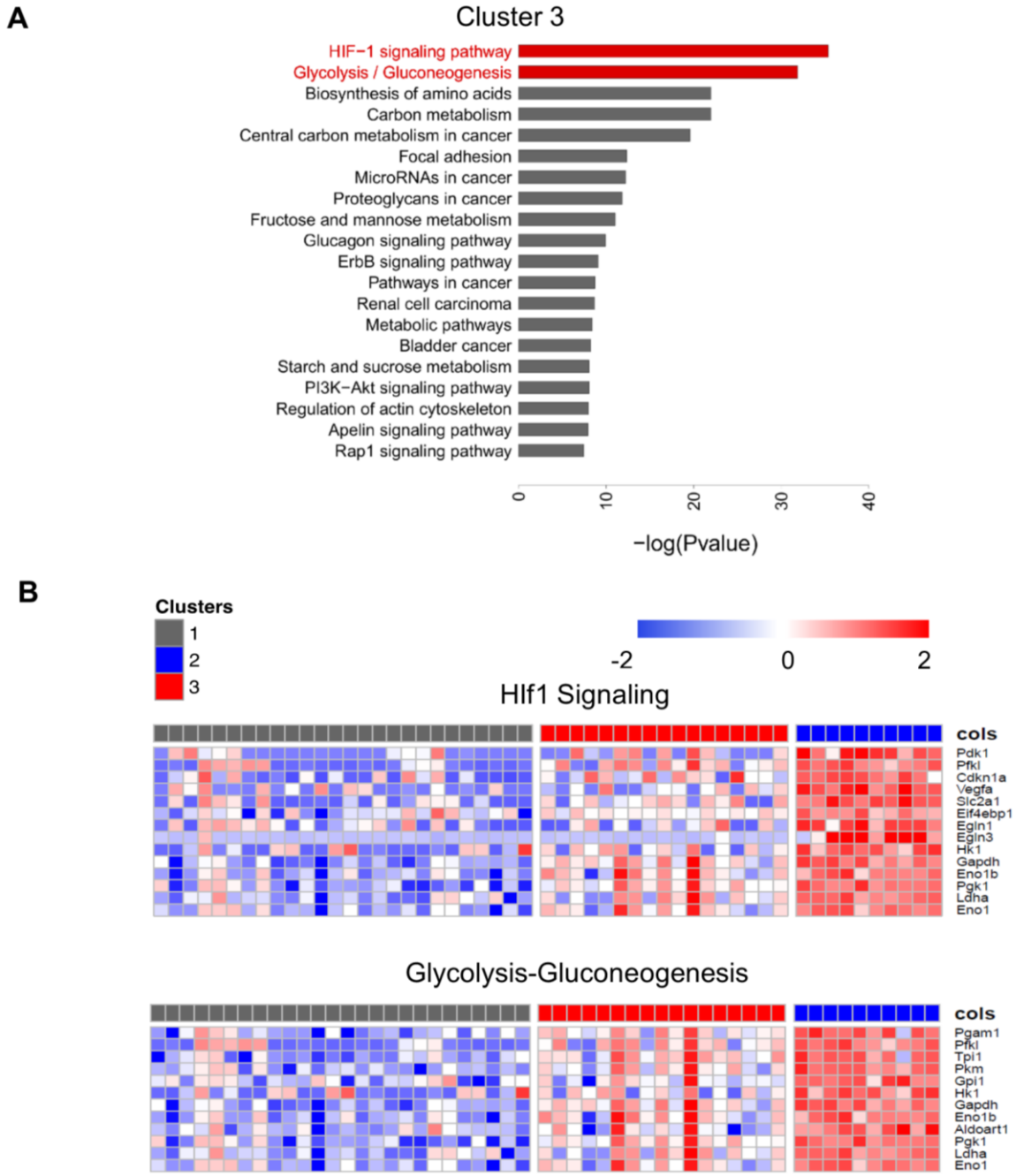

Fig. 3.13 GO analysis reveals functional phenotypes of Cluster 3

(A) GO analysis was performed on the significantly upregulated ($p < 0.05$) genes for each cluster. Plots show the top 20 pathways and the -log(p values) associated with Cluster 3. (B) Heatmaps show the z score expression of genes in selected pathways of interest. Red indicates high expression, blue indicates low expression.

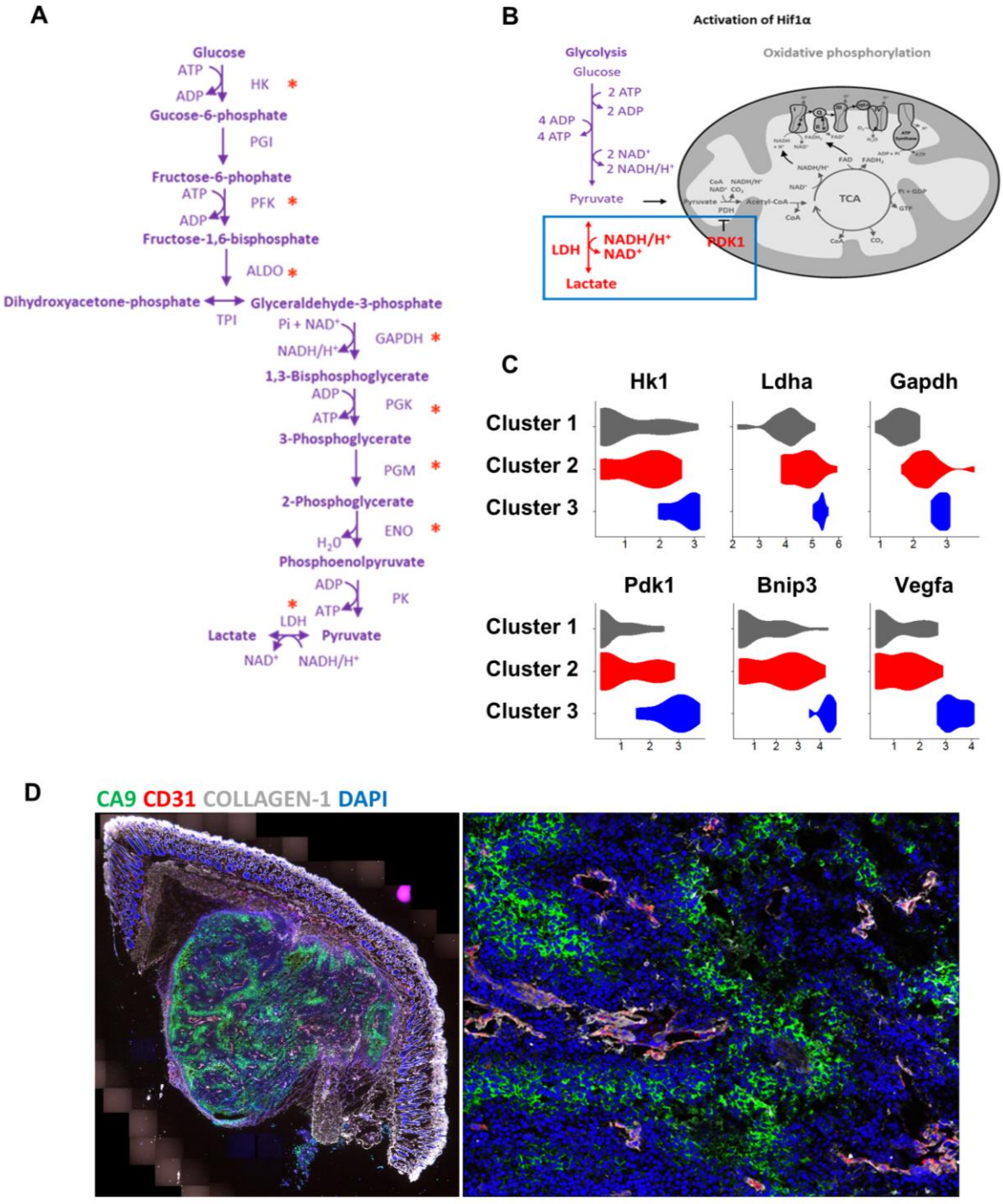

Fig. 3.14 Hypoxia and HIF1 may drive increased glycolysis in Cluster 3

(A) The glycolysis pathway. * denotes enzymes upregulated in cluster 3. (B) Schematic showing the metabolic switch induced by increased expression of PDK1. (C) Violin plots showing expression of glycolytic enzymes *Hk1* and *Gapdh* and HIF1 targets *Pdk1*, *Bnip3* and *Vegfa*. Plots show log(counts+1). (D) Representative confocal images of day 11 B16 tumours. 20x tile scan (left) and 63x region of interest (right). Sections were stained for the Hypoxia marker CA9 (green), CD31 (red), COLLAGEN-1 (grey) and DAPI (blue).

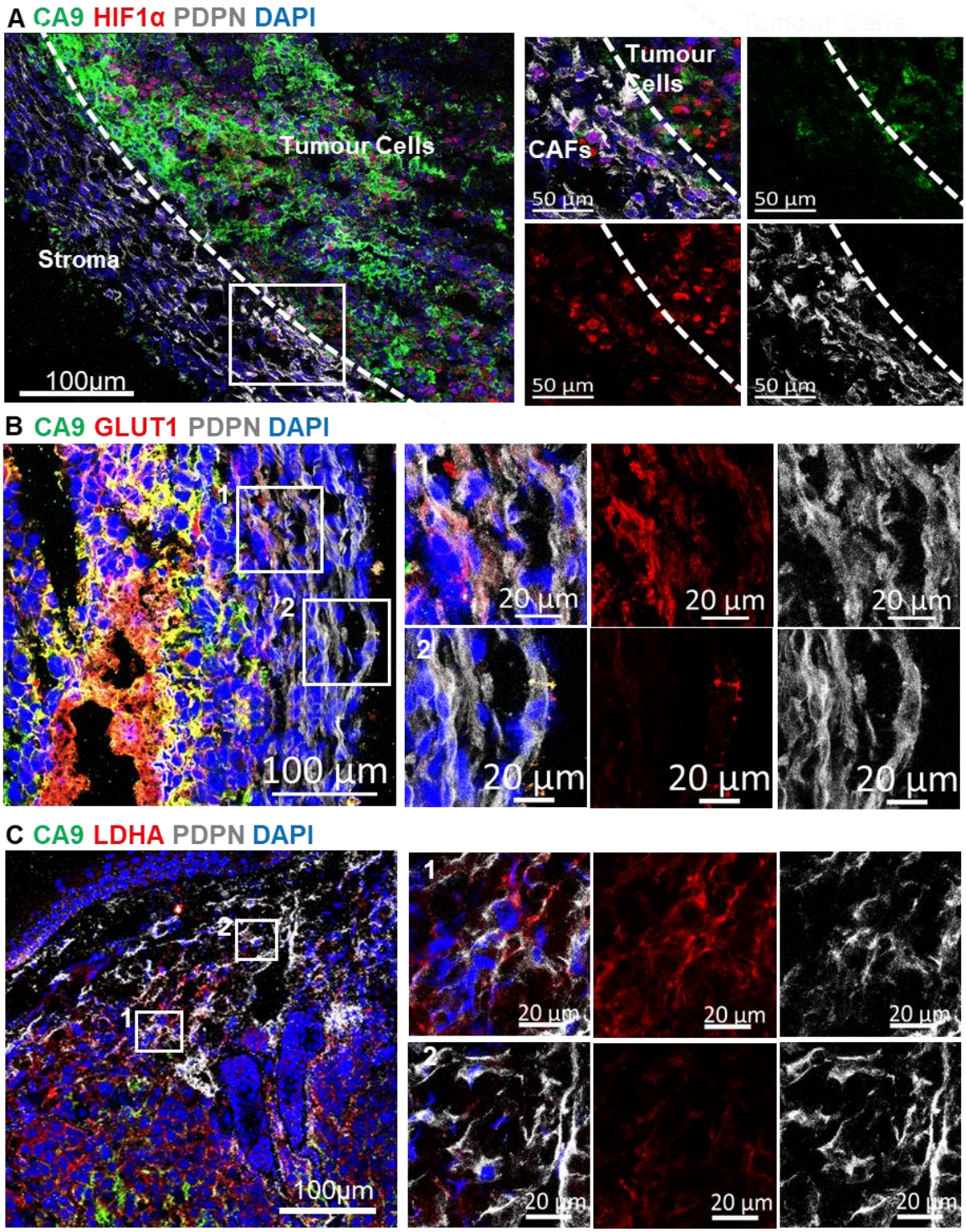

Fig. 3.15 HIF1α, GLUT1 and LDHA are upregulated in fibroblasts close to regions of hypoxia

Day 11 B16 melanomas were stained for (A) CA9 (green), HIF1α (red), PDPN (grey) and DAPI (blue), (B) CA9 (green), GLUT1 (red), PDPN (grey) and DAPI (blue) and (C) CA9 (green), LDHA (red), PDPN (grey) and DAPI (blue). Regions of interest are highlighted inset and a dotted line indicates the divide between the tumour and stromal compartments. Images represent (A) n=1 (B) n=3 and (C) n=3 melanomas from independent mice.

3.2.2.5 *Cluster 2 represents a proliferating sub-population*

While upregulation of cell-cycle genes in cluster 2 could indicate a proliferative sub population, it is also possible that the tSNE algorithm has clustered the cells according to their cell cycle stage. The cell cycle is known to confound single cell sequencing analysis, as cell cycle genes are highly expressed [382]. In addition, the expression of other genes that are not involved in this process can also be affected by cell cycle stage. Thus, the cell cycle can account for much of the variance within sequencing data, meaning dimensional reduction algorithms often group cells according to their cycle position.

To assess whether this was the case here, cell cycle stage was allocated to each cell using the cyclone R package (Fig. 3.16 A). This assigned clusters 1 and 3, as well as half of the cells in cluster 2, to the G1 phase, whereas the other half of cluster 2 was assigned to the G2/M stage. This may indicate that cluster 2 contains cells that are undergoing mitosis, whereas the other cells remain in G1. However, the cyclone algorithm cannot detect quiescent cells, therefore, it is likely that cells residing in G0 have been miss labelled G1. This was supported by expression of Ki67 in cluster 2, which marked all proliferating cells irrespective of stage (Fig. 3.16 B).

To confirm that our sequencing data has correctly identified a proliferating population of CAFs, we treated B16-F10 tumour bearing mice with the thymidine analogue EdU. EdU incorporates into the DNA of proliferating cells and can be detected by conjugating a fluorophore to the compound. To ensure all proliferating cells were labelled, 4 days prior to culling, mice were injected with EdU every 24hs (Fig. 3.16 C). Tumours were stained for melanoma marker TRP2 and the fibroblast marker PDPN to determine if a proliferating CAF population exists. While EdU strongly labelled tumours cells, as would be expected, EdU incorporation could also be identified in a small fraction of CAFs (Fig. 3.16 D), indicating that our sequencing data accurately detected a small pool of cycling fibroblasts, while the majority are quiescent.

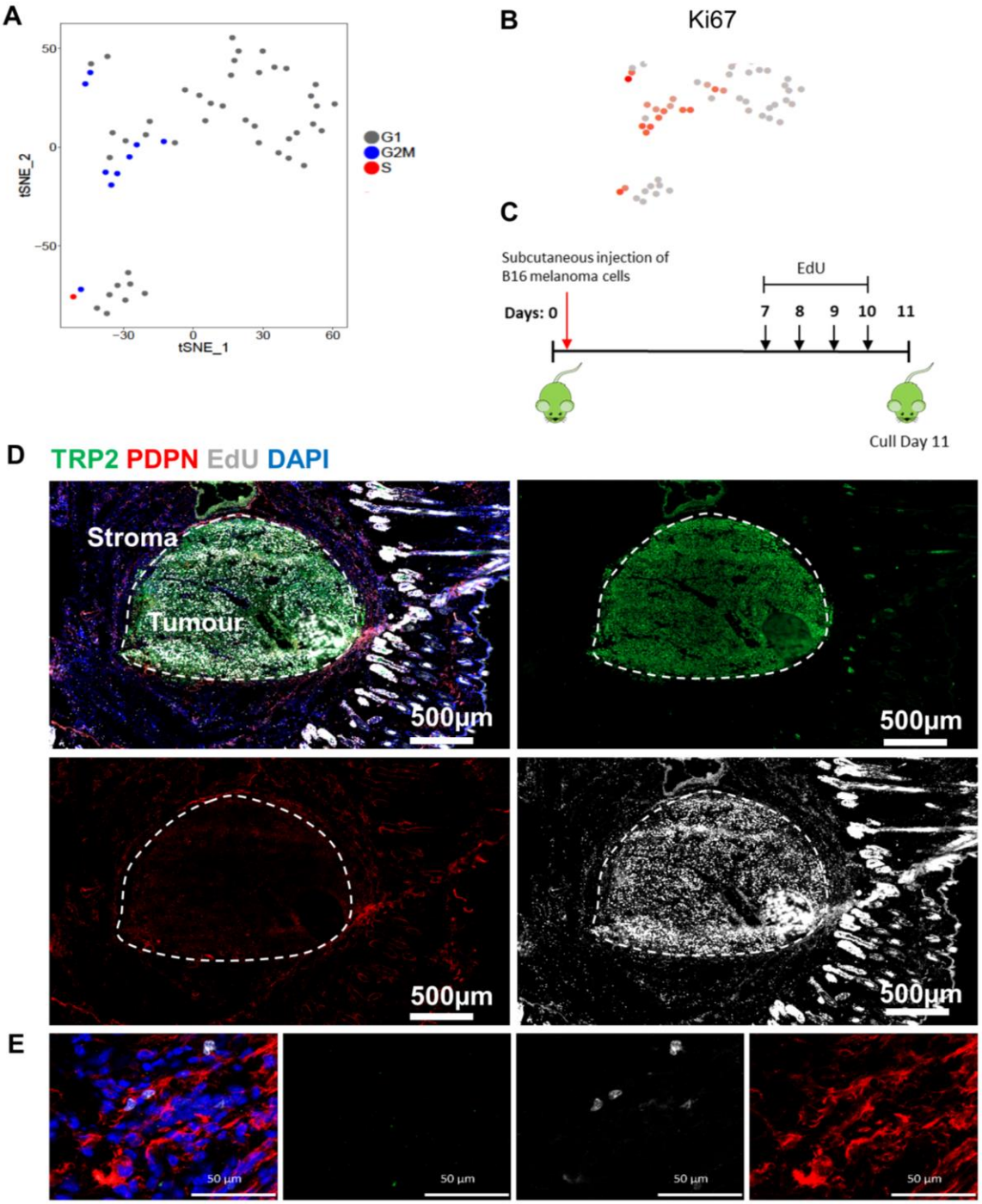

Fig. 3.16 Cluster 2 represents a proliferating sub population of fibroblast

(A) The cell cycle stage of each cell was calculated using the R package. (B) tSNE plot showing expression of the proliferation marker Ki67, red indicates high expression grey indicates low expression. (C) Schematic showing experimental design, EdU was injected every day for 4 days prior to culling. (D) IF imaging of EdU incorporation, including 20x tile scans of tumours (top) and (E) 63x images within the stromal compartment (bottom). Tumours were stained for the melanoma marker TRP2 (green), fibroblast marker PDPN (red) and Alexa647 was conjugated to incorporated EdU (grey). Tumour/stromal borders are defined (dashed white line) and scale bars represent 200µm (D) and 50µm (E).

3.2.2.6 *Keratinocyte contamination enabled identification of possible Pan-CAF markers*

As well as investigating transcriptional differences between CAF populations, the presence of contaminating keratinocytes also provided an opportunity to investigate similarities. Genes upregulated within the fibroblasts cluster were identified and further filtered to ensure they were expressed in 99% of these cells. The 10 most significant genes are displayed in Fig. 3.17, however, no genes were expressed by all CAFs in this dataset. Many of these genes are involved in functions associated with the fibroblast phenotype. For example, *Emilin1*, *Nid1*, *Lama4* and *Serpinh1* are all ECM components or their regulators, while *Dpysl2* and *Lgals1* are involved in adhesion and migration. While these genes may represent possible pan-CAF markers, in many cases, it is important to note that the expression is gradated across the fibroblast pool. Variable levels, as well as expression by other cell types, may placate the usefulness of such candidates to identify fibroblasts in the TME.

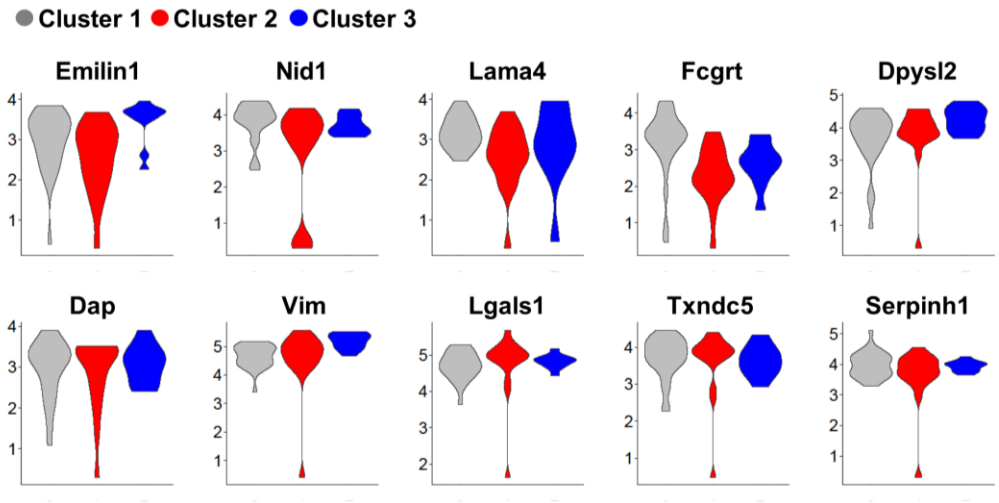

Fig. 3.17 Identification of possible Pan-CAF markers

Violin plots depicting expression of to 10 most significant genes, upregulated in CAFs compared to keratinocytes, that were expressed in 99% of fibroblasts. Plots organised according to identified clusters.

3.3 *Summary*

A combination of Flow cytometry and imaging was used to characterise the fibroblast compartment of the murine BRAFV600E model of melanoma using four common CAF markers. These tumours are heavily fibrotic, as staining indicated that 20-30% of these tumours were positive for PDPN, FAP, THY1 and PDGFRα. In addition, fluorescent staining of skin and tumours from early and later stages, showed considerable expansion of the fibroblast compartment. Closer inspection revealed these markers were not uniformly expressed, with varying patterns of co-expression, indicating that tumours contain heterogeneous fibroblast populations. Such variability emphasized the drawbacks of using single markers to isolate and profile CAFs.

With the inherent limitations of imaging and conventional FACS hierarchies, a slightly different approach was adopted. SPADE analysis enabled the clustering and visualisation of the different fibroblast populations at a greater resolution, incorporating all markers tested. This revealed that CAFS, labelled by four different surface antigens, split into two predominant groups; one that expressed all four markers and a double positive $PDPN^{+}$ FAP^{+} population. These populations were also present in normal skin and persisted through to large desmoplastic tumours, suggesting that tissue resident fibroblasts may shape the identity of CAF populations in the tumour stroma.

Although these methods were sufficient to confirm the presence of fibroblast heterogeneity in murine melanomas, the use of only four markers likely masked the true scale of CAF diversity. Furthermore, these results do not provide information regarding population function. Thus, whether identified sub-sets perform the same, or distinct roles, in the tumour microenvironment, remains unanswered. However, functional characterisation requires profiling expression of many proteins simultaneously, exceeding the capabilities of flow cytometry-based methods. Furthermore, by pre-selecting marker combinations to investigate, true differences between CAF populations may not be detected, biasing interpretation. Therefore, to perform an unbiased investigation of fibroblast heterogeneity, a combination of negative selection and scRNAseq was employed. A feasibility pilot was performed and optimised by Dr. Angela Riedal (Shields Lab) in collaboration with the Teichmann Group. Although, a small degree of keratinocyte contamination was observed, this

served as a useful internal control, confirming the identity of fibroblasts and some potential Pan-CAF markers. Importantly, this approach enabled the identification of 3 CAF subsets which exhibit specific and distinct functional signatures. Validation of glycolytic and proliferating subpopulations, using IF staining and EdU incorporation, demonstrated the reliability of this method to identify transcriptional variation within the fibroblast compartment. The ability to detect such signatures highlights the sensitivity and resolution of single cell sequencing approaches. Furthermore, our data was not confounded by cell-cycle stage and implies that external factors, such as hypoxia, may underlie a proportion of CAF heterogeneity.

While expression of HIF1 and its target CA9 implies B16-F10 tumours are hypoxic, HIF1 activity in tumour cells can be activated by aberrant cell signalling [378,379]. Indeed, activation of this transcription factor under normoxic conditions is one of the proposed mechanisms driving the 'Warburg effect'. However, the restriction of positive cells to regions devoid of vasculature, suggests that low oxygen tension is responsible for HIF1 activation in this setting. Nevertheless, this could be verified by incorporating oxygen sensitive dyes. Other mechanisms have also been shown to induce glycolytic metabolism in CAFs, such as the 'Revere Warburg' effect. Here, H_2O_2 produced by tumour cells, induces oxidative stress and ROS production in neighbouring fibroblasts [383]. Potentiated by autophagic degradation of CAV1, ROS activates HIF1 and NFκB, inducing transcription of glycolytic enzymes, glucose transporters and LDHA [384–387]. In this model, Lactate secreted by fibroblasts as a biproduct of increased glycolysis, is taken up by tumour cells and used to support their mitochondrial metabolism [387]. However, the use of oxidative phosphorylation by malignant cells is not consistent with expression of glycolytic enzymes and HIF1 in B16-F10 tumours. Other studies have also reported induction of HIF1 in fibroblasts as a result of tumour secreted ROS [388]. As ROS is produced under hypoxic conditions, its production by tumour cells may indirectly drive HIF1 activity in fibroblasts, that are not themselves hypoxic. Irrespective of the underlying mechanism, whether the resulting metabolic switch or transcription of HIF1 downstream targets, impacts CAF function remains to be investigated in this model.

In addition to hypoxia, the tumour microenvironment is exposed to many external factors, such as nutrient deprivation and fibrosis [389–393]. These factors are in constant flux and likely change as the tumour grows and develops. Furthermore, the stromal

compartment is composed of numerous cell types, which each possess their own secretome and add to the local cytokine milieu [1–3]. These interacting populations are simultaneously influenced by changes in external factors as the tumour evolves. Thus, the developing tumour microenvironment comprises a complicated and dynamic system. Owing to the success of single cell sequencing in revealing fibroblast sub populations, in a single snapshot of time, this technique was next employed to investigate stromal interactions and dynamics across time. This project was undertaken in collaboration with Sarah Teichmann's group, in which I have largely focussed on the fibroblast compartment.

4

Identification and validation of CAF populations in the developing melanoma microenvironment

4.1 *Introduction*

Our previous results demonstrated the limitations of conventional approaches to investigate fibroblast subsets. However, by combining scRNAseq with a negative selection protocol, we were able to visualise CAF heterogeneity at high resolution within the B16-F10 murine model of melanoma. This data revealed distinct metabolic and proliferative populations, which may have been masked by bulk analysis. Furthermore, diverse expression of CAF markers was evident, highlighting the importance of negative selection when characterising fibroblasts.

Owing to this success, the study was expanded to investigate changes in both immune and non-immune stromal populations, across melanoma development. This chapter concentrates on the fibroblast compartment, using bio-informatic approaches to identify functionally distinct populations. Importantly, isolating fibroblasts from different stages of tumour development enabled investigation of how the fibroblast compartment and associated heterogeneity changes throughout tumour growth. Although populations displaying unique functional signatures have been reported in other cancer types, this data represents a snapshot of the subsets present in developed tumours [298–301]. Indeed, Fibroblast adaptation across tumour development remains under-studied. In particular, whether the phenotypes or prevalence of individual populations is altered by malignant growth has not been investigated. Thus, the composition of the CAF compartment was investigated across this time course. Further analysis was performed to identify key changes between early and late time points within CAFs as a whole, as well as within each subset.

4.2 *Results*

4.2.1 *Applying single cell technologies to profile stromal cells across tumour development*

Immune and non-immune stromal cells were isolated from both the primary tumour and draining lymph nodes. Similar to tumours, lymph nodes comprise an interacting network of immune and non-immune stromal cells, which together orchestrate an immune response. However, tumours have been shown to corrupt draining lymph nodes and influence stromal populations [394]. By sequencing both the tumour and the lymph node in tandem, we were able to profile development of the tumour associated immune responses and examine their manipulation in the presence of malignancy.

To enrich for rare immune populations, cells were FACS sorted from B16-F10 melanomas based on markers such as CD45R, CD4, CD8, CD11b and CD11c. However, a negative selection approach, similar to methods previously described (Section 3.2.2), was employed to isolate non-immune cells. Here, tumour cells were injected into CAG-EGFP mice, allowing stromal populations to be selected based on GFP expression. CD45+ immune cells were then excluded, and endothelial cells and fibroblasts separated based on CD31 expression

Importantly, to investigate how stromal populations change as the tumour develops, cells were isolated at different points in tumour growth (day 5, 8 and 11) and normal skin. Tumour induction was performed by Dr. Angela Reidel (Shields lab), who with the aid of Dr. Bidesh Mahata (Teichmann Lab), isolated immune and non-immune stromal populations. Together, Dr. Angela Reidel and I produced cDNA from non-immune populations, while immune cells were processed by Dr. Bidesh Mahata. Library preparation and sequencing was conducted Sanger core facilities. Finally, alignment and quality control was performed by Dr. Mirjana Efremova, to produce TPMs. Together, we performed downstream data analysis, once TPMs were generated. In particular, I analysed sequenced fibroblast populations.

After quality control 4627 cells were successfully sequenced, including endothelial, fibroblast, T-cell, B-cell and myeloid populations, identified based on displayed markers (Fig. 4.2). Importantly, this data enabled comparison between tumour and

lymph node sites, as well as adaptations across time, in multiple cell types. Interestingly, some populations showed unique site-specific signatures, while others were unaffected by location. However, in this project we have particularly focussed on tumour fibroblasts, which were clustered and re-analysed.

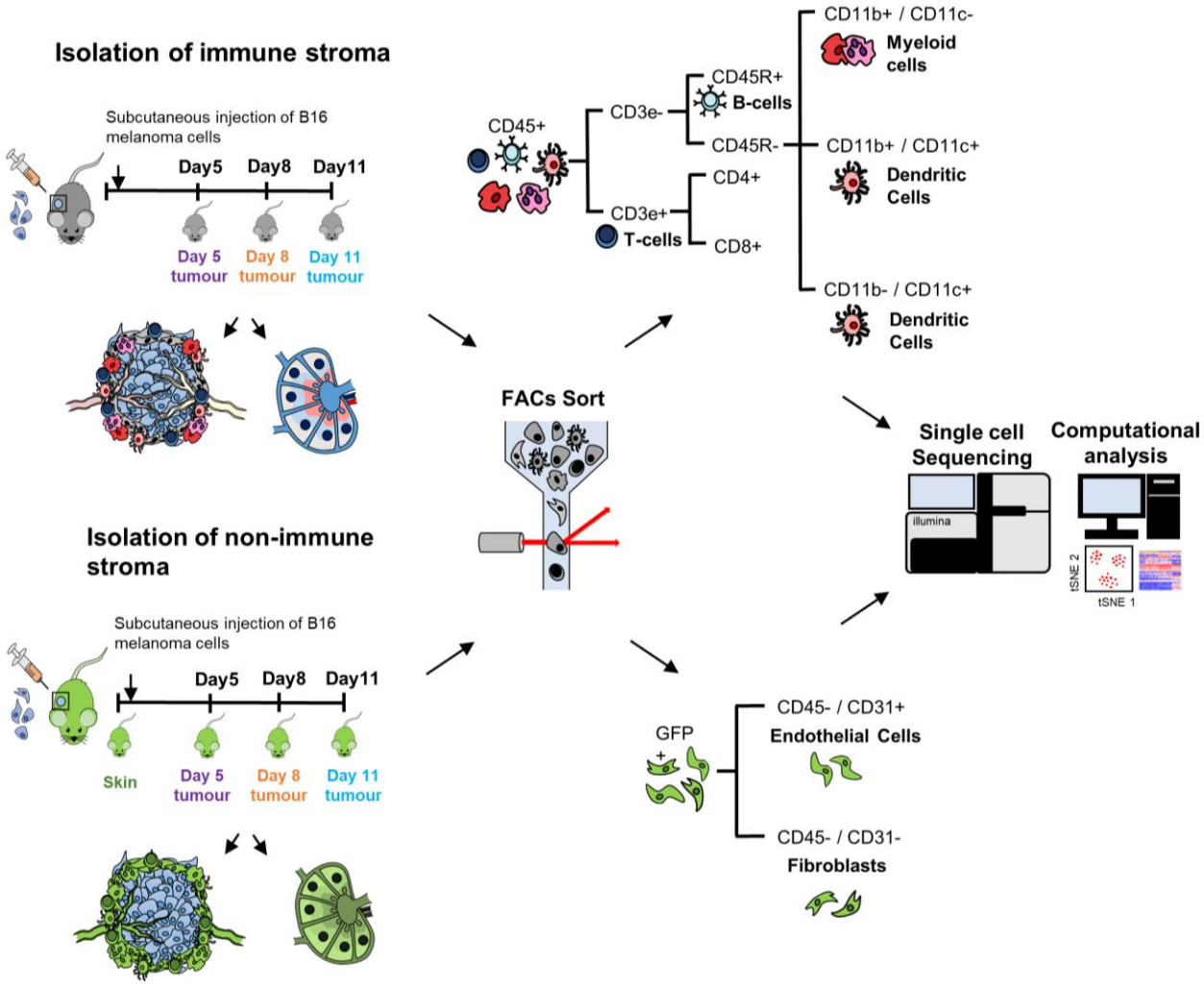

Fig. 4.1 Immune and non-immune stromal populations were isolated from the primary tumour and draining lymph nodes for single cell RNA sequencing.

Schematic depicting the isolation of immune and non-immune stromal populations for scRNAseq. To enrich for immune populations, cells were sorted based on marker combinations. Stromal populations were isolated based on a negative selection approach, in which tumour and immune cells were removed (GFP-, CD45+). Endothelial cells and fibroblasts were separated based on CD31 expression.

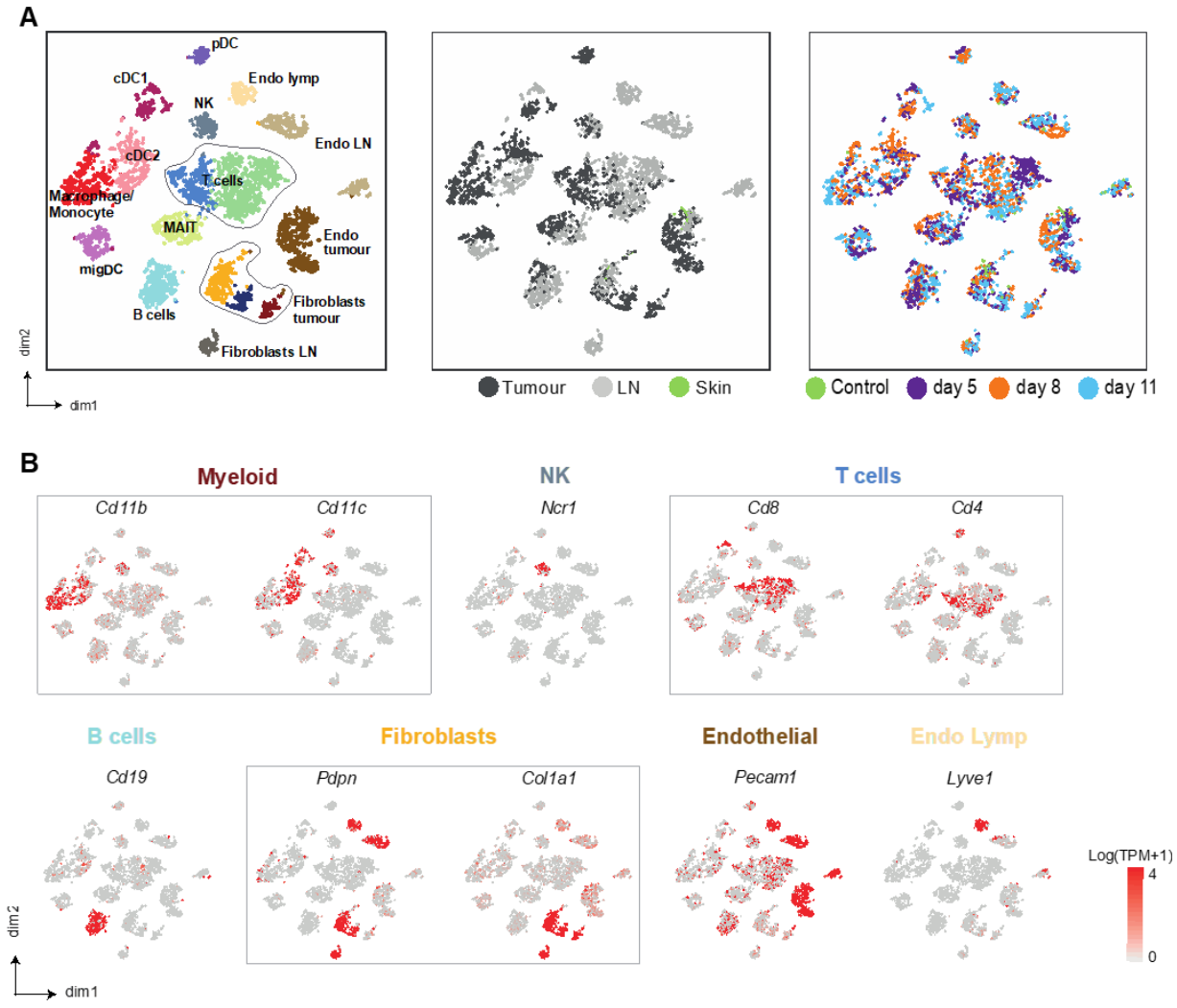

Fig. 4.2 Numerous stromal populations were identified within the tumour and lymph node, across different stages of tumour development.

(A) tSNE plots generated by Dr. Mirjana Efremova, display all populations isolated (4627 cells), coloured according to their cell type (left), location (middle) and the time point from which they were isolated (right) (B) Markers used to identify each stromal population.

4.2.2 *CAFs cluster into 3 phenotypically distinct populations*

4.2.2.1 *CAF populations could be identified by distinct marker repertoires*

$CD45^{-}CD31^{-}$ fibroblasts from all time points were subsetted and re-clustered, forming 3 transcriptionally distinct populations (termed CAF1, 2 and 3; (Fig. 4.3 A). These populations were un-affected by batch or sequencing depth as clusters do not separate by the number of detected genes or by the mouse from which cells were isolated (Fig. 4.3 B and C). Similar to our previous results, commonly used CAF markers were heterogeneously expressed (Fig. 4.3 D), yet expression of certain markers correlated with specific clusters. For example, high levels of *Pdpn* and *Pdgfra* were observed within CAF 1 and 2 clusters, whereas *Acta2* (αSMA) was upregulated by CAF 3 and showed intermediate expression within CAF2. Similarly, *Cd34* was highly expressed by CAF 1 and displayed intermediate expression in a subset of CAF2 cells. By combining these markers, we can identify each population as CAF1: $CD34^{high}$ $PDPN^{high}$ $PDGFRa^{high}$, CAF2: $PDPN^{high}$ $PDGFRa^{high}$, CAF3: $aSMA^{high}$.

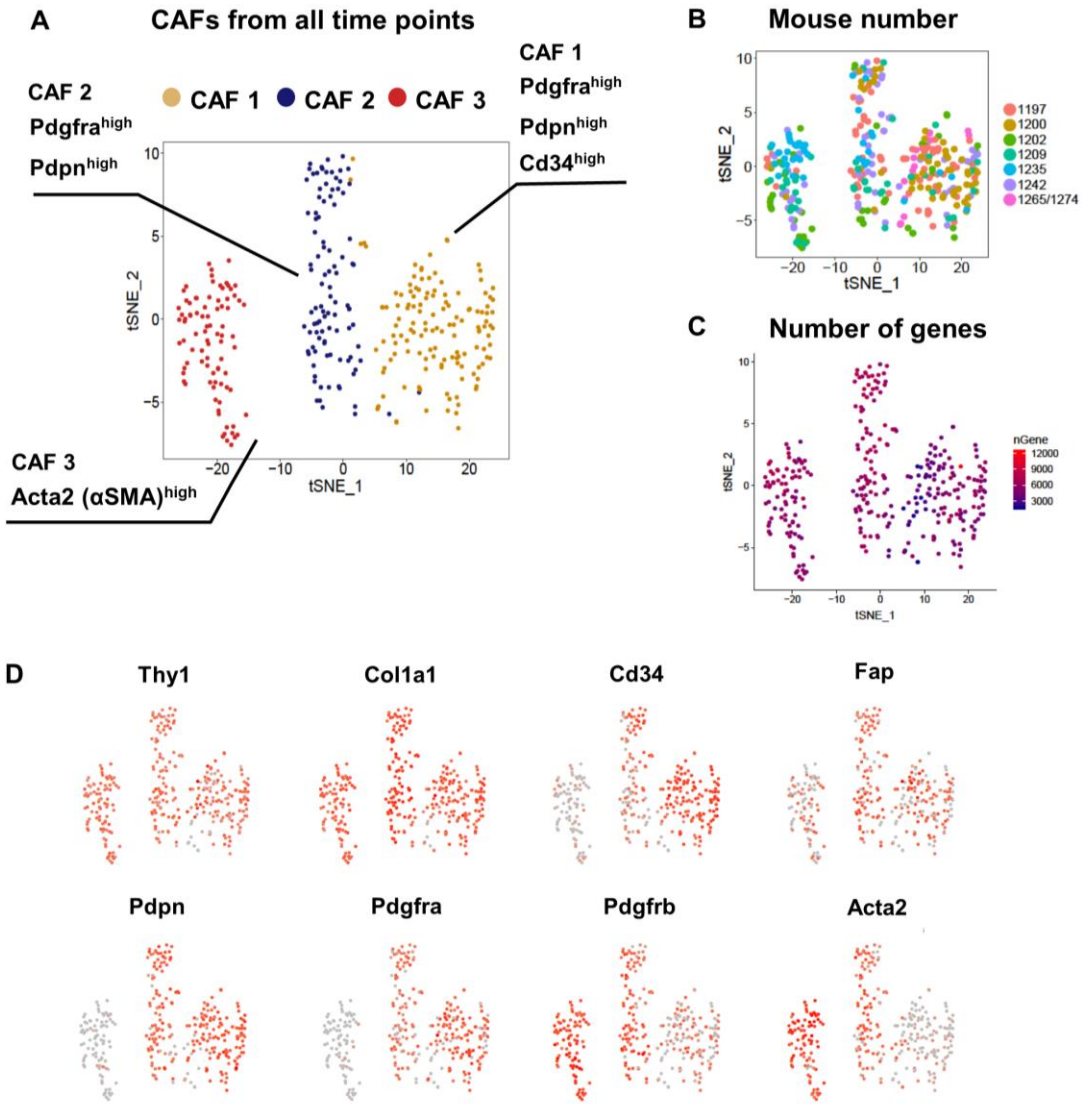

Fig. 4.3 CAFs clustered into three transcriptionally distinct populations

(A) Tumour fibroblasts were subsetted, re-clustered and displayed using tSNE (321 Cells)). *Pdpn*, *Pdgfra*, *Cd34* and *Acta2* expression correlated with specific populations (A and D). (B) tSNE plots coloured according to the mouse from which cells were isolated. (C) tSNE plot coloured according to the number of genes identified within each cell (nGene). This shows that clusters are un-effected by batch or sequencing depth. (D) tSNE plots are coloured according to the individual expression of each gene, where red indicates high expression and grey indicates low expression.

4.2.2.2 *Each CAF population displays unique functional signatures*

To examine the functional properties of each population, gene ontology analysis was performed on genes upregulated in each cluster and the top 20 terms displayed (Fig. 4.4 A, Fig. 4.5 A). Unique GO terms were produced for each population, indicating the presence of distinct phenotypes. The CAF1 subset upregulated secreted cytokines and cytokine receptors, such as *Cxcl12*, *Csf1*, *Cxcl13*, *Il11ra1* and *Il6st*, which are involved in immune cell recruitment and regulation. Furthermore, this population upregulated components of the complement cascade including *C3*, *C4b* and complement regulator *Cd55* (Fig. 4.4 B).

The complement system is activated during inflammation and involves the formation of convertases which cleave central proteins C3 and C5 to their respective a and b products. C3b and C5b form complexes with other complement factors, contributing to the creation of the membrane attack complex (MAC), which forms on the surface of targeted cells, causing calcium influx and cell death [395]. On the other hand, anaphylatoxins C3a and C5a trigger inflammation and recruit immune cells to the site of activation. Thus, expression of central component C3 and upstream activators of the classical and alternative pathways *C4b*, *C1rb C1ra* and *Cfb* (factor B), imply that CAF1 may be instrumental in complement activation in the tumour. However, this population also upregulates the complement regulator *Cd55*, which prevents formation of MAC on host cells [396]. Therefore, CAF1 fibroblasts may aid activation of this cascade, yet remain protected from its harmful effects. In addition, this CAF subset may be more widely involved in immune recruitment by production of C3 cleavage product C3a and cytokines *Cxcl12*, *Csf1, Cxcl13*.

Interestingly, the GO term “ECM-receptor interactions” was highlighted in both CAF1 and CAF2 populations. However, CAF1 fibroblasts expressed matrix components associated with the basement membrane, such as, laminin fibres *Lama2* and *Lamc2*, which underlie normal epithelial tissues (Fig. 4.4 B) [397]. In contrast, the CAF2 population upregulated genes associated with pathological matrix deposition and remodelling, including *Col1a1*, *Col1a2* and *Tnc* (Fig. 4.5 A and C) [197,398,399]. This indicates that the CAF2 subset may be primarily involved in the desmoplastic response associated with tumour development. Lastly, fibroblasts within CAF3 also expressed genes involved in matrix remodelling, however, the stronger functional signature

related to genes involved in contraction and rearrangement of the actin cytoskeleton (Fig. 4.5 B and C). In particular, these cells upregulated *Myl9* (myosin light chain 2) and *Mylk* (myosin light chain kinase), which participate in stress fibre contraction. Furthermore, expression of *Itgb1* (β1 integrin) and *Vcl* (vinculin) is increased, which are important members of focal adhesion complexes and transduce mechanical force [400–402]. Indeed, *Itgb1* expression is upregulated by heightened cytoskeletal tension [403], suggesting CAF3 fibroblasts may represent a contractile population under high tensile stress. Owing to these unique functional signatures, CAF1, CAF2 and CAF3 populations were designated ‘immune’, ‘desmoplastic’ and ‘contractile’ respectively.

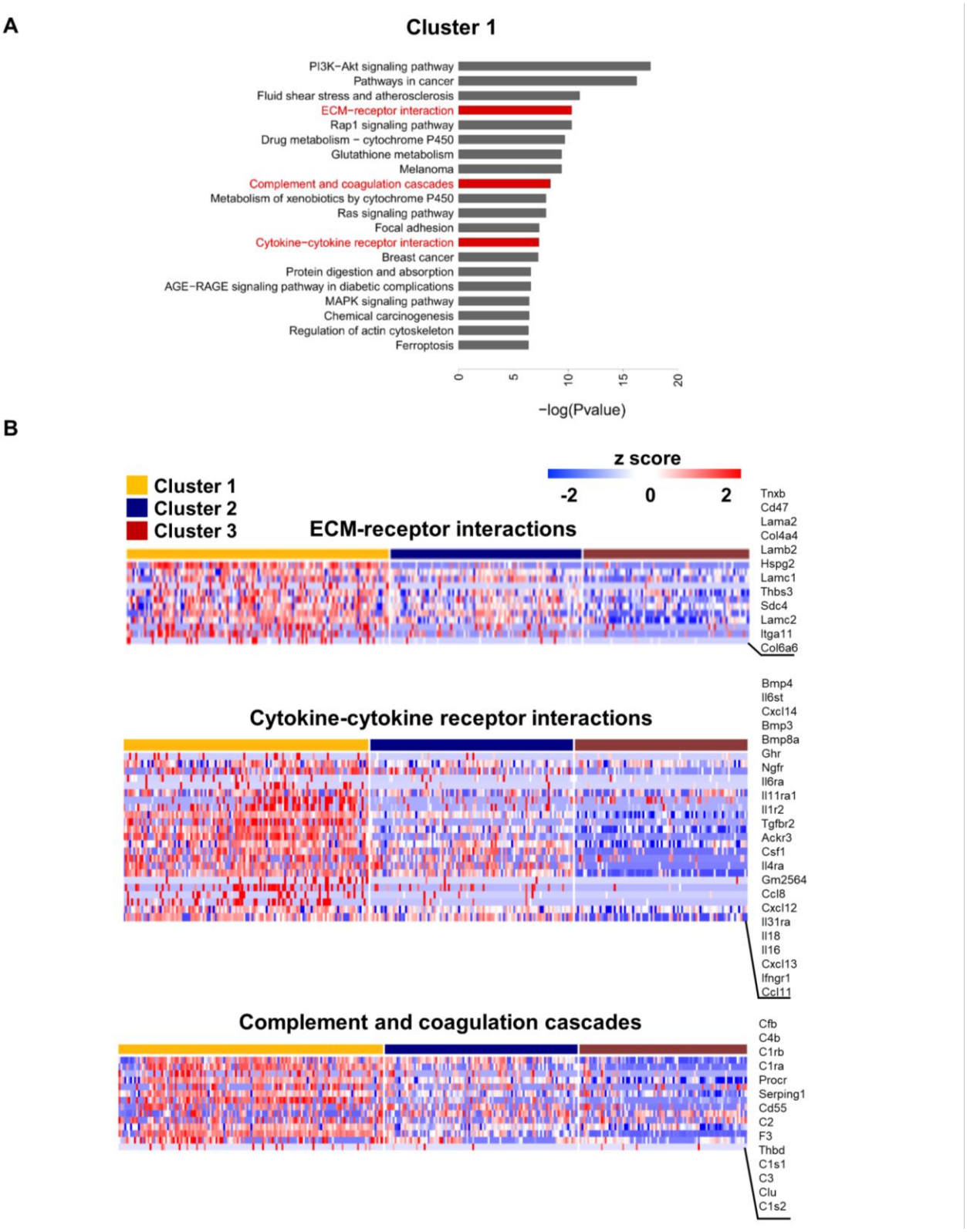

Fig. 4.4 GO pathway analysis of the CAF1 population revealed it may be involved in immune-crosstalk

(A) Top 20 GO terms generated from genes upregulated within the CAF1 population. (B) Heatmaps depicting selected pathways of interest, where rows correspond to genes and columns represent individual cells. z scores are displayed.

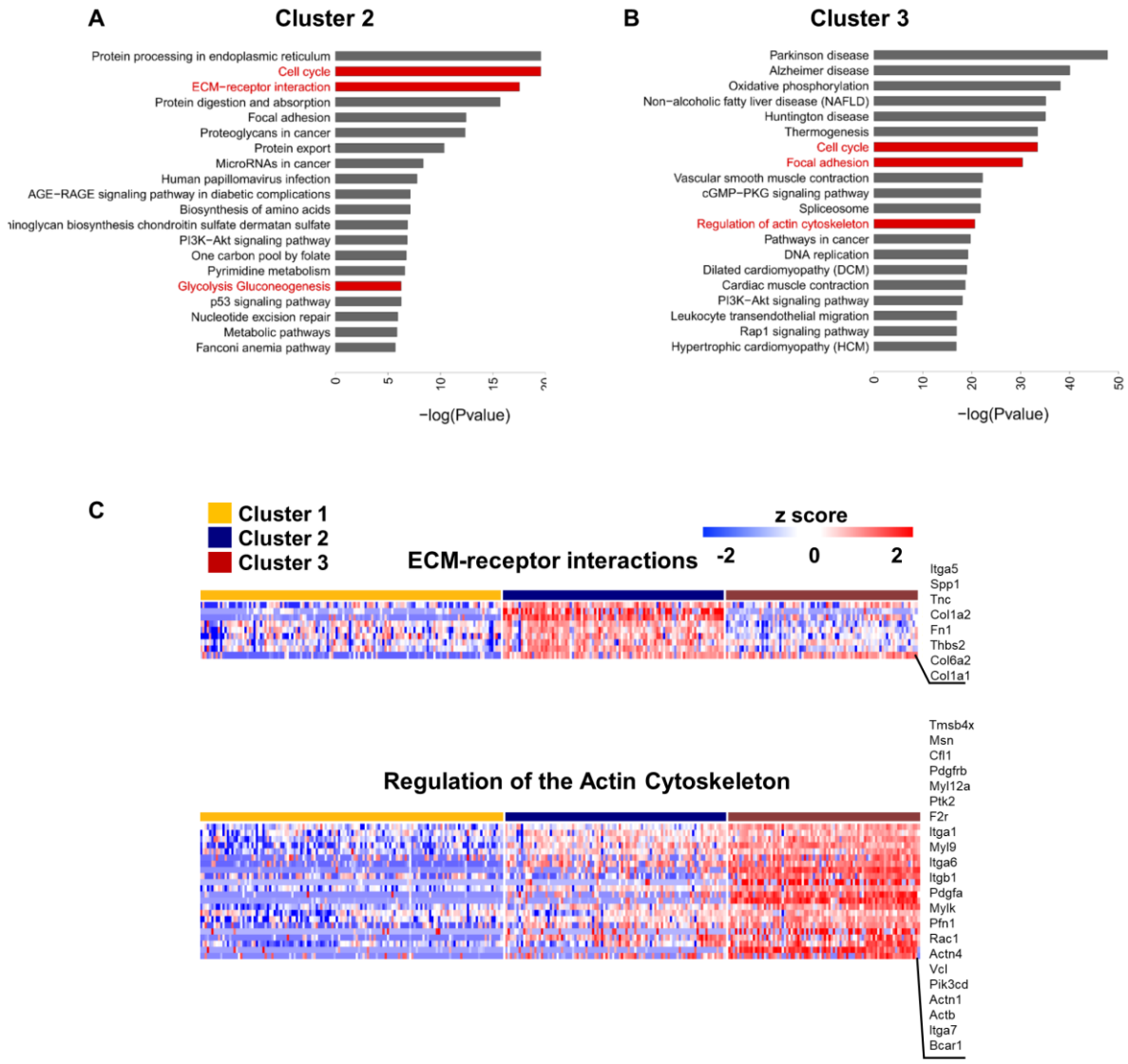

Fig. 4.5 GO pathway analysis of the CAF2 and 3 reveal ‘desmoplastic’ and ‘contractile’ phenotypes

Top 20 GO terms generated by upregulated genes within the CAF2 (A) and CAF3 (B) population. (C) Heatmaps depicting selected pathways of interest where rows correspond to genes and columns represent individual cells. z scores are displayed.

4.2.2.3 *Within CAF2 and CAF3 populations, subsets of glycolytic and proliferative fibroblasts are present*

Reiterating our previous results, GO analysis highlighted glycolysis and the cell cycle signatures in clusters 2 and 3 respectively (Fig. 4.5 A and B). However, high expression of glycolytic enzymes and cell cycle factors, was neither uniform across all cells in each population, nor exclusive to CAF2 or 3. Instead, a subset of cells in both groups highly expressed these gene signatures, suggesting that while glycolytic and proliferating fibroblasts exist, clusters are not defined by these factors (Fig. 4.6 A). The existence of proliferating subpopulations within CAF2 and CAF3 was supported by cyclone analysis and *Ki67* expression (Fig. 4.6 B). Similar to our preliminary data, the cyclone algorithm assigned most cells to G1, yet allocated a subset of fibroblasts to S phase and G2/M. This subset also expressed proliferation marker *Ki67*, thus, likely represent actively proliferating cells. tSNE plots displaying cyclone labels and *Ki67* expression, show that proliferating cells cluster together within their respective CAF subsets. This suggests that the cell-cycle remains a source of variance within our data, however, other factors have a larger effect on the transcriptional profiles of these cells.

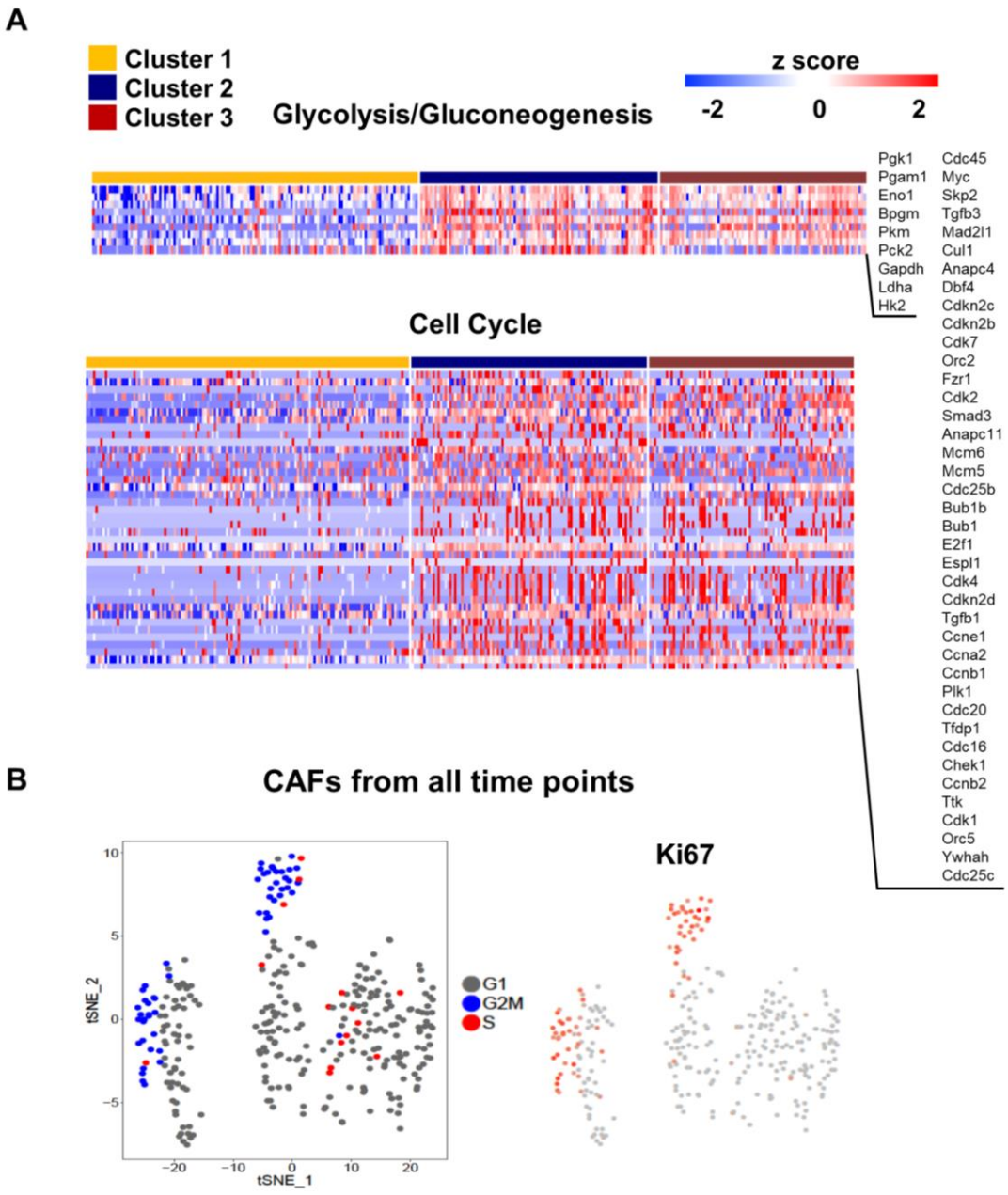

Fig. 4.6 Glycolytic and Proliferating subsets are present within CAF 2 and 3

(A) Heatmaps depicting genes associated with glycolysis / gluconeogenesis and cell-cycle GO terms. Rows represent genes, columns represent individual cells and z scores are displayed. (B) Cyclone analysis was performed and displayed as a tSNE plot in which cells are coloured according to their assigned stage (left). tSNE plot displaying *Ki67* expression in which red indicates high expression and grey indicates low expression (right). tSNE plots display CAFs from all time points (321 cells).

4.2.2.4 ***Similar transcriptional signatures are present in the pilot data set***

As glycolytic and proliferative signatures were identified in both our pilot run and time course experiment, we investigated whether the ‘immune’, ‘desmoplastic’ and ‘contractile’ signatures were also present within our preliminary data. Interestingly, GO analysis highlighted upregulation of the complement cascade in cluster 1 (section 3.2.2.3). This included factors such as *C4b*, *C2*, *C1ra* and *C1rb*, suggesting that complement components are consistently upregulated within a subset of fibroblasts. To explore other phenotypic signatures associated with our time course data, we selected key genes and investigated their expression across the pilot data set. Clustering both cells and selected genes revealed a subset of fibroblasts that displayed high expression of immune recruitment factors *C3*, *Csf1* and *Cxcl12* (Fig. 4.7 A). Furthermore, this subset also highly expressed CAF markers *Cd34*, *Pdgfra* and *Pdpn* but not *Acta2* (αSMA), reflecting our time course data. In particular, the complement component *C3* was associated with high *Cd34* expression (Fig. 4.7 B). On the other hand, while matrix components such as *Postn*, *Col1a1* and *Col1a2* clustered together, a clear ‘desmoplastic’ subset was not observed. Thus, while there is clear overlap between our two data sets, gene signatures differ in their prominence.

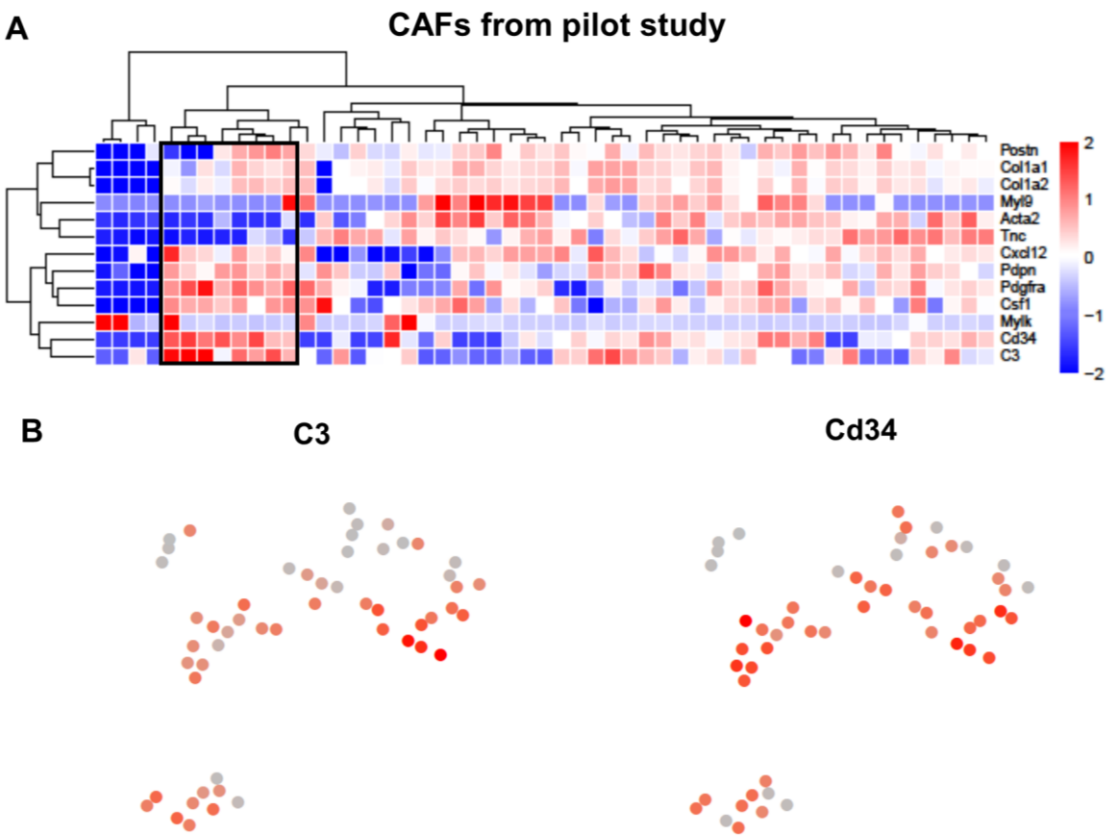

Fig. 4.7 Investigation of 'immune', 'desmoplastic' and 'contractile' signatures in pilot data

(A) Heatmap depicting expression of selected genes related to 'immune' 'desmoplastic' and 'contractile' phenotypic signatures within pilot data. Columns represent individual cells while rows represent selected genes, z scores are displayed. Both columns and rows were clustered to investigate related signatures. A subset of fibroblasts expressing immune recruitment factors are highlighted (black box). (B) tSNE plot coloured according to *C3* and *Cd34* expression, red indicates high expression, grey indicates low expression.

4.2.3 *The CAF compartment is a dynamic niche, changing and adapting as the tumour progresses*

4.2.3.1 *CAF populations dominate at different stages of tumour development*

Sequencing fibroblasts from different stages of tumour development offered the opportunity to investigate the prevalence of these populations at different time points. Unfortunately, cells isolated from skin contained a large amount of keratinocyte contamination, leaving only 15 fibroblasts. Nevertheless, all of these cells were observed within the CAF1 subset, suggesting that this population may reside in normal tissue. However, owing to the limited number of skin fibroblasts recovered, this requires further corroboration.

Investigation of the remaining time points revealed a dynamic compartment, in which the composition of populations changes as the tumour develops. While CAF1 and CAF2 populations dominate at day 5, the CAF1 subset receded at day 8 and 11 and CAF3 became more prevalent. This suggests that CAF1 and CAF2 are present from early stages of tumour development, whereas CAF3 is associated with later time points.

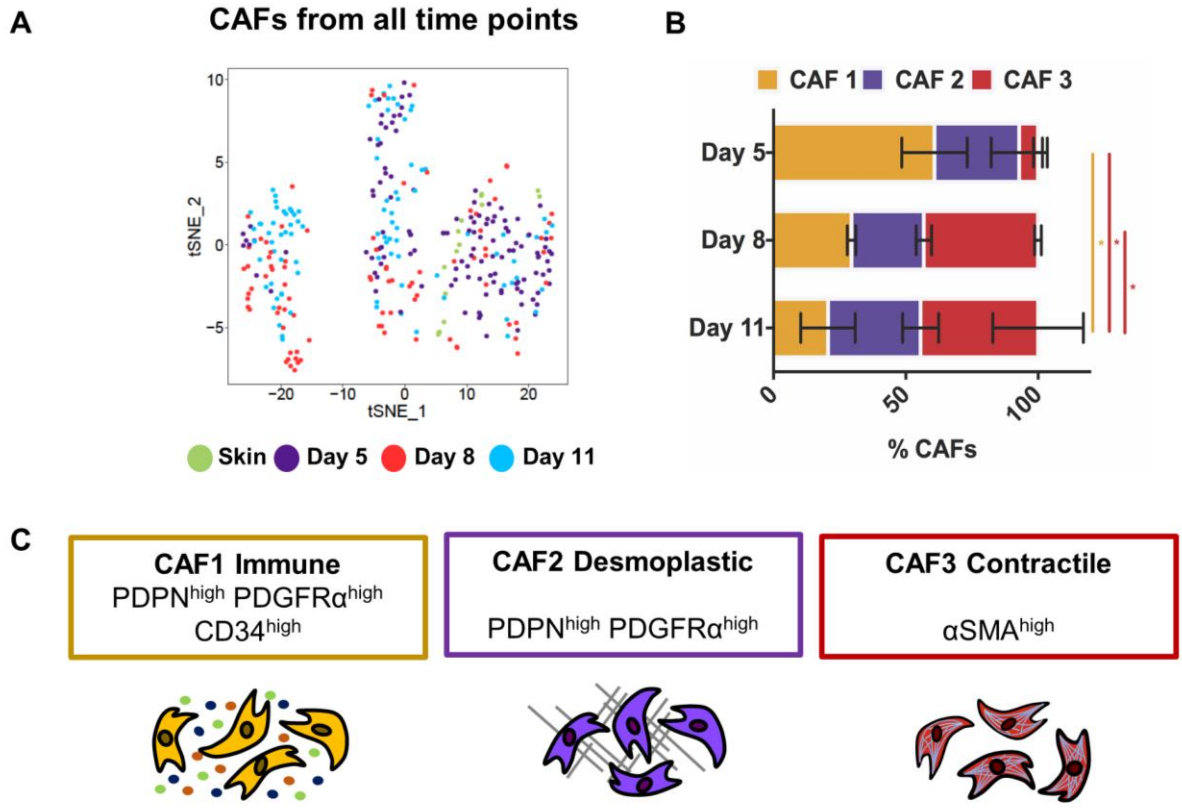

Fig. 4.8 The abundance of each CAF population changes as the tumour develops.

(A) tSNE plot in which each cell is coloured according to the time point from which it was isolated. (B) Sequencing data represented as a bar graph, in which the size of each bar is proportional to the percentage of each CAF populations at day 5, 8 and 11. * < 0.05 (two way anova with Tukey post-hoc test), yellow indicates significance between CAF1 populations at different time points, red indicates significance between CAF3 populations. Data presented as SEM ±, n = 2 mice. (C) Schematic showing CAF populations, their defining markers, phenotypes and the time points from which they are present.

4.2.3.2 *Individual populations retain a similar phenotype throughout tumour growth, yet develop increased hypoxic signatures*

As well as investigating changes in the abundance of fibroblast populations at different time points, the transcriptional profiles of fibroblasts isolated at day 5 were also compared to day 11. This revealed that the complement pathway was upregulated at early stages, whereas Hif1 signalling and contractile signatures were upregulated at later time points (Fig. 4.9 A and B).

However, by including all CAFs in this analysis, the results may be biased by population dynamics. For example, upregulation of the complement pathway at day 5 may reflect the abundance of CAF1 fibroblasts at this time point. This raised the question of whether individual populations change over time and how universal these changes are across subsets. Thus, whether the signatures highlighted in Fig. 4.9 A, as well as the 'immune', 'desmoplastic' and 'contractile' phenotypes, temporally change within individual populations was investigated. This showed that generally, phenotypic signatures associated with each population where not influenced by tumour development. For example, from early time points CAF2 cells produced pathological matrix components and the CAF1 population secreted inflammatory factors. Furthermore, expression of these genes was generally consistent throughout tumour growth (Fig. 4.9 C). This suggests that key differences between CAFs at early and late time points, such as production in complement factors, likely results from shifts in population abundance, rather than transitions in phenotype. However, most fibroblasts in CAF1 and CAF3 subsets were isolated from either day 5 or day 11 respectively. Thus, the number of cells isolated from other time points may be too few for a fair comparison.

On the other hand, glycolytic signatures observed within the whole CAF compartment (Fig. 4.9 A), were upregulated at late time points, in both CAF2 and CAF3 populations (Fig. 4.10). As previously discussed (Section 3.2.2.4), this glycolytic signature is likely induced by tumour hypoxia, indicating that hypoxia may be associated with more developed tumours. This indicated that while defined fibroblast subsets exist in the tumour, external factors that arise during tumour development can further influence their transcriptional profiles and increase diversity.

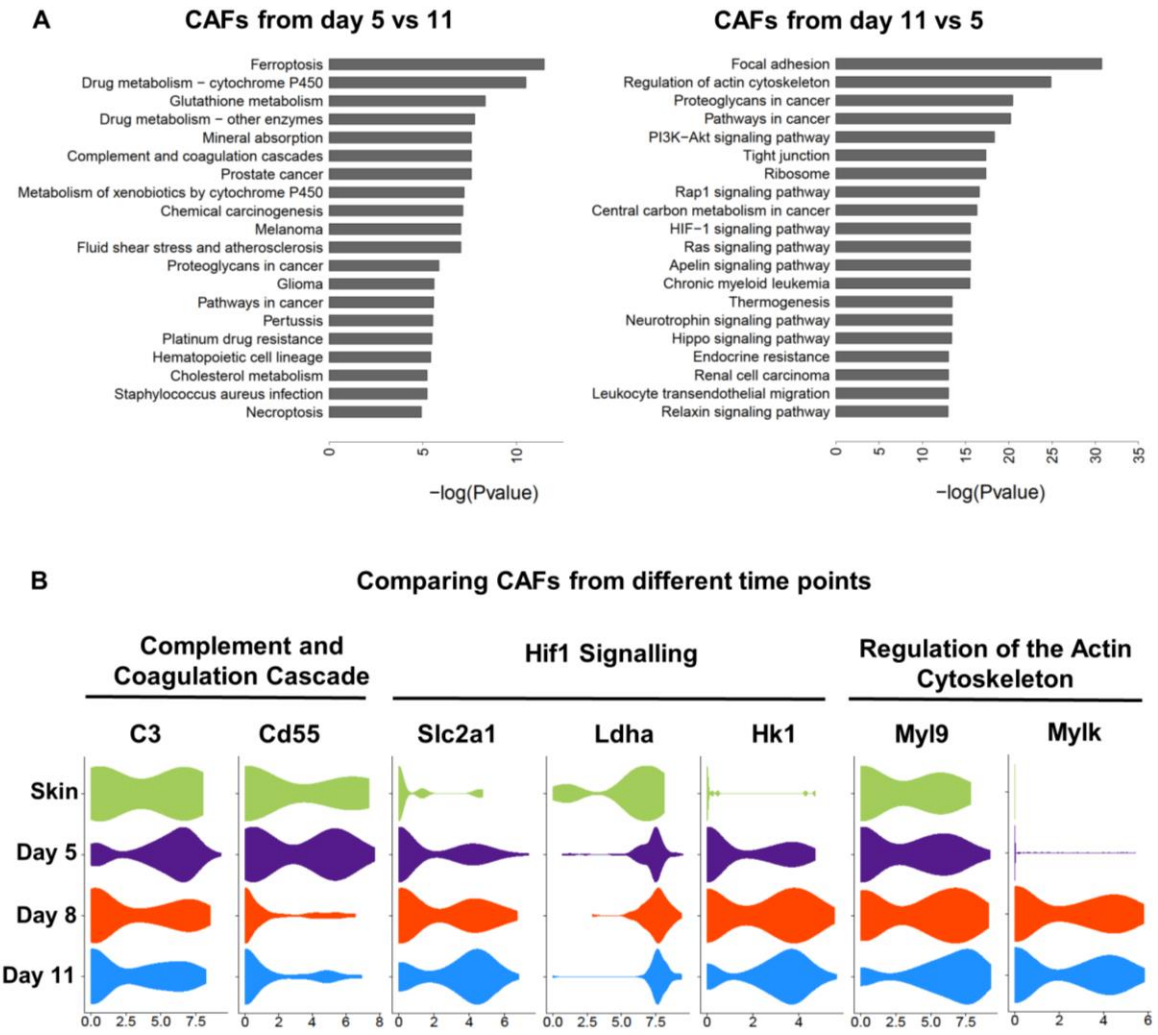

Fig. 4.9 Comparison of CAFs from different time points.

(A) GO analysis of genes deregulated between CAFs from day 5 and day 11 across all populations. Terms upregulated at day 5 (left) and day 11 (right) are shown. (B) Violin plots showing expression of selected genes mapped to GO terms, across all fibroblasts, at different time points. Skin = 15 cells, day 5 = 124 cells, day 8 = 89 cells, day 11 = 94 cells

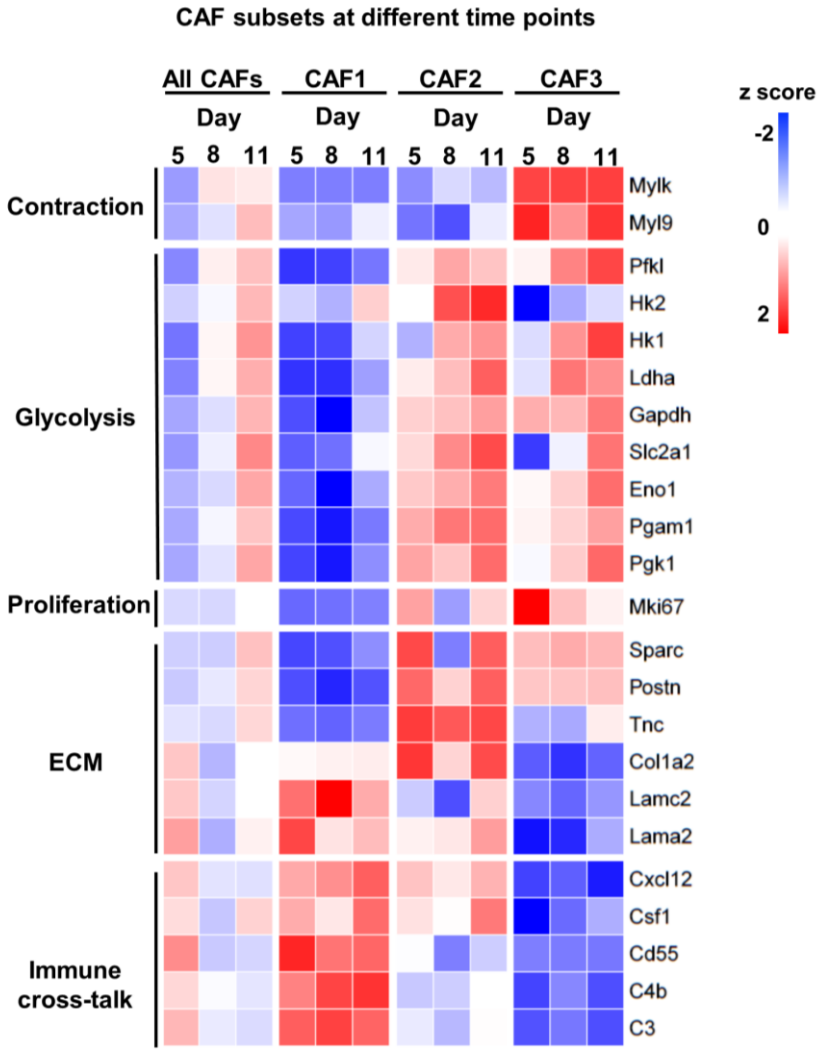

Fig. 4.10 Individual phenotypes of each CAF population remain similar over time, CAF 2 and CAF3 develop glycolytic signatures at later time points.

(Heatmap displaying the average expression of selected genes at different time points within all CAFs, CAF1, CAF2 and CAF3, z scores are displayed. All CAFs day 5 = 124 cells, All CAFs day 8 = 89 cells, All CAFs day 11 = 94 cells, CAF1 day 5 = 74 cells, CAF1 day 8 = 26 cells, CAF1 day 11 = 21 cells, CAF2 day 5 = 41, CAF2 day 8 = 24 cells, CAF2 day 11 = 34 cells, CAF3 day5 = 9 cells, CAF3 day 8 = 38 cells, CAF3 day 11 = 39 cells.

4.2.3.3 *Pseudo-time analysis implies CAFs may transition between populations*

Examination of the CAF compartment across tumour development suggested populations are autonomous, retaining their functional phenotypes and merely shrinking or expanding in response to malignant growth. However, it is also possible that these populations are not mutually exclusive and represent phenotypic states, through which fibroblasts transition. To examine this possibility, we created diffusion maps and employed pseudo-time analysis. Typical methods of visualising single cell data, such as PCA and tSNE, organise cells with similar transcriptomes into clusters. However, this does not reflect the transitional nature of biological processes, such as differentiation. Diffusion maps are another form of dimensional reduction that order cells into continuous trajectories, rather than clustering them into discreate groups.

The r package 'destiny' creates both diffusion maps and performs pseudo-time analysis, known as diffusion pseudo-time (DPT) [374,375]. DPT orders cells according to their transcriptional similarity and is performed independently from the generation of diffusion maps. Starting with one cell, DPT calculates the probability of transition to all other cells, repeating this process until such probability networks are calculated for every cell. By ordering these probabilities, a trajectory for any cell in the dataset is produced. These trajectories are projected onto diffusion maps, displaying the transition order of a specific cell.

Interestingly, plotting the first two diffusion components showed a transition from CAF1 towards CAF 2 and then from CAF2 to CAF3. The DPT trajectory for the first, or "tip", cell in the diffusion map was overlaid, showing a clear progression through the populations. This implies that fibroblasts transition between populations, rather than existing in a single state (Fig. 4.11 A). Furthermore, expression of CAF markers and signature genes was graduated along this trajectory, reflecting this transitional nature (Fig. 4.11 B). As CAF 1 is more dominant at early time points and CAF 3 arises at later stages, it is tempting to suggest CAFs evolve along this path. However, while the displayed DPT maps a trajectory from CAF1 to CAF3, this merely reports how cells are related to one another and does not dictate the direction of transition. Indeed, this trajectory could begin with any population. Nonetheless, this data highlights CAF 2 as an intermediate population, sharing features with both CAF 1 and CAF3.

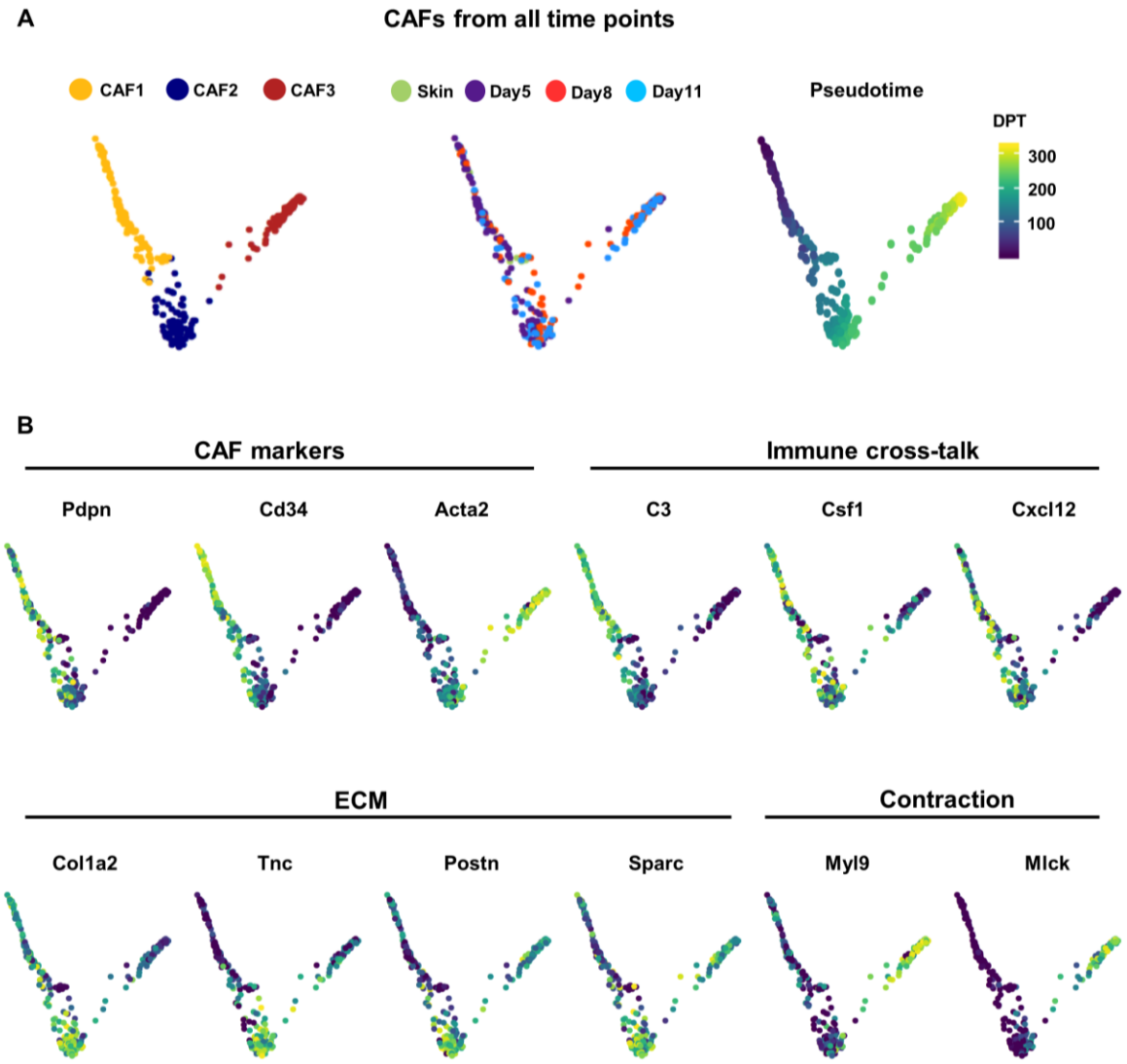

Fig. 4.11 Diffusion maps and pseudo-time analysis suggest transition between CAF populations

(A) Diffusion maps are coloured to show CAF 1, CAF 2 and CAF 3 populations (left) and the time points from which each cell was isolated (centre). The DPT trajectory orders cells from most similar to most different and can be produced for any cell in the dataset. Here, the map has been coloured according to the DPT order produced for the first (tip) cell in the diffusion map. Blue indicates CAFs that are closely related to the tip cell, whereas as yellow indicates CAFs that are more distant. (B) Diffusion maps coloured according to the expression of CAF markers and selected genes. Blue indicates low expression, while yellow indicates high expression.

4.2.4 *Identifying CAF populations in the tumour microenvironment and validating their functional signatures*

Having identified these CAF populations using single cell sequencing, conventional techniques were employed to validate their existence in the tumour microenvironment. Using IF and flow cytometry, we attempted to identify each population in B16-F10 melanomas, based on their unique marker repertoires.

4.2.4.1 *CAF subsets were identified in the tumour stroma using IF and flow cytometry*

As previously described (section 4.2.2.1), markers *Pdpn* and *Pdgfra* where highly expressed by CAF1 and CAF2 subsets, whereas *Cd34* and *Acta2* (αSMA) expression was more prominent within CAF1 and CAF3 respectively. Thus, to identify CAF populations within B16-F10 tumours, sections from day 5 and day 11 were stained for these 4 markers. Extensive colocalization between PDPN and PDGFRα was observed at both time points, while CD34 also colocalised with a subset of PDGFRα^{+} and PDPN^{+} cells. αSMA staining was more distinct, although colocalization was also observed. This colocalization likely represents the intermediate CAF2 population, which express lower levels of both αSMA and CD34. Furthermore, as highlighted by our pseudo-time analysis, fibroblasts are extremely plastic and sit on a spectrum of marker expression.

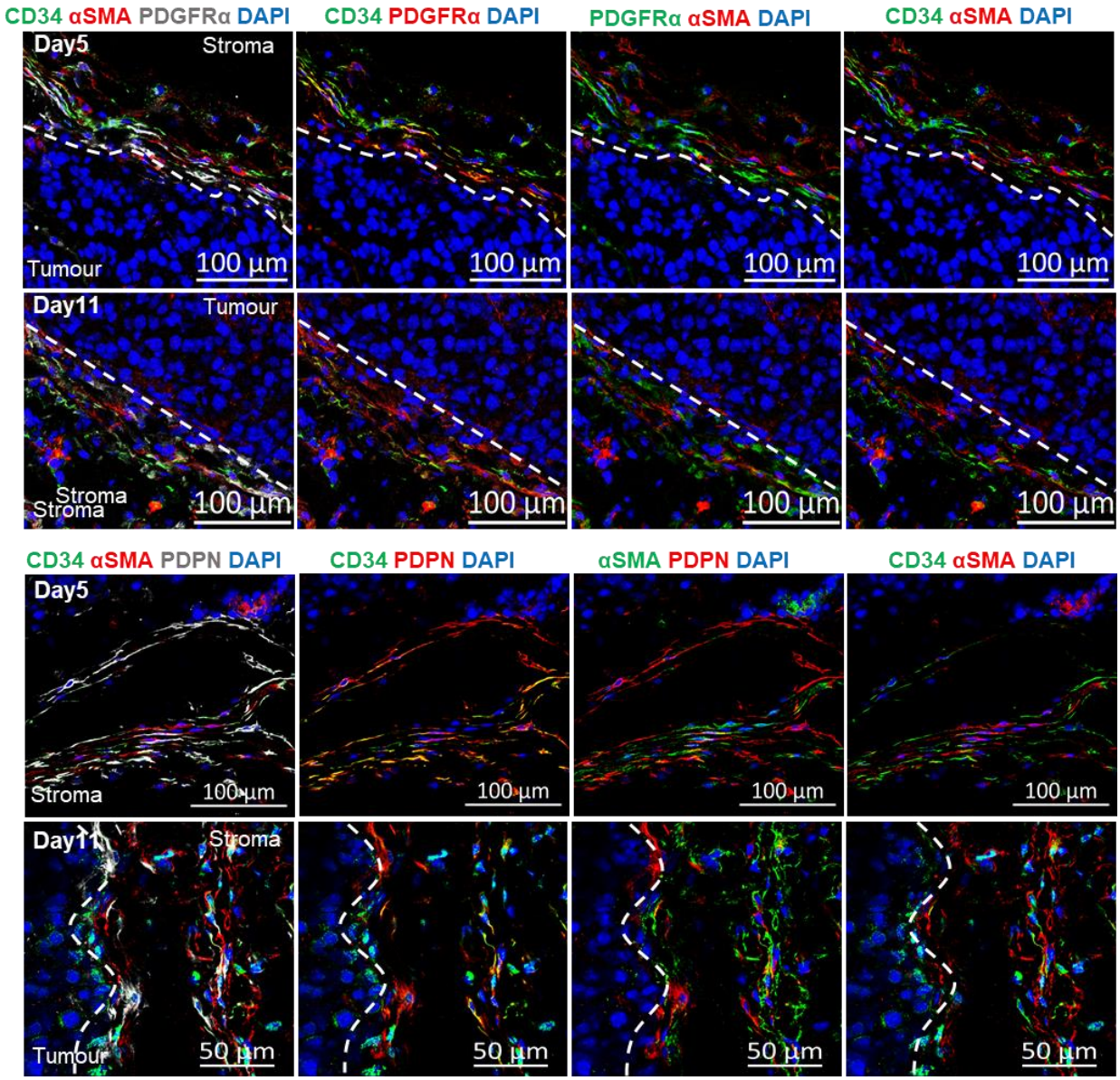

Fig. 4.12 Confocal imaging shows CD34 colocalization with PDGFRα and PDPN yet more distinct αSMA staining

Representative confocal images showing the combination of CD34, αSMA and PDGFRα (top) and CD34, αSMA and PDPN (bottom) in day 5 and 11 B16-F10 tumours. A merged image of all 3 markers is displayed, as well as images showing two channels at a time. Pseudo-coloured green or red, these images emphasise colocalization. Dashed line indicates the tumour border and scale bars are displayed. Images represent at least n=3 independent mice.

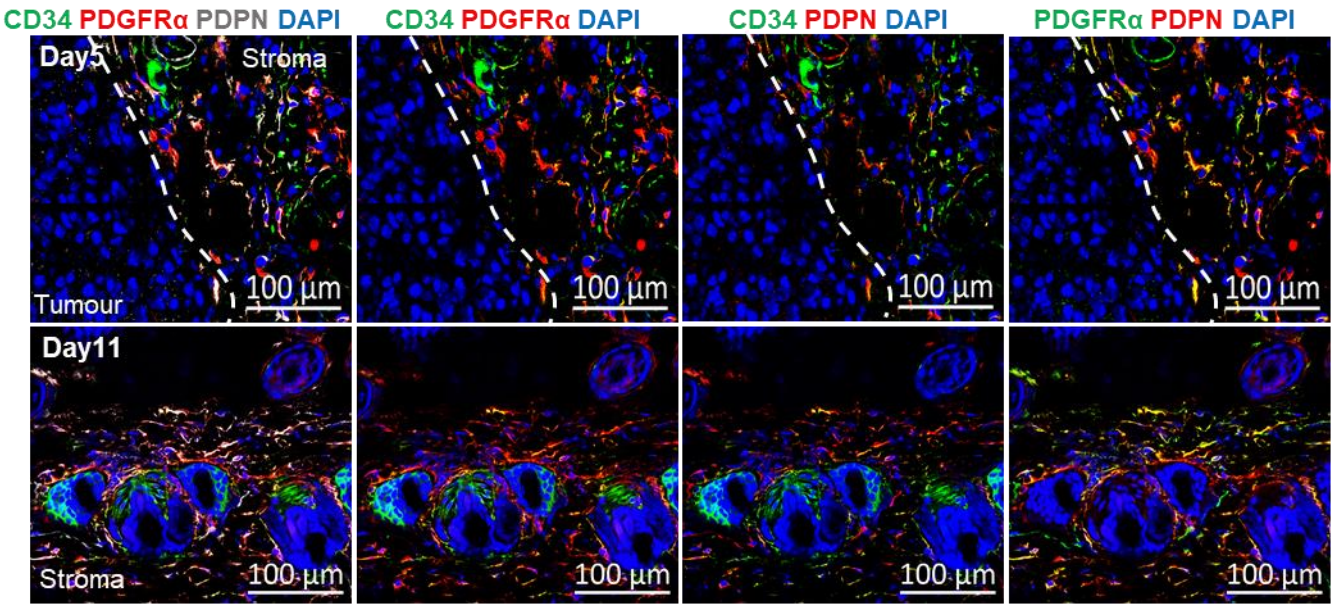

Fig. 4.13 Confocal imaging shows CD34 PDGFRα and PDPN colocalise

Representative confocal images showing the combination of CD34, PDGFRα and PDPN in day 5 and 11 B16-F10 tumours. Images taken form day 11 tumours were taken further away from the tumour edge, blue structures represent hair follicles. A merged image of all 3 markers is displayed, as well as images showing two channels at a time. Pseudo-coloured green or red, these images emphasise colocalization. Dashed line indicates the tumour border. Scale bars are displayed, and images represent at least n=3 independent mice.

While the expression pattern of CAF markers observed within our sequencing data was reflected by IF imaging, it remained difficult to identify individual populations. Thus, flow cytometry was employed to further investigate CAF subsets. After removal of doublets and dead cells, immune and endothelial cells were excluded based on CD45 and CD31 expression. As previously discussed, flow cytometric analysis is restricted to comparison of two markers in tandem. Thus, staining for CAF markers individually would complicate identification of CAF populations. Instead, we separated fibroblasts from tumour cells using the combination of Thy1, PDGFRα and PDGFRβ, which our sequencing data indicated would collectively identify all fibroblast populations. Within this compartment, fibroblasts could then be separated into populations resembling CAF1, CAF2 and CAF3, based on CD34 and αSMA expression. Here CD34^{high} αSMA^{low}, CD34^{low} αSMA^{low} and CD34^{low} αSMA^{high}, were termed CAF1 CAF2 and CAF3 respectively.

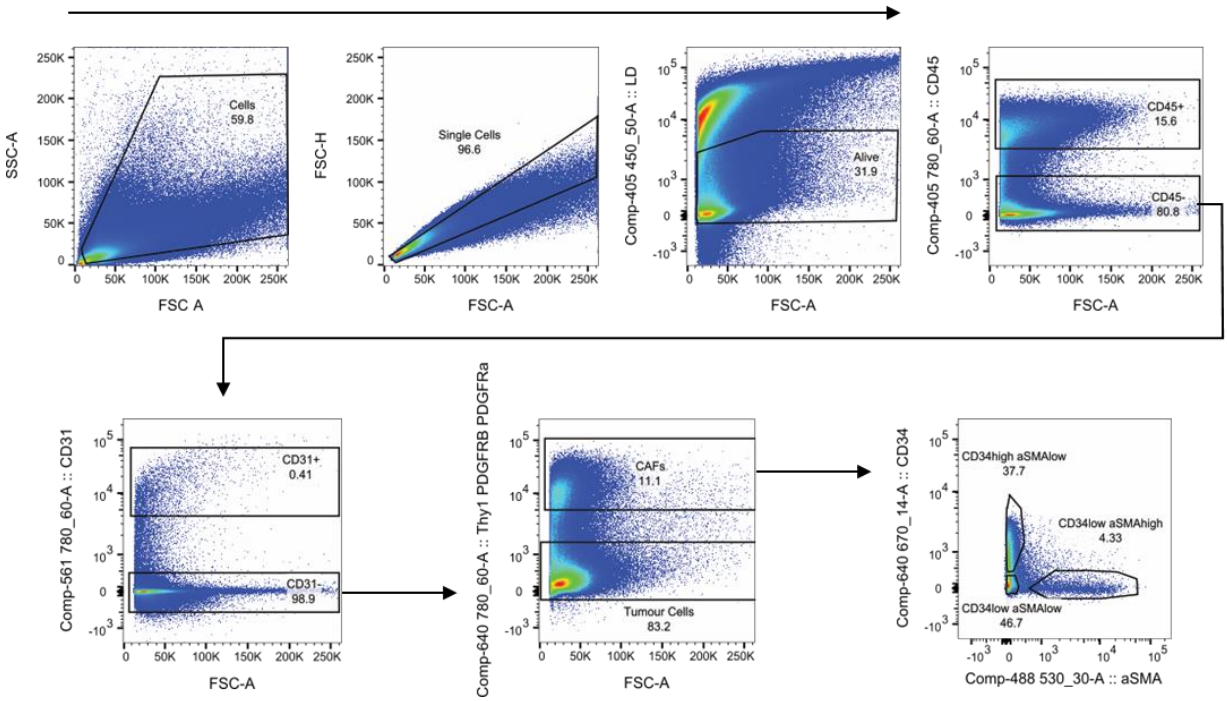

Fig. 4.14 Identifying CAF populations using flow cytometry

Representative gating strategy for the identification of CAF populations in B16-F10 melanomas. Debry, doublets, dead cells, immune cells (CD45^{+}) and endothelial cells (CD31^{+}) were excluded and CAFs were selected by combined expression of PDGFRα, PDGFRβ and Thy1. CAF populations were divided based on CD34 and αSMA expression into CAF1: CD34^{high} αSMA^{low}, CAF2: CD34^{low} αSMA^{low} and CAF3: CD34^{low} αSMA^{high}.

4.2.4.2 *Investigation of CAF populations over time confirmed CAF 3 was more prominent at later time points*

Having developed a method to detect CAF populations, we next sort to validate their temporal dynamics across tumour development. While we observed expansion of the CD34^{low} αSMA^{high} CAF3 population at day11, we did not detect a decrease in the number of CAF1 CD34^{high} αSMA^{low} cells (Fig. 4.15). Furthermore, both CAF 1 and CAF2 populations were present in normal skin, contradicting our sequencing data which suggested CAF1 cells represented resident fibroblasts. It was also noted that the CAF3 populations only represented 5% of the CAF compartment by flow cytometry, yet both the sequencing data and IF images suggest higher numbers are present. While trends are maintained, this discrepancy in prevalence may be due to the intracellular location of αSMA, as poor permeabilization can prevent antibody entry and reduce signal.

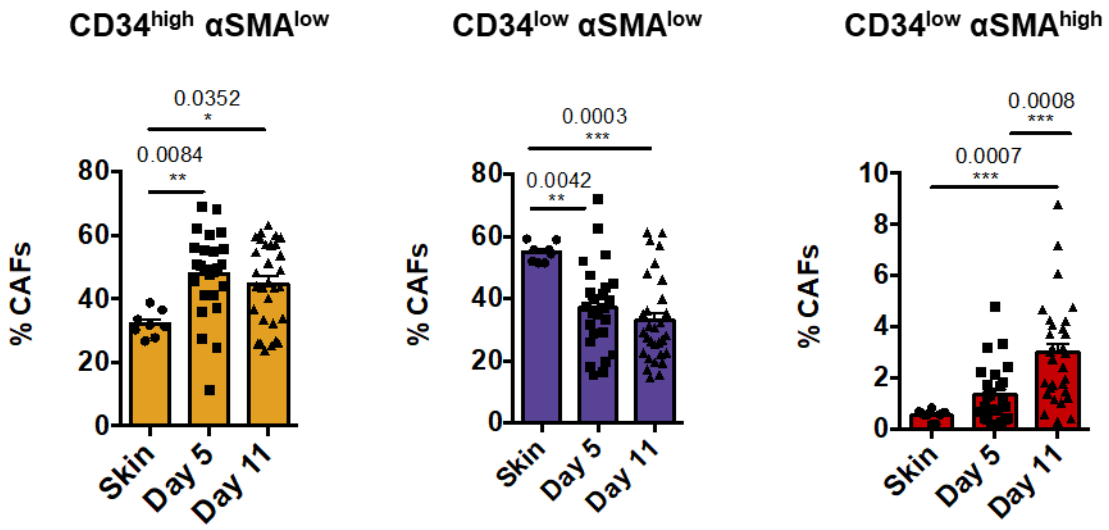

Fig. 4.15 Examining CAF populations at different time points confirmed CAF3 is more prevalent at later stages.

Quantification of the CAF populations at day 5 and day 11 tumours using flow cytometry. Populations are displayed as a percentage of total CAFs. Each point represents a tumour and data presented as mean ± SEM. * P<0.05, ** P<0.01, *** P<0.001, **** P<0.0001 (one way anova with Tukey post-hoc test). Skin n = 8 mice, day 5 n = 25 mice, day 11 n = 30 mice.

4.2.4.3 *Immune recruitment factors are produced by CAF 1*

The ability to separate these populations using flow cytometry enabled us to examine production of immune recruitment factors associated with CAF 1 that were identified by the sequencing data, including CSF1, CXCL12 and C3. To enable cytokine detection and ensure their secretion was not affected by processing steps, tumours were incubated with BFA during digestion (1.5hs) and for a further (2.5hs) in media. BFA disrupts ER/Golgi transport, inhibiting secretion and causing proteins to build up in the cytoplasm. Average expression (geometric mean of fluorescence intensity) was calculated from each CAF population using the gating strategy previously described (Fig. 4.14). Our data showed that CXCL12 and C3 expression was greater in CAF1 and CAF2, compared to CAF3. In agreement with our sequencing data, the highest expression of C3 was detected in the CAF1 population. However, the highest expression of CXCL12 was observed in the CAF2 subset, conflicting our previous findings (Fig. 4.16 A and B).

This abnormality led us to investigate whether antibodies against CXCL12 and C3 were binding to cytokines coating the cell surface. Indeed, surface staining revealed CXCL12 specifically bound to CAF 2 fibroblasts. Furthermore, expression of surface CXCL12 was greater than combined surface and intracellular staining, detected after fixation and permeabilization. This may be due to disruption of the membrane upon permeabilization, as well as changes in epitope structure caused by fixation. These technical caveats make it difficult to determine the proportion of total expression originating from surface or intracellular staining. Thus, while we have shown that CAF1 acts a source of CXCL12, we were unable to confirm increased expression in comparison to CAF2.

On the other hand, little to no C3 was detected on the surface of fibroblast subsets, verifying production of this factor specifically within CAF1 cells. Thus, we also investigated changes in C3 expression at different stages of tumour development (Fig. 4.16 B). Compared to other populations, C3 expression was highest within the CAF1 subset across all time points, including normal skin. However, upon tumour initiation C3 production significantly increased, yet remained consistent from day 5 onwards. This implies that C3 expression is upregulated at early stages and is sustained at a similar level throughout tumour development, reflecting our sequencing

data. Finally, CSF1 could not be detected by flow cytometry, yet IF imaging showed colocalization with CD34^{high} fibroblasts (Fig. 4.16 C). This implies the CAF1 population may represent a significant source, yet it was difficult to determine corresponding levels in other populations as IF quantification is challenging.

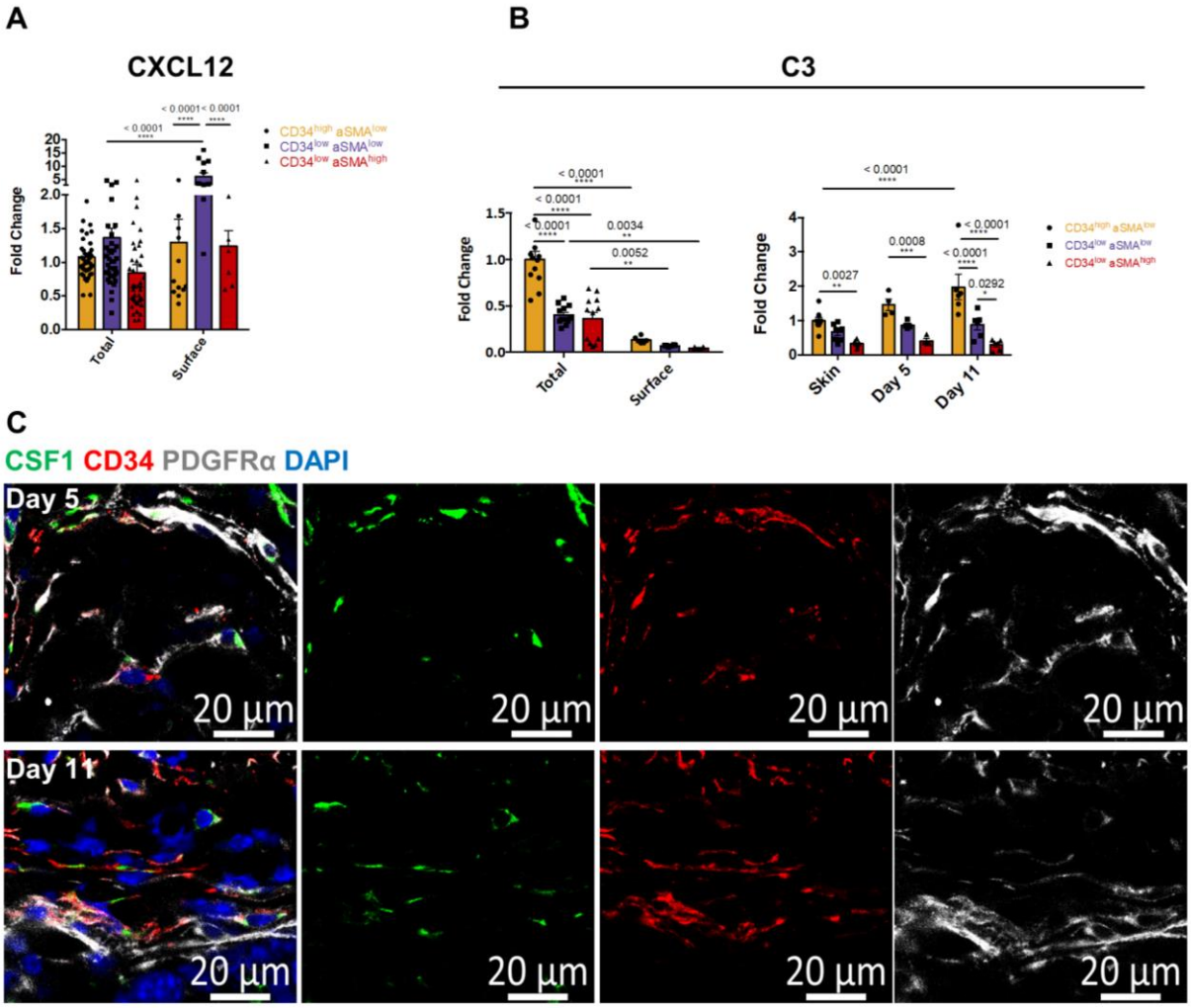

Fig. 4.16 Immune recruitment factors are produced by CAF 1

Flow cytometric quantification of total and surface CXCL12 (A) and C3 (B, left) expression in each population at day 11, presented as fold change in mean fluorescence and normalised to the CD34^{high} αSMA^{low} population. C3 expression was also examined in skin, day 5 and day 11 tumours (B, right) **(C)** Representative confocal images of CSF1 expression in CD34+ CAF populations in day 5 and day 11 tumours, indicated by arrow heads. Scale bars 20um,images represent n=3 (day 5) and n=2 (day 11) independent mice. Data presented as mean ± SEM. * P<0.05, ** P<0.01, *** P<0.001, **** P<0.0001 (A and B (left, C3 total vs surface) two way anova with Sidak post-hoc test, B (right, C3 across time) two way anova with Tukey post-hoc test). CXCL12: n = minimum of 12 mice, C3: day 11 n = minimum of 6 mice, day 5 n = 4 mice, skin n = 6 mice.

4.2.4.4 *Increased matrix deposition was observed at later time points*

To validate the desmoplastic phenotype, we performed confocal imaging of matrix proteins Collagen, Periostin and Tenascin-C, upregulated in CAF2 at the RNA level. Staining of normal skin, day5 and day11 tumours, showed increased matrix deposition at later stages of tumour development (Fig. 4.17). However, staining was mostly extracellular, making it difficult to determine their source. In an attempt to confirm matrix production by CAF2 cells, BFA incubation was performed prior to intracellular staining, yet matrix proteins could not be detected by flow cytometry.

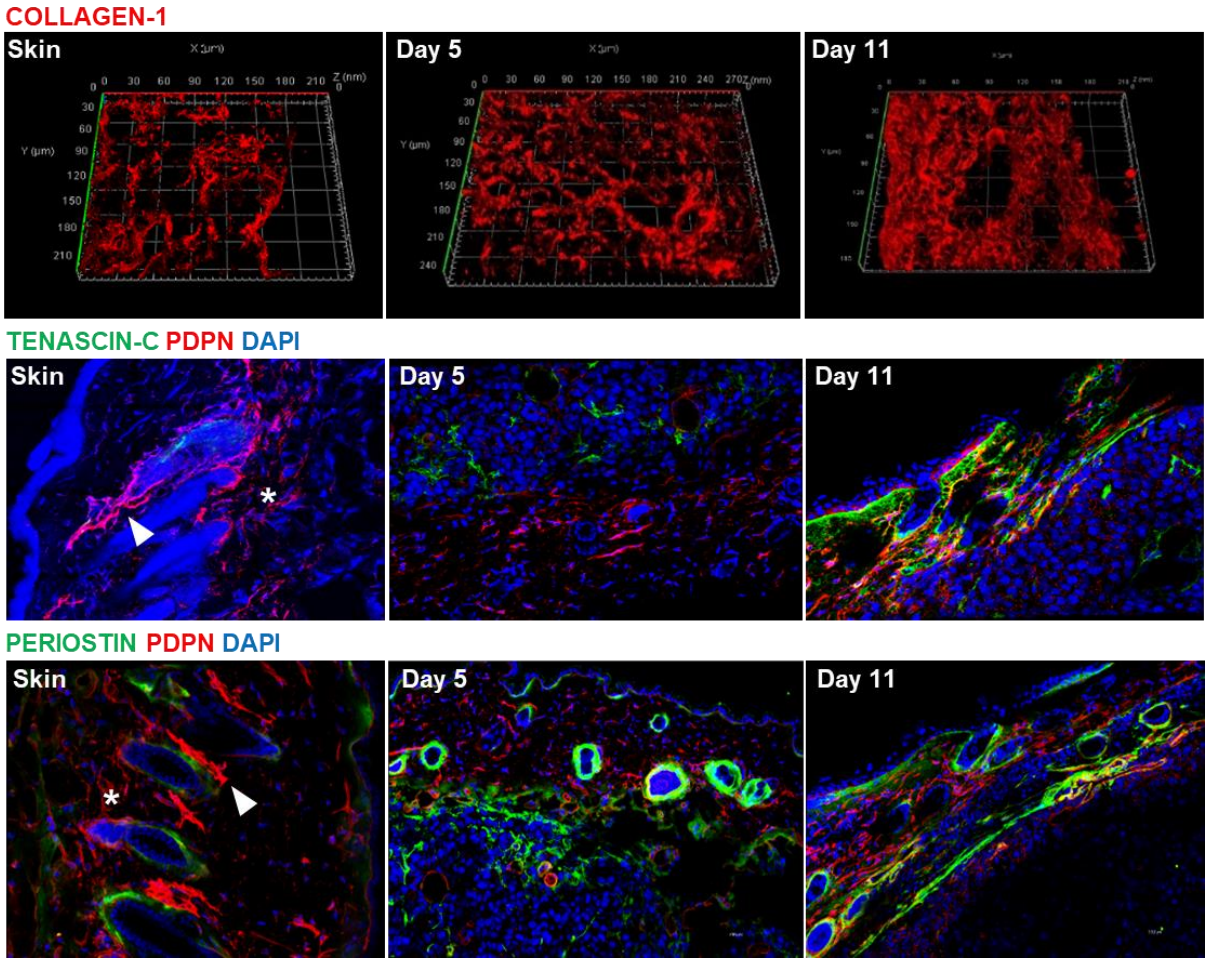

Fig. 4.17 Increased matrix deposition was observed at later time points

IF images of matrix components COLLAGEN (top) TENASCIN-C (centre) and PERIOSTIN (bottom) in skin, day 5 and day 11 samples. In normal skin, bright red ($PDPN^{+}$) structures represent lymphatic vessels (arrow heads) while fibroblasts (*) were mostly restricted to the reticular dermis. COLLAGEN staining is displayed as a 3D reconstruction of z-stack images, while TENASCIN-C and PEROSTIN are shown as compressed z-stack images, in combination with PDPN. n= minimum of 2 tumours per time point.

4.2.4.5 *Validation of CAF phenotypes using in vitro functional assays was technically challenging*

As well as validating expression of specific proteins, we attempted to isolate each population from the tumour microenvironment for *in vitro* functional assays. However, as αSMA is an intracellular protein, it not possible to isolate live cells by antibody staining for FACS sorting. Thus, B16-F10 tumours were implanted into αSMA-DsRed mice, in which the fluorophore DsRed is expressed under the *Acta2* (αSMA) locus. Within the fibroblast compartment, each population was isolated based on CD34 and αSMA expression and seeded for culture (Fig. 4.18 A). However, within 48hs of isolation, live cell imaging showed that all populations developed expression of αSMA, likely due to culture on a stiff plastic surface (Fig. 4.18 B). Furthermore, after 2 weeks tumour cell contamination was significant, leaving only a small population of cells that still expressed CAF markers (Fig. 4.18 C). As B16-F10 tumour cells grow rapidly in culture, even small amounts of contamination can quickly outgrow stromal populations. Thus, to perform further functional phenotyping of this nature, additional optimization will be required.

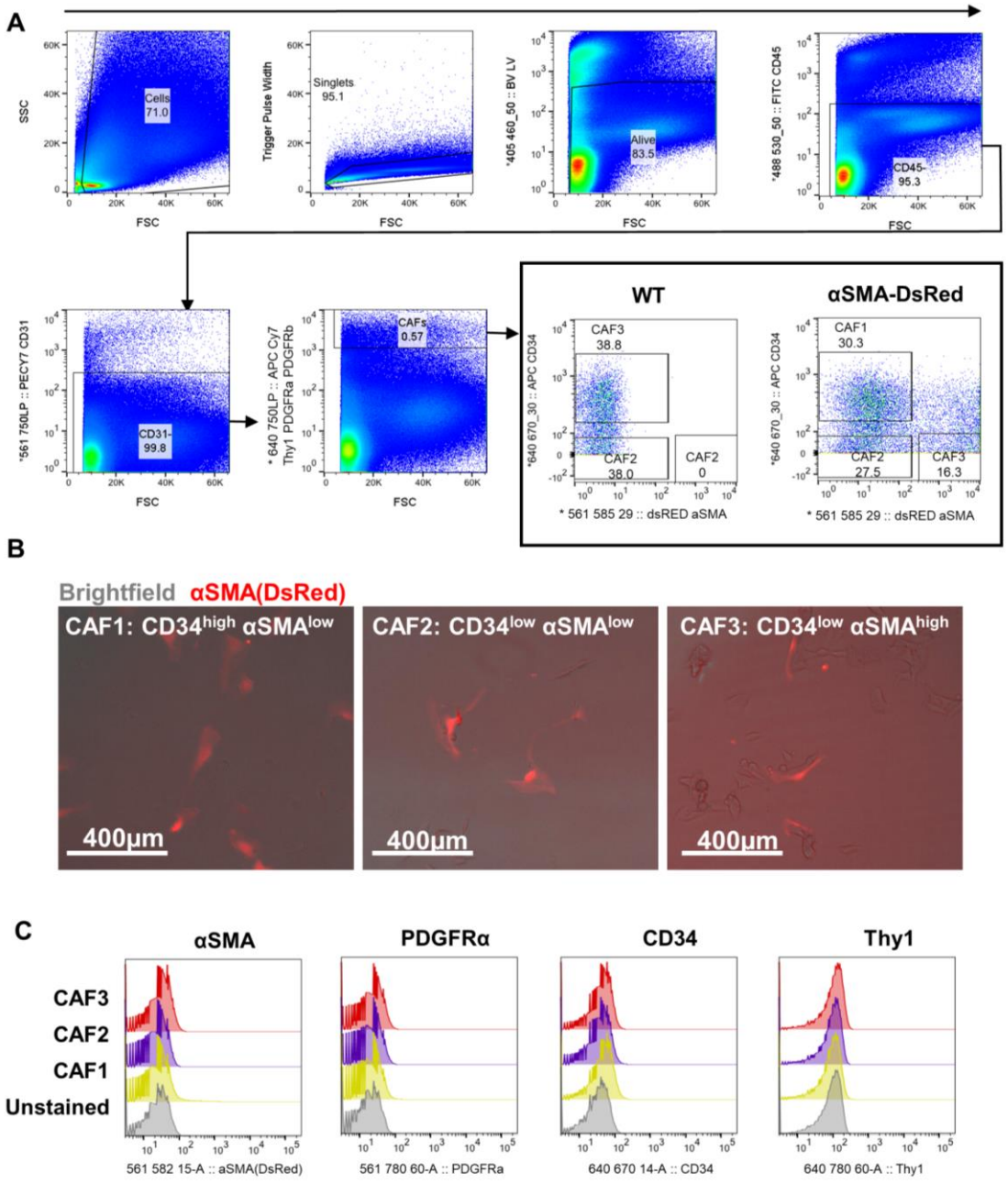

Fig. 4.18 Isolation and culture of CAF populations

(A) Gating strategy describing selection of CAF populations isolated from aSMA-DsRed mice by FACS. Debry, doublets, dead cells, immune cells ($CD45^+$) and endothelial cells ($CD31^+$) were excluded and CAFs were selected by combined expression of PDGFRα, PDGFRβ and Thy1. CAF populations were divided based on CD34 and αSMA (DsRed) expression into CAF1: $CD34^{high}$ $αSMA^{low}$, CAF2: $CD34^{low}$ $αSMA^{low}$ and CAF3: $CD34^{low}$ $αSMA^{high}$. DsRed positive cells were identified by comparison with tumours from WT mice (black box). (B) Merged images showing brightfield and DsRed (aSMA) expression of sorted populations after 48hs in culture. Scale bars 400 µm. (C) Histograms show expression of CAF markers, determined by flow cytometry, in cultured populations after 2 weeks compared to an unstained control.

4.2.4.6 *EdU incorporation reveals different proliferative dynamics between CAF populations*

Sequencing data implied that proliferating populations resided within CAF 2 and CAF 3 subsets, yet not within CAF1. Thus, EdU incorporation was utilised to determine which CAF populations contained actively cycling cells. To investigate which stage of tumour development proliferating CAFs emerge, EdU was injected 24 and 48hs prior to tissue collection and samples were collected from normal skin, day 5 and day 11 tumours (Fig. 4.19 A and B). Interestingly, proliferating cells were observed in all three CAF subsets, yet CAF3 contained the greatest proportion (15-30%), whereas CAF1 and 2 contained 2-10% (Fig. 4.19 C). Furthermore, very few cells within CAF1 and CAF2 actively cycle in normal skin, yet a significant proportion of the CAF 3 population proliferates. However, only a limited number of CAF3 fibroblasts were detected at this time point, possibly skewing this result. Upon tumour initiation the proportion of EdU+ fibroblasts within CAF1 and CAF2 increases, remaining a similar percentage throughout tumour growth. This indicates that the dynamics of fibroblast proliferation, across tumour development, vary between CAF subsets. Interestingly, within the CAF compartment as a whole, the percentage of proliferating cells remains similar between day 5 and 11. Although the total number of cycling cells increases, this is in proportion to the expansion of the CAF compartment (Fig. 4.19 D).

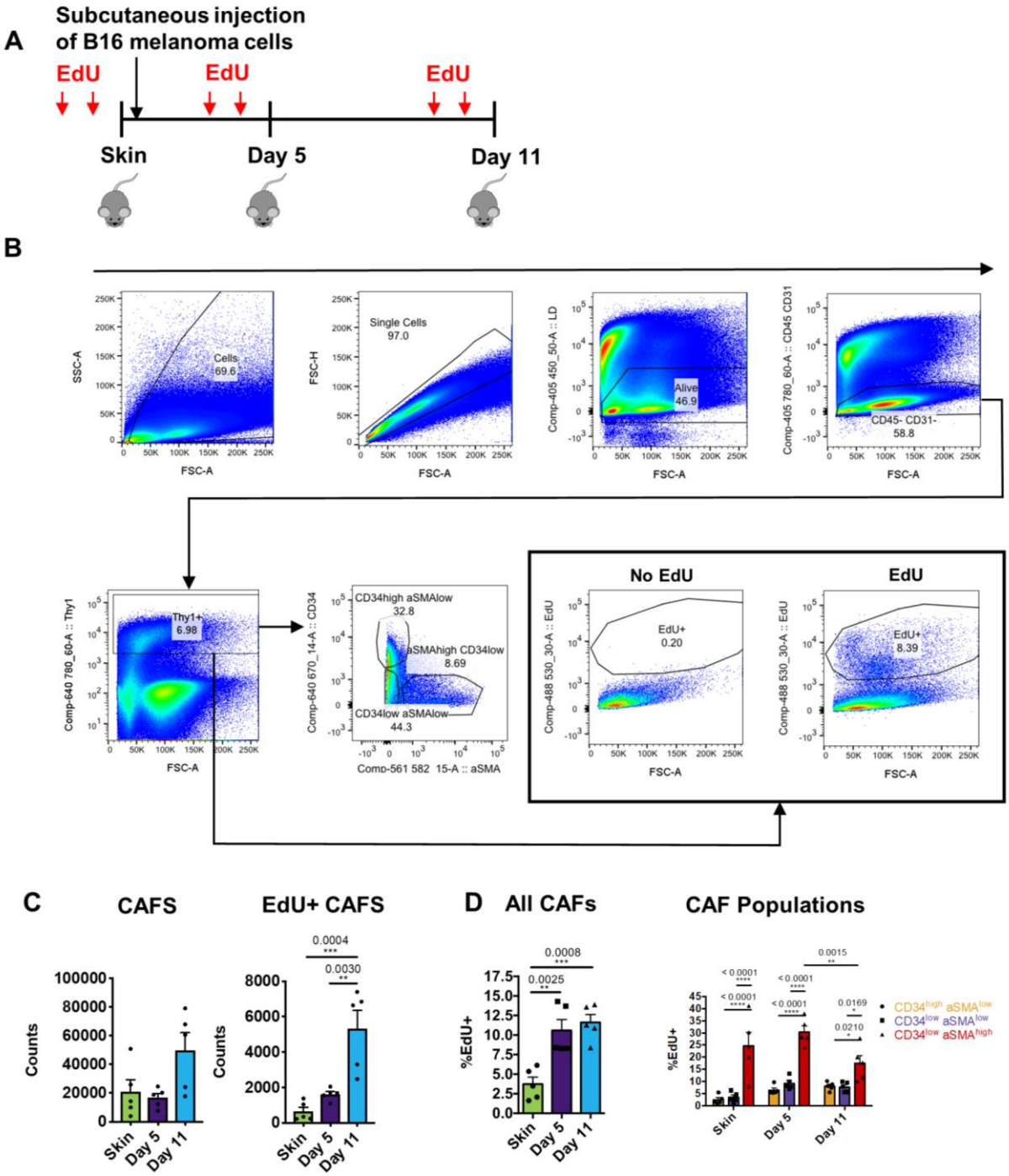

Fig. 4.19 EdU incorporation reveals cycling subsets within all CAF populations

(A) Schematic showing experimental design; EdU was injected 48 and 24hs before samples were collected. Both day 5 and day 11 tumours were isolated from different mice, as well as normal skin. (B) Gating strategy for CAF populations, EdU positive cells were identified by comparing tumours from mice that were not injected with EdU (black box). (C) EdU positive cells as a percentage of individual populations at different time points. (D) Graphs displaying the % EdU positive across all CAFs, as well as raw counts for CAFs and EdU+ CAFs. Data presented as mean ± SEM. * P<0.05, ** P<0.01, *** P<0.001, **** P<0.0001 (C two way anova with Tukey post-hoc test, D one way anova with Tukey post-hoc test), n = 5 mice.

4.2.4.7 *Increased expression of glycolytic enzymes at later time points may reflect the development of tumour hypoxia*

Glycolytic CAF populations were observed in both our pilot study and time course data (Sections 3.2.2.4 and 4.2.2.3). Interestingly, within the latter data set, this metabolic signature was more prominent at later stages of tumour development. We previously showed glycolytic fibroblasts in close proximity to hypoxic regions, suggesting poor perfusion may increase expression of enzymes in this pathway. Therefore, to investigate at what stage of tumour growth hypoxia develops, we stained day 5, and day 11 tumours, as well as normal skin, for the hypoxic marker CA9 and the glycolytic enzymes GLUT1 and LDHA. CA9 staining showed that hypoxia develops at day 5 yet progresses as the tumour grows, forming an extensive hypoxic network by day 11 (Fig. 4.20).

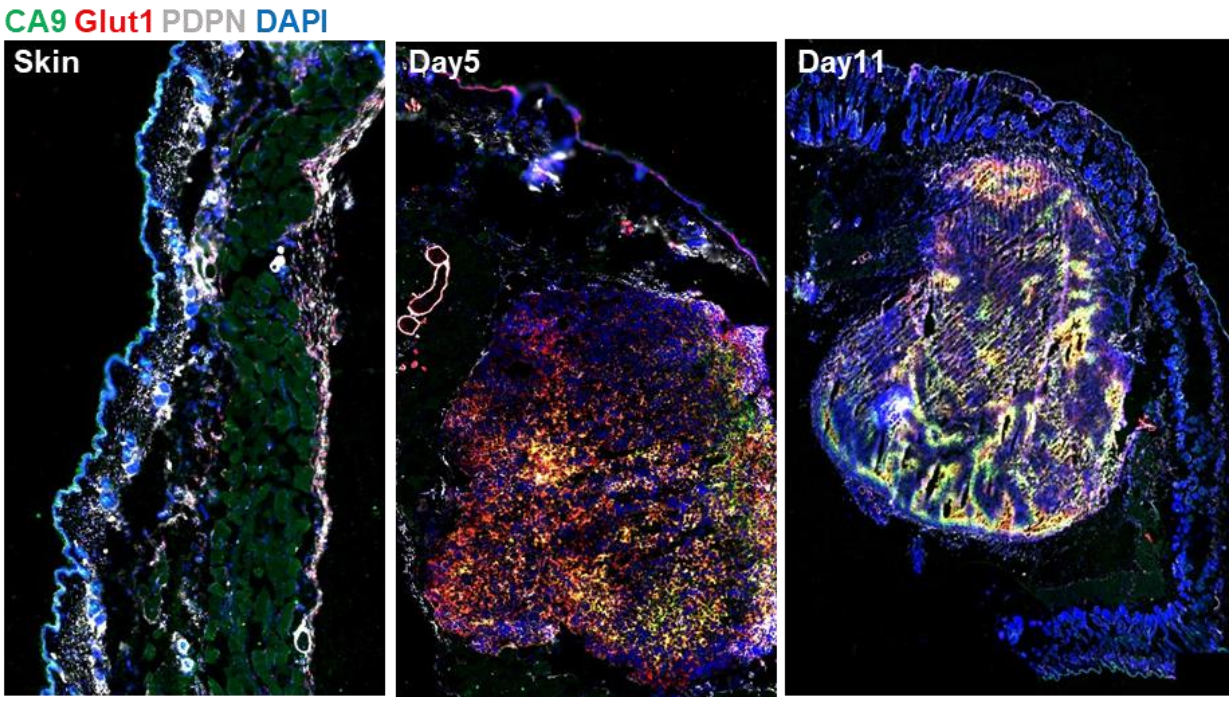

Fig. 4.20 The development of hypoxia across tumour development

Tile scans of Skin from control (non-tumour bearing mice), as well as day 5 and day 11 tumours. Sections were stained for CA9 (green), Glut1 (red), PDPN (grey) and DAPI (blue). Images represent n=2 mice.

4.2.4.8 *CAF 3 express pericyte markers yet were identified dissociated from blood vessels*

On further examination of the CAF 3 subset, we observed expression of several markers associated with pericytes including *Des, Cspg4* (Ng2), *Mcam* and *Rgs5* (Fig. 4.21 A). Pericytes are another member of the mesenchymal family and are associated with blood vessels, regulating their functional properties and providing structural support. However, pericytes share a number of markers with fibroblasts, making these populations hard to distinguish [269]. It is possible that increased vascularisation of the tumour as it grows, is accompanied by an expansion of pericyte populations. If CAF3 comprises pericytes, this may explain the increased prevalence of this population at later time points. However, while pericyte markers were observed within this population, they also express *Aspn (Asporin)*, and matrix components *Fn1* (fibronectin1), *Col1a1*, *Col1a2* and *Sparc*, which are more commonly associated with fibroblasts (Fig. 4.21 A). Furthermore, expression of pericyte markers NG2 and MCAM, have also been observed in fibroblast populations in other studies [273,294,297,299]. The promiscuity of these markers was reflected within our data, as *Des* and *Rgs5* were also expressed by *Pdpn*$^{+}$ fibroblasts of the lymph node (Fig. 4.21 B). Furthermore, examination of our pilot data also revealed expression of pericyte markers dispersed throughout fibroblast populations (Fig. 4.21 C).

For these reasons, discerning the identity of this population based on known markers is difficult. Thus, we investigated expression of CAF3 markers NG2 and αSMA in relation to CD31^{+} endothelial cells. Confocal Imaging revealed NG2^{+} and αSMA^{+} cells in association with blood vessels, indicating there are pericytes present within the tumour microenvironment (Fig. 4.22). However, these cells were mainly located at the periphery, which formally comprised normal skin. While endothelial cells developed in the tumour bulk, these were largely immature and un-supported by pericyte populations. Furthermore, in accordance with sequencing data, both NG2^{+} and αSMA^{+} spindle shaped cells were observed, distinct from the vasculature. Thus, it is possible that the CAF3 subset may contain contaminating pericytes, yet also comprise fibroblast populations that share pericyte markers.

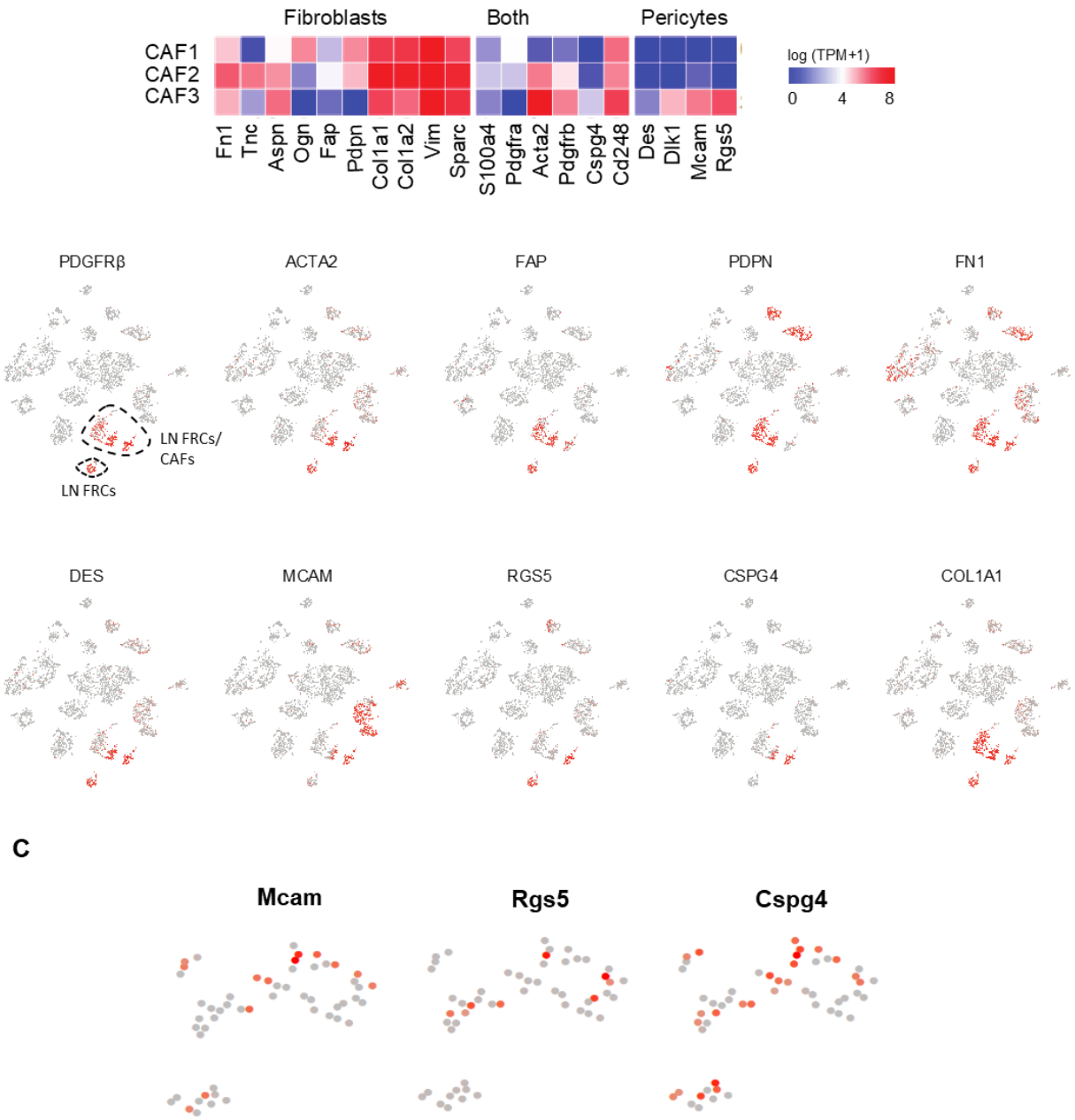

Fig. 4.21 CAF3 express some pericyte markers

Heatmap showing expression of canonical fibroblasts and pericytes markers in the CAF populations. Log(TPM+1) expression is displayed. (B) tSNE plots of all sequenced cells. Expression of typical pericyte markers was also detected in PDPN^{+} lymph node fibroblasts. (C) tSNE plots showing expression of pericyte markers in original pilot data set.

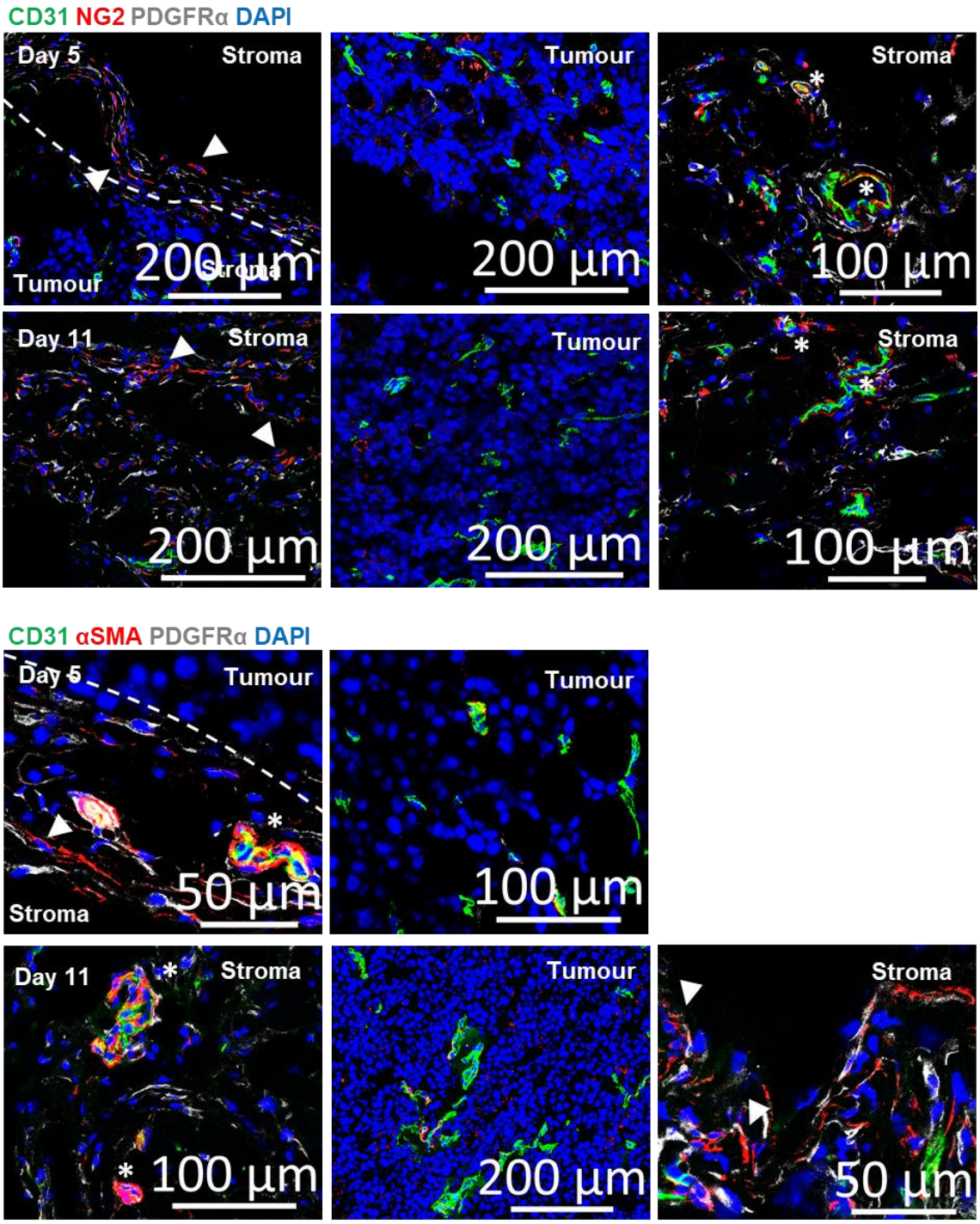

Fig. 4.22 αSMA and NG2 expressing cells were observed dissociated from blood vessels

(A) and (B) IF imaging showing αSMA^{+} and NG2^{+} cells both distinct from (arrow heads) and associated with CD31^{+} blood vessels (*) in peripheral stromal regions of day 5 and day 11 tumours. Vessels in the tumour mass are also shown, which lack pericyte coverage. White dotted lines inidcate boundries between tumour and stromal regions. Images are representative of n=3 tumours, scale bars are displayed.

4.3 *Summary*

To date, only a handful of studies have investigated the differences between fibroblasts from normal tissues and their tumour resident counterparts[192–194], as well as changes in CAF phenotype as the tumour progresses[404]. The discovery of multiple fibroblast populations adds another layer of complexity, as the development of heterogeneity has not been documented. Thus, how these populations arise or whether their composition or phenotype change as the tumour grows, remains unclear. The success of combining negative selection with single cell sequencing (Chapter 3), prompted the application of these techniques to isolate and profile fibroblasts from different stages of tumour growth. This data offered the opportunity to examine the evolution of fibroblast heterogeneity at single cell resolution.

Three distinct CAF populations were uncovered (CAF1-3), displaying different functional signatures and a unique combination of CAF markers. CAF1 fibroblasts expressed cytokines, cytokine receptors and components of the complement cascade, implying a role in immune-crosstalk. On the other hand, the CAF2 population upregulated pathological matrix components such as collagens *Col1a1* and *Col1a2*, *Tnc* and *Postn*. Lastly, the CAF3 subset highly expressed cytoskeletal regulators *Myl9* and *Mylk*, that drive contraction of actin stress fibres. Using flow cytometry and IF imaging we were able to verify presence of these populations within the tumour microenvironment at the protein level, based on expression of CAF markers CD34, PDGFRα, PDPN and αSMA. Furthermore, production of immune regulatory factors CXCL12, CSF1 and C3 by the CAF1 subset was confirmed at the protein level. However, due to technical caveats, only expression of C3 was accurately quantified and shown to be specifically upregulated by this population. In addition, C3 was only investigated at the intracellular level. Thus, whether this factor is actively secreted at by our CAF1 subset remains to be determined. This could be clarified by performing an enzyme-linked immunosorbent assay (ELISA) on isolated populations. However, considering the difficulties associated with *in vitro* culture of CAF subsets, such as the development of αSMA expression and tumour cell contamination, this may be technically challenging. Further technical limitations also prevented validation of CAF 2 and CAF 3 functional signatures. While the development of a fibrotic ECM was

observed as the tumour progressed, it was not possible to identify the source of these matrix components.

Substrate rigidity is known to regulate fibroblast phenotype and increased stiffness can induce activation and expression of αSMA [404–407]. Thus, the stiffness of plastic culture likely induced αSMA expression in isolated CAFs, which may be prevented by culture on collagen gels or in matrigel. While these changes in marker expression may not equate to altered functions, fibroblasts are extremely plastic and likely change their phenotype if removed from their local environment. This was demonstrated by Salzer *et al,* who showed considerable changes in gene expression of fibroblasts isolated from the dermis after one passage [408]. In combination with tumour cell contamination, performing functional assays *in vitro*, will be extremely difficult. Thus, to further validate the functional properties of these populations a different approach must be taken.

Interestingly, proliferating subsets identified in our pilot dataset, were also observed within CAF2 and CAF3 populations but not CAF1. However, EdU incorporation revealed proliferating cells within all CAF subsets, although CAF3 contained the greatest proportion. Mice were exposed to EdU for 48hs prior to sample collection, enabling all cycling cells to incorporate this label and suggesting only a subset in each population actively divide. In the absence of pathology, fibroblasts are described as quiescent and their expansion in disease has been attributed to increased proliferation [409]. Our results support this model in part, as the number of cycling cells in CAF 1 and 2 increased upon initiation of malignant growth. Furthermore, this pool of cycling cells expanded in tandem with the CAF compartment, potentially driving its growth. While proliferating cells within the CAF 3 subset were present in normal skin, very few cells were detected at this time point, possibly biasing these results. It remains unclear whether proliferating cells represent an isolated population undergoing continuous self-renewal, or if cells inter-change between quiescent and cycling phenotypes. This could be investigated by BrdU and EdU double labelling, in which cells are initially labelled with BrdU, followed by EdU at a later stage. The presence of single positive BrdU cells would suggests fibroblasts proliferate for a limited period of time.

Sequencing fibroblasts from different stages of tumour progression revealed a dynamic fibroblast niche, in which the composition of populations changed as the tumour progressed. However, it is unclear whether these subsets represent discreate

populations that emerge and regress at different stages, or phenotypic states in which fibroblasts transition. Our sequencing data suggests that CAF1 may represent resident fibroblasts, that dominate at early stages of tumour development yet recede at later time points. A decrease in this population was also concomitant with the emergence of the CAF 3 subset. As pseudo-time analysis ordered CAFs in a trajectory from CAF1 to CAF2, and CAF2 to CAF3, it is tempting to suggest this reflects differentiation from resident CAF1 fibroblasts, towards an activated 'CAF3' state.

However, this hypothesis was not supported by experimental validation which showed both $CD34^{high}\alpha SMA^{low}$ CAF1 and $CD34^{low}\alpha SMA^{low}$ CAF 2 fibroblasts were present in skin samples. Furthermore, while the expansion of the CAF3 population at later time points was confirmed, the proportion of CAF1 fibroblasts remained consistent. In addition, the presence of a proliferating pool within each CAF subset suggests populations are maintained separately. Growth of the CAF 3 population at later time points may be explained by increased proportions of cycling cells within this group. Moreover, the presence of multiple populations in normal skin has been previously documented[291,293,410] and raises the possibility that CAF populations pre-exist in the absence of pathology. Whether certain populations are specifically expanded upon tumour onset is unknown. Although differential marker expression suggested heterogeneity, our data also showed a significant increase in both C3 and ECM production upon tumour formation. Thus, while these populations may be present in normal skin, their functional properties are still manipulated in the presence of malignant cells. Indeed, whether fibroblast populations are pre-disposed to specific functions, or are entirely regulated by their local environment, is an interesting question.

Overall, it is unclear whether CAF populations expand independently or represent different stages in a differentiation trajectory. It is also possible that discrete subsets exist yet, due to their innate plasticity, CAFs may freely transition between populations. However, this is difficult to determine in the absence of lineage tracing experiments. Regardless of whether populations are related, increased heterogeneity was observed in more advanced tumours. The emergence of the CAF3 subset was likely induced by changes in soluble factors, such as cytokines and growth factors, as well as mechanical cues. Furthermore, the development a hypoxic network may drive the appearance of 'glycolytic' subpopulations at later time points. This highlights how

environmental pressures, that arise as a consequence of tumour growth, can induce further heterogeneity. The local microenvironment is a critical regulator of fibroblast phenotype, thus the turbulent and evolving atmosphere of a developing tumour inevitably induces diversity.

Owing to the expression of markers such as *Rgs5*, *Cspg4* (Ng2) *Mcam* and *Des*, it is possible that the CAF3 population may contain pericyte contamination. However, all of these markers have been reported in fibroblast populations [214,298,299,411] and both *Rgs5* and *Des* were observed in lymph node FRCs, a phenomenon previously reported [412]. Furthermore, CAF3 also produced matrix components such as *Col1a1, Col1a2*, *Fn1* and *Sparc* which indicate a fibroblast phenotype. Thus, it is difficult to distinguish CAFs from pericytes based on marker expression, emphasizing the poor characterisation of the mesenchymal compartment.

Consequently, to differentiate pericytes from fibroblasts, association with the vasculature was examined. While aSMA and NG2 expressing cells were observed surrounding vessels, the majority of new vessels formed in the centre of the tumour and were not accompanied by pericytes. Furthermore, cells expressing these markers were also present dissociated from the vasculature in peripheral regions. Therefore, CAF3 may represent a mixed population of mesenchymal cells that share similar surface marker expression and functional properties. Other studies have attempted to remove pericytes, based on NG2 expression, yet populations expressing pericyte markers were still isolated. The close relationship between these populations has led the suggestion that pericytes may act as source of CAFs in the tumour microenvironment. This has been reported during liver and kidney fibrosis, as well as tumour development [270,271,273,298,411]. Thus, it is possible that the CAF3 population may be pericyte derived.

Having identified distinct CAF populations within the melanoma microenvironment, we next wished to investigate how each subset influences tumour growth. In particular we have focussed on the CAF 1 population, which has been implicated in immune cross-talk. Yet, it is unclear with which immune populations these CAFs are interacting and whether the promote anti-tumour immunity or induce tolerance. To explore this in more detail, we have examined the immune-stromal compartment which was also sequenced as part of this study. Other key questions include how these populations

arise and whether similar populations exist in other tumour types, as well as human cancer. These themes were explored in the following chapter, providing more function and global relevance.

5

Investigating the functional significance of CAF populations in melanoma and their conservation in other cancer types

5.1 *Introduction*

scRNA sequencing of B16-F10 melanomas revealed a diverse CAF compartment, whose composition changed in as the tumour develops. 3 phenotypically distinct populations were identified and validated, including 'immune' CAF1, 'desmoplastic' CAF2 and 'contractile' CAF 3 subsets. However, whether these fibroblast subsets promote or inhibit tumour development remains elusive. Thus, in this chapter the functional significance of these populations in the tumour microenvironment was investigated. In particular, we focussed on CAF1 fibroblasts, which were implicated in immune-cross talk. Here, scRNAseq data from immune cells, isolated in parallel to fibroblasts, was used to assess immune phenotypes and identify potential interactions. This data, in combination with *in vivo* functional studies, was used to examine the role of CAF1 populations in the development of tumour associated inflammation.

What drives the formation of different CAF populations is another pertinent question. One potential source of heterogeneity is the different origins from which CAFs are derived. We have previously discussed that pericytes may contribute to CAF3 populations in B16-F10 melanoma. However, assessing this *in vivo* would require lineage tracing models. Bone marrow mesenchymal cells have also been reported to migrate and form populations in the primary tumour [274,275,278]. Thus, bone marrow chimeric mice were used to investigate the contribution of this compartment to CAF subsets in melanoma.

Lastly, whether the three CAF populations identified are specific to melanoma or are present in other cancer models is unclear. Therefore, using additional murine models and publicly available sequencing data, conservation of these CAF subsets was explored in different cancer types. Publicly available data was also used to investigate whether these populations were present in human tumours. This revealed the translational relevance of our findings and potential for therapeutic intervention.

5.2 *Results*

5.2.1 *Characterising the Immune Compartment*

To uncover the role of the 'immune' CAF1 population in shaping the tumour immune landscape, it was first necessary to characterise infiltrating leukocyte populations. Thus, scRNAseq data from immune populations, isolated in tandem with CAFs, was used to evaluate their respective phenotypes in both the primary tumour and draining lymph node. Initial clustering of immune cells was performed by Dr. Mirjana Efremova. Together we identified specific immune-subsets and investigated their phenotypes.

5.2.1.1 *T-cells*

As previously discussed (section 1.1.1.1), the presence and functional status of T-cells is a key determinant of disease outcome [13–17,40–44] . Thus, to determine if immune populations support or inhibit in the melanoma development in this model, initial investigations focussed on T-cell phenotypes. Clustering revealed the presence of classical CD8 and CD4 T-cells, as well as γδ, MAIT and iNK T-cells (Fig. 5.1 A). The latter were identified by expression of *Trdc1* (T-cell receptor δ constant region 1) *Trdgj1* (T-cell receptor γ joining region 1), *Trdgj2*, *Klrb1a* and *Klrb1b* (NK1.1) (Fig. 5.1 B). Interestingly, *Foxp3* expressing T-regs were only detected in the primary tumour, suggesting they are enriched at this site compared to the lymph node.

Furthermore, CD8 and CD4 T-cells clustered according to their location in either the tumour and lymph node, indicating site specific programmes. Crucially LN T-cells expressed naïve markers (*Sell*, *Tcf7* and *Lef1*), whereas activation markers (*CD44*, granzyme enzymes and *Ki67*) were highly expressed by T-cells at the tumour. However, tumour resident T-cells also expressed dysfunction markers (*Lag3*, *Pdcd1* (Pd1), *Clta4 and Tigit)*, suggesting T cells may be more activated in the primary tumour yet become exhausted (Fig. 5.1 C).

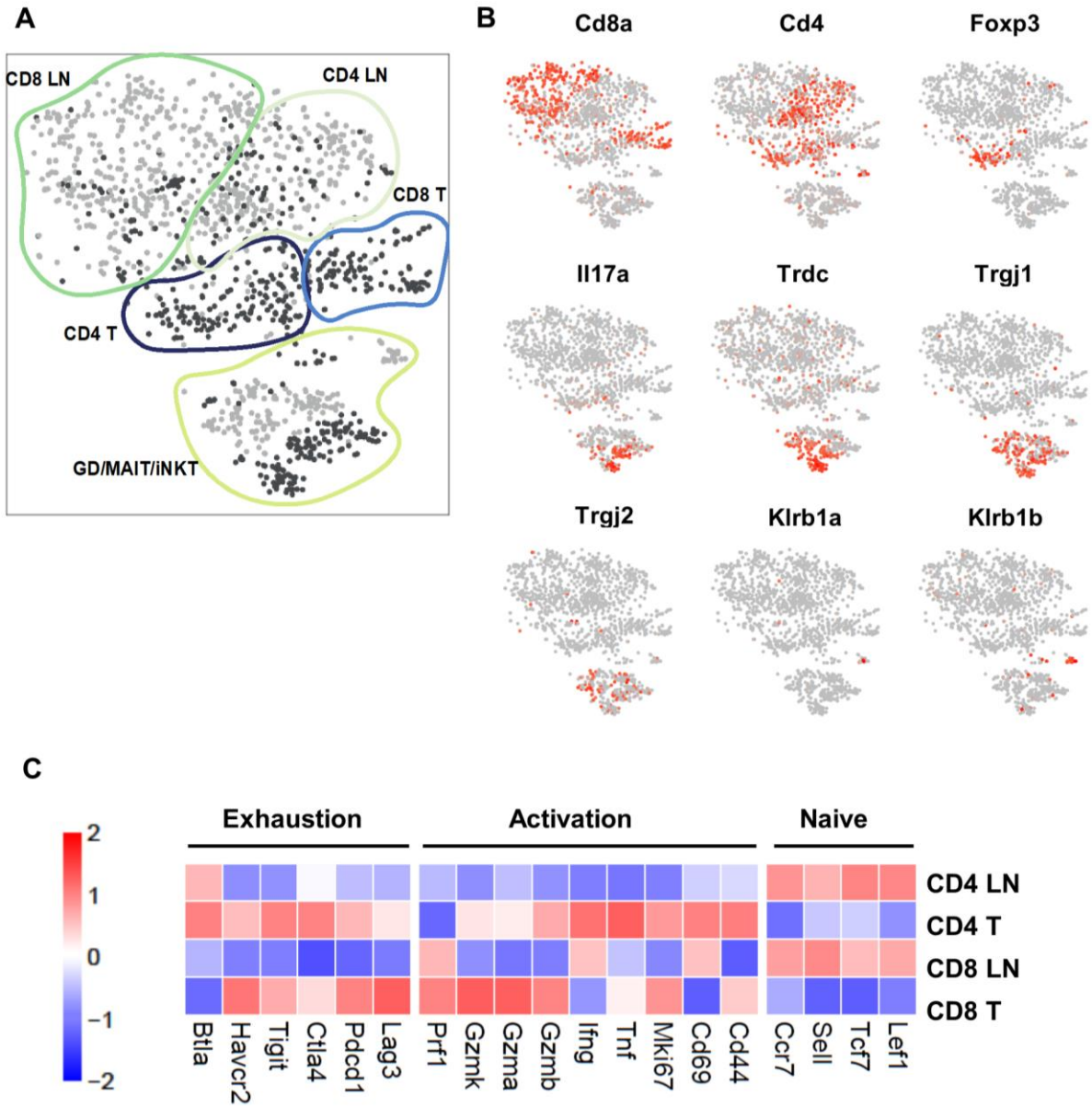

Fig. 5.1 Multiple T-cell populations were identified

1298 T-cells were selected based on CD3e expression and re-clustered. (A) tSNE plot showing T-cell subsets, produced my Dr. Mirjana Efremova and coloured according to location (T tumour (black), LN lymph node (grey)). (B) tSNE plots showing expression of genes associated with T-cell subsets, red indicates high expression grey indicates low expression. (E) Heatmap showing expression of naïve, activation and exhaustion markers in lymph node and the tumour T-cell populations. Expression was averaged across each population and z scores are displayed.

5.2.1.2 *Pseudo-time analysis showed CD8 T-cells become activated and display dysfunctional markers in the primary tumour*

In particular, CD8 T-cells have the ability detect and kill tumour cells [11,12]. Thus, their activation and function are critical for tumour growth and progression. Having shown a difference in the maturation state of these cells, between the LN and tumour sites, pseudo-time analysis was employed to further investigate differentiation in a malignant context. Strikingly, this trajectory ordered CD8 T-cells from the lymph node towards the tumour (Fig. 5.2 A and B). As we also possessed “real time” data, this could be mapped onto the trajectory, confirming that within the tumour compartment, cells were organised from early to late time points (Fig. 1.5 B). Furthermore, expression of naïve markers decreased from the LN towards the tumour, while activation and exhaustion markers increased (Fig. 5.2 A and C). The smart seq2 protocol also enables sequencing of the TCR and identification of clonal cells. This analysis was performed by Dr. Mirjana Efremova and showed that T-cells clonally expanded specifically within the tumour compartment (Fig. 5.2 B). Thus, in contrast to the current dogma, our results indicate that CD8 T-cells leave the lymph node naïve and are activated in situ at the primary tumour. Here, they clonally expand and ultimately become dysfunctional. This was supported by experimental validation which showed an increase in the number of PD1+ and Ki67+ CD8 T-cells in the tumour compared to the lymph node, particularly at day 11 (Fig. 5.2 D). While proliferating cells were identified in the lymph node, their proportion was consistent between tumour draining nodes and those isolated from control mice.

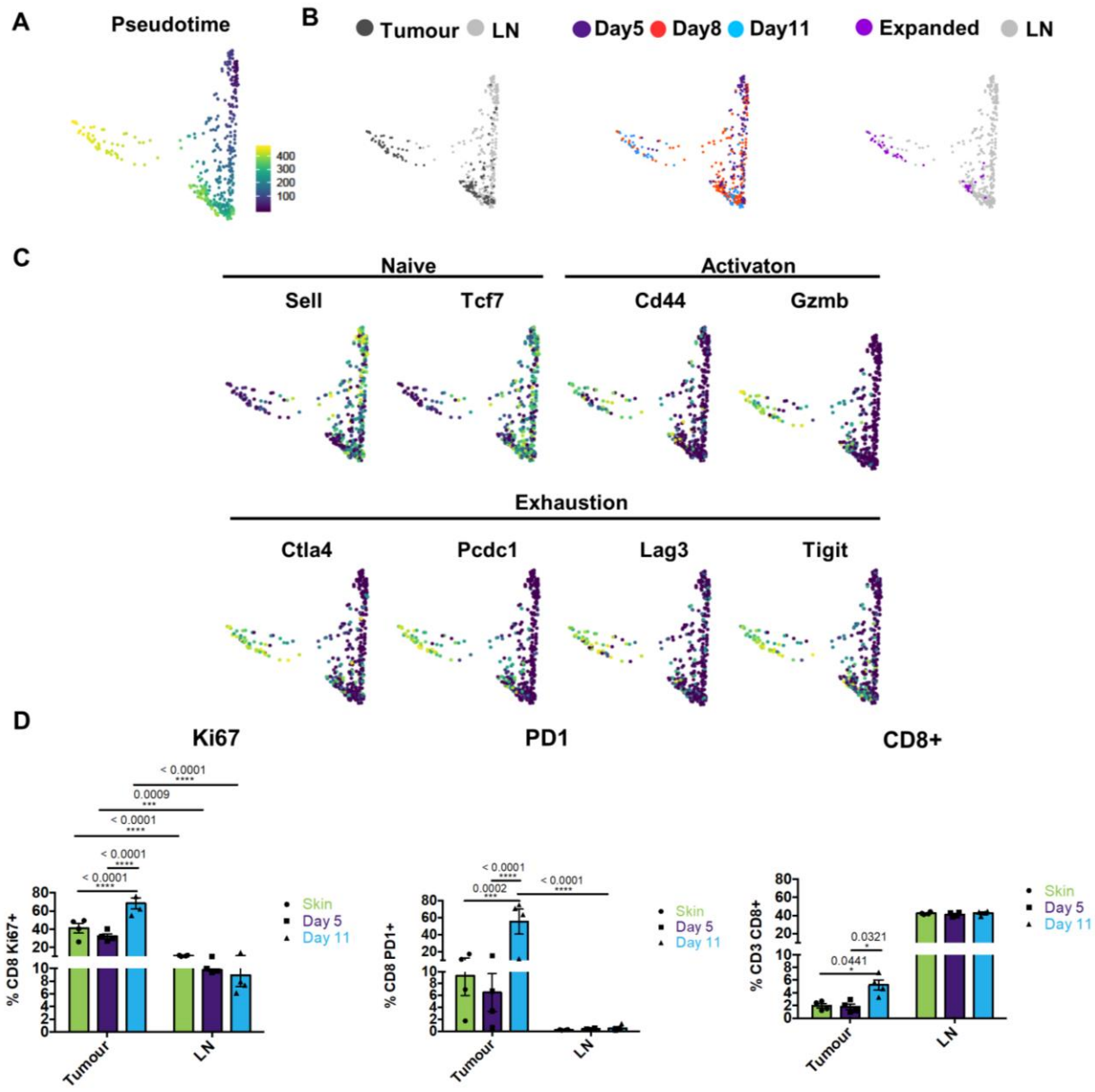

Fig. 5.2 Diffusion maps and pseudo-time analysis suggests T-cell activation occurs in the tumour and the development of dysfunctional markers at later time points.

(A) Diffusion maps showing the DPT trajectory (left), blue indicates cells that are closely related to the starting or (tip) cell, whereas as yellow indicates cells that are more distant. (B) Diffusion maps coloured according to the location (left) and time points (centre) from which each cell was isolated. Clonally expanded cells were determined by matching TCRs and shown on the diffusion map (right). Clonally expanded cells were identified by Dr. Mirjana Efremova, while I produced diffusion maps and DPT analysis (C) Diffusion maps coloured according to the expression of selected genes. Blue indicates low expression, while yellow indicates high expression. (D) Percentage of Ki67 and PD1 expressing CD8 T-cells (% CD8) and the number of CD8 T-cells (% CD3e) in the tumour and draining lymph node at different time points. Data presented as mean ± SEM. * P<0.05, ** P<0.01, *** P<0.001, **** P<0.0001 (two way Anova with Sidak post-hoc test), n=4 mice per condition.

5.2.1.3 ***Innate Immune Populations***

The innate arm of the immune system is able to detect the presence of tumour cells and coordinate an adaptive response. However, these cells are often corrupted by the tumour, supporting its growth and promoting immune tolerance [7]. Owing to their ability to both stimulate and supress T-cell functions, innate populations may regulate the sequential development of lymphocyte activation and dysfunction in the primary tumour. Thus, to investigate which populations were present, as well as their phenotypes, T and B cells were removed from analysis (based on Cd3e and CD19 expression) and the remaining populations re-clustered (Fig. 5.3 A). Cells formed 10 distinct subsets which were identified as NK cells, Phagocytes and multiple DC populations, based on common markers: NK: *Ncr1, Prf1* (Perforin), phagocytes: *Itgam* (Cd11b), DCs: *Itgax* (Cd11c). Cluster 8 was composed of cells in which a low number of detected genes and was excluded from the analysis (Fig. 5.3 B and C). Further investigations into marker expression enabled more detailed phenotyping of innate populations. The majority of Phagocytes expressed *Adgre1* (F4/80), indicating significant macrophage infiltration. However, some *Ly6g* and *Ly6c* positive cells were also observed, which likely represent neutrophils and monocytes respectively (Fig. 5.3 D). It is possible this cluster also contains MDSCs, however it is difficult to identify these cells based on marker expression. On the other hand, classical DC populations cDC1 and cDC2, as well as plasmacytoid DCs (pDCs), clustered separately. These were identified based on expression of cDC1: *Clec9a, Tlr3, Tlr11, Ly75,* and *Xcr1*, cDC2: *Cd11b*, *Fcγr1* and *Sirpa*, pDC: *Bst2* and *Siglech*. Cluster 3 represented a lymph node resident *Cd11b Cd11c* double positive population, witch expressed both cDC2 markers as well as Monocyte/macrophage markers such as *Cx3cr1* (Fig. 5.3 D and E).

Interestingly, DC clusters also separated according to their location in the tumour or lymph node. Similar to T-cells, this suggests these cells possess site-specific transcriptional signatures. cDC1 cells in the tumour expressed the dermal marker *Itgae* (CD103), a marker that defines populations known to migrate to the LN and cross present antigen to CD8 T-cells. However, their lymph node counterparts expressed CD8a, suggesting these cells represent LN resident populations and have not

migrated from the tumour. Nevertheless, expression of *Ccr7* by *Cd103*+ DCs implies these cells are capable of trafficking to secondary lymphoid organs (Fig. 5.3

E). Clusters 5 and 7 also represented closely related populations separated by location, yet their identity was difficult to define. Low expression of myeloid markers *Cd11b* and *Cd11c* and high expression of the *Il7r*, initially indicated an innate lymphoid phenotype. However, expression of other innate lymphoid markers, as well as mast cell and eosinophil markers *Siglecf*, *cd200r3* and *Enpp3* and *Fcε1* were very low or undetected. On the other hand, DC transcription factors such as *Flt3*, *Baft3*, *Zbtb46* and *Id2* were highly expressed. Interestingly, in addition to classical *CD103*+ DCs, the tumour resident half of this population (cluster 5), also expressed *Ccr7* (Fig. 5.3 E). This suggested these cells also traffic to the lymph node, thus were termed migratory DCs (migDC). However, these cells may represent DC progenitors, although low expression of *Kit* and *Cd34* implies they are restricted to a pre-DC phenotype.

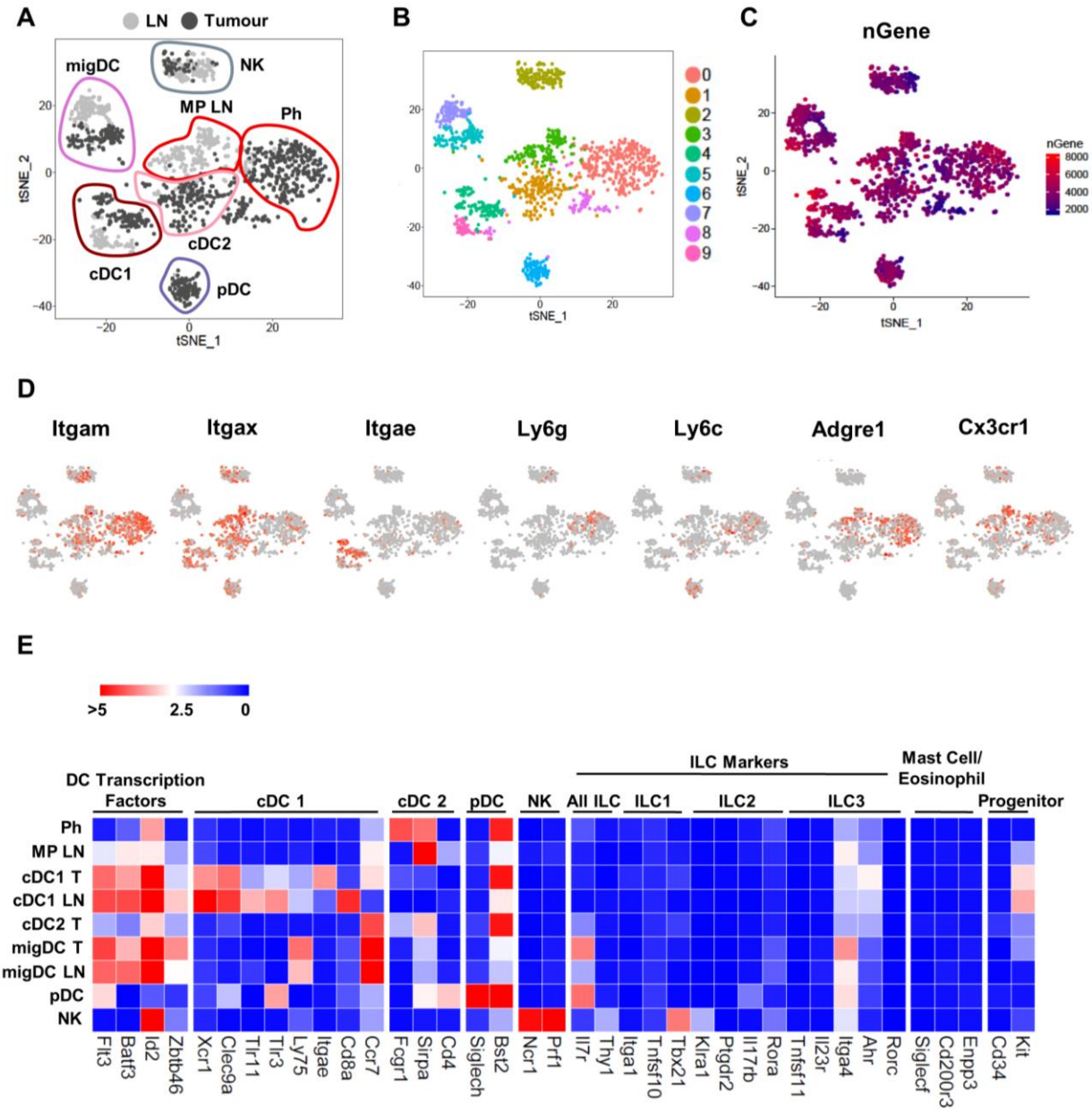

Fig. 5.3 NK cells, Phagocytes and numerous DC populations were identified in the innate compartment

T and B cells were excluded based on Cd3e and Cd19 expression and the remaining 1444 immune cells were re-clustered. (A) tSNE plots coloured according to location, the assigned cell identity based on (D and E) are shown. tSNE plots showing the original clusters identified (B) and the number of genes detected (C) and expression of selected genes (D). (E) Heatmap showing expression of innate cell markers across all populations, Log(tpm+1) is displayed. Ph: Phagocytes, NK: NK cells, MP LN: Mononuclear Phagocytes Lymph Node, cDC1: Classical DC 1, cDC2: Classical DC 2, pDC: plasmacytoid DC, migDC: migratory DC. T and LN denote tumour and lymph node respectively. (A) and (B) were produced by Dr. Mirjana Efremova, I produced all other plots.

5.2.1.4 *Innate cells were more activated yet suppressive in the tumour compared to the lymph node*

To assess interactions that may dictate T-cell function, expression of known costimulatory molecules, inflammatory cytokines and suppressive factors were investigated (Fig. 5.4 A). Interestingly, costimulatory molecules and inflammatory factors such as *Pvr*, *Il1b* and *4-1bbl* were upregulated in tumour resident DC populations, compared to those in the lymph node. While expression of suppressive molecules *Pdl1* and *Gal9*, as well as *Pdl2* were increased in tumour cDC1 and migDC subsets respectively. The observation that the innate compartment within the tumour may be more inflammatory, yet also suppressive, was counterintuitive, hence this phenotype was investigated further by examining expression of these molecules at different time points. This revealed that expression of *Arg1* in Phagocytes and *Pdl1* in both Phagocytes and cDC1 cells, increased at later time points. Furthermore, increased expression of these factors in CD11b+ cells was confirmed at the protein level, implying populations may become more suppressive as the tumour develops (Fig. 5.4 B). Functional differences between tumour and lymph node populations, as well as changes over time are summarised in Fig. 5.5.

Another feature of tumour associated inflammation is the polarisation of macrophages from an M1 to an M2 phenotype. However, macrophages in this data set expressed a collection of typical M1 and M2 markers, making it difficult to determine their polarisation state (Fig. 5.4 C). However, as discussed above, expression of suppressive markers *Pdl1* and *Arg1* suggest they promote immune tolerance. This is consistent with current thinking, in which polarisation states are insufficient to describe tumour macrophage populations. Instead, it is better to categorise these cells according to specific functional properties.

Overall, the innate compartment mirrors the adaptive, showing heightened inflammatory phenotypes within the tumour, compared to the lymph node, as well increased expression of suppressive molecules at later time points. Thus, it is possible that upregulation of costimulatory molecules and inflammatory cytokines, by tumour resident innate populations, is responsible for T-cell activation at this site. Furthermore, increased expression of PDL1 and ARG1 may contribute to the

development of T-cell dysfunction at later stages. This suggests melanomas cultivate an immunosuppressive environment to prevent detection and enable their growth.

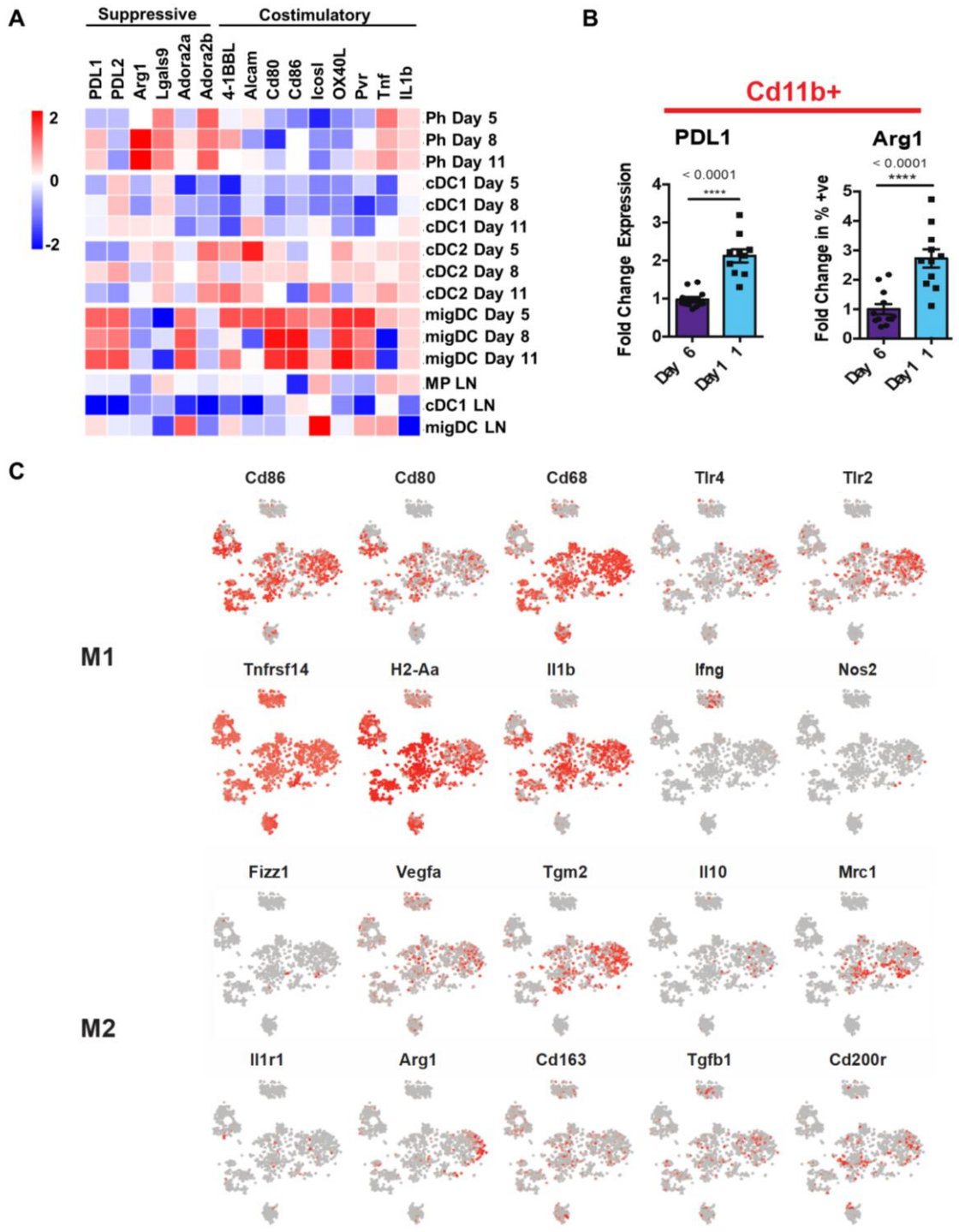

Fig. 5.4 Myeloid cells are more activated yet suppressive in the tumour compared to the lymph node

(A) Heatmap displaying expression of suppressive and costimulatory molecules across location and time points. Z score is displayed. (B) Flow cytometry data showing mean fluorescence intensity of PDL1 and percentage ARG1+ cells in CD11b+ myeloid populations, normalised to day 6. (C) tSNE plots showing expression M1 and M2 markers, red indicates high expression and grey indicates low expression. **** P<0.0001 (T-test), B: n=12 mice per condition. Ph: phagocytes, MP LN: mononuclear phagocytes lymph node, cDC1: classical DC 1, cDC2: classical DC 2, migDC: migratory DC.

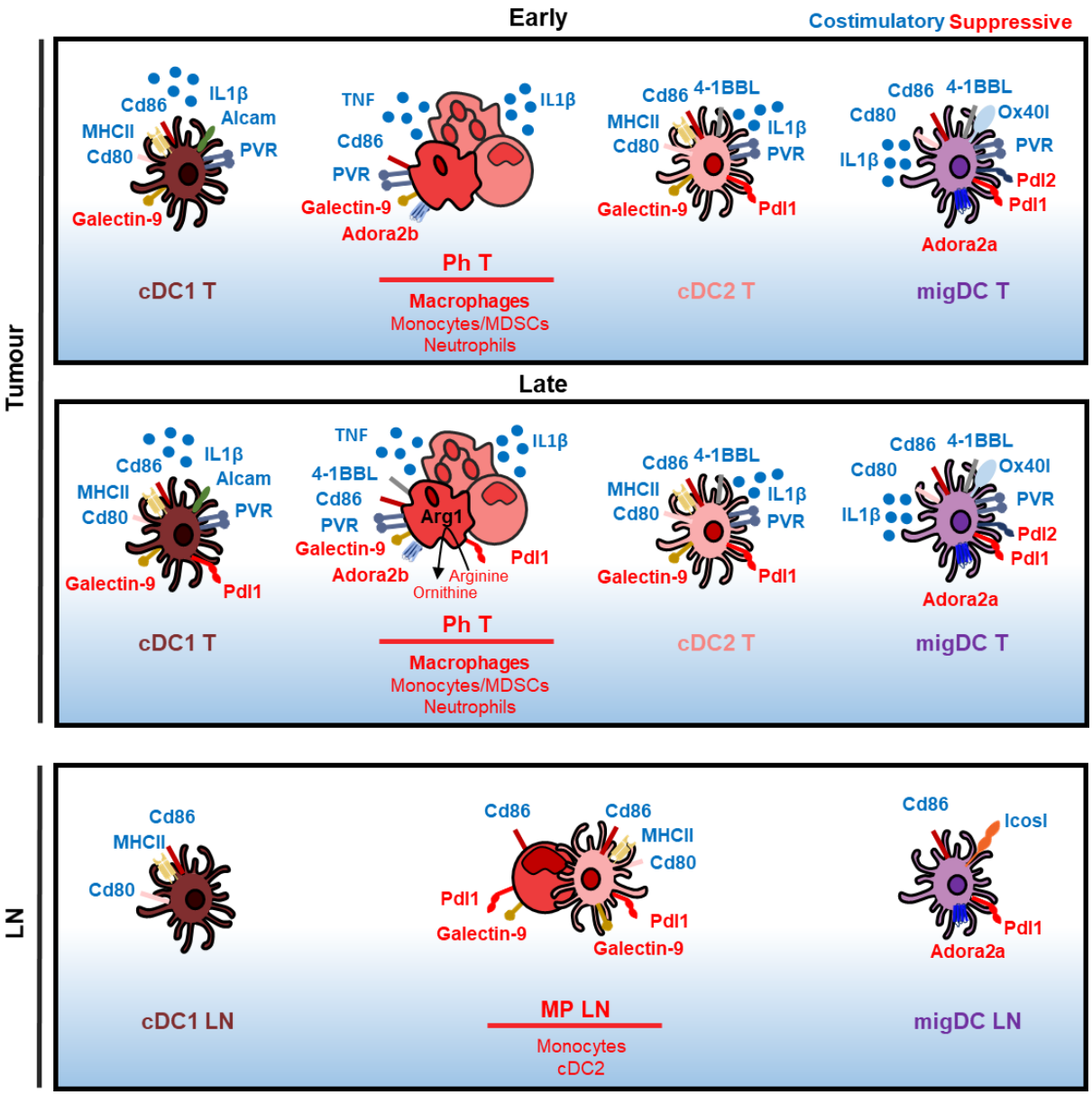

Fig. 5.5 Phenotypes of myeloid cells in the tumour and the lymph node.

Schematic depicting the expression of costimulatory and suppressive molecules on myeloid cells in the lymph node and at early and late time points in the tumour. Blue indicates costimulatory molecules and red indicates suppressive molecules. All molecules are significantly de-regulated between conditions. Ph: phagocytes, MP LN: mononuclear phagocytes lymph node, cDC1: classical DC 1, cDC2: classical DC 2, migDC: migratory DC.

5.2.2 *Examining the role of 'immune' CAF1 fibroblasts in the development of an immunosuppressive microenvironment*

5.2.2.1 *The CAF1 population may be involved in cross-talk with tumour macrophages*

Having discovered the development of an immunosuppressive microenvironment, we next sought to identify the role of the CAF1 population in this process. In particular, this subset secreted immune recruitment factors CXCL12, CSF1 and C3, of which the latter is cleaved to produce the anaphylatoxin C3a. Thus, to infer potential immune interactions, expression of their cognate receptors *Cxcr4*, *Csf1r* and the *C3ar* was investigated (Fig. 5.6 A). While *Cxcr4* and the *Csf1r* were expressed on T-cell populations and cDC2 cells respectively, all three receptors were expressed by Phagocytic cells. As macrophages were the most dominant population within this cluster, this suggests CAF1 fibroblasts may be involved in their recruitment or regulation. Furthermore, confocal imaging of tumour sections using macrophage marker F4/80 showed macrophages expressing all three receptors adjacent to $CD34^{high}$ CAFs (Fig. 5.6 B). The close proximity of these populations affords potential for these cells to interact.

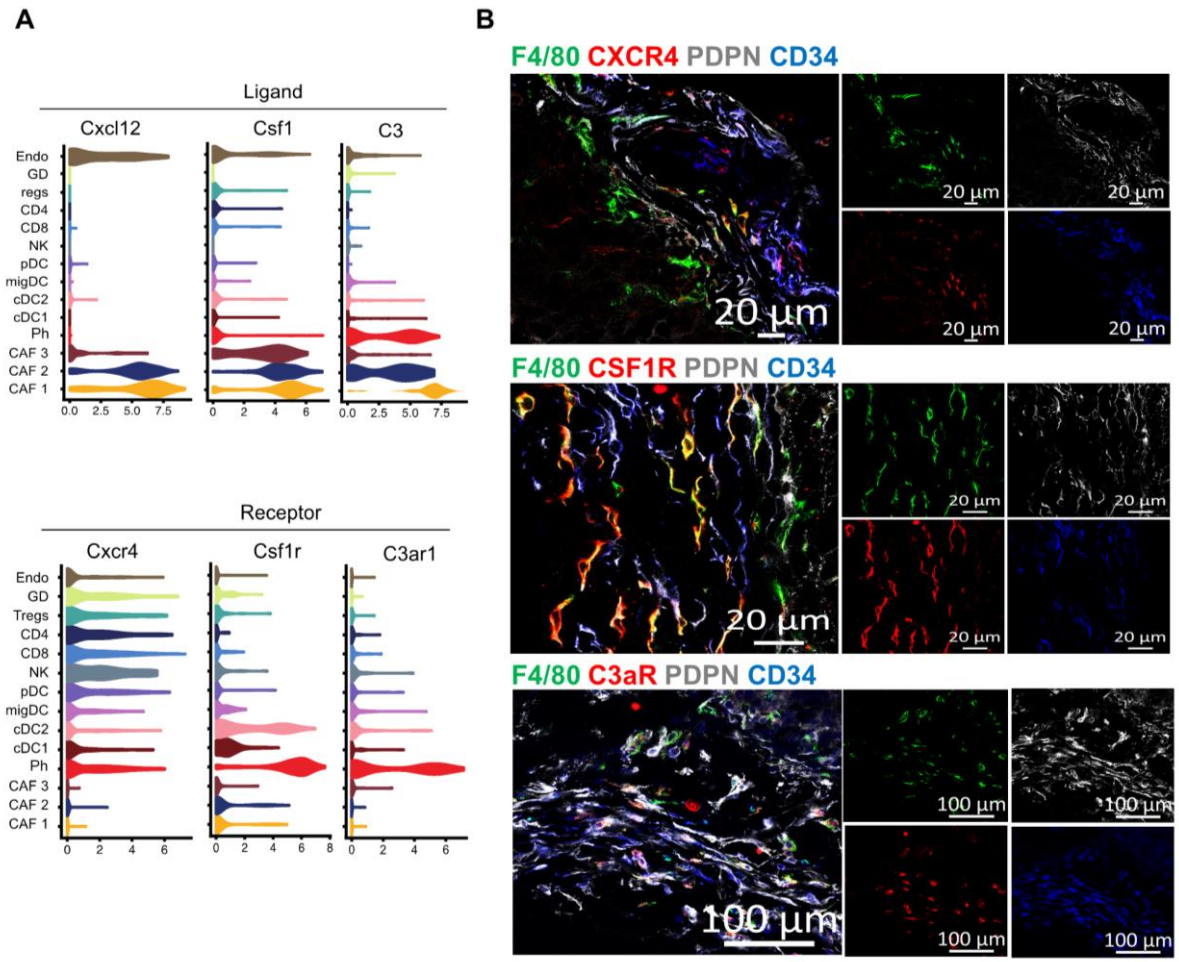

Fig. 5.6 Cognate receptors for key CAF1 inflammatory factors are expressed on macrophage populations

(A) Violin plots showing expression of inflammatory factors *Cxcl12*, *Csf1* and *C3* and their cognate receptors *Cxcr4*, *Csf1* and *C3ar* in stromal populations in the tumour. (B) IF images of day 5 B16-F10 tumours showing the close proximity of CD34^{high} CAFs and macrophages expressing CXCR4, CSF1R or C3aR. IF images represent n=3 tumours, scale is indicated.

5.2.2.2 *C3 was specifically produced by CD34+ Fibroblasts in the tumour microenvironment*

Next, we wished to investigate the nature of the interactions between the CAF1 population and macrophages. For example, whether CAF1 cells are involved in their recruitment or induction of suppressive properties is unclear. However, devising a method to investigate interactions was difficult. As previously discussed, isolation of these cells for *in vitro* assays was technically challenging and would likely lead to loss of phenotype. Thus, *in vivo* blocking of CAF produced factors was employed to assess their influence on the myeloid compartment. However, in addition to sticking to the cell surface (4.2.4.3), CXCL12 was also produced by other microenvironment components including both tumour and endothelial cells. Thus, whether the effects of blocking this interaction are specific to the CAF compartment is difficult to evaluate (Fig. 5.7). Similarly, our sequencing data implied exclusive production of CSF1 by fibroblasts within the stroma. However, expression of this cytokine by other populations, including tumour cells, was not validated at the protein level. On the other hand, C3 was specifically produced by $CD34^{high}$ CAF1 fibroblasts, thus, the C3a/C3aR axis was selected for these studies.

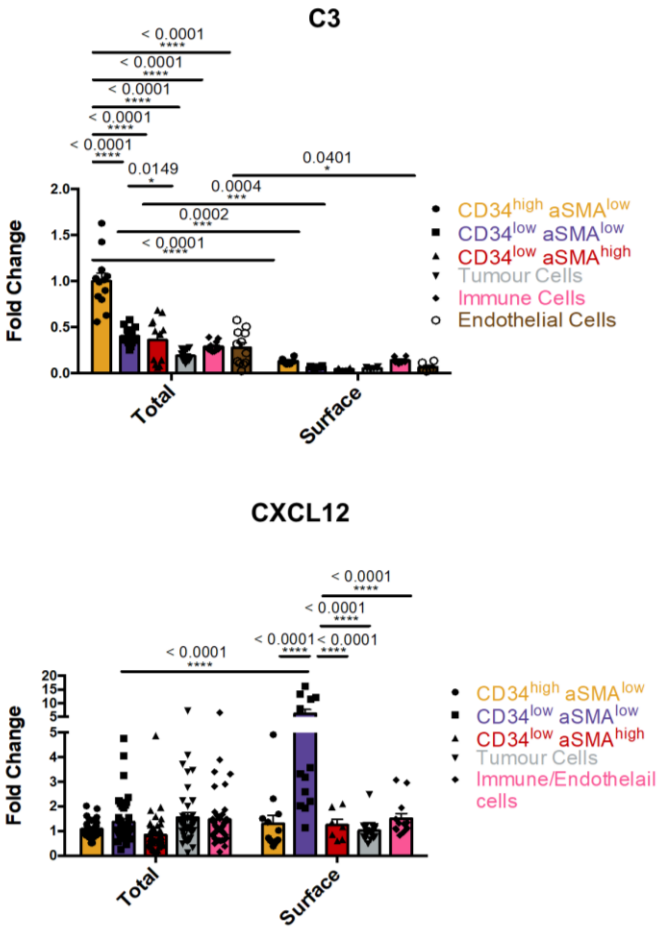

Fig. 5.7 Expression of CXCL12 and C3 in the tumour microenvironment

Flow cytometric quantification of total and surface CXCL12 and C3 expression in CAFs, tumour, immune and endothelial cells at day 11. Graphs are presented as fold change in mean fluorescence and normalised to the $CD34^{high}$ αSMA^{low} population. Data presented as mean ± SEM. * P<0.05, ** P<0.01, *** P<0.001, **** P<0.0001 (two way anova with Sidak post-hoc test). CXCL12: n = minimum of 12 mice, C3: n = minimum 6 mice

5.2.2.3 *Inhibition of C3a/C3aR signalling axis in the TME*

In vivo perturbation of C3a signalling enabled a broad evaluation of the role of CAF 1 populations in the tumour microenvironment. To begin with, the effects of C3a on both myeloid recruitment and the development of suppressive phenotypes was evaluated. Furthermore, our data implicates the involvement of myeloid cells in T-cell suppression Thus, changes in the numbers or phenotypes of myeloid cells could influence the adaptive compartment. C3aR expression did not colocalise with Cd3e, indicating that alterations in T-cells, upon inhibition of C3a signalling, are a consequence of changes in myeloid populations (Fig. 5.8). Thus, the wider effects of CAF1-myeloid interactions on the development of T-cell dysfunction and tumour growth were investigated.

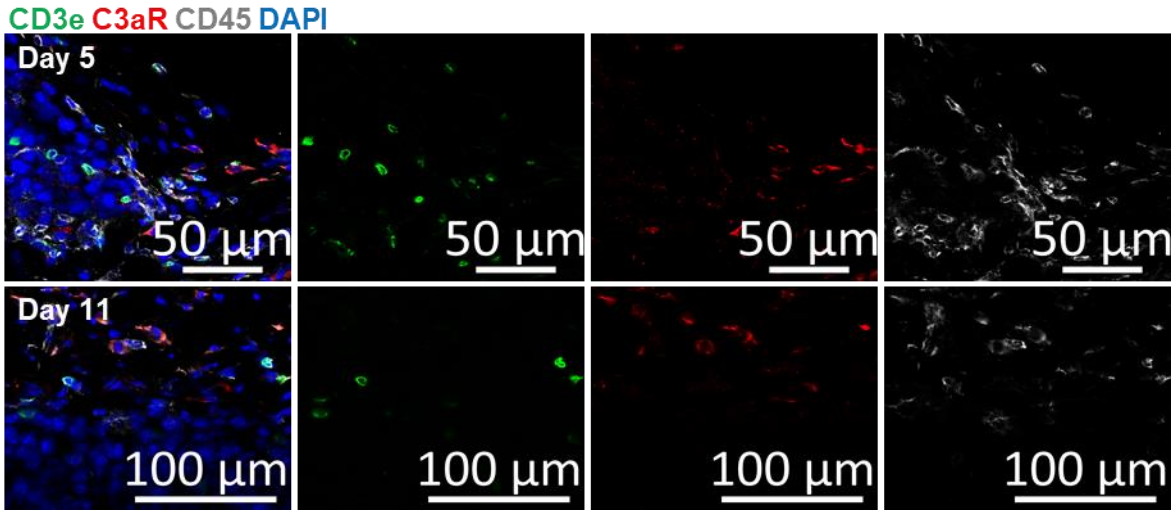

Fig. 5.8 C3aR does not colocalise with CD3e.

IF images of day 5 and day 11 tumours showing expression of Cd3e (green), C3aR (red) and CD45 (grey). C3aR was observed on CD45+ immune cells but did not colocalise with CD3e. Images represent n=3 tumours, scale is indicated.

Mice with established tumours were treated with C3a neutralising antibody, according to (Fig. 5.10 A and B). To assess the immediate and long-term effects of C3a inhibition on myeloid populations, mice were sacrificed 24hs after the first treatment (day 6) and at day 11. Although macrophages represented the principal population within the C3aR+ phagocytic cluster, Ly6C+ monocytes and Ly6G+ neutrophils were also present. Expression of C3aR on CD11b+ Ly6C+ myeloid cells was confirmed by

confocal imaging (Fig. 5.9), thus, changes in Ly6C, Ly6G and F4/80 populations were assessed in treated mice. A small yet significant decrease in F4/80+ macrophages was observed in in treated samples at day6, suggesting C3a is important for their recruitment (Fig. 5.10 D). However, F4/80+ cells were rare in blood samples and most likely recruited to the tumour as Ly6C+ monocytes, which then differentiate to a macrophage phenotype. As, monocyte recruitment was not reduced at day6, this signifies that C3a may be involved in monocyte differentiation to macrophages. Interestingly, neutralisation of C3a did not affect expression of suppressive molecules Arg-1 or PDL1 on macrophages, although a slight decrease was observed at early time points in Ly6C+ monocytes.

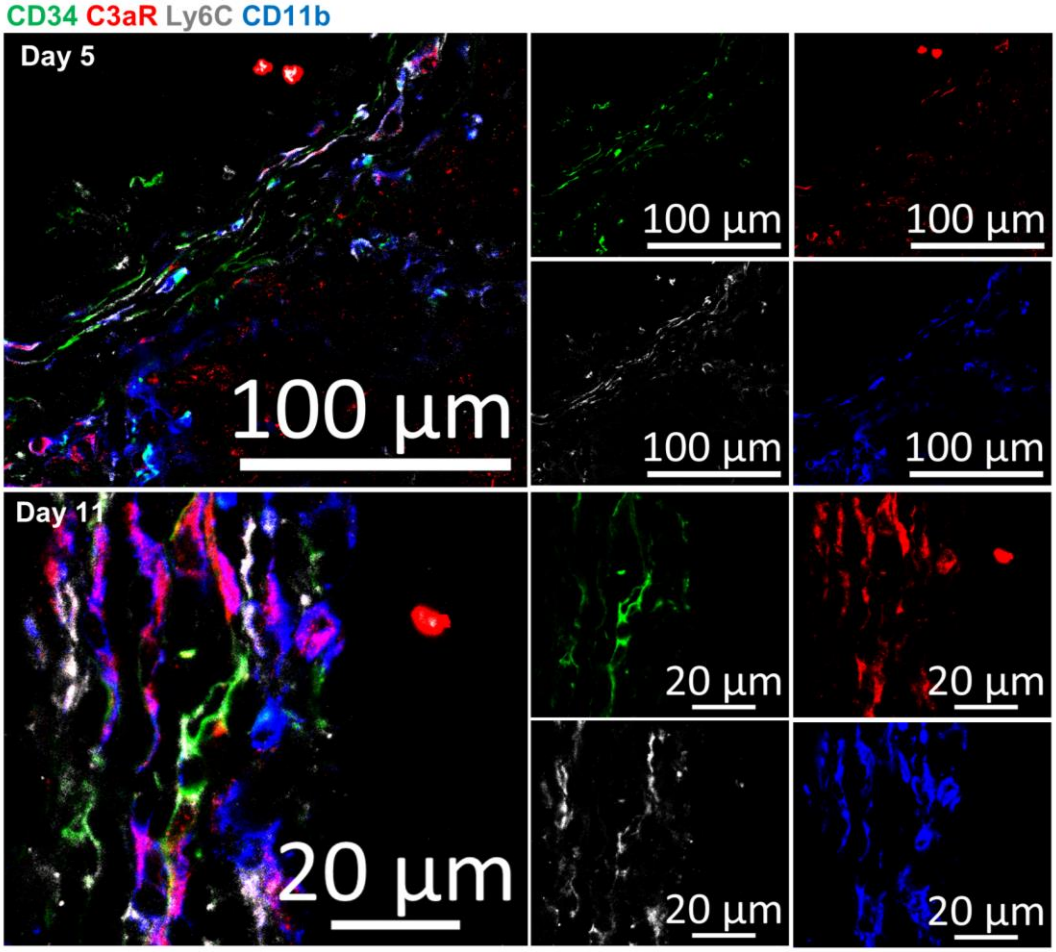

Fig. 5.9 C3aR was expressed by Ly6C+ monocytes

IF images of day 5 and day 11 tumours showing expression of Cd34 (green), C3aR (red) and Ly6C (grey) and CD11b (blue). C3aR was observed on CD11b+, Ly6C+ monocytes in close proximity to $CD34^{high}$ CAFs. Images represent n=3 tumours, scale is indicated.

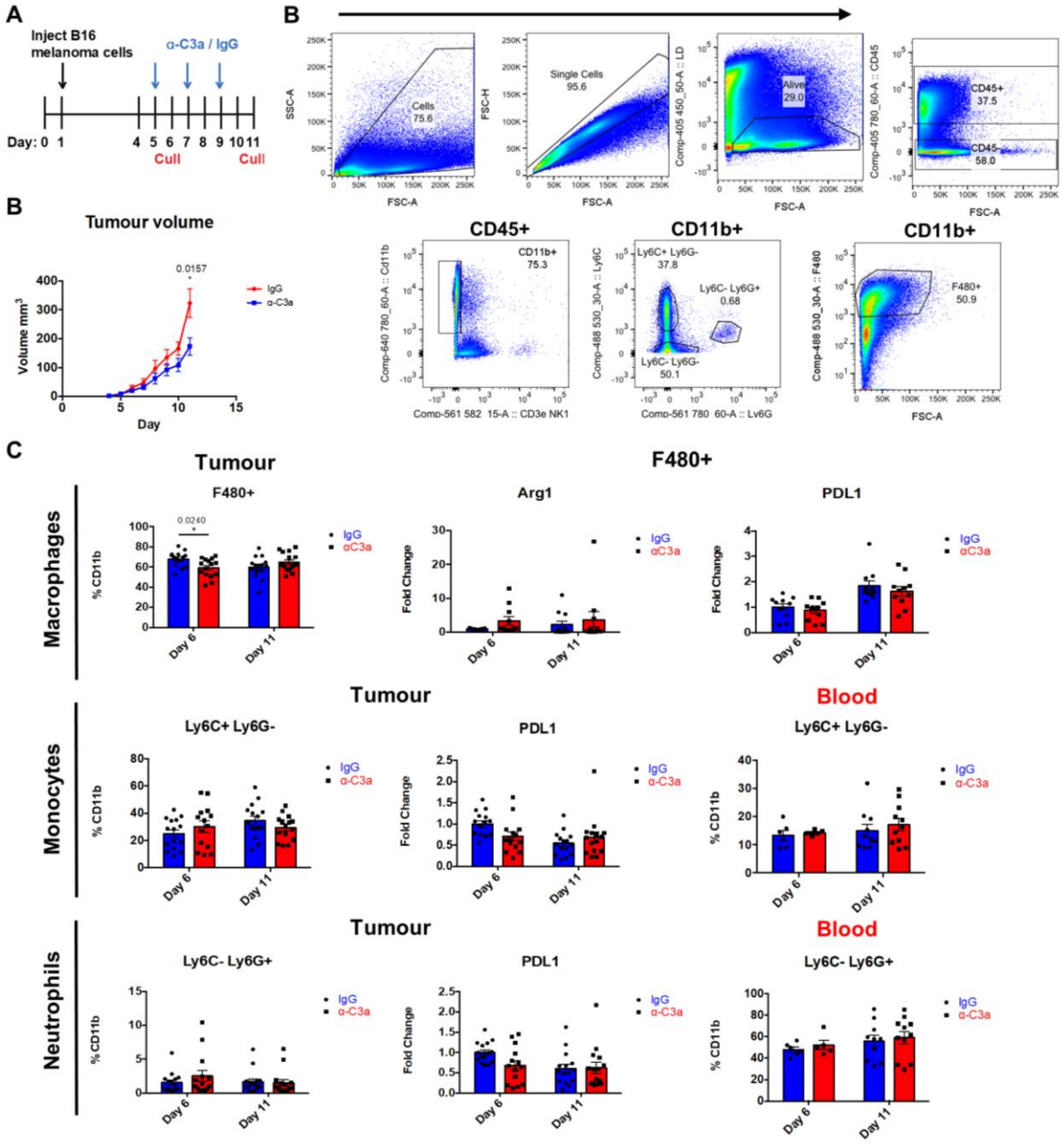

Fig. 5.10 The effects of neutralising C3a on tumour growth and myeloid composition

(A) Schematic showing treatment regime, mice received injections of IgG or anti-C3a at day 5, 7 and 9 and were sacrificed at either day 6 or 11. (B) Graph showing tumour volume (mm^3) of treated mice. (C) Gating strategy for identification of myeloid populations. Dead cells and doublets were removed and CD45+ immune cells selected. Within immune cells CD3e+ T-cells and NK1.1 NK cells were excluded and CD11b+ cells were divided into populations based on Ly6C and Ly6G or F4/80 expression. (D) Tumour infiltrating and blood myeloid populations are displayed as a percentage of CD11b. Mean fluorescence intensity of suppressive markers ARG1 and PDL1 in different populations are displayed, normalised to IgG day6. Data presented as mean ± SEM, *P<0.05, ** P<0.01 (B: T-test performed on day 11 treated and non-treated volumes D: two way anova with Sidak post-hoc test), n = minimum of 13 tumours. Statistical significance was tested for all data in this figure. If no star is displayed, comparisons were not significant

Crucially, this decrease in macrophage populations was accompanied by an increase in CD8 T-cells at later time points and a reduction in the rate of tumour growth (Fig. 5.11 B). Although a small increase in CD8-T cells was observed as a percentage of CD3e, this was obscured by a large amount of variation between samples. Thus, CD8 T-cell counts were normalised to tumour volume, showing a significant difference in their number upon treatment. However, T-cell dysfunction molecules PD1 and LAG3 were slightly increased, although expression was extremely variable. This is consistent with unaltered expression of myeloid ARG1 and PDL1 and indicates that inhibiting C3a does not prevent T cell suppression. However, it appears that by reducing myeloid numbers, CD8 T-cell recruitment is increased or their survival is promoted. While this is sufficient to decelerate tumour growth, this modest effect may be boosted by restoration of cytotoxic functions. Importantly, the anti-C3a antibody was well tolerated by mice in this study and no significant changes in immune populations were observed in blood samples. This indicates treatment does not cause damaging systemic effects.

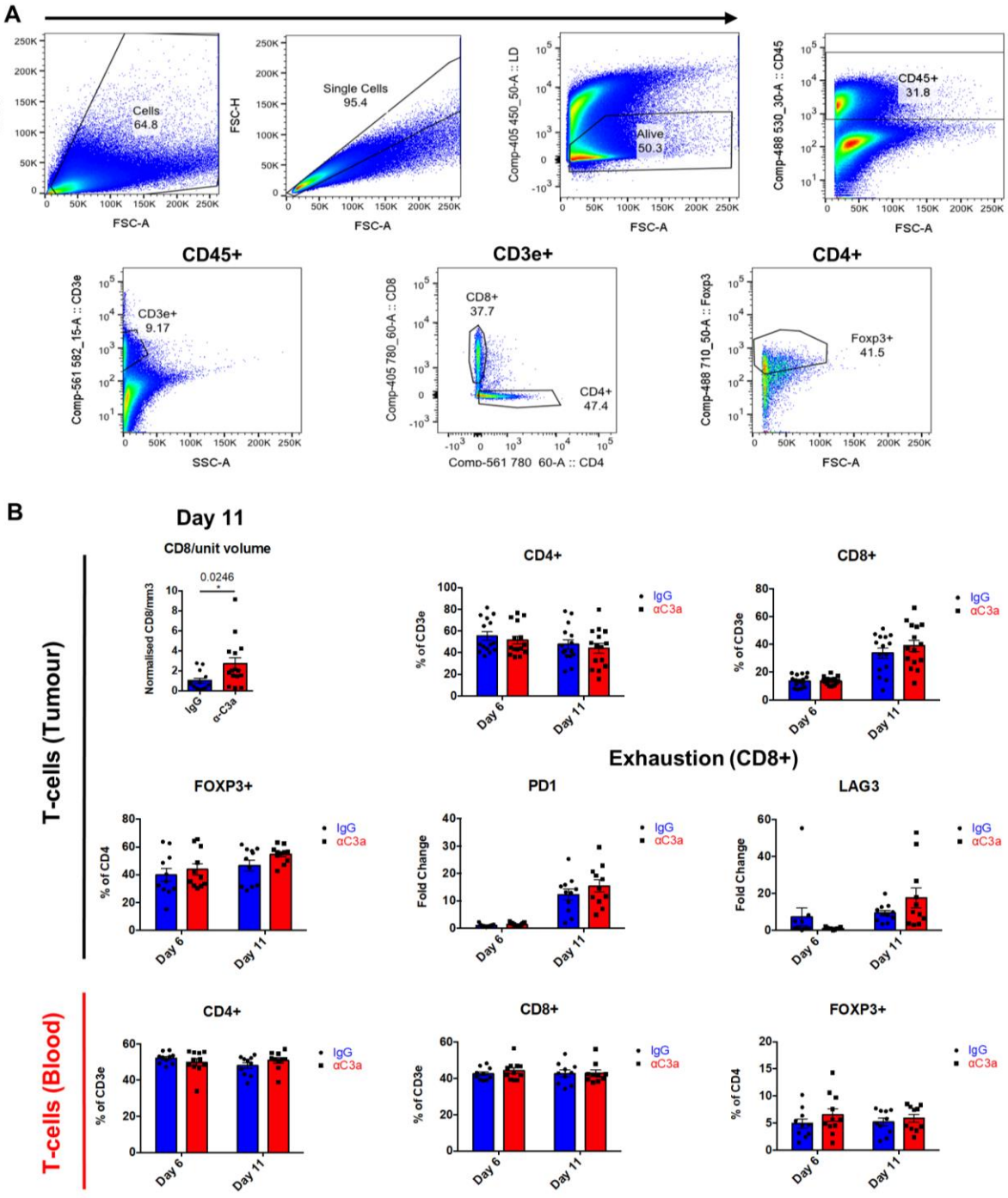

Fig. 5.11 The effects of neutralising C3a on T-cell composition

(A) Gating strategy for identification of T-cell populations. Dead cells and doublets were removed and CD45+ immune cells selected. Within immune cells CD3e+ T-cells were divided into CD8+ and CD4+populaitons. Tregs were identified within CD4 cells based on FOXP3 expression. (B) Tumour Infiltrating and blood T-cell populations are displayed as a percentage of CD3e of CD4 cells. CD8 T-cells counts were also normalised to tumour volume (mm^3). Mean fluorescence intensity of T-cell exhaustion markers PD1 and Lag3 in CD8 T cells, is shown, normalized to IgG day 6. Data presented as mean ± SEM, *P<0.05,: two way anova with Sidak post-hoc test), n = minimum of 13 tumours. Statistical significance was tested for all data in this figure. If no star is displayed, comparisons were not significant

To corroborate these findings, the effects of C3aR antagonist SB290157 on immune cell infiltration were also investigated. Two time-courses were performed, of which one was identical to the C3a neutralisation study, while the other assessed the effect of treatment at different time points. The results of the first study, in which mice were treated every two days and culled at either day 6 or day 11, were extremely variable. A decrease in macrophage populations and an increase in Ly6C+ cells was initially observed, yet this trend was not present when the experiment was repeated (combined results displayed in (Fig. 5.12 C). In the second time course, C3aR was perturbed at either early stages (day4 and day 6) or later stages (day 8 and day 10) and all tumours were allowed to develop for 11 days. Interestingly, in this experiment, a decrease in F4/80 macrophages and an increase in Ly6C+ cells was observed after inhibition of the C3aR at either early or late time points (Fig. 5.12 F). These dynamics suggest that treatment at early time points is long lasting, which differs from the C3a neutralisation study where this trend was not observed at day 11. Thus, while trends in myeloid populations are retained upon C3aR antagonism, there are subtle differences in timing of these events. However, in both time courses, inhibition of C3aR did not increase in the number of CD8 T-cells, nor slow tumour growth (Fig. 5.12 B and E). Indeed, treatment with SB290157 at day 4 and 6 actually increased tumour volume.

Overall, these results are preliminary and require optimisation. However, common trends suggest that CAF1 production of C3 regulates macrophage accumulation in the tumour and may be important for monocyte to macrophage differentiation. Furthermore, reduction in macrophage numbers increased CD8 T-cells and slowed tumour growth. Thus, via regulation of suppressive myeloid cells, the CAF1 population may be an important player in the development of the immunosuppressive melanoma microenvironment.

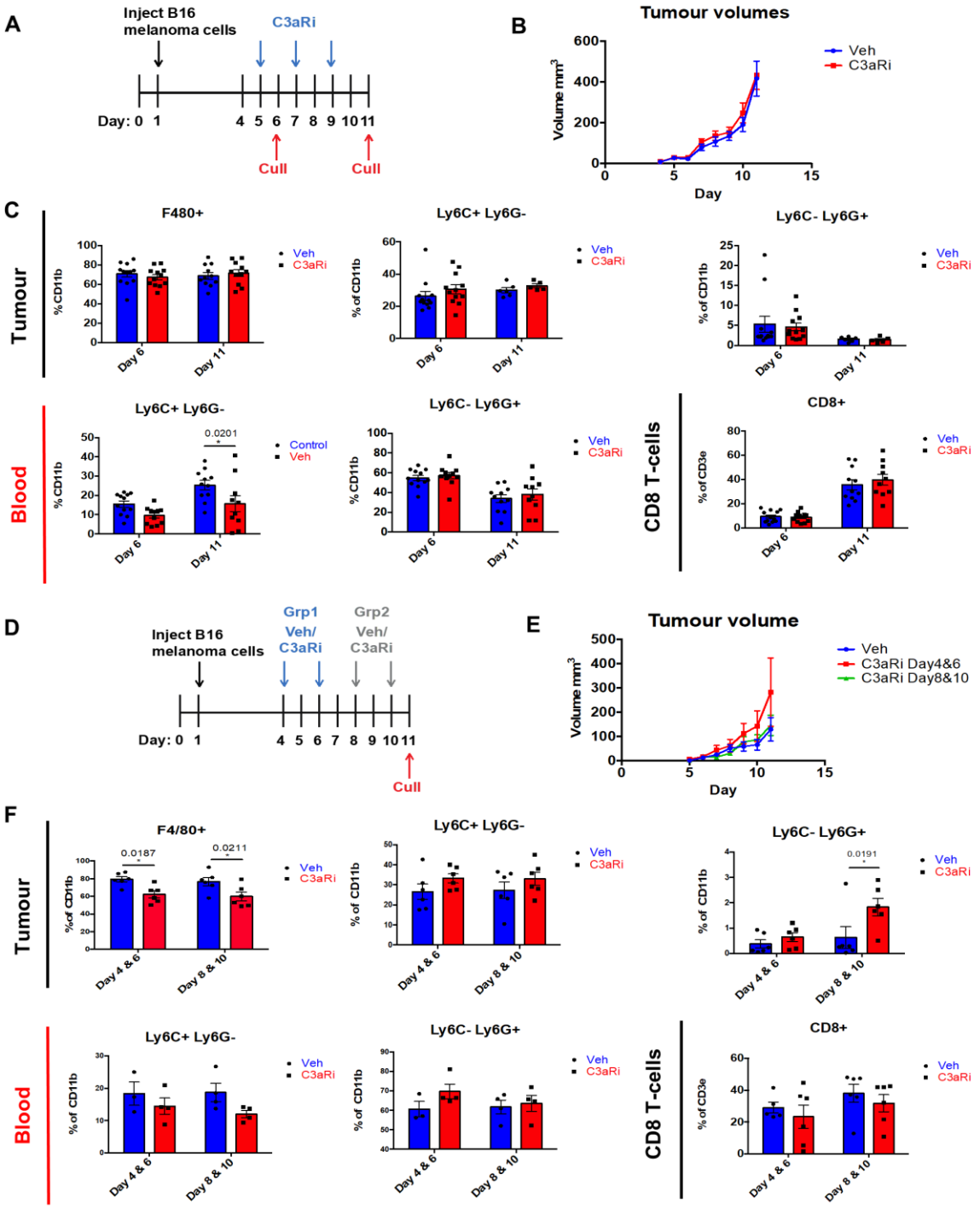

Fig. 5.12 The effects of C3aR antagonism on tumour growth and immune composition (A and D) Schematics showing treatment regimes. (A) Mice received injections of vehicle or C3aR inhibitor (C3aRi) at day 5, 7 and 9 and were sacrificed at either day 6 or 11. (D) Mice were treated at either day 4 and 6 or day 8 and 10, and all mice were sacrificed at day 11. (B, E) Graphs showing tumour volume (mm^3) of treated mice. (C and F) Tumour infiltrating myeloid, CD8 T-cell populations and blood neutrophils are displayed. Myeloid cells are shown as a percentage of CD11b, while CD8 T-cells are shown as a percentage of CD3e. Data presented as mean ± SEM, *P<0.05, (two way anova with Sidak post-hoc test), n = minimum of 13 tumours. Statistical significance was tested for all data in this figure. If no star is displayed, comparisons were not significant

5.2.3 *Investigating whether fibroblasts derived from different origins form functionally distinct populations*

As well as environmental cues, one potential source of fibroblast heterogeneity is their cellular origin. In addition to resident fibroblasts, stromal cells recruited from the bone marrow represent another potential source. Thus, to investigate whether the bone marrow contributes to the milieu of fibroblast populations in the tumour stroma, a chimeric model was developed.

5.2.3.1 *Establishment of a chimeric mouse model enabled the identification of bone marrow derived CAFs*

Chimeric mice were created by transplanting bone marrow extracted from CAG-EGFP^{+} mice into irradiated WT strains. This enabled the detection of fibroblasts recruited from the bone marrow, based on GFP expression (Fig. 5.13 A). To ensure bone marrow engraftment was successful blood samples were analysed to assess the proportion of GFP+ cells. After 3 weeks, over 90% of cells were GFP+ indicating successful engraftment (Fig. 5.13 B and C). Analysis of day 11 B16-F10 tumours showed that only 1-2% of CAFs were bone marrow derived (GFP^{+}). Furthermore, the level of GFP expression appeared significantly lower than immune populations in tumours, raising the possibility that either CAFs do not express as much GFP or they have phagocytosed immune cells or immune cell debris. Consequently, it is unlikely that bone marrow stromal cells are responsible for fibroblast heterogeneity in this model.

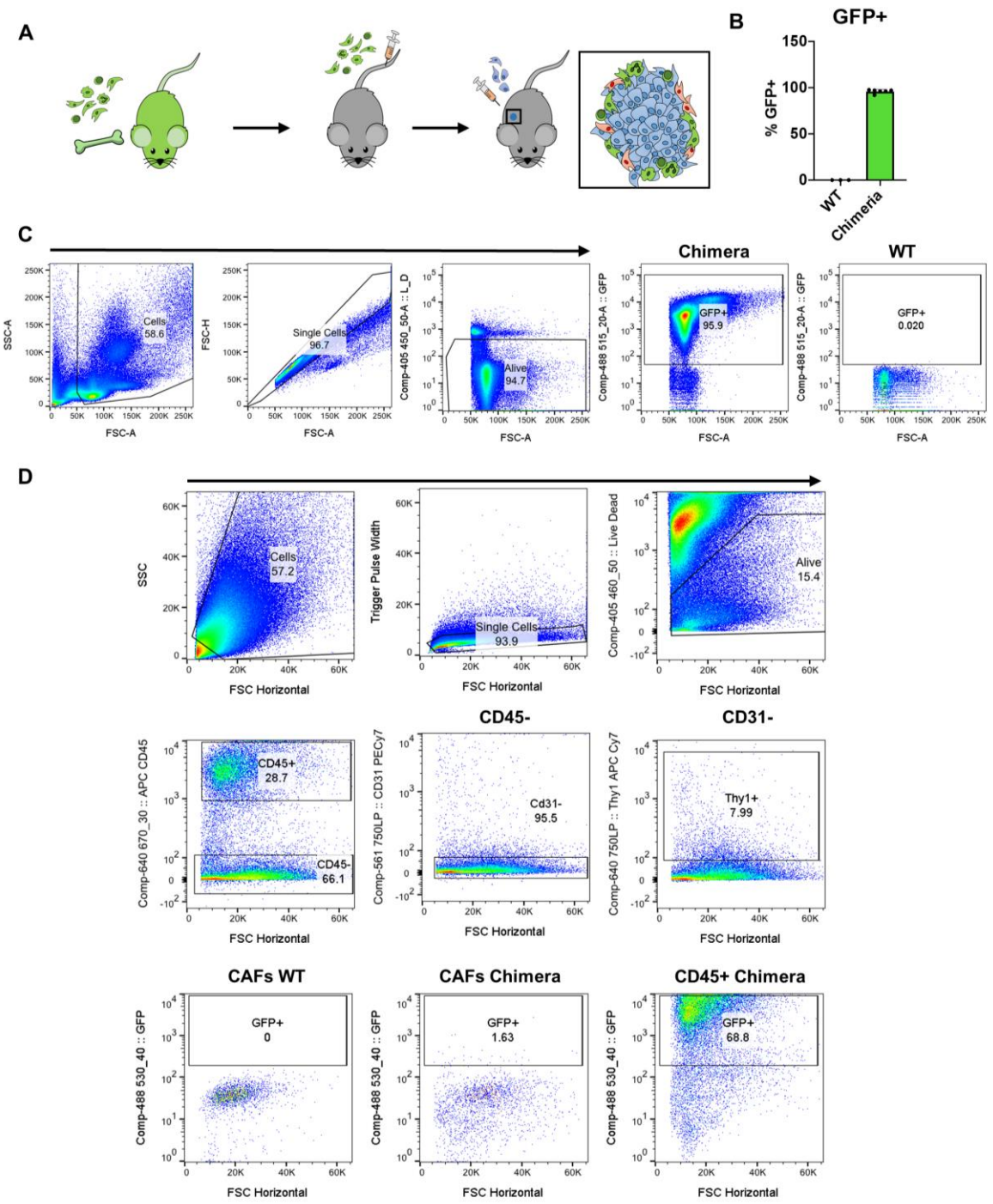

Fig. 5.13 The bone marrow does not represent a significant source of fibroblasts

(A) Schematic depicting the formation of the bone marrow chimeric mice. The bone marrow of CAG.EGFP mice were extracted and implanted into irradiated WT mice. B16-F10 tumours were established in chimeric mice, enabling the identification of bone marrow derived cells based on GFP expression. (B) To check engraftment was successful the percentage of GFP+ cells in blood samples from chimeric and WT mice was quantified. WT n=3 mice, Chimeras n=6 mice. (C) Gating strategy for (B). (D) Representative FACs plots (n=6) showing GFP expression in CAFs and immune cells from chimeric models. CAFs were selected by excluding doublets, dead cells, CD45+ immune and CD31+ endothelial cells and cells were removed. Fibroblasts were then identified by expression of Thy1 and PDGFRα. And GFP measured within this gate

5.2.4 *Investigation of 'immune', 'desmoplastic' and 'contractile' CAF populations in other murine cancer models and human cancers*

The critical role of CAF1 fibroblasts in the regulation of immune populations and the potential of anti-C3a therapies, lead us to investigate whether these populations were limited to the B16-F10 model or were relevant to other cancer types. Thus, the presence of these CAF populations was examined in breast and pancreatic murine models, as well as the $BRAF^{V600E}PTEN^{-/-}$ model (described in section1.6.2), which better resembles the slow development of human melanoma.

5.2.4.1 *$BRAF^{V600E}PTEN^{-/-}$ murine model of melanoma*

Staining of spontaneously arising $BRAF^{V600E}PTEN^{-/-}$ tumours for CAF markers CD34, PDGFRα, PDPN and αSMA, showed a different distribution. CAFs predominantly expressed αSMA and PDPN, for which double positive populations were abundant and mutually exclusive populations were rare. Interestingly, while CD34+ cells were present throughout the tumour, a large proportion of these cells did not display a fibroblast morphology nor express CAF markers. These cells may represent immune populations or progenitors (Fig. 5.14 A and B). Furthermore, in support of our initial characterisation of these tumours (section 3.2.1), only a small subset of CAFs expressed PDGFRα. These fibroblasts were restricted to peripheral regions and did not penetrate the tumour core.

Despite the small number of $CD34^{high}$ CAFs in this model, C3 levels were higher in this population comparison to the $CD34^{low}$ fibroblasts (Fig. 5.15 B). Although C3 was also detected in immune and endothelial cells, this may be due to cell surface sticking. Thus, despite the different distribution of CAF markers, CD34+ CAFs are still the primary source of C3 in this melanoma model.

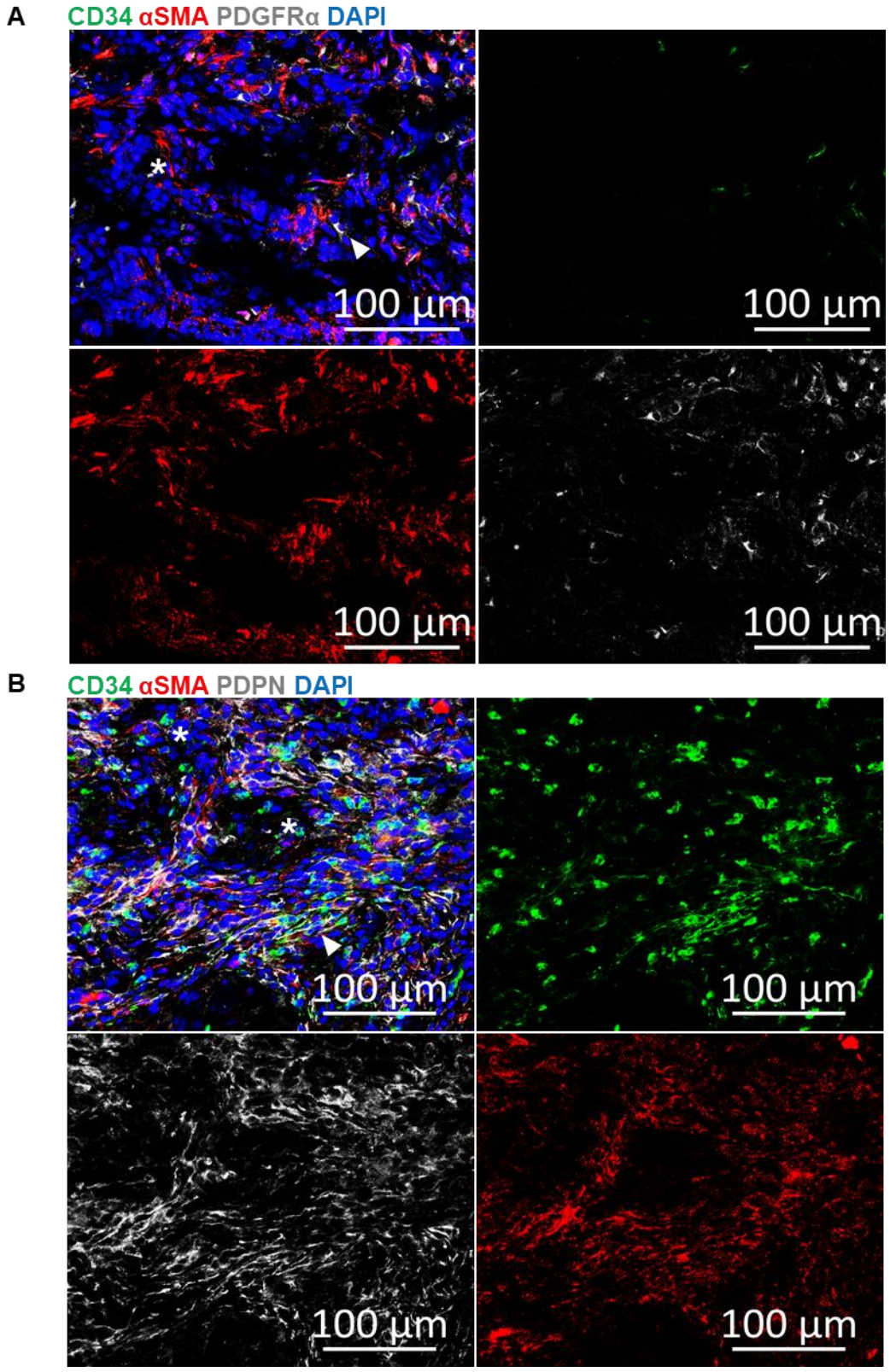

Fig. 5.14 Confocal images of CAF markers in BRAF^{V600E}PTEN$^{-/-}$ tumours

IF images of spontaneous BRAF^{V600E}PTEN$^{-/-}$ tumours. (A) Sections stained for CD34, αSMA and PDGFRα. Arrow heads indicate PDGFRα^{+} cells, * indicate αSMA^{+} cells. (B) Sections stained for CD34 αSMA and PDPN. Arrow heads indicate CD34+ fibroblasts * indicate CD34+ cells that do have a fibroblast morphology nor express fibroblast markers. Scale is indicated.

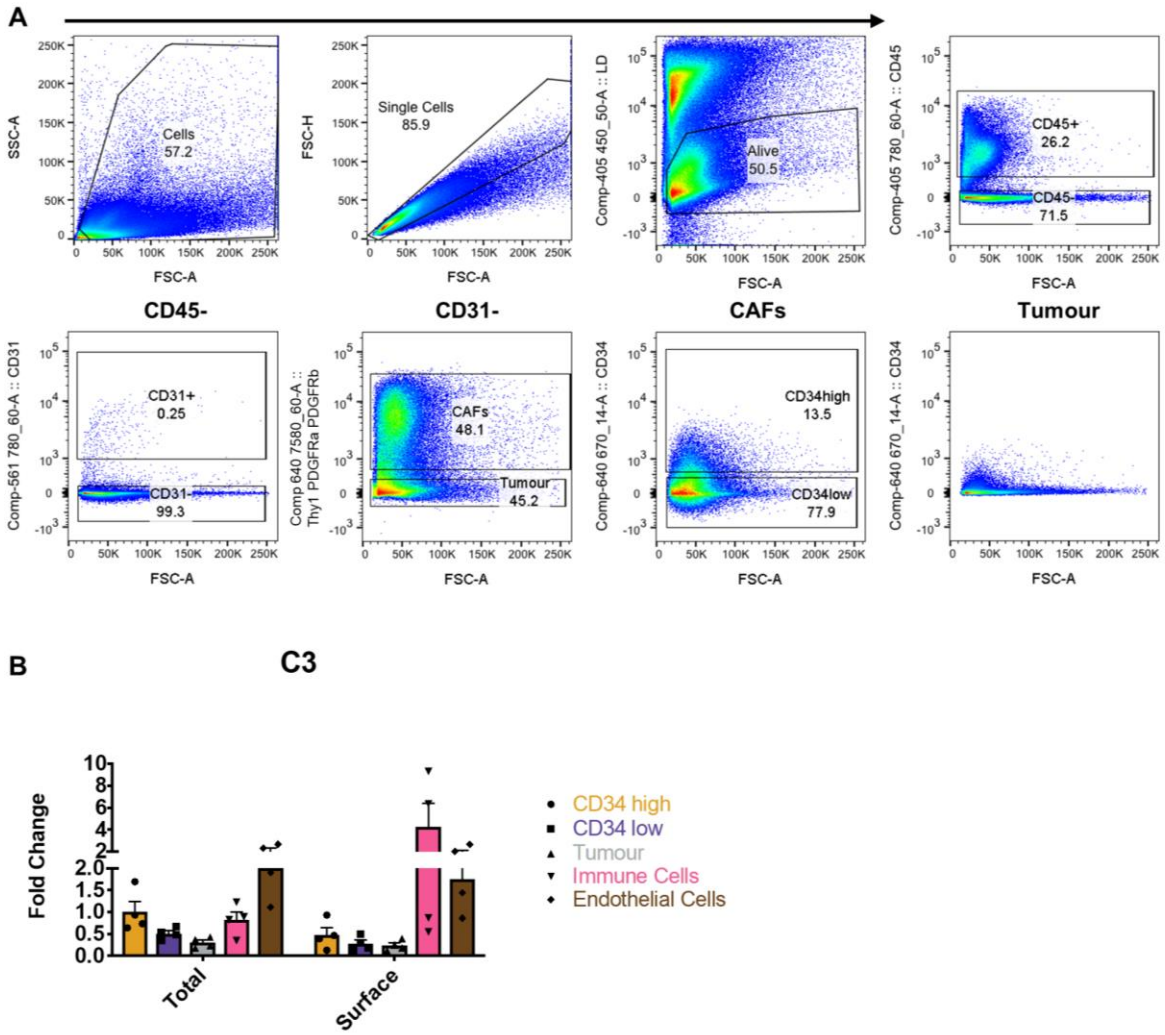

Fig. 5.15 CD34+ CAFs were the primary source of C3 in BRAF^{V600E}PTEN$^{-/-}$ tumours

Flow cytometric analysis of C3 in the microenvironment of spontaneous BRAF^{V600E}PTEN$^{-/-}$ tumours. (A) Gating strategy showing identification of populations. Doublets and dead cells were excluded, and endothelial and immune cells were selected based on CD31 and CD45 expression respectively. CAFs were identified based on combined expression of THY1, PDGFRα and PDGFRβ once immune and endothelial cells were excluded. Expression of CD34 was determined based tumour cells, which should act as a negative control. (B) Mean fluorescence intensity of total and surface C3 was quantified and normalised to CD34 high CAFs for each population. Data presented as mean ± SEM. Statistical significance was tested for all data in this figure. However, comparisons were not significant, thus, no star is displayed.

5.2.4.2 *Murine models of breast cancer*

The E0771 orthotopic model was used in which tumour cells were injected into the mammary fat pad, to investigate CAF populations in breast cancer. These tumours grew at a slightly slower rate than their B16-F10 counterparts and mice were culled after 8 or 16 days. Confocal imaging revealed a similar marker distribution, in which PDGFRα colocalised with CD34, while αSMA exhibited more distinct staining (Fig. 5.16). Furthermore, flow cytometry confirmed that C3 was expressed by $CD34^{high}$ CAFs (Fig. 5.17 B) and that these CAFs are the dominant source of this factor in theTME (Fig. 5.17C). Interestingly, consistent with the B16-F10 model, C3 expression was low in fibroblasts from normal tissue yet increased as the tumour developed (Fig. 5.17 B). However, the prevalence of these populations did not change as breast tumours developed (Fig. 5.17 D). This indicates differences in the temporal dynamics of CAF populations between models.

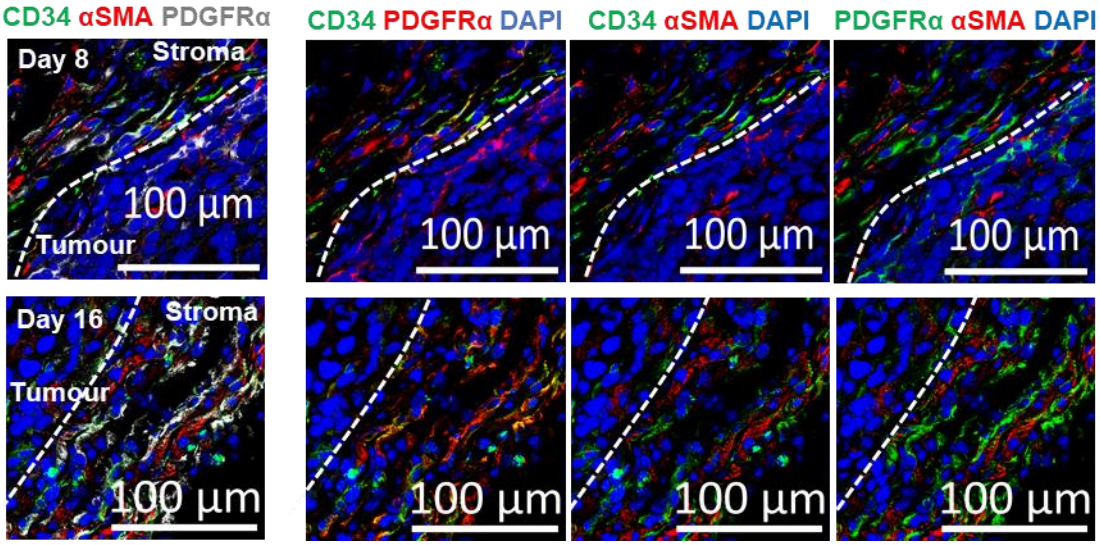

Fig. 5.16 IF of CAF markers in the tumour microenvironment of E0771 breast tumours

Representative confocal images showing the combination of CD34 (green), αSMA (red) and PDGFRα (grey) in day 8 and day16 E0771 tumours. A merged image of all 3 markers is displayed, as well as images showing two channels at a time. Pseudo-coloured green or red, these images emphasise colocalization. White dotted lines represent the divide between tumour and stromal regions, scale is indicated. Images represent at least n=3 independent mice.

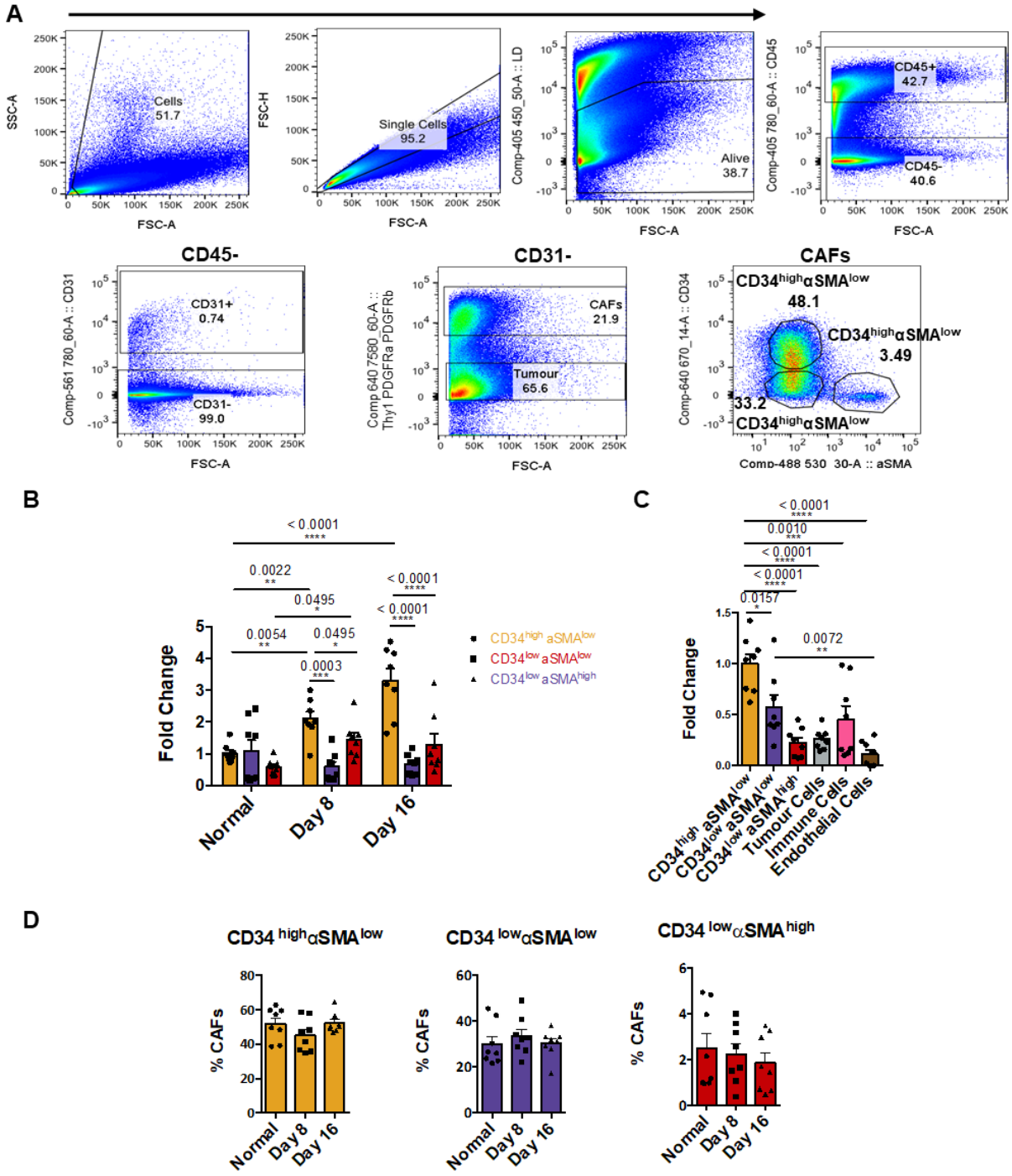

Fig. 5.17 CAF populations in the tumour microenvironment of E0771 breast tumours

(A) Gating strategy showing identification of populations in the microenvironment of E0771 breast tumours. Doublets and dead cells were excluded, and endothelial and immune cells were selected based on CD31 and CD45 expression respectively. CAFs were identified based on combined expression of THY1, PDGFRα and PDGFRβ, once immune and endothelial cells were excluded, and further separated based on CD34 and αSMA expression. Flow cytometric quantification of C3 expression in CAF populations at different time points (B) and all populations at day 16 (C). Displayed as mean fluorescence intensity and normalised to the CD34^{high} αSMA^{low} population. (D) CAF populations at different time points as a percentage of the CAF compartment. Data presented as mean ± SEM. * P<0.05, ** P<0.01, *** P<0.001, **** P<0.0001 (B: two way anova with Tukey post-hoc test, C: one way, anova with Tukey post-hoc test), n = 8 mice.

To investigate these CAF populations in an additional breast cancer model, we examined gene signatures related to each population in publicly available data. Bartoschek *et al* isolated CAFs form the MMTV-PyMT mode,l by excluding Epcam+, CD45+, CD31+ and NG2+ cells[299]. Here, they discovered 4 populations termed vascular (vCAFs), matrix (mCAFs), developmental (dCAFs) and cycling CAFs (cCAFs), which are a proliferating subset of vCAFs, based on their unique functional signatures. These results were recapitulated in our hands, as 4 similar populations were identified that expressed the reported markers (Fig. 5.18 A and B). Interestingly, examination of genes associated with our 'immune', 'desmoplastic' and 'contractile' subsets showed some similarities with these populations (Fig. 5.18 C and D). Although neither *C3* nor *Cd34* were high highly expressed by fibroblasts in this data set, other immune recruitment factors *Cxcl12* and *Csf1* were specifically associated with mCAFs. This population also expressed matrix components *Col1a2* and *Tnc*, as well as CAF markers *Pdpn* and *Pdgfra*, suggesting it resembles features of our 'immune' and 'desmoplastic' populations. Furthermore, vCAFs displayed high expression of contractile genes *Myl9* (Mlc2) and *Mylk* (Mlck), as well as pericyte markers *Cspg4* (Ng2), *Mcam, Rgs5* and *Des* resembling 'contractile' CAF3 cells (Fig. 5.19). This population was observed both surrounding blood vessels, as well as the leading edge, suggesting pericyte origins and reflecting our findings.

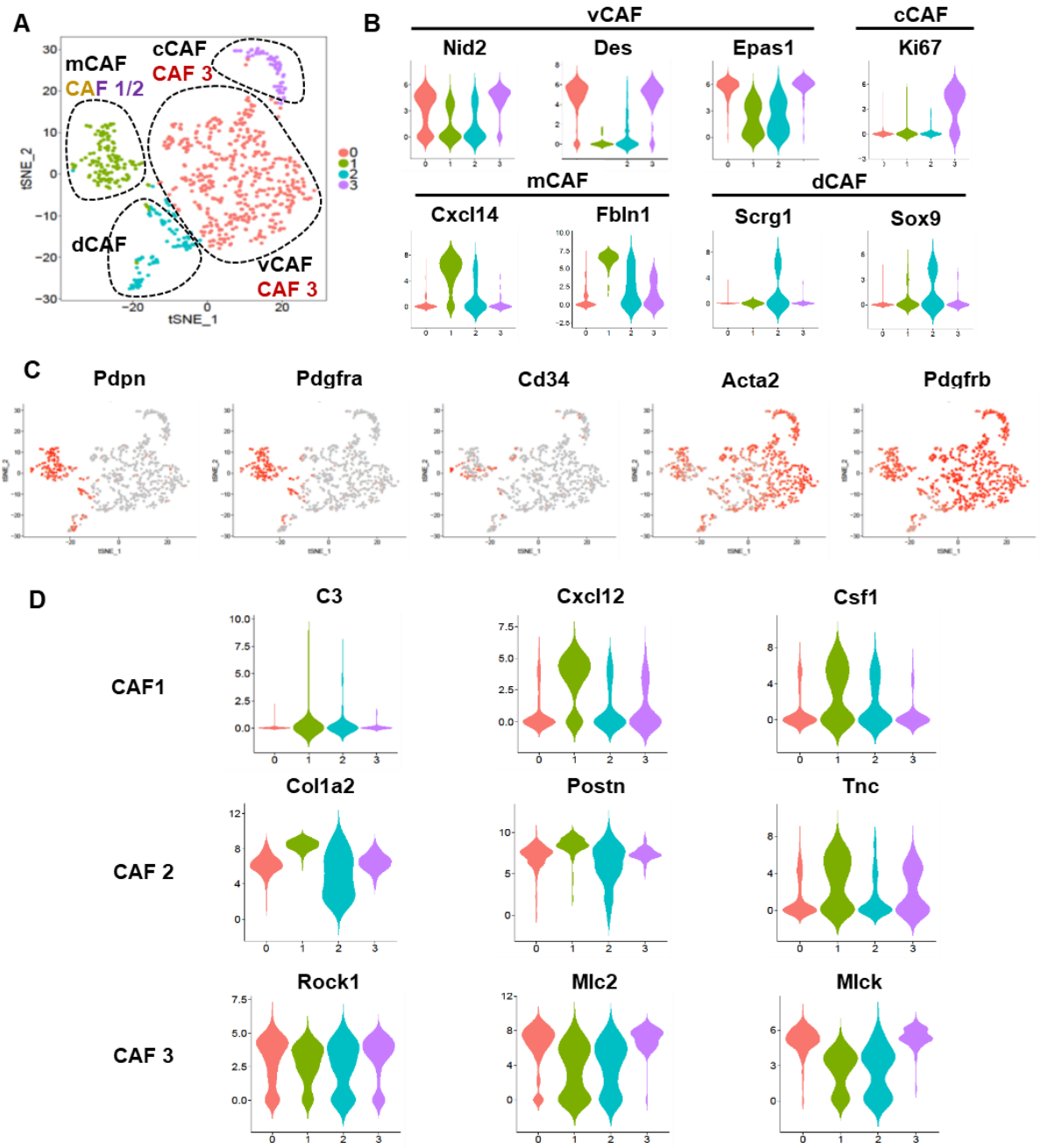

Fig. 5.18 CAF populations in the MMTV-PyMT model of breast cancer share some phenotypes with subsets identified in B16-F10 melanoma.

Publicly available sequencing data from Bartoschek *et al* [299] of EpCAM- CD45- CD31- NG2- CAFs isolated from the MMTV-PyMT murine model of breast cancer. (A) Sequencing data was processed and re-clustered, displayed here as a tSNE plot. Labels indicate the populations that correspond to those identified by Bartoschek *et al* (vCAF, mCAF, cCAF and dCAF), as well as those that share features with our CAF subsets. These were assigned based on expression of genes depicted in B-D. (B) Violin plots displaying expression of population markers identified by Bartoschek *et al*, confirming similar clusters were found. (C) tSNE plots coloured according to expression of typical CAF markers, red indicates high expression and grey indicates low expression. (D) Violin plot showing expression of genes associated with CAF1 'immune', CAF 2 'desmoplastic' and CAF3 'contractile' phenotypes.

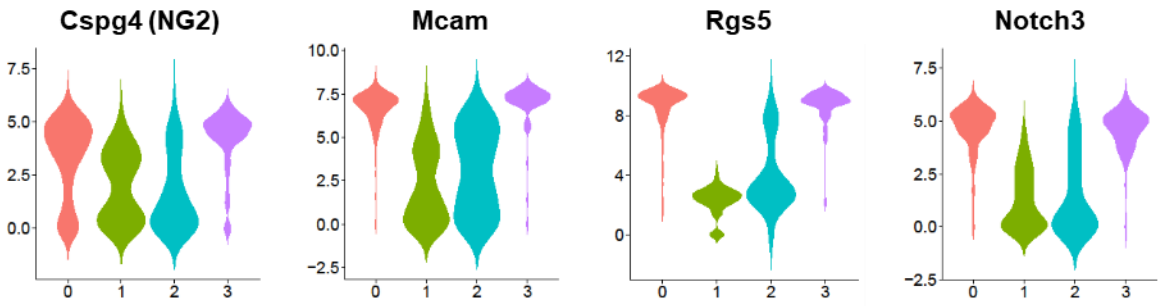

Fig. 5.19 Pericyte markers were strongly expressed by CAF populations displaying a CAF3 'contractile' phenotype in the MMTV-PyMT model of breast cancer.

Publicly available sequencing data from Bartoschek *et al* [299] of the MMTV-PyMT murine model of breast cancer. Violin plots displaying expression of pericyte markers across identified populations.

5.2.4.3 *KPC murine model of PDAC*

CAFs constitute a large proportion of pancreatic tumours[413], thus, uncovering the different populations present is particularly pertinent. Feig *et al* previously reported distinct expression of CD34 and αSMA in the KPC model of PDAC[248]. However, in the present study, staining of PDAC samples from KPC mice (donated by Dr. Tobias Janowitz, CRUK Cambridge institute department of Oncology) showed CD34 expression was restricted to CD31+ vessels. However, when examining normal pancreatic tissue, the majority of pancreatic stellate cells (PSCs) expressed CD34 (Fig. 5.20 B). In contrast, aSMA expression was limited to perivascular cells in normal tissue, yet was abundant in PDAC samples (Fig. 5.20 A and C). This suggests $CD34^{high}$ fibroblasts represent resident populations in normal pancreatic tissue. However, similar to B16-F10 melanomas, upon tumour initiation these cells either transform into αSMA expressing CAFs or are replaced by a second population. This was supported by flow cytometry, which showed large numbers of $CD34^{high}$ cells in WT tissue yet fewer were detected in advanced tumours. The infrequency of this population in PDAC may make them difficult to detect by confocal imaging (Fig. 5.20 D). Interestingly, PDGFRα colocalised strongly with both CD34 and αSMA in pancreatic samples, although some discrepancy was observed between this marker and the latter. This suggests, while similar CAF populations are present in PDAC, although marker expression is not identical.

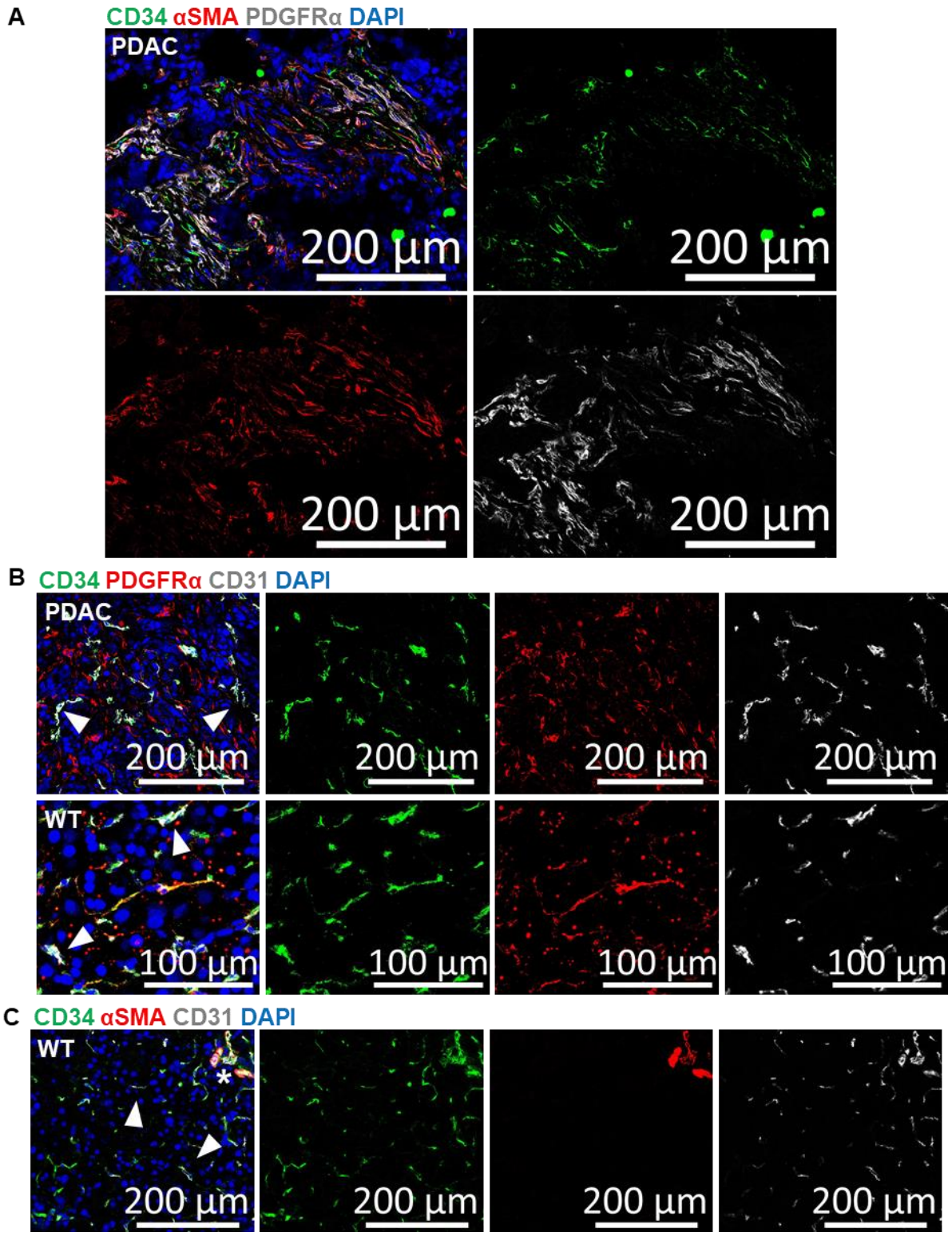

Fig. 5.20 Fibroblast populations in WT pancreas and KPC PDAC

IF images of normal (WT) pancreatic tissue and PDAC from KPC models. (A) PDAC Sections stained for CD34 (Green) αSMA (red) and PDGFRα (grey). (B) WT and PDAC sections stained for CD34 (Green) PDGFRα (red) and CD31 (grey). (C) WT sections stained for CD34 (green), αSMA (red) and CD31 (grey). Arrow heads indicate blood vessels, * indicates pericytes, scale is indicated, n = minimum of 3 mice.

Due to the limited number of samples available we were not able to explore the functional phenotypes of these populations experimentally. However, CD34 positive and negative CAFs were sorted and sequenced by Feig *et al*, who made this data publicly available [248]. GO term analysis, performed on DE genes, showed CD34+ CAFs upregulated cytokines and cytokine receptors, as well as complement components such as C3 (Fig. 5.21 A). Furthermore, *Acta2* (αSMA) was upregulated by CD34- CAFs, which also expressed matrix components and contractile machinery (Fig. 5.21 A and B). This suggests CD34+ CAFs in pancreatic tissue also possess an 'immune' phenotype, while αSMA+ populations are both 'desmoplastic' and 'contractile'.

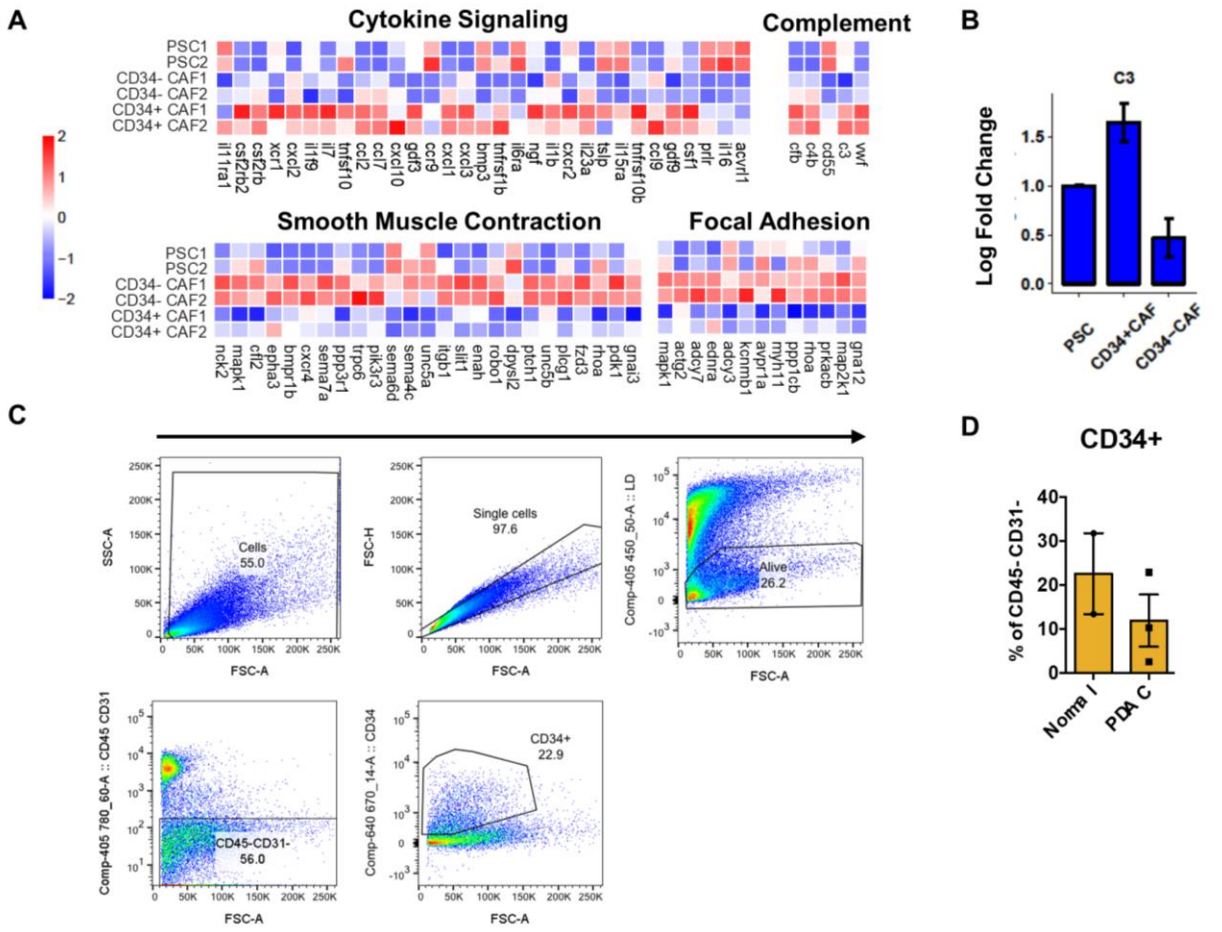

Fig. 5.21 Phenotype and prevalence of CD34+ CAFs in pancreatic tissue

Publicly available RNA seq data form Feig *et al* [248] of CD34+ and CD34- CAFs isolated from the KPC model of PDAC, as well as normal pancreatic stellate cells (PSCs). (A) Heat maps show selected pathways from GO analysis performed on differentially expressed genes between CD34+ and CD34- populations, z scores are displayed. (B) Log Fold Change in C3 and Acta2 (αSMA) RNA expression from PSCs, CD34+ CAFs and CD34- CAFs. (C) Gating strategy showing identification of CD34+ fibroblasts in pancreatic tissue. CAFs were selected by excluding doublets, dead, CD45+ immune and CD31+ endothelial cells. Graph displays FACs quantification of CD34+ fibroblasts as a percentage of CD45-CD31- cells in normal pancreatic tissue and KPC tumours. normal pancreas: n = 2 mice, KPC tumours: n = 3 mice.

This was further supported by data recently published by Elyada *et al*, acquired from the same model [301]. Here 'immune' iCAFs, 'myofibroblastic' myCAFs and 'antigen presenting' apCAFs were detected. Based on markers reported for these populations, including *Clec3b*, *Il6* and *Has1* (iCAF), *Thy1*, *Thbs2*, and *Col12a1* (myCAF) and *H2-Ab1*, *Cd74* and *Saa3* (apCAFs), fibroblasts were sub-setted and re-clustered (Fig. 5.22 A and B). *Cd34* was highly expressed in iCAF populations, as well as apCAFs at a lower level. *Acta2* (αSMA) expression was restricted to the myCAF population and, consistent with our experimental data, did not overlap with *Cd34* (Fig. 5.22 C). Interestingly, iCAF and myCAF populations expressed similar features to the CAF subsets identified in B16-F10 melanoma. For example, iCAFs upregulated inflammatory mediators *Cxcl12* and *C3* while myCAFs upregulated matrix components *Col1a2* and *Tnc* and contractile factor *Myl9* (Mlc2) (Fig. 5.22 D). Critically, in addition to C3, other complement components such as, *C4b*, *C1s1* and *C1ra* were upregulated by iCAFs, as well as the regulatory factor *Cd55* (Fig. 5.22 E). This suggests that, similar to 'immune' CAFs in melanoma, iCAFs also activate the complement pathway yet protect themselves from complement mediated lysis.

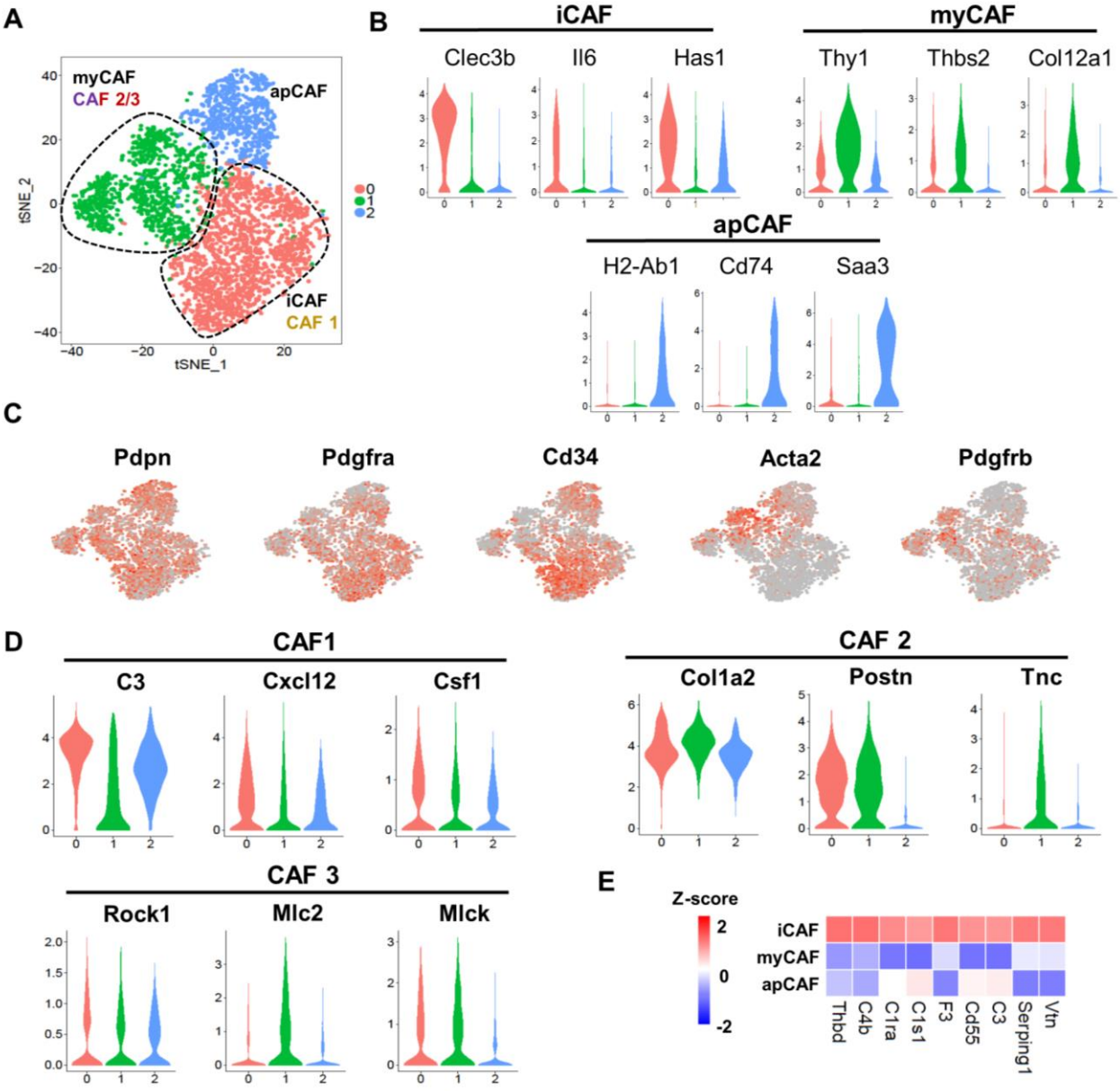

Fig. 5.22 CAF populations in the KPC model of PDAC share similar phenotypes with subsets identified in B16-F10 melanoma.

Publicly available sequencing data from Elyada *et al* [301] of CAFs isolated from the KPC murine model of PDAC . (A) Sequencing data was processed and re-clustered, displayed here as a tSNE plot. Labels indicate the populations that correspond to those identified by Elyada *et al* (iCAF, myCAF, apCAF), as well as those that share features with our CAF subsets. These were assigned based on expression of genes depicted in B-E. (B) Violin plots displaying expression of population markers identified by Elyada *et al*, confirming similar clusters were found. (C) tSNE plots coloured according to expression of typical CAF markers, red indicates high expression and grey indicates low expression. (D) Violin plot showing expression of genes associated with CAF1 'immune', CAF 2 'desmoplastic' and CAF3 'contractile' phenotypes. (E) Heatmap displaying the average expression across each population of factors belonging to the complement pathway identified by GO analysis, z score displayed.

5.2.4.4 ***Human cancers***

The conservation of ‘immune’, ‘desmoplastic’ and ‘contractile’ phenotypes in other murine models was exiting, but to determine clinical relevance, investigation into their presence in human cancers was needed. Again, to examine fibroblast populations in different types of human cancer, publicly available single cell data was used. Firstly, whether these CAF populations were present in human melanoma was examined. Tirosh *et al* sequenced the tumour and stromal compartments of 19 human melanomas at different stages of progression, which contained various activating mutations [414]. Re-clustering CAFs revealed two distinct populations of which one displayed both ‘immune’ and ‘desmoplastic’ phenotypes, while the other resembled the ‘contractile’ CAF3 population (Fig. 5.23 A). Furthermore, *CD34* and *ACTA2* (αSMA) expression was associated with the CAF1/2 and CAF3 populations respectively, reflecting our murine model (Fig. 5.23 B). In addition, pericyte markers *CPSG4* (Ng2), *MCAM*, *RGS5* and *NOTCH3* were also present within these CAF clusters, although expression was divided across the two populations (Fig. 5.24 A).

Although a clear separation between *ACTA2* and *CD34* expressing CAFs was present, the small number of CAFs isolated in this study likely masks further sub populations. For example, this may obscure the distinction between ‘desmoplastic’ and ‘immune’ fibroblasts. However, consistent with the mouse models and relevant to the clinic, *CD34* expressing CAFs exhibited the highest levels of *C3* within the fibroblast compartment, as well as the tumour as a whole (Fig. 5.23 C and 1.24 B). In addition, expression of C3aR was restricted to macrophage populations, suggesting the interaction between these populations is conserved in human melanoma (Fig. 5.24 B).

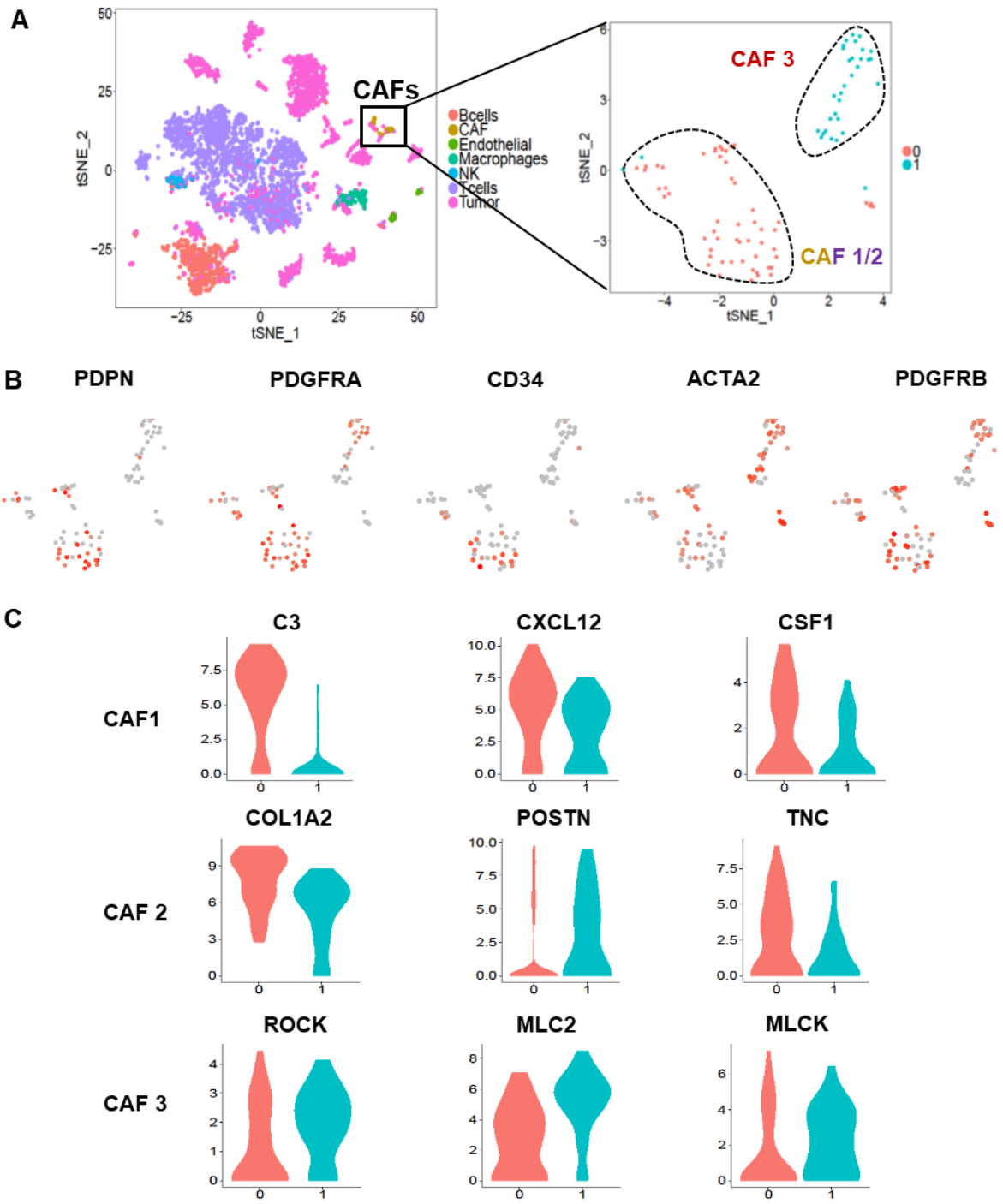

Fig. 5.23 Similar CAF populations were identified in human melanoma

Publicly available sequencing data from Tirosh *et al* [414] of CAFs isolated from the human melanoma. (A) tSNE plot (left) showing all sequenced populations, labels indicate cell identities assigned by Tirosh et al. CAFs were subsetted and re-clustered (tSNE right) populations that that share features with our CAF subsets are indicated. These were assigned based on expression of genes depicted in B-C. (B) tSNE plots coloured according to expression of typical CAF markers, red indicates high expression and grey indicates low expression. (C) Violin plot showing expression of genes associated with CAF1 'immune', CAF 2 'desmoplastic' and CAF3 'contractile' phenotypes.

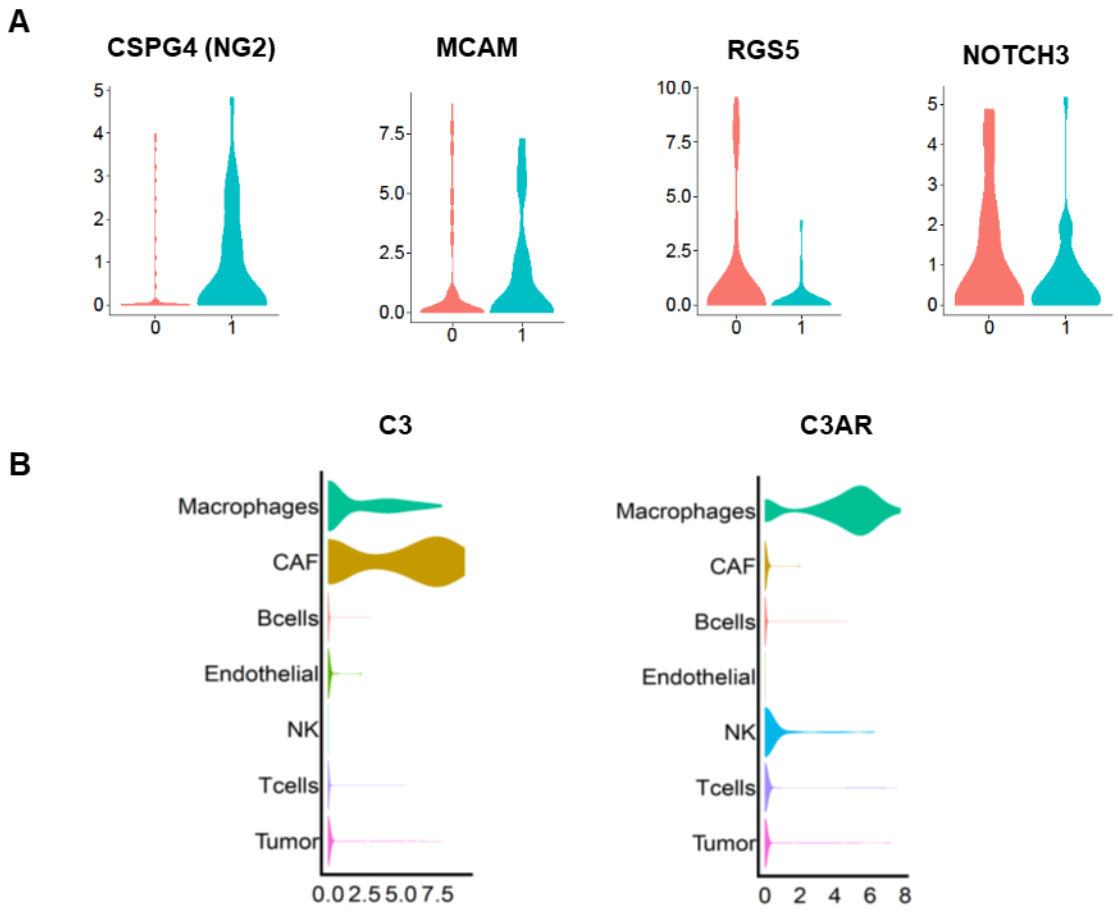

Fig. 5.24 Expression of Pericyte markers, C3 and C3aR in CAFs and other populations in Human melanoma

Publicly available sequencing data from Tirosh *et al* [414] of human melanoma. Violin plots displaying expression of pericyte markers across fibroblast populations (A) and C3 and C3aR expression across all populations identified (B).

To investigate whether these populations translate to other human cancers, single cell data sets from head and neck and colorectal cancer were examined [300,415]. Fibroblast sub-sets in these data sets also resembled ‘immune’, ‘desmoplastic’ and ‘contractile’ populations, although there were some differences in associated surface markers (Fig. 5.25 and Fig. 5.26). Again, in both data sets, pericyte markers were associated with ‘contractile’ populations (Fig. 5.27 A). Importantly, *Cd34*^{high} populations from both tumour types expressed complement component *C3*, and the specificity of interactions between *C3* producing CAFs and *C3aR*$^{+}$ macrophages was retained (Fig. 5.27 B). Furthermore, fibroblasts were the key sources of *C3* in both tissues, although it was also expressed by macrophages in head and neck cancer. This suggests that *CD34*^{high} fibroblasts could act as a biomarker for the application of anti-C3a therapies.

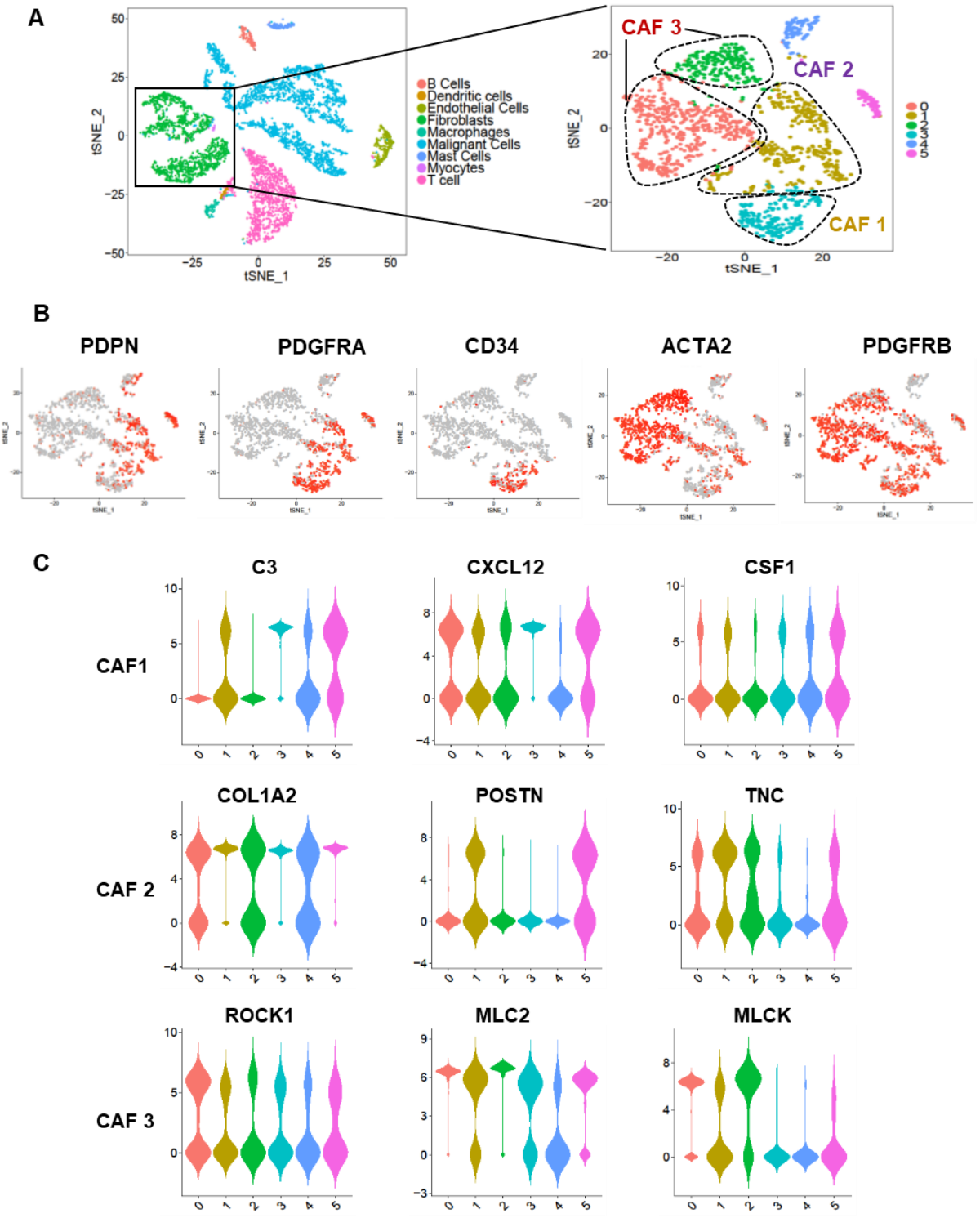

Fig. 5.25 Similar CAF populations were identified in human head and neck cancer

Publicly available sequencing data from Puram *et al* [300] of CAFs isolated from human head and neck squamous carcinoma. (A) tSNE plot (left) showing all sequenced populations, labels indicate cell identities assigned by Puram *et al*. CAFs were subsetted and re-clustered (tSNE right) populations that that share features with our CAF subsets are indicated. These were assigned based on expression of genes depicted in B-C. (B) tSNE plots coloured according to expression of typical CAF markers, red indicates high expression and grey indicates low expression. (C) Violin plot showing expression of genes associated with CAF1 'immune', CAF 2 'desmoplastic' and CAF3 'contractile' phenotypes.

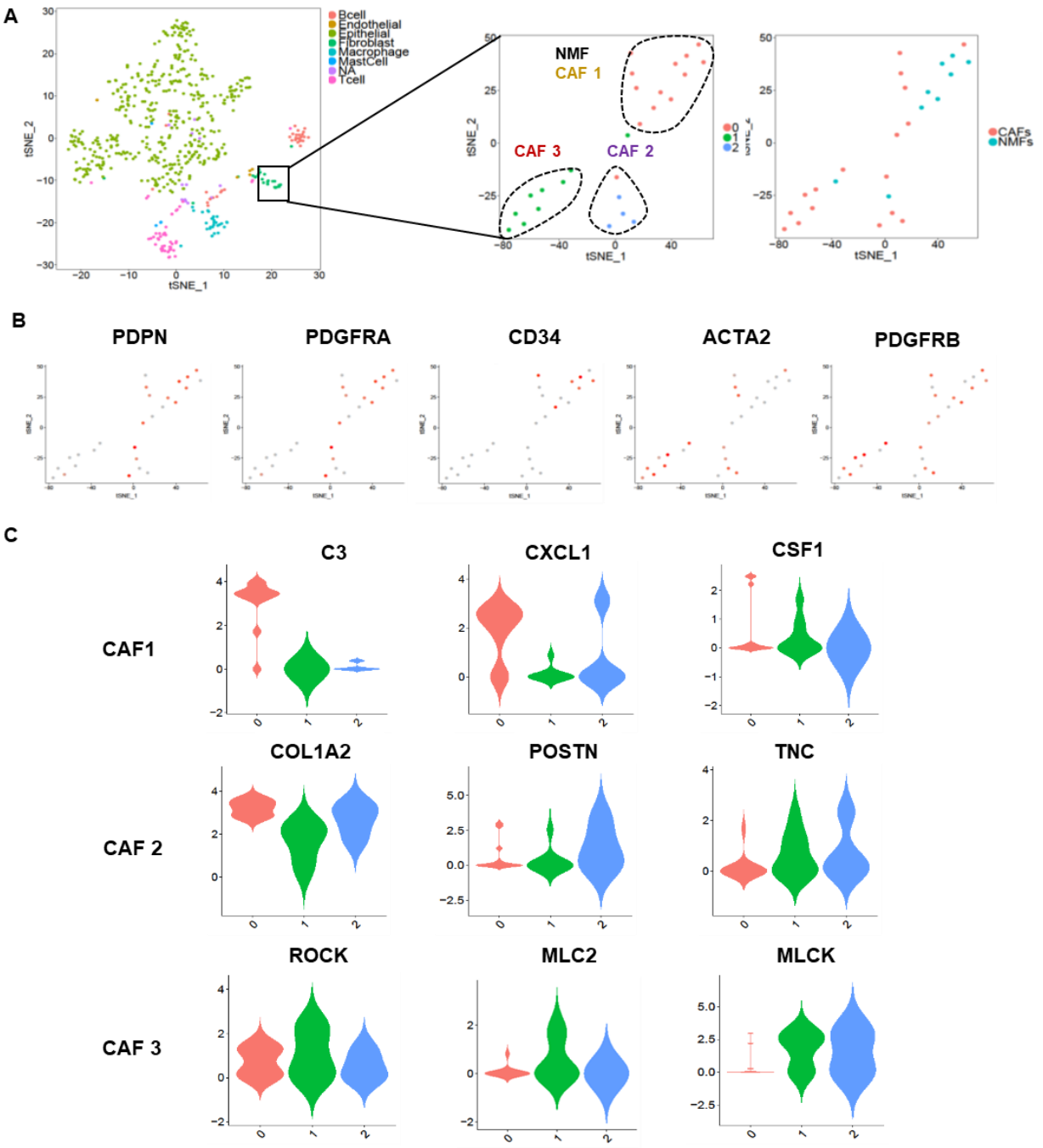

Fig. 5.26 Similar CAF populations were identified in human colorectal cancer

Publicly available sequencing data from Li *et al* [415]of CAFs isolated from human head and neck squamous carcinoma. (A) tSNE plot (left) showing all sequenced populations, labels indicate cell identities assigned by Li *et al*. CAFs were subsetted and re-clustered. tSNE plots show identified populations (centre) and whether these populations were isolated from malignant (CAF) or normal (NMF: Normal Mucosal Fibroblasts) tissue (right). Fibroblasts that that share features with our CAF subsets are indicated. These were assigned based on expression of genes depicted in B-C. (B) tSNE plots coloured according to expression of typical CAF markers, red indicates high expression and grey indicates low expression. (C) Violin plot showing expression of genes associated with CAF1 'immune', CAF 2 'desmoplastic' and CAF3 'contractile' phenotypes.

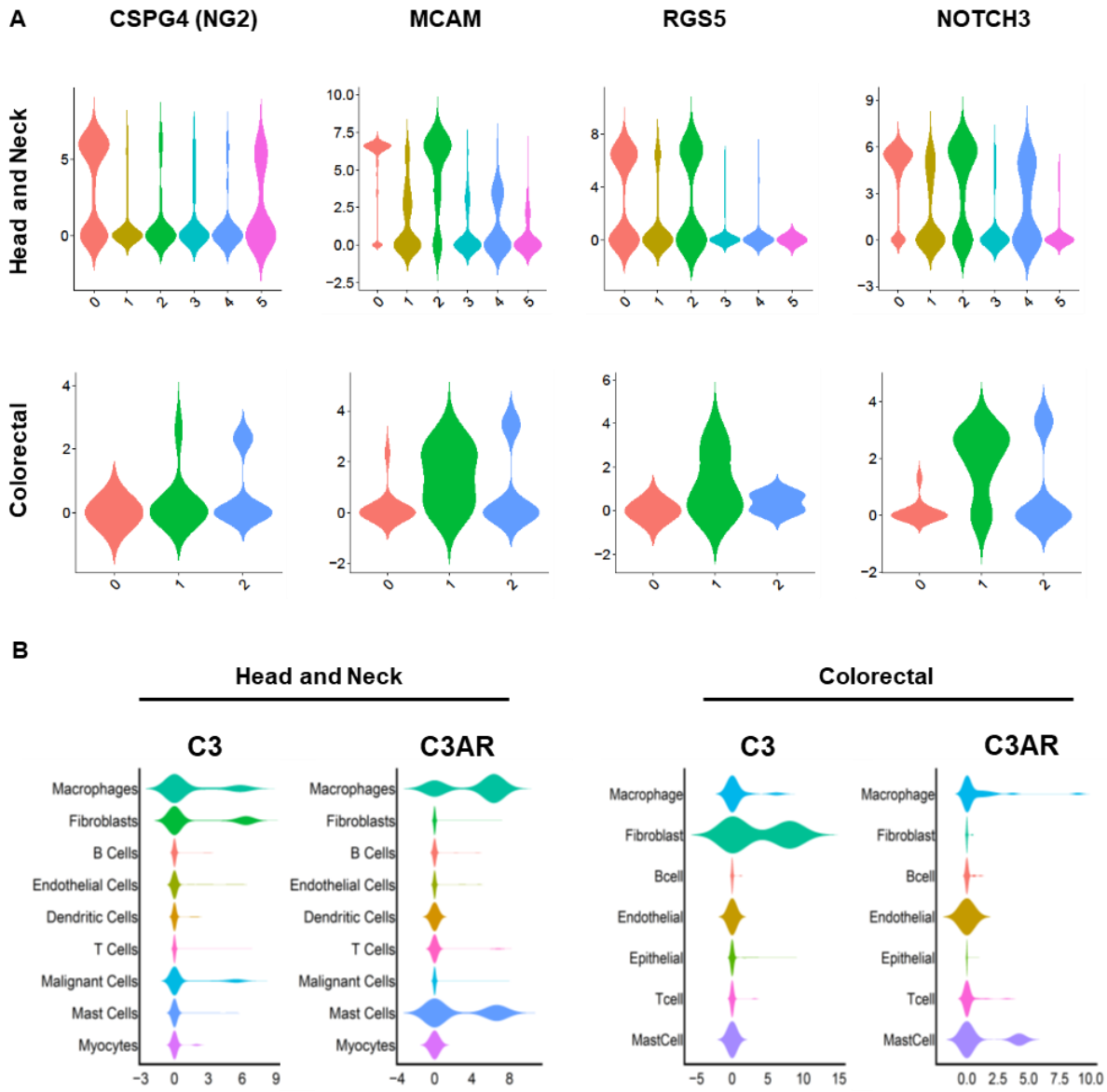

Fig. 5.27 Expression of Pericyte markers, C3 and C3aR in CAFs and other populations in Human head and neck cancer and colorectal cancer.

Publicly available sequencing data from Puram *et al* [300]and Li *et al* [415] of human head and neck cancer and colorectal cancer respectively. Violin plots displaying expression of pericyte markers across fibroblast populations (A) and C3 and C3aR expression across all populations identified (B).

5.3 ***Summary***

Having identified three functionally distinct CAF subsets, this chapter explored their impact on melanoma development, as well as their conservation in other types of cancer. Here we have focussed on the 'immune' CAF1 subset and their interactions with tumour leukocytes. Although immune populations have the ability to detect and kill malignant cells, anti-tumour immunity depends on the particular populations present and their functional state[7]. Thus, to determine the potential impact of CAF1-Leukocyte cross-talk on tumour growth, characterisation of the melanoma immune compartment was performed using sequencing data obtained from immune cells, isolated in tandem with fibroblasts. This revealed recruitment of inflammatory cells, as well as the development of an immunosuppressive microenvironment at later time points. Investigation of the innate compartment showed increased expression of costimulatory and inflammatory factors, in tumour resident cells, compared to those in the lymph node. However, at later stages, these cells increased expression of suppressive molecules such as PDL1 and Arg1. Furthermore, these dynamics were mirrored by the adaptive compartment. Here, CD8 T-cells predominantly displayed a naïve phenotype in the lymph node, becoming activated in the tumour and undergoing clonal expansion. However, at later time points, T-cells also developed expression of dysfunction markers *Ctla4*, *Pd1* and *Lag3*. This suggests that, rather than undergoing activation in the lymph node, these cells are recruited to the tumour in a naïve state and are activated *in situ*, a phenomenon reported in other murine models. [403].

The simultaneous development of activating and suppressive phenotypes in tumour resident innate and adaptive populations, suggested myeloid cells contribute to activation and dysfunction of T-cells. While increased expression of PDL1 and ARG1 in myeloid cells, and PD1 in T-cells, was confirmed in day 11 tumours, functional validation is still required to verify a suppressive phenotype. This is particularly pertinent in regard to CD8 T-cells, as exhaustion markers are also upregulated during the activation process [416]. Furthermore, T-cells in our model retained expression of granzyme enzymes, suggesting their cytotoxic functions may still be intact. However, T-cell exhaustion involves the progressive downregulation of effector molecules, in which these enzymes are only lost at advanced stages [37]**.** Nevertheless, to conclusively determine their functional state, *ex vivo* assays could be performed on

cells from different time points. Furthermore, it is possible that activated T-cells are present in draining lymph nodes yet were masked by the overwhelming numbers of naïve cells. Thus, to confirm activation of adaptive cells in the tumour, further characterisation of activation and naïve markers in both compartments is required.

Following the identification of suppressive and tolerogenic immune phenotypes, the involvement of CAF1 fibroblasts in this process was assessed. The cognate receptors to CAF1 cytokines were expressed predominantly by macrophages, monocytes and neutrophils, suggesting cross-talk between these populations. As C3 was specifically expressed by CAF1 cells in the tumour microenvironment, the effects of blocking C3a signalling were investigated. Neutralisation of C3a reduced the number of macrophages at early time points, increased CD8 T-cell infiltration, and decreased the rate of tumour growth. In agreement with the literature, C3aR was not detected in T-cell populations, suggesting that changes in lymphocyte abundance were induced indirectly [417–421]. Thus, we propose that a reduction in suppressive myeloid populations increases T-cell recruitment or survival. Indeed, *C3ar* was uniquely expressed by phagocytic myeloid cells, at the transcript level, indicating this population alone should be impacted by treatment directly. However, the presence of the receptor in other stromal populations, or malignant cells, was not confirmed at the protein level. As macrophages are likely monocyte derived, if C3a impacted their recruitment, a parallel decrease in Ly6C+ cells would be expected. Thus, the slight increase in their number indicates that C3a is potentially involved in monocyte to macrophage differentiation, rather than acting as a chemotactic stimulus. Similar trends in myeloid populations upon C3aR antagonism support these findings, although, all experiments were highly variable and require repeating. Furthermore, it is crucial to stress that changes in macrophage abundance, in both treatment regimes, are small (~10-20%), suggesting other mechanisms are likely involved.

Despite the small scale of these alterations, a >2fold reduction in CD8 T-cells was observed upon C3a neutralisation. This suggests that even such small and variable changes in macrophage numbers, are sufficient to increase CD8 T-cell survival or recruitment. However, these results were not corroborated by C3aR antagonism, in which CD8-Tcells appeared unaffected by treatment. While this could suggest C3a neutralising antibodies have off-target effects, other possible causes are discussed in Chapter 6. While treatment with anti-C3a also reduced the rate of tumour growth,

again, these changes were moderate. This may reflect the retention of dysfunction markers PD1 and LAG3 on CD8 T-cells, which suggests their cytotoxic functions remain impaired. To restore T-cell functionality, a greater decrease in macrophage numbers, or a reduction in suppressive molecule expression, may be required.

Although these experiments are decidedly preliminary, the initial results suggest that CAF derived C3/C3a is involved in the maintenance of tumour macrophages. While the small scale of changes, upon blockade of C3a signalling, may suggests functional redundancy, both treatment regimens require optimisation. Thus, the importance of the C3/C3a pathway in the development of an immunosuppressive microenvironment, as well as the utility of this axis as a therapeutic target, requires further investigation. This is discussed in more detail in Chapter 6, along with possible optimisation strategies.

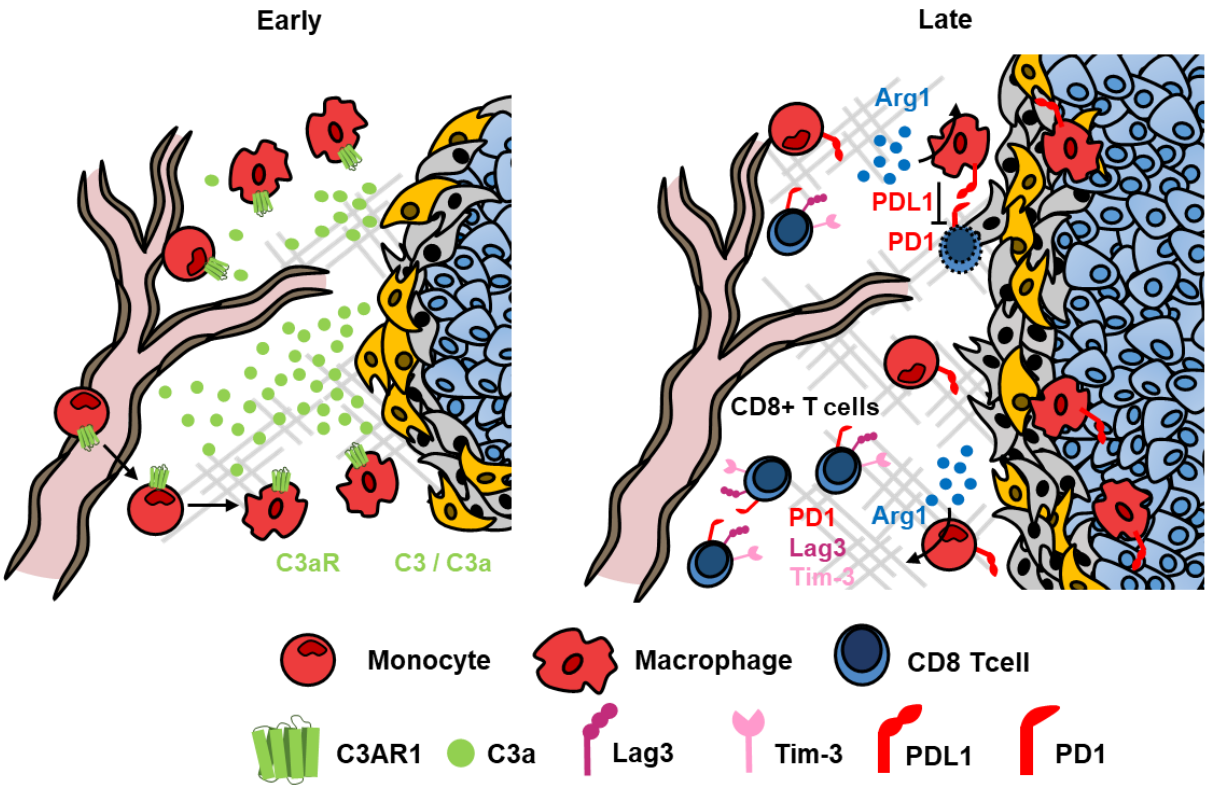

Fig. 5.28 C3 production by CAFs in important for the development of an immunosuppressive environment

Schematic showing the proposed role of C3/C3a production in the tumour microenvironment. Monocytes are recruited to the tumour at early stages where the undergo differentiation to macrophages, promoted by C3a At later time points macrophages increase expression of suppressive molecules PDL1 and ARG1. These molecules further induce suppression of CD8 T-cell populations, which increase expression of dysfunction markers.

Despite uncertainty surrounding the role of C3/C3a in the TME, our data indicate blocking this pathway my provide some therapeutic benefit. Consequently, conservation of C3 expressing CD34+ CAFs, in other models of murine and human cancer, was assessed both experimentally and using online sequencing data. To begin with, we utilised the $BRAF^{V600E}PTEN^{-/-}$ melanoma model, which recapitulates the genetic landscape of human melanoma and contains a fibrotic stromal compartment. $CD34^{high}$ fibroblasts were present in this model, although represented a much rarer population. Nevertheless, these CAFs also expressed the highest levels of C3, compared to tumour and other stromal cells. The small number of $CD34^{high}$ CAFs detected, may be due to the use of advanced spontaneous tumours for these investigations, that contain a dense fibrotic core. Therefore, it is possible that this population is more prevalent in BRAF melanomas at earlier time points. Indeed, we previously showed that CD34+ CAFs were abundant in normal skin (4.2.4.3) and displayed increased expression of C3. This suggests that discrepancies between the B16 and BRAF melanoma models are caused by differences in local cues. However, it is remains unclear which model more accurately resembles the CAF compartment of human melanoma. Although human tumours and the BRAF model share similar genetic mutations and growth kinetics, few comparisons of stromal components have been made. In particular, it is unclear whether reported increases in matrix components, in human melanoma, are as extensive as the fibrosis observed in spontaneous BRAF tumours. However, the presence of CD34+ C3+ CAFs in publicly available sequencing data from human melanoma [414], suggests this population is conserved.

In addition to melanoma, the composition of CAF populations was also investigated in pancreatic and breast murine models, as well as human colon and head and neck cancer. Similar to the BRAF model, CD34+ CAFs were rare in the KPC model of PDAC yet represented the dominant population in the normal pancreas. This is consistent with Feig *et al's* findings, in which $CD34^{high}$ fibroblasts were found surrounding early PanIn lesions [248]. However, despite their infrequency, this population also highly expressed C3, suggesting this function is conserved. Interestingly, like melanoma, investigation of CAF populations in murine breast cancer also revealed discrepancies between models. While CD34+ C3+ CAFs were abundant in the E0771 injectable

model, sequencing data from MMTV-PyMT tumours revealed little expression of *C3* and *Cd34* [299]. Again, this may reflect inherent differences between the two systems, such as the rate of tumour growth and oncogenic mutations [422–424]. It is also possible that, similar to the BRAF model, as only advanced MMTV-Pymt tumours were examined, CD34+ CAFs may be more abundant at earlier stages. In addition, while both models are classified as 'Triple Negative' (owing to low expression of the Oestrogen, Progesterone and HER2 receptors), E0771 tumours display a basal phenotype whereas as MMTV-PyMT tumours are described as luminal [425,426]. Such differences in latency, genetic landscape and subtype, likely effect production of secreted factors, which could alter the local cytokine milieu and significantly influence the development of CAF heterogeneity. Interestingly, regardless of disparity between models, C3 expression was increased in CD34+ CAFs compared to normal fibroblasts in the same tissue, across all three types of cancer examined. This suggests C3 is upregulated upon tumour initiation.

Importantly, *C3* expression was associated with $CD34^{high}$ fibroblasts in other human malignancies, including colorectal and head and neck cancer. Moreover, consistent with murine models, this CAF population was the dominant source of C3 expression in the tumour microenvironment. This data implies multiple cancers may benefit from anti-C3a therapies and highlights the potential of CD34 expressing CAFs may as a biomarker for its application. In addition to the conservation of CAF1-like populations, populations that resemble our 'contractile' CAF3 subset were also identified in both murine and human datasets. Interestingly, these CAF 3-like fibroblasts also expressed pericyte markers *Cspg4* (Ng2), *Mcam*, *Rgs5* and *Notch3*. Similar to our findings, this population was observed both surrounding blood vessels and at the leading edge of MMTV-PyMT breast tumours. This suggests pericytes dissociate from the endothelium and form a subset of fibroblast populations in the periphery. However, it remains unclear whether our CAF3 population represents pericytes or fibroblasts and highlights the poor characterisation of mesenchymal cells.

Finally, we explored the contribution of different fibroblast origins to the development of CAF heterogeneity. As previously discussed, pericytes could represent the source of CAF3 fibroblasts in this model. However, investigating this hypothesis would require complicated lineage tracing models. Thus, we focused on recruitment of mesenchymal cells from the bone marrow, which has been reported to contribute to the fibroblast

compartment in pancreatic and gastric cancer [274,275,278]. However, chimeric models showed only 1-2% of CAFs were recruited from the bone marrow. Thus, it is unlikely that the bone marrow represents a source of fibroblasts in the B16-F10 model. However, the rapid growth of B16 tumours may not provide enough time for recruitment of bone marrow cells, or do not produce the required recruitment factors. Thus, while the bone marrow does not contribute to CAF heterogeneity in this model, it could serve as a significant source in other cancer types.

In conclusion, this chapter highlighted a potential role for CAF1 cells in the development of an immunosuppressive environment. Furthermore, similar CAF populations were observed in additional murine models and different types of human cancer. Subtle differences in marker expression and temporal dynamics likely reflect physical and soluble factors unique to each cancer type. Variations in driver mutations, immune infiltration and tissue type all influence the local cytokine milieu, sculpting CAF phenotypes. However, despite this diversity, C3 expression was consistently upregulated in $CD34^{high}$ fibroblasts. In addition, the interaction between these cells and myeloid populations was conserved across cancer type and species. The factors contributing to diversity among CAF populations across cancer, as well as the utility of anti-C3a therapies, is discussed in more detail in the following Chapter.

6

Discussion

Despite the development of targeted therapies and immune checkpoint inhibitors, melanoma still suffers from a severe clinical unmet need. The numerous mechanisms through which CAFs support tumour growth and development, highlights their potential as therapeutic targets for this disease [409]. This is emphasised by their involvement in therapy resistance and raises the possibility of targeting fibroblast in combination with existing therapeutics. However, as previously discussed, the innate heterogeneity and plasticity of these cells represents a significant barrier to drug development. While recent studies have revealed the existence of functionally distinct CAF populations, whether similar subsets are present in melanoma is unclear [298–301]. Furthermore, how CAF populations arise and adapt to the developing tumour microenvironment remains poorly examined. Thus, this project aimed to profile the composition of the CAF compartment, in murine models of melanoma, at different stages of tumour development. This included the identification of distinct populations and investigating their functional properties.

6.1 *Functionally distinct CAF populations were identified in melanoma*

Initial studies were conducted in the $BRAF^{V600E}$ $PTEN^{-/-}$ murine melanoma model, as it recapitulates the genetic landscape of a large proportion of human disease. Profiling fibroblast markers and matrix proteins, across different stages of tumour growth, revealed the development of an extensive fibrotic core at later time points. However, fibrosis was most prominent in spontaneously arising melanomas. SPADE analysis of the 4 markers FAP, PDPN, Thy1 and PDGFRα, revealed significant heterogeneity in their expression. While there was considerable variability between time points and individual animals, the existence of a population expressing all 4 markers and a subset only expressing PDPN and FAP, was a common theme. These two populations were present at all time points, including induced skin from non-carriers.

Interestingly, both Thy1 and PDGFRα are not merely CAF markers but possess functional properties. While PDGFRα and PDGF signalling has long been associated with activation of fibroblasts, the role of Thy1 in this process is more controversial. Thy1 does not follow normal ligand-receptor relationships but engages with an

abundance of surface molecules [427]. These include both paracrine and autocrine interactions with surface proteins on neighbouring cells, as well as in the adjacent membrane space [428]. In fibroblasts, it is involved in TGFβR signalling[429] and is a key regulator of mechanotransduction. By altering integrin avidity to ECM substrates and recruiting signalling molecules to focal adhesions, Thy1 influences the ability of cells to sense their physical surroundings. Indeed, its loss rendered these cells incapable of responding to changes in matrix stiffness [430]. Although both TGFβ signalling and increased substrate rigidity are important contributors to fibroblast activation (discussed in detail below), the impact of Thy1 on their differentiation is varied and may be context dependent. For example, in lung fibrosis, Thy1 is epigenetically downregulated and loss of expression is correlated with disease pathology [431,432]. On the other hand, expression of this glycoprotein is positively associated with dermal and liver fibrosis, as well as expansion of the fibroblast compartment in hepatocellular carcinoma [433–435]. Considering the involvement of both Thy1 and PDGFRα in fibroblast activation, it is possible that the two populations observed in BRAF melanomas, reside in different differentiation states.

However, it is doubtful that 4 CAF markers alone, capture the true scale of fibroblast heterogeneity. Furthermore, functional diversity may not be related to expression of surface proteins. Thus, restricting investigations to these markers, may introduce bias and mask more important differences. This is supported by homogeneous expression of Thy1 across previously identified functional dermal subsets [436,437]. Therefore, to obtain a broader picture of CAF diversity, scRNAseq technology was combined with a 'negative selection' approach to isolate and sequence melanoma fibroblasts. This technology offers the unique opportunity to visualise the transcriptomes of multiple cells in tandem, giving unprecedented insight into the populations and phenotypes that reside in complex systems. Unfortunately, a marker of tumour cells was not available for the $BRAF^{V600E}$ $PTEN^{-/-}$ system, thus, the B16-F10 syngeneic model of melanoma, was used instead.

A pilot study showed CAFs, isolated from a single time point, displayed unique transcriptional profiles which were validated *in vivo*. This data highlighted that environmental cues, such as hypoxia, play an important role in fibroblast heterogeneity. While it is unclear whether low oxygen tension directly activated HIF1 in CAFs, or whether this was indirectly induced by hypoxic tumour cells (discussed in

section 3.2.2.6), fibroblasts situated close to hypoxic regions upregulated glycolytic enzymes. Although we have focussed on the metabolic implications of HIF1 activity, this transcription factor has a diverse range of targets and may directly regulate CAF function. For example, by inducing expression of CXCL13, VEGFA and MCP-1, HIF1 enhances the ability of fibroblasts to recruit leukocytes [438–440]. In addition, hypoxic CAFs can modify the immune compartment by secreting lactic acid, a biproduct of glycolysis. This metabolite is known to induce macrophage polarisation towards an M2 phenotype[110] and promotes T-reg induction [246]. Thus, fibroblasts under low oxygen conditions may contribute to immune suppression in the melanoma environment. While the impact of hypoxia on CAF function in the TME is interesting, the identification and validation of this glycolytic subset demonstrates the advantage of scRNAseq to discern distinct transcriptional programs. Such differences may have been lost if populations were pre-defined by marker expression. Indeed, these subsets were not defined by the pattern of markers previously identified in the $BRAF^{V600E}$ $PTEN^{-/-}$ model. However, expression of these markers was variable, indicating these populations may still exist, but are not transcriptionally distinct.

To investigate how fibroblast phenotypes and their composition adapt within the evolving microenvironment, scRNAseq was applied to CAFs isolated at different stages of melanoma development. This revealed three transcriptionally distinct populations, each possessing a unique marker repertoire. The first population, CAF1, displayed high expression of PDPN, PDGFRα and CD34. This group upregulated cytokines and cytokine receptors, consistent with a role in immune cross-talk. In particular, ‘immune’ CAFs highly expressed factors involved in activation of the complement cascade, including the central component C3. Furthermore, expression of cognate receptors to CAF1 derived inflammatory factors, on tumour macrophages, suggested this population may be involved in recruitment and regulation of myeloid cells.

Other populations included a $PDPN^{high}$ $PDGFR\alpha^{high}$ $CD34^{low}$ ‘desmoplastic’ subset, which may be responsible for pathological matrix remodelling, as well as an αSMA^{high} ‘contractile’ group. Interestingly, these populations were dynamic, changing in prevalence as the tumour developed. Here, the fibroblast compartment was dominated by ‘immune’ and ‘desmoplastic’ populations at early stages, while the ‘contractile’ subset became more abundant at later time points. The discovery of a diverse and

evolving fibroblast niche has significant implications for therapeutics targeting these cells. We have previously discussed the contrasting effects of depleting fibroblasts from the tumour stroma, based on expression of αSMA and FAP [248,303]. As our data indicates these markers delineate two distinct populations, targeting cells based on their expression could remove specific functional subsets. Furthermore, CAFs expressing αSMA appear to be more prominent in advanced tumours, highlighting that the presence of certain populations governs both therapeutic strategy, as well as the timing of application.

Interestingly, when examined at different time points, the identifying phenotypes of individual populations were unchanged. This suggests that the functional roles of each CAF subset are not altered by increased malignant growth, but merely expand or contract as the tumour develops. However, the limited number of cells belonging to CAF1 at day 11 or CAF3 at day 5, reduce the validity of these results. Thus, more cells are required to truly identify changes in fibroblast phenotype across time, at the population level. Nevertheless, a subset of both CAF2 and CAF3 populations developed additional glycolytic signatures, at later time points. This coincided with increased staining of hypoxic marker CA9, suggesting that hypoxia induces metabolic heterogeneity in more advanced tumours. These results highlight that factors arising from increased strain on the local environment, imparted by the expanding tumour, can induce further diversity in the CAF compartment.

Validation of these populations revealed all 3 are present in normal skin and throughout tumour development, however, the CAF3 subset expands at later time points. Thus, different CAF populations may resemble pre-existing functional subsets in the dermis, whose abundance adapts during tumour growth. This theory is further supported by our initial studies of the $BRAF^{V600E}$ $PTEN^{-/-}$ model. Although only defined by expression of 4 CAF markers, all populations were present in skin samples, through to advanced spontaneous tumours. However, population defining markers identified in the B16 model, do not show the same expression pattern in advanced spontaneous $BRAF^{V600E}$ $PTEN^{-/-}$ tumours. To begin with, PDGFRα expression was restricted to a subpopulation of fibroblasts in the upper layer of the dermis. This reflects our earlier findings that show PDGFRα and Thy1 may mark a subpopulation of cells. In addition, αSMA expression was less distinct from the other markers and CD34+ CAFs represented a much smaller population. However, despite their reduced abundance,

this population also upregulated C3. The reasons underlying such vast differences in these models have been previously discussed (section 5.3) but may represent variation in the local environmental factors. Again, it is important to emphasize that, despite recapitulating the genetic landscape of human melanoma, stromal and immune populations in the BRAF model are not well characterised. Thus, it is unclear whether features of human disease, such as immune dysfunction, are recapitulated. Furthermore, the extensive collagen deposition, observed in spontaneous tumours, is not commonly reported in melanoma. Indeed, owing to this fibrosis, B16 tumours may be more comparable to earlier stages of BRAF tumour development. Moreover, the malignant compartment in both models resides in the dermis, whereas human melanomas develop at the dermal/epidermal junction. As discussed in section 6.4, fibroblast populations located in hair follicles or the papillary and reticular dermis have distinct phenotypes. Thus, owing to the identity and abundance of surrounding local fibroblasts, the anatomical position of the tumour may impact CAF composition. Although, it is unclear which model, if any, accurately captures the melanoma fibroblast compartment, similar populations were conserved in sequencing data obtained from patients.

While this data represents a significant delineation of fibroblast heterogeneity in melanoma, the functions of each population are implied based on transcriptional expression. Furthermore, the broader role of these subsets during tumour development, or whether they promote or constrain malignant growth, remained unclear. Concomitant to changes in the CAF compartment, immune infiltrates develop tolerogenic phenotypes at later time points. This includes expression of suppressive molecules on macrophage populations, as well as the upregulation of lymphocyte dysfunction markers. Considering potential cross-talk between tumour leukocytes and ‘immune’ CAFs, the involvement of these fibroblasts in the generation of this immunosuppressive environment was investigated.

Expression of population defining markers by other stromal components, precluded depletion studies as a method to investigate their role in the TME. Consequently, functional studies focussed on inhibiting C3a, the pro-inflammatory cleavage product of C3, which is uniquely expressed by this subset. Both antibody neutralisation of C3a and antagonism of the C3aR receptor, induced a small reduction in macrophage numbers, validating predicted interactions between CAF1 fibroblasts and myeloid

populations. This is consistent with reported effects of this anaphylatoxin on myeloid cells, during an number of biological processes [441–444]. Interestingly, no reduction in monocyte recruitment was observed upon treatment, conversely, the number of Ly6C+ cells marginally increased. Thus, C3a may be important for monocyte-macrophage differentiation, rather than recruitment.

However, as previously discussed (section 5.3), observed changes in population size are limited. This may be due to functional redundancy (discussed in section 5.3), however, both treatment regimens require further optimisation. To begin with, the concentration of intertumoral C3a was not measured, making it difficult to determine the amount of the neutralising antibody required. Furthermore, only one publication has performed *in vivo* studies using the same antibody clone [445]. Owing to concerns regarding adverse reactions, the same concentration (2µg per injection) was administered. However, compared to other antibody regimes, this concentration is relatively low. As treatment is well tolerated, increased amounts of antibody could be injected, at more frequent intervals. Increased sequestration of C3a, may heighten observed changes in macrophage abundance. Similarly, the dose and treatment regime for the C3aR antagonist, was determined using published studies [444,446]. Thus, the extent to which either treatment inhibits C3a signalling is unknown.

Despite these caveats, blocking C3a also increased T-cell infiltration and modestly reduced the rate of tumour growth. As tumour resident T-cells do not express C3aR, it was hypothesised that changes in their abundance was driven by concomitant decreases in macrophage numbers. As myeloid cells highly expressed suppressive markers, it is possible that a reduction in population size may promote T-cell survival and anti-tumour cytotoxicity. However, neutralising C3a did not impact expression of lymphocyte dysfunction markers, suggesting increased cell numbers was not accompanied by restoration of function. This is consistent with the limited effects of treatment on macrophage expression of T-cell modulating factors, PDL1 and Arg1. Thus, the combination of C3a neutralisation with immune checkpoint inhibition may synergise to constrain tumour growth, by both promoting T-cell infiltration and enhancing their cytotoxic properties. This concept is discussed in more detail in section 6.5.

However, it is important to stress that these trends in T-cell infiltration and tumour growth, were not recapitulated by inhibition of C3aR. As targeting both C3a and its receptor reduced the number of macrophages in the TME, this may not mediate parallel changes in the T-cell compartment. However, the C3aR antagonist, SB290157, has been reported to have additional agnostic effects, which may impact macrophage function and their interactions [447]. In addition, such discrepancies may also be a product of the pharmacokinetic properties of the drugs used in these studies. As highlighted above, the extent to which C3a signalling is inhibited, by use of either treatment, remains unknown. It is possible that C3a modulation of macrophage biology is concentration dependent. Thus, the level of C3a/C3aR inhibition may affect their concurrent interactions with T-cells. A similar phenomenon has been described for the related anaphylatoxin C5a. Here, different concentrations C5a promoted macrophages to induce either Th1 or T-reg differentiation [448].

Overall, several additional experiments are required to corroborate these results and confirm the underlying mechanisms. Firstly, whether treatment efficacy underlies the limited scale of changes in population size, can be addressed by conditional deletion of C3aR *in vivo*. Establishing B16 tumours in C3aR floxed models, would also enable a comparison of C3aR deletion, at different stages of melanoma development. In addition, macrophage depletion in these models would confirm their involvement in promoting CD8 T-cell infiltration, upon C3a blockade. Bulk sequencing of macrophages from C3aR knockout mice, or those treated with an inhibitor, may provide further mechanistic insights into this process. Moreover, comparing the transcriptome of macrophages, isolated from tumours treated with either the C3aR antagonist or the C3a neutralising antibody, may reveal if these inhibitors differentially impact macrophage function. Finally, the impact of C3a signalling on macrophage biology could be validated *in vitro*. This could include testing the involvement of C3a in monocyte to macrophage differentiation, by addition of recombinant anaphylatoxin to cultures in which C3aR has been deleted or knocked down. The effect of C3a signalling on macrophage interactions with T-cells, could also be assessed by incorporating lymphocytes in these cultures. Possible outputs include, regulation of T-cell proliferation, survival, migration and cytotoxicity.

6.2 *CAF populations across different types of Cancer*

As previously discussed, functionally distinct fibroblast populations have been reported in cancers other than melanoma. Similar to our findings, Feig *et al* observed that CD34 and αSMA delineated two different populations in the KPC model of PDAC [248]. Despite the availability of bulk sequencing data from these two populations, we are the first to compare their transcriptomes. This showed that, analogous to melanoma, CD34 also marks a subpopulation of CAFs that upregulate cytokines and cytokine receptors in pancreatic tumours, indicative of a role in immune cross-talk. While the cytokine profile of these cells differed between the two types of cancer, expression of complement component C3 is conserved. In addition, CD34- CAFs display both 'desmoplastic' and 'contractile' features, suggesting this population may represent an amalgamation of these two phenotypic subsets. Interestingly, the pancreatic CAF compartment also mirrors the temporal changes in composition, observed in melanoma. Here, CD34+ cells were observed surrounding early lesions, while αSMA+ cells were located in the tumour core [248], consistent with the expansion of the CAF3 population in the dermis. Furthermore, IF staining of PDAC and WT tissue revealed pancreatic stellate cells were predominantly CD34+ and αSMA-. This suggests that this CD34+ fibroblasts represent resident stellate cells, while αSMA demarcates a subset, or phenotypic state, only present in disease.

The functional signatures uncovered by bulk sequencing, are consistent with 'myCAFs' and 'iCAF' phenotypes described by Ohland et al [295], which occupy discrete locations in the pancreatic TME. Here, myCAFs encapsulated malignant cells, while iCAFs were restricted to peripheral regions [449] [295]. However, no differences in the spatial distribution of CAF populations was observed in melanoma. This disparity may be due to the reduced size of the CAF compartment in this model. Though fibroblasts are abundant in pancreatic tumours and infiltrate the tumour core, in B16 melanomas, they are mostly confined to the outer stromal layer surrounding malignant cells. These iCAF and myCAF populations were phenotyped further, in both KPC and human pancreatic tumours, by single cell RNA sequencing. This also revealed a novel MHCII+, antigen presenting subset, which was not observed in melanoma.

In addition to pancreatic cancer, other single cell sequencing studies have also identified fibroblast groups displaying similar functional signatures. Thus, to directly

compare gene expression profiles, this data was downloaded from public repositories. Strikingly, data sets obtained from pancreatic, colon and head and neck cancer all contain a CD34+ fibroblast subpopulation, which upregulates the complement component C3. However, expression of other factors associated with the 'immune' CAF profile varied from tumour to tumour. Despite conservation across many types of cancer, the presence of CD34+ C3+ CAFs in breast cancer was more controversial. While this population was detected in E0771 orthotopic breast tumours, by IF and flow cytometry, it was not observed in sequencing data taken from the MMTV-PyMT model.

Interestingly, 'immune' CAFs have been described in human breast cancer [214]. This subset aided the development of a tolerogenic microenvironment, by attracting, retaining and activating T-regs. This was mediated by production of recruitment factor CXCL12, adhesion molecules OX40L, PDL2 and JAM2, as well as expression of B7H3, DPP4 and CD73, which activate T-reg suppressive properties [214]. The recruitment factor *Cxcl12,* is also upregulated at the transcriptional level within our 'immune' CAF population. This thesis has concentrated on cross-talk between this subset and macrophages, owing to their expression of receptors for CAF1 derived factors. However, T-cells also express CXCR4, the cognate receptor for CXCL12, suggesting melanoma 'immune' CAFs may regulate tumour lymphocytes. Despite this similarity, these two fibroblast populations express vastly different immune modulators and are defined by different marker repertoires. This includes expression of αSMA, which is upregulated by 'immune' breast CAFs yet is distinctly absent from their melanoma counterparts. Importantly, production of complement components by any breast fibroblast subset, was not described in this study. However, similar to our early investigations in the $BRAF^{V600E}PTEN^{-/-}$ model, a selection of markers were used to pre-define populations. Thus, this paper suffers from the same limitations and may represent a biased perspective. Hence, the presence and role of 'immune' CAFs in breast cancer is unclear and may depend on the tumour system investigated.

In addition to the ambiguity surrounding 'immune' fibroblasts in breast cancer, it is also unclear whether 'contractile' and 'desmoplastic' populations are a consistent feature. In the MMTV-PyMT model the subset termed 'mCAFs' produced pathological matrix proteins, while 'vCAFs' strongly resembled 'contractile' fibroblasts in melanoma. Furthermore, this population was more prominent at later time points, mirroring the temporal dynamics associated with the contractile CAF3 subset. However, the

phenotype of CAF populations, other than 'immune' subsets, was not examined in either the murine E0771 model or by *Costa et al*. in human breast tumours [214]. While CD34, PDGFRα and αSMA showed a similar pattern of expression in E0771 tumours, suggesting equivalent populations may be present, the functional signatures associated with CAF2 and CAF3 populations were not investigated. Moreover, αSMA^{high} CAFs did not change in abundance across the tumour development. This suggests that, even in the same tissue, the functional properties and temporal composition of fibroblasts vary in malignancy. Possible reasons for such discrepancies, have been previously discussed (Section 5.3) and likely reflect inherent differences in intratumoural signalling. The relationship between tumours, their tissue of origin, and the resulting impact on CAF composition, is explored in more detail below.

Distinct 'contractile' and 'matrix producing' populations, were detected in several other datasets, including colon and head and neck cancer. However, of the three ECM components associated with 'desmoplastic' CAFs in melanoma, not all were expressed by equivalent populations. This may reflect the specific matrix requirements of the tissue in which they reside. Thus, while fibroblast subsets in other types of cancer display similar functions, the particular genes expressed, as well as their relative marker repertories, are tissue dependent. However, only key genes associated with each of the 3 melanoma CAF phenotypes were investigated. Owing to the increasing number of single cell data sets becoming available, new computational algorithms have been developed to enable their integration. For example, Seurat version 3 permits datasets to be analysed simultaneously, even if sequenced on different platforms [450]. This may permit a more comprehensive comparison of populations across tissues.

6.3 *Local environmental factors may impact the composition of the CAF compartment and population dynamics as the tumour develops*

The incongruity between CAF populations, across different types of cancer, is likely the result of their unique surroundings. The TME encompasses diverse soluble, physical and environmental factors, that are irregularly distributed throughout the tumour. This creates varied local environments, that may contribute to the

development of fibroblast heterogeneity. Indeed, phenotypic regulation of fibroblasts is a complex process, in which the underlying mechanisms remain unclear. To begin with, CAFs are exposed to an array of different soluble cues, that can differentially impact their behaviour. For example, factors such as TGFβ, PDGF and sonic hedgehog promote desmoplasia, contractility and upregulate αSMA expression[427,451–458], while IFNγ inhibits fibroblast activation and reduces proliferation [459]. Furthermore, interplay between different soluble cues also regulates cell signalling, adding another layer of complexity. This is illustrated by interactions between WNT7a and the TGFβR, which potentiate TGFβ induced activation of resident fibroblasts [460]. Thus, fibroblast function is likely a product of integrated signals from multiple pathways.

Interestingly, the transcription factor NFκB, orchestrates fibroblast production of inflammatory cytokines, upon exposure to TNFα and IL1β [199,461]. Our sequencing data indicates that these cytokines are produced by innate immune infiltrates, that are present from early stages of tumour development. Thus, such factors may induce the 'immune' CAF1 phenotype in melanoma. Although C3 is not a known target of NFκB, monocyte derived TNFα and IFNγ were shown to increase C3 production in keratinocytes [462]. Thus, similar inflammatory factors may also induce C3 expression in 'immune' CAFs by a different mechanism. This suggests reciprocal signalling between 'immune' CAFs and leukocytes, may be crucial for the maintenance of both populations.

NFκB signalling is also central for the maintenance of the iCAF phenotype in PDAC [449]. Here, iCAFs and myCAFs, represent interchangeable phenotypic states, governed by exposure to specific chemical cues [295]. Principally, the iCAF phenotype is induced by IL1β induction of NFκB, which is sustained in a positive feedback loop [449]. Here, production of Leukaemia Inhibitory Factor (LIF), a downstream target of NFκB, upregulates expression of IL1R via JAK/STAT3 signalling. This augments the CAF response to IL1β and maintains the iCAF phenotype. However, the presence of TGFβ reduces expression of IL1R, disrupting this feed forward mechanism and inducing the myCAF phenotype. This illustrates how complicated networks of soluble factors regulate the functional properties of fibroblasts in the TME. However, in breast cancer, TGFβ cooperates with LIF to induce JAK/STAT3 signalling, driving the acquisition of contractile and pro-invasive properties in fibroblasts [463]. These contradicting results may be explained by the wider chemical environment, specific to

these systems. For example, while JAK/STAT3 signalling maintains iCAF phenotypes in PDAC, this population is primarily regulated by IL1 induction of NFκB. As the JAK/STAT signalling is also implicated in cytoskeletal regulation, in the absence of IL1, activation of this pathway may enhance contractility and invasiveness [464]. This highlights the importance of chemical context, and the multifaceted nature of signalling pathways that control CAF phenotypes. Thus, the specific soluble milliue of different cancer types may account for discrepancies in CAF populations.

In addition to soluble cues, CAFs sense the deposition of matrix components and increased stiffness of malignant tissue, through a network of integrins, focal adhesion complexes and cytoskeletal apparatus [465]. Indeed, Calvo *et al.* demonstrated matrix stiffness is critical for the maintenance of CAF functions [404]. Here, they show that induction of the transcription factor YAP, enhances the ability of CAFs to induce angiogenesis and remodel the ECM. However, matrix remodelling and increased cytoskeletal tension propagated YAP activity, generating a positive feedback loop. Considering the impact of ECM composition on CAF phenotype and function, it is likely matrix interactions are involved in the development of CAF heterogeneity. This was demonstrated by differential enrichment of two populations, FAP^{high} αSMA^{low} and FAP^{low} αSMA^{high}, upon alteration of ECM substrate or stiffness. Here, culture on malleable fibronectin increased the proportion of FAP^{high} αSMA^{low} populations, while increased stiffness or culture on collagen promoted the expansion FAP^{low} αSMA^{high} populations [466]. Furthermore, similar to our results, the FAP^{low} $aSMA^{high}$ subsets displayed enhanced contractility. In combination, these studies suggest that matrix stiffness and cytoskeletal tension may be critical for the upregulation of αSMA and induction of a contractile phenotype in CAF3 fibroblasts. Furthermore, owing to their role in the production of a stiff and fibrotic matrix, ‘desmoplastic’ CAF2 cells may be vital for this process. This highlights potential interplay between fibroblast subsets during the development of the CAF compartment. In addition, contraction and stiffening of the matrix by CAF3 cells may augment cytoskeletal tension and contractility, suggesting this phenotype could be self-perpetuating.

Importantly, soluble and physical factors likely act in concert to dictate CAF function. Indeed, interacting stromal compartments reside in a dynamic equilibrium, in which changes to one compartment are reciprocated by another. For example, cytokines secreted by malignant cells, such as TNFα, induce autocrine expression of VEGFA,

CXCL12, IL6 and CCL2. These soluble factors then have paracrine effects on the tumour microenvironment, promoting angiogenesis and leukocyte recruitment [2,3]. This is known as a 'cytokine network' and highlights the interactive and cooperative nature of the tumour microenvironment. Consequently, changes in stromal features or intratumoral signalling, as the tumour develops, are augmented by these dynamic interactions. Such transformation of the local environment likely effects fibroblast phenotype and behaviour. We have described several changes in the B16-F10 microenvironment, across tumour development, which may contribute to the temporal dynamics of CAF populations in melanoma (**Error! Reference source not found.**). To begin with, the development of an immunosuppressive microenvironment may significantly alter local soluble cues, orchestrating changes in CAF composition. In addition, the importance of matrix rigidity for the development of 'contractile' fibroblast populations has been discussed. Thus, increased ECM deposition in more advanced tumours may contribute to the emergence of CAF3 'contractile' subset, at later time points. Although we have also considered the possibility that this population may be derived from pericytes, it is conceivable that increased matrix stiffness mediates this process. Finally, the emergence of hypoxic pockets in more advanced tumours, may induce further functional, as well as metabolic heterogeneity. This is supported by the coinciding development of 'glycolytic' signatures, in both 'desmoplastic' and 'contractile' subsets, with enhanced staining of the HIF1 target CA9.

Fluctuations in the abundance of melanoma CAF populations, raises the question of whether these cells transition between phenotypes, in response to changes in local cues. In addition, increased expression of the active myofibroblast marker αSMA, suggests populations may represent different states in fibroblast activation. This process is not well understood, although, cytoskeletal changes such as formation of stress fibres and focal adhesions have been described. Interestingly, incorporation of αSMA into stress fibres occurs at later stages of the differentiation process [452,467], in keeping with a this hypothesis. This was further supported by pseudo-time analysis, which ordered CAFs in a trajectory from 'immune' to 'desmoplastic' to 'contractile', implying that these populations are inter-related. However, it is unclear whether CAFs transition through these phenotypes in a single direction, or whether cells switch between three independent populations. As all populations were detected in normal skin, we suggest, that CAF subsets in melanoma mirror the interchangeable

iCAF/myCAF system, in which populations are polarised from one phenotypic state to another, by combined soluble and mechanical stimuli. However, this is difficult to determine in the absence of lineage tracing experiments. *Ex vivo* assays or an *in vitro* system, similar to Ohland et al 2017, may enable investigation of phenotypic changes in response to different factors. Though, the difficulties associated with isolation and culture of CAF from these tumours, may make this challenging.

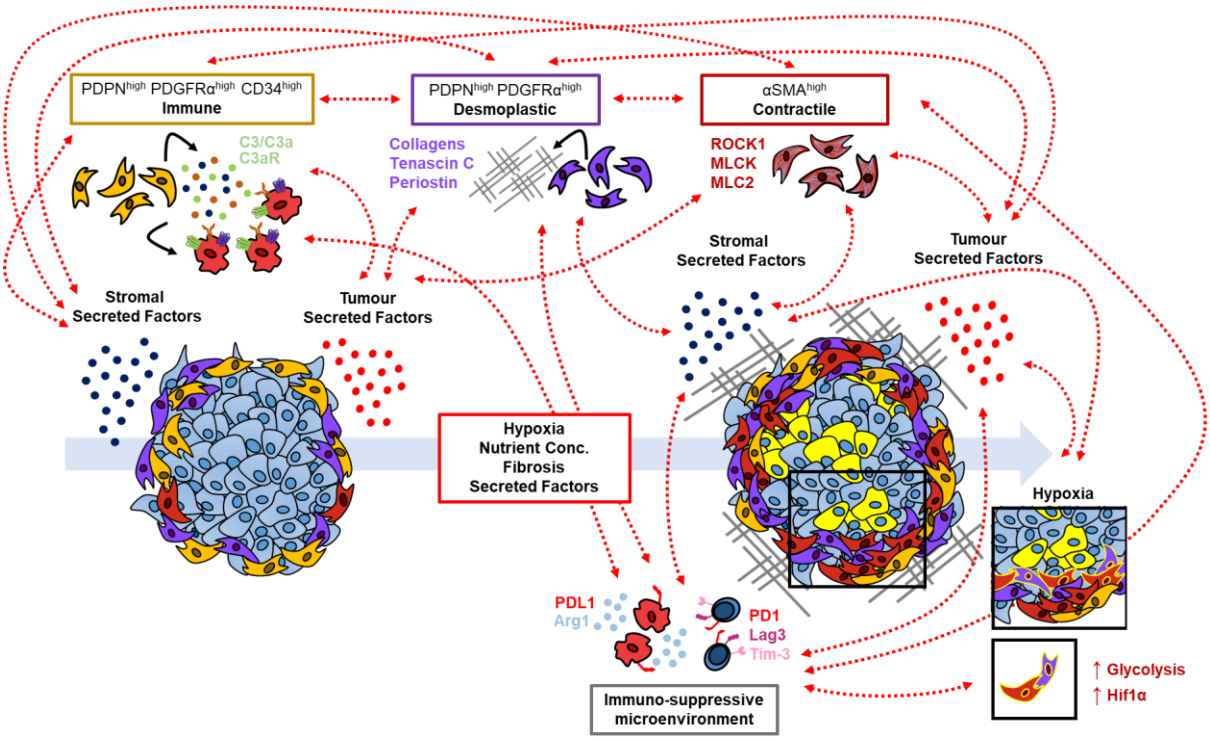

Fig. 6.1 Tumour and stromal interactions influence fibroblast heterogeneity in the developing microenvironment of B16-F10 melanoma.

Fibroblast phenotypes are influenced by local soluble and physical cues derived from resident stromal and malignant populations. Importantly, these populations interact (red arrows), forming a complicated signalling network. In the B16-F10 melanoma model, additional factors such as hypoxia and fibrosis arise at later stages of tumour development. This disrupts the signalling network, which may lead to changes in tumour and stromal secreted factors. Furthermore, the gain of suppressive phenotypes, by leukocyte populations, alters the local chemical environment. These factors may induce the increase in prevalence of the 'contractile' CAF subset, at later time points. In addition, factors such as hypoxia induce further, compartmentalised, fibroblast heterogeneity by induction of Hif1 signalling.

6.4 *The interplay between tumour biology the surrounding tissue in shaping CAF heterogeneity*

Considering the complicated nature of cross-talk between fibroblasts and their local environment, it is unsurprising that their precise functions and marker expression varied between different types of cancer. Furthermore, even cancers of the same tissue, contained different fibroblast populations, suggesting that intrinsic properties of the tumour itself, alter local fibroblast phenotypes. This was evident in BRAF and B16 melanomas, as well as the E0771 and MMTV-PyMT breast models. Thus, the interplay between the tissue of origin and tumour intrinsic properties, on sculpting the CAF landscape, is extremely interesting.

Fibroblasts isolated from different parts of the body have been shown to possess unique transcriptional signatures. Largely, these signatures differentiated cells along proximal-distal and anterior-posterior axes, as well as dermal and non-dermal location [290]. Retention of these transcriptional programs *in vitro*, in the absence of local cues, suggests fibroblasts possess an intrinsic memory of their anatomical location. Positional identify during embryogenesis is dictated by expression of specific HOX transcription factors, which are differentially expressed along the anterior-posterior and proximal-distal axes [468]. This pattern of HOX gene expression was emulated in cultured fibroblasts, that were isolated along these trajectories. Thus, fibroblasts present in adult tissues, may preserve embryonic programs that provide a 'positional memory' [290]. In addition, this 'positional memory' has been shown to supersede local environmental stimuli, dictating fibroblast function during wound healing. Here, fibroblasts from the dorsal dermis and oral dermis produce distinctive ECM structures upon injury. When transplanted to opposing regions, upon wound initiation, these cells continued to produce matrix resembling their original site [437]. Thus, resident fibroblasts from different tissues may have distinct intrinsic programs, that determine their function in a malignant setting. This could have further implications in the context of metastasis, where stromal populations are vital for the establishment of secondary lesions [469]. For example, the phenotypes of local fibroblasts at certain locations, may either promote or inhibit metastatic seeding. Moreover, the competing effects of tumour manipulation, compared to intrinsic fibroblast programs, can be investigated by examining CAFs at the primary and secondary site.

However, the mutational landscape of tumours in the same tissue, can influence fibroblast behaviour. In pancreatic cancer, a gain of function mutation in p53 increased the ability of CAFs to promote invasion and chemotherapy resistance, compared to p53 null tumours [470]. This was mediated by increased NFκB signalling in tumour cells, which induced paracrine activity of the same pathway in adjacent fibroblasts. Indeed, by impacting tumour cell signalling, genetic mutations can directly alter the local soluble environment. For example, Protein Kinase C Iota (PRKCI) amplification leads to increased TNFα production by tumour cells, while PTEN loss can activate NFκB inflammatory signalling, and RAS mutations induce expression of IL6 and IL8 [471–474]. However, through paracrine interactions with the stromal components, the mutational signature of malignant cells can also indirectly manipulate local chemical cues. This particularly pertains to the immune compartment, owing to its potent release of inflammatory factors. For example, Stat-3 activation in melanoma cells prevented immune infiltration by supressing the release of pro-inflammatory cytokines [475]. Considering the possible role of leukocytes in the induction of CAF1 properties, immune exclusion may supress the emergence of this population.

In addition to identifying CAF populations in breast cancer, *Costa et al* compared CAF subsets in different types of breast cancer [214]. This provides a unique opportunity to investigate the influence of tumour intrinsic factors on the tissue specific programs of resident fibroblasts. Indeed, distinct CAF populations were differentially enriched in luminal A, HER2 and triple negative cancers [214]. Two of these populations were isolated and sequenced from both luminal and triple negative tumours. When plotted together using PCA, CAFs clustered according to their population identity, rather than tumour subtype. This suggests that fibroblast populations and their associated phenotypes may be predetermined by their tissue of origin. However, the presence of specific soluble and physical cues, unique to each tumour, governs their prevalence and activates their specific functions.

These concepts are particularly relevant to melanoma, as fibroblast heterogeneity in the adult human dermis is well documented. Interestingly, key differences between papillary and reticular fibroblasts, the two dominant populations, include upregulation of complement and extracellular matrix components respectively [293]. Thus, these cells may represent dormant pre-cursors of our CAF1 and CAF2 populations. Increased production of matrix proteins in combination with a positive association between

dermal depth and scaring, suggest that fibroblasts of the lower reticular dermis are responsible ECM remodelling during wound healing [476–478]. This has been attributed to increased expression of TGFβR II on the surface of this population, which potentially renders these cells more responsive to TGFβ [477]. Thus, it is possible that expression of surface receptors, may pre-prime specific dermal populations to respond to particular cues. Our data indicates that, even under homeostatic conditions, C3 expression is higher in $CD34^{high}$ fibroblasts compared to other populations. However, this complement component is upregulated upon the onset of malignancy. As previously mentioned, exposure to immune secreted factors may increase expression of C3 in the CAF1 subset. Thus, the repertoire of surface receptors, specific to this population, may sensitize these cells to inflammatory factors produced by early immune infiltrates.

Furthermore, a study investigating the effects of aging on local fibroblast populations, identified two similar subsets in the dermis of young (2 months) mice, that differentially expressed complement and ECM components [408]. While these two populations were also present in older mice (18 months), their transcriptional separation was reduced. Moreover, bulk sequencing revealed an overall increase in expression of complement components in fibroblasts of older mice, concomitant with a downregulation in ECM genes. However, changes in these transcriptional signatures could be reduced by calorie restriction. If the functions of CAFs in melanoma are predetermined by existing dermal populations, this data suggests that age and diet may contribute to their prevalence and phenotype. This is intriguing as mice used in our experiments were typically 2-3 months old, similar to mice categorised as ‘young’. Thus, it would be interesting to investigate whether fibroblasts in older mice have an increased propensity for C3 secretion in the tumour stroma, or whether expression of this component is already at full capacity.

It is also important to note that additional sources of heterogeneity, present in human melanoma, are not captured by our murine model. To begin with, as an injectable model, the tumour compartment of B16-F10 melanomas are relatively uniform and does not contain significant clonal heterogeneity. Furthermore, experiments were performed in genetically identical mice, of similar ages, housed under matching conditions. Human tumours develop in hosts with distinct genetic backgrounds, that are exposed to a number of different environmental factors. We have already

discussed the effects of age and diet on dermal fibroblasts, which could impact population prevalence and function upon tumour initiation. However, the effect of cancer therapies on CAFs and the wider stromal compartment, are not well understood. Nonspecific therapies such as radio and chemotherapies may directly induce changes in fibroblast populations. We have previously described how DNA damage in CAFs, induced by chemotherapy, caused NFκB activation and therapy resistance [243]. However, targeted drugs such as oncogene inhibitors and immunotherapies, may indirectly impact tumour fibroblasts. By depleting specific tumour clones, or restoring immune cell cytotoxicity, these drugs may disrupt the delicate balance of signalling networks in this dynamic microenvironment. Indeed, as human samples are rarely treatment naïve, many published scRNAseq datasets are obtained from patients who have received different combinations of therapies [414]. Thus, to truly understand the development of diverse fibroblast populations, these additional factors must be considered.

6.5 *The complement pathway as a therapeutic target*

Despite differences in the functional properties and marker expression of CAF populations, across different types of cancer, a $CD34^{high}$ C3 producing subset was a common feature. Furthermore, the interaction between this CAF population and C3aR expressing macrophages was also conserved. Considering the unique composition of each tumour microenvironment, the preservation of this interaction is significant. Although still preliminary, our data demonstrated that blockade of the C3 cleavage product C3a, reduced tumour macrophage populations, which may boost the number of CD8 T-cells and decrease malignant growth. This suggests C3a may represent a therapeutic target in a range of cancers.

Activation of the complement system has been linked to cancer development. In several solid cancers C3 and C3a are elevated at both the primary tumour site and in patient serum [479–482]. Furthermore, C3 and C5aR were associated with poor prognosis in ovarian cancer [483]. Thus, in recent years, investigations into the role of complement activation in the tumour microenvironment has gained traction. However, the cellular source of complement components remains unclear, and may vary depending on the

type of cancer. The results of C3 deficiency models, in which cancer cells are injected in C3-/- mice, indicate that C3 is produced by the host in melanoma, breast and cervical cancer models, yet produced by the tumour itself in ovarian cancer [446,483,484]. While, fibroblasts *in vitro* and in malignant settings are reported to produce complement factors [301,414,485,486], this pathway is not the focus of these studies and the role of fibroblasts in cascade activation is not appreciated.

Our data highlights the potential therapeutic benefit of inhibiting C3a/C3aR interactions between fibroblasts and monocytes/macrophages in multiple different cancers. Owing to immune-suppressive properties of these macrophage populations, potential synergy between C3a neutralisation and immune checkpoint inhibitors was previously suggested (section 5.3). Targeting macrophage recruitment in conjunction with immunotherapies represents a current strategy to improve therapeutic responses, with several combinations undergoing clinical trials [87]. Similar to C3a, C5a also acts on immune populations, increasing MDSC accumulation in the tumour and promoting their suppressive activity [484,487]. Blocking C5a in combination with PD1 inhibitors was more effective than either monotherapies [484,487,488], suggesting a combined approach may improve clinical efficacy.

Beyond the cancer setting, complement activation also underpins pathogenesis in diseases such as rheumatoid arthritis, lupus and kidney disorders [489,490]. Thus, inhibitors of different components of the cascade are being developed, yet few are approved for clinical use. The C5 inhibitor Eculizumab is currently used to treat uncontrolled complement activation in Paroxysmal nocturnal haemoglobinuria (PNH) [491] yet it is also being tested for treatment of other diseases [489]. While, clinical trials are ongoing for several inhibitors of C5a and C5aR, few drugs have been developed that target the C3a/C3aR axis. Instead, blocking C3 cleavage has been the key focus, leading to the development of Compstatin and its derivatives AMY-101 and APL2 [489]. C3 is a central component of the complement cascade, acting as a convergent and amplification point for the classical, lectin and alternative activation pathways (**Error! Reference source not found.**). Thus, inhibition of its cleavage will prevent further activation of the complement cascade, including formation of the MAC and anaphylatoxins C3a and C5a. As these components have varied effects on tumorigenesis [396], it will be interesting to examine whether blocking the cascade at specific stages impacts clinical efficacy. For example, inhibiting C3a or C5a signalling

prevents anaphylatoxin activity while permitting formation of MAC, which may have tumoricidal activity. Importantly, as the primary source of C3 in our melanoma model, CD34^{high} CAFs regulate the activation of all axes of the complement pathway.

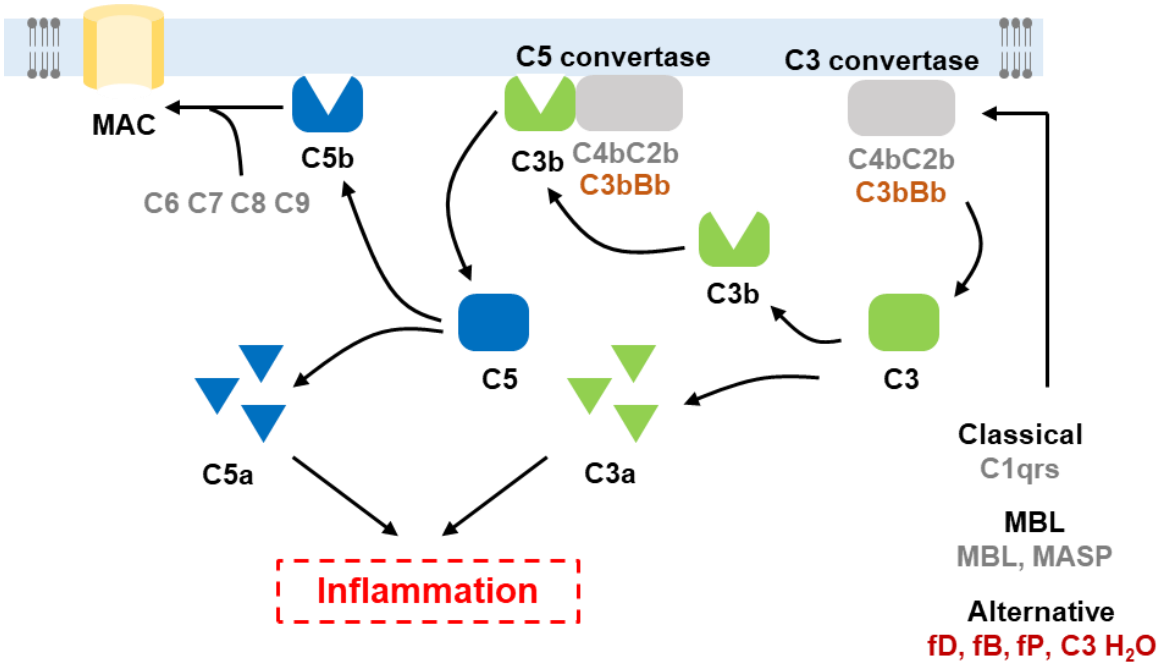

Fig. 6.2 The complement cascade

Classical, Mannose Binding Lectin (MBL) and Alternative pathways generate a C3 convertase consisting of C4b,C2b (Classical and MBL) and C3bBb (Alternative), which cleaves central component C3 to C3b and C3a. C3a acts as an anaphylatoxin, inducing inflammation, while C3b binds to the C3 convertase to form the C5 convertase. Similar to C3, C5 is cleaved to form the anaphylatoxin C5a and C5b which binds to other complement components and forms the membrane attack complex (MAC). This permeabilises the membrane and induces cell death.

6.6 *Conclusions and future directions*

This project highlights the complexity of the CAF compartment in melanoma development. We identify functionally distinct populations with a diverse marker repertoire, stressing the futility of bulk analysis and single marker approaches to characterise CAFs. This also emphasises the importance of fibroblast composition in cancer therapy. The presence of certain populations may dictate the efficacy of drugs targeting specific markers or functions, while their temporal dynamics control the timing of therapeutic application. Our work identified C3a as a possible target for

treatment of melanoma and other cancer types, as well as CD34 as biomarker for its application. However, further optimisation of C3a neutralisation is required, including increasing antibody concentration and possible combination with immune checkpoint therapies. Furthermore, a better understanding of the effects of C3a neutralisation on immune phenotypes is needed. For example, mechanistic insight into myeloid regulation of the T-cell compartment upon treatment, may identify additional targets. This involves a more comprehensive profile of macrophage/monocyte signalling molecules and the spatial location of immune populations in treated samples.

Ultimately fibroblast heterogeneity is determined by the tissue or origin, tumour intrinsic signalling and exposure to extrinsic factors, such as cancer therapy, age and diet. Identification of soluble or mechanical cues that regulate individual populations could be used to establish *in vitro* models, similar to the pancreatic iCAF / myCAF system. The inability to isolate and culture fibroblasts from B16-F10 melanoma as part of this study, limited their functional characterisation *in vitro*. However, if normal skin fibroblasts can be induced to resemble certain populations, by cytokine exposure or culture on specific substrates, functional assays can be performed.

Improvement in throughput, availability and cost of single cell technologies, such as scRNAseq and CyTOF, is creating an increasing pool of publicly available data spanning tissues and pathologies. This enables investigations into fibroblast populations present in cancers of different tissues and other disease states, such as chronic inflammatory disorders. Interestingly, functionally distinct fibroblast populations have been reported in colitis and rheumatoid arthritis [492,493], including a C3 producing subset in the latter [493]. In addition, sequencing of human cancers includes information regarding therapeutic treatment. This may be used to compare the effect of anti-cancer drugs on fibroblast composition. However, such studies are currently impeded by a lack of single cell data from patients exposed to similar therapies, in which a sufficient number of fibroblasts have been sequenced. Furthermore, due to obvious ethical reasons, the number of treatment naive samples are limited. Performing scRNAseq on mice treated with specific anti-cancer drugs, compared to non-treated controls, would reveal their effects on CAF composition and may uncover novel mechanisms of resistance.

Moreover, a shortage of sequencing data from homeostatic conditions limits our understanding of the contribution of location in shaping the fibroblast compartment in both inflammatory and malignant disease. ScRNAseq data from different tissues, under resting conditions, would uncover if fibroblasts are heterogenous in the absence of pathology. Site specific transcriptional signatures have already been identified, however, single cell resolution would highlight differences at the population level. Moreover, this would indicate whether certain subsets are conserved across tissues. Profiling the development of the fibroblast compartment at different stages of malignant disease may indicate whether phenotypes and functions in the resting state, impact CAF composition.

In combination with other published studies, our data indicates that two CAF populations present in the melanoma model may be derived from existing dermal subsets, while the third may originate from resident pericytes. The contribution of 'normal' populations to the CAF compartment could be tracked using lineage tracing models. For example, tamoxifen inducible cre could be expressed under the control of genes associated with a specific tissue resident population. If crossed to a mouse in which cre recombination induces expression of a fluorescent protein, downstream of the ubiquitous Rosa26 promoter, exposure to tamoxifen prior to tumour initiation would label this population throughout malignancy. Interestingly, lineage tracing is currently being combined with single cell sequencing, using barcoding technology. This involves labelling cells *in vivo* with specific sequences or inducing mutational bar codes with recombinase or CRISPR systems. If these sequences are transcribed, they can be detected using scRNAseq and used to identify clonal lineages. However, this technology is still being optimised and is largely restricted to embryonic studies [494]. However, mRNA encoding fluorescent proteins can be detected by RNA sequencing. Thus, the lineage tracing model proposed above could be combined with scRNAseq. This would enable the identification of cells derived from a specific resident subset, within tumour fibroblast populations. Furthermore, if performed as a time course, the transcriptional processes that govern phenotypic transition of a specific dermal population, during tumour development, could be investigated.

In summary, while we are beginning to understand the diverse contributions of fibroblast populations to the tumour microenvironment, there remains much to be

uncovered. The development of single cell technologies is enabling a growing appreciation of the complexity of interactions across compartments.

References

1. Balkwill, F. R., Capasso, M. & Hagemann, T. The tumor microenvironment at a glance. *J. Cell Sci.* **125**, 5591–5596 (2012).

2. Kulbe, H. *et al.* The inflammatory cytokine tumor necrosis factor-α generates an autocrine tumor-promoting network in epithelial ovarian cancer cells. *Cancer Res.* **67**, 585–592 (2007).

3. Kulbe, H. *et al.* A dynamic inflammatory cytokine network in the human ovarian cancer microenvironment. *Cancer Res.* **72**, 66–75 (2012).

4. Shields, J. D., Kourtis, I. C., Tomei, A. A., Roberts, J. M. & Swartz, M. A. Induction of lymphoidlike stroma and immune escape by tumors that express the chemokine CCL21. *Science (80-.).* **328**, 749–752 (2010).

5. Balkwill, F. & Mantovani, A. Inflammation and cancer: Back to Virchow? *Lancet* **357**, 539–545 (2001).

6. Vinay, D. S. *et al.* Immune evasion in cancer: Mechanistic basis and therapeutic strategies. *Semin. Cancer Biol.* **35**, S185–S198 (2015).

7. Gonzalez, H., Hagerling, C. & Werb, Z. Roles of the immune system in cancer: From tumor initiation to metastatic progression. *Genes and Development* **32**, 1267–1284 (2018).

8. Zhang, N. & Bevan, M. J. CD8+ T Cells: Foot Soldiers of the Immune System. *Immunity* **35**, 161–168 (2011).

9. Segal, N. H. *et al.* Epitope landscape in breast and colorectal cancer. *Cancer Res.* **68**, 889–892 (2008).

10. Germano, G. *et al.* Inactivation of DNA repair triggers neoantigen generation and impairs tumour growth. *Nature* **552**, 1–5 (2017).

11. Hanson, H. L. *et al.* Eradication of established tumors by CD8+ T cell adoptive immunotherapy. *Immunity* **13**, 265–276 (2000).

12. Matsushita, H. *et al.* Cancer exome analysis reveals a T-cell-dependent

mechanism of cancer immunoediting. *Nature* **482**, 400–404 (2012).

13. Galon, J. *et al.* Type, density, and location of immune cells within human colorectal tumors predict clinical outcome. *Science (80-.).* **313**, 1960–1964 (2006).

14. Pagès, F. *et al.* Effector memory T cells, early metastasis, and survival in colorectal cancer. *N. Engl. J. Med.* **353**, 2654–2666 (2005).

15. Pautu, J. L. & Kumar, L. Intratumoral T cells and survival in epithelial ovarian cancer. *Natl. Med. J. India* **16**, 150–151 (2003).

16. Rusakiewicz, S. *et al.* Immune in filtrates are prognostic factors in localized gastrointestinal stromal tumors. *Cancer Res.* **73**, 3499–3510 (2013).

17. Azimi, F. *et al.* Tumor-infiltrating lymphocyte grade is an independent predictor of sentinel lymph node status and survival in patients with cutaneous melanoma. *J. Clin. Oncol.* **30**, 2678–2683 (2012).

18. Yamamoto, R. *et al.* PD-1 PD-1 ligand interaction contributes to immunosuppressive microenvironment of Hodgkin lymphoma. *Blood* **111**, 3220–3224 (2008).

19. Fourcade, J. *et al.* PD-1 Is a Regulator of NY-ESO-1-Specific CD8 + T Cell Expansion in Melanoma Patients. *J. Immunol.* **182**, 5240–5249 (2009).

20. Ahmadzadeh, M. *et al.* Tumor antigen-specific CD8 T cells infiltrating the tumor express high levels of PD-1 and are functionally impaired. *Blood* **114**, 1537–1544 (2009).

21. Saito, H., Kuroda, H., Matsunaga, T., Osaki, T. & Ikeguchi, M. Increased PD-1 expression on CD4+ and CD8+ T cells is involved in immune evasion in gastric cancer. *J. Surg. Oncol.* **107**, 517–522 (2013).

22. Sakuishi, K. *et al.* Targeting Tim-3 and PD-1 pathways to reverse T cell exhaustion and restore anti-tumor immunity. *Journal of Experimental Medicine* **208**, 1331 (2011).

23. Fourcade, J. *et al.* Upregulation of Tim-3 and PD-1 expression is associated with tumor antigen-specific CD8+ T cell dysfunction in melanoma patients. *J.*

Exp. Med. **207**, 2175–2186 (2010).

24. Woo, S. R. *et al.* Immune inhibitory molecules LAG-3 and PD-1 synergistically regulate T-cell function to promote tumoral immune escape. *Cancer Res.* **72**, 917–927 (2012).

25. Matsuzaki, J. *et al.* Tumor-infiltrating NY-ESO-1-specific CD8+ T cells are negatively regulated by LAG-3 and PD-1 in human ovarian cancer. *Proc. Natl. Acad. Sci. U. S. A.* **107**, 7875–7880 (2010).

26. Zajac, A. J. *et al.* Viral immune evasion due to persistence of activated T cells without effector function. *J. Exp. Med.* **188**, 2205–2213 (1998).

27. Joller, N. *et al.* Cutting Edge: TIGIT Has T Cell-Intrinsic Inhibitory Functions. *J. Immunol.* **186**, 1338–1342 (2011).

28. Fourcade, J. *et al.* CD8 + T cells specific for tumor antigens can be rendered dysfunctional by the tumor microenvironment through upregulation of the inhibitory receptors BTLA and PD-1. *Cancer Res.* **72**, 887–896 (2012).

29. Blackburn, S. D. *et al.* Coregulation of CD8+ T cell exhaustion by multiple inhibitory receptors during chronic viral infection. *Nat. Immunol.* **10**, 29–37 (2009).

30. Crawford, A. & Wherry, E. J. The diversity of costimulatory and inhibitory receptor pathways and the regulation of antiviral T cell responses. *Current Opinion in Immunology* **21**, 179–186 (2009).

31. Jin, H. T. *et al.* Cooperation of Tim-3 and PD-1 in CD8 T-cell exhaustion during chronic viral infection. *Proc. Natl. Acad. Sci. U. S. A.* **107**, 14733–14738 (2010).

32. Barber, D. L. *et al.* Restoring function in exhausted CD8 T cells during chronic viral infection. *Nature* **439**, 682–687 (2006).

33. Kuang, D. M. *et al.* Activated monocytes in peritumoral stroma of hepatocellular carcinoma foster immune privilege and disease progression through PD-L1. *J. Exp. Med.* **206**, 1327–1337 (2009).

34. Rodig, N. *et al.* Endothelial expression of PD-L1 and PD-L2 down-regulates

CD8 + T cell activation and cytolysis. *Eur. J. Immunol.* **33**, 3117–3126 (2003).

35. Lakins, M. A., Ghorani, E., Munir, H., Martins, C. P. & Shields, J. D. Cancer-associated fibroblasts induce antigen-specific deletion of CD8 + T Cells to protect tumour cells. *Nat. Commun.* **9**, 948 (2018).

36. Iwai, Y. *et al.* Involvement of PD-L1 on tumor cells in the escape from host immune system and tumor immunotherapy by PD-L1 blockade. *Proc. Natl. Acad. Sci. U. S. A.* **99**, 12293–12297 (2002).

37. Wherry, E. J., Blattman, J. N., Murali-Krishna, K., van der Most, R. & Ahmed, R. Viral Persistence Alters CD8 T-Cell Immunodominance and Tissue Distribution and Results in Distinct Stages of Functional Impairment. *J. Virol.* **77**, 4911–4927 (2003).

38. Topalian, S. L. *et al.* Safety, Activity, and Immune Correlates of Anti–PD-1 Antibody in Cancer. *N. Engl. J. Med.* **366**, 2443–2454 (2012).

39. Topalian, S. L., Drake, C. G. & Pardoll, D. M. Targeting the PD-1/B7-H1(PD-L1) pathway to activate anti-tumor immunity. *Current Opinion in Immunology* **24**, 207–212 (2012).

40. Zhang, Y. *et al.* Protein expression of programmed death 1 ligand 1 and ligand 2 independently predict poor prognosis in surgically resected lung adenocarcinoma. *Onco. Targets. Ther.* **7**, 567–573 (2014).

41. Hamanishi, J. *et al.* Programmed cell death 1 ligand 1 and tumor-infiltrating CD8+ T lymphocytes are prognostic factors of human ovarian cancer. *Proc. Natl. Acad. Sci. U. S. A.* **104**, 3360–3365 (2007).

42. Muenst, S. *et al.* Expression of programmed death ligand 1 (PD-L1) is associated with poor prognosis in human breast cancer. *Breast Cancer Res. Treat.* **146**, 15–24 (2014).

43. Gao, Q. *et al.* Overexpression of PD-L1 significantly associates with tumor aggressiveness and postoperative recurrence in human hepatocellular carcinoma. *Clin. Cancer Res.* **15**, 971–979 (2009).

44. Ohigashi, Y. *et al.* Clinical significance of programmed death-1 ligand-1 and programmed death-1 ligand-2 expression in human esophageal cancer. *Clin.*

Cancer Res. **11**, 2947–2953 (2005).

45. Akasaki, Y. *et al.* Induction of a CD4 + T Regulatory Type 1 Response by Cyclooxygenase-2-Overexpressing Glioma. *J. Immunol.* **173**, 4352–4359 (2004).

46. Thomas, D. A. & Massagué, J. TGF-β directly targets cytotoxic T cell functions during tumor evasion of immune surveillance. *Cancer Cell* **8**, 369–380 (2005).

47. Uyttenhove, C. *et al.* Evidence for a tumoral immune resistance mechanism based on tryptophan degradation by indoleamine 2,3-dioxygenase. *Nat. Med.* **9**, 1269–1274 (2003).

48. Pandya, P. H., Murray, M. E., Pollok, K. E. & Renbarger, J. L. The Immune System in Cancer Pathogenesis: Potential Therapeutic Approaches. *J. Immunol. Res.* **2016**, 4273943 (2016).

49. Chakravarti, A., Raquil, M.-A., Tessier, P. & Poubelle, P. E. Surface RANKL of Toll-like receptor 4-stimulated human neutrophils activates osteoclastic bone resorption Activation of neutrophil membrane-bound RANKL was linked to tyrosine phosphorylation of Src-homology domain-containing cytosolic phospha-tase 1 with. *Blood* **114**, 1633–1644 (2009).

50. Dobrzanski, M. J. Expanding roles for CD4 T cells and their subpopulations in tumor immunity and therapy. *Frontiers in Oncology* **3 MAR**, 63 (2013).

51. Tosolini, M. *et al.* Clinical impact of different classes of infiltrating T cytotoxic and helper cells (Th1, Th2, Treg, Th17) in patients with colorectal cancer. *Cancer Res.* **71**, 1263–1271 (2011).

52. Kondo, T. *et al.* Favorable prognosis of renal cell carcinoma with increased expression of chemokines associated with a Th1-type immune response. *Cancer Sci.* **97**, 780–786 (2006).

53. De Monte, L. *et al.* Intratumor T helper type 2 cell infiltrate correlates with cancer-associated fibroblast thymic stromal lymphopoietin production and reduced survival in pancreatic cancer. *J. Exp. Med.* **208**, 469–478 (2011).

54. Ochi, A. *et al.* MyD88 inhibition amplifies dendritic cell capacity to promote pancreatic carcinogenesis via Th2 cells. *J. Exp. Med.* **209**, 1671–1687 (2012).

55. Huang, H. *et al.* CD4+ Th1 cells promote CD8+ Tc1 cell survival, memory response, tumor localization and therapy by targeted delivery of interleukin 2 via acquired pMHC I complexes. *Immunology* **120**, 148–159 (2007).

56. Knutson, K. L. & Disis, M. L. Tumor antigen-specific T helper cells in cancer immunity and immunotherapy. *Cancer Immunology, Immunotherapy* **54**, 721–728 (2005).

57. Surman, D. R., Dudley, M. E., Overwijk, W. W. & Restifo, N. P. Cutting Edge: CD4 + T Cell Control of CD8 + T Cell Reactivity to a Model Tumor Antigen. *J. Immunol.* **164**, 562–565 (2000).

58. Nishikawa, H. & Sakaguchi, S. Regulatory T cells in tumor immunity. *International Journal of Cancer* **127**, 759–767 (2010).

59. Lahl, K. *et al.* Selective depletion of Foxp3+ regulatory T cells induces a scurfy-like disease. *J. Exp. Med.* **204**, 57–63 (2007).

60. Kim, J. M., Rasmussen, J. P. & Rudensky, A. Y. Regulatory T cells prevent catastrophic autoimmunity throughout the lifespan of mice. *Nat. Immunol.* **8**, 191–197 (2007).

61. Sakaguchi, S., Sakaguchi, N., Asano, M., Itoh, M. & Toda, M. Immunologic self-tolerance maintained by activated T cells expressing IL-2 receptor alpha-chains (CD25). Breakdown of a single mechanism of self-tolerance causes various autoimmune diseases. *J. Immunol.* **155**, 1151–64 (1995).

62. Tadokoro, C. E. *et al.* Regulatory T cells inhibit stable contacts between CD4+ T cells and dendritic cells in vivo. *J. Exp. Med.* **203**, 505–511 (2006).

63. Tang, Q. *et al.* Visualizing regulatory T cell control of autoimmune responses in nonobese diabetic mice. *Nat. Immunol.* **7**, 83–92 (2006).

64. Thornton, A. M. & Shevach, E. M. CD4+CD25+ immunoregulatory T cells suppress polyclonal T cell activation in vitro by inhibiting interleukin 2 production. *J. Exp. Med.* **188**, 287–296 (1998).

65. Takahashi, T. *et al.* Immunologic self-tolerance maintained by CD25+CD4+ naturally anergic and suppressive T cells: Induction of autoimmune disease by breaking their anergic/suppressive state. *Int. Immunol.* **10**, 1969–1980 (1998).

66. Peggs, K. S., Quezada, S. A., Chambers, C. A., Korman, A. J. & Allison, J. P. Blockade of CTLA-4 on both effector and regulatory T cell compartments contributes to the antitumor activity of anti-CTLA-4 antibodies. *J. Exp. Med.* **206**, 1717–1725 (2009).

67. Wing, K. *et al.* CTLA-4 control over Foxp3+ regulatory T cell function. *Science (80-.).* **322**, 271–275 (2008).

68. Collison, L. W., Pillai, M. R., Chaturvedi, V. & Vignali, D. A. A. Regulatory T Cell Suppression Is Potentiated by Target T Cells in a Cell Contact, IL-35- and IL-10-Dependent Manner. *J. Immunol.* **182**, 6121–6128 (2009).

69. Kobie, J. J. *et al.* T Regulatory and Primed Uncommitted CD4 T Cells Express CD73, Which Suppresses Effector CD4 T Cells by Converting 5′-Adenosine Monophosphate to Adenosine. *J. Immunol.* **177**, 6780–6786 (2006).

70. Borsellino, G. *et al.* Expression of ectonucleotidase CD39 by Foxp3+ Treg cells: Hydrolysis of extracellular ATP and immune suppression. *Blood* **110**, 1225–1232 (2007).

71. Schaefer, C. *et al.* Characteristics of CD4+CD25+ regulatory T cells in the peripheral circulation of patients with head and neck cancer. *Br. J. Cancer* **92**, 913–920 (2005).

72. Wolf, A. M. *et al.* Increase of regulatory T cells in the peripheral blood of cancer patients. *Clin. Cancer Res.* **9**, 606–612 (2003).

73. Ormandy, L. *et al.* Increased populations of regulatory T cells in peripheral blood of patients with hepatocellular carcinoma. *Cancer Res.* **65**, 2457–2464 (2005).

74. Liyanage, U. K. *et al.* Prevalence of Regulatory T Cells Is Increased in Peripheral Blood and Tumor Microenvironment of Patients with Pancreas or Breast Adenocarcinoma. *J. Immunol.* **169**, 2756–2761 (2002).

75. Curiel, T. J. *et al.* Specific recruitment of regulatory T cells in ovarian carcinoma fosters immune privilege and predicts reduced survival. *Nat. Med.* **10**, 942–949 (2004).

76. Mougiakakos, D. *et al.* Intratumoral forkhead box p3-positive regulatory t cells

predict poor survival in cyclooxygenase-2-positive uveal melanoma. *Cancer* **116**, 2224–2233 (2010).

77. Onizuka, S. *et al.* Tumor rejection by in vivo administration of anti-CD25 (interleukin-2 receptor α) monoclonal antibody. *Cancer Res.* **59**, 3128–3133 (1999).

78. Shimizu, J., Yamazaki, S. & Sakaguchi, S. *Autoimmunity Between Tumor Immunity and T Cells: A Common Basis + CD4 + CD25 Induction of Tumor Immunity by Removing*. *J Immunol References* **5211**, (2019).

79. Lutsiak, M. E. C. *et al.* Inhibition of CD4+25+ T regulatory cell function implicated in enhanced immune response by low-dose cyclophosphamide. *Blood* **105**, 2862–2868 (2005).

80. Kono, K. *et al.* Dendritic cells pulsed with HER-2/neu-derived peptides can induce specific T-cell responses in patients with gastric cancer. *Clin. Cancer Res.* **8**, 3394–3400 (2002).

81. Bates, G. J. *et al.* Quantification of regulatory T cells enables the identification of high-risk breast cancer patients and those at risk of late relapse. *J. Clin. Oncol.* **24**, 5373–5380 (2006).

82. Sato, E. *et al.* Intraepithelial CD8+ tumor-infiltrating lymphocytes and a high CD8+/regulatory T cell ratio are associated with favorable prognosis in ovarian cancer. *Proc. Natl. Acad. Sci. U. S. A.* **102**, 18538–18543 (2005).

83. Najafi, M., Farhood, B. & Mortezaee, K. Contribution of regulatory T cells to cancer: A review. *J. Cell. Physiol.* **234**, 7983–7993 (2019).

84. Zhang, Q. wen *et al.* Prognostic Significance of Tumor-Associated Macrophages in Solid Tumor: A Meta-Analysis of the Literature. *PLoS One* **7**, e50946 (2012).

85. Komohara, Y., Jinushi, M. & Takeya, M. Clinical significance of macrophage heterogeneity in human malignant tumors. *Cancer Sci.* **105**, 1–8 (2014).

86. Gentles, A. J. *et al.* The prognostic landscape of genes and infiltrating immune cells across human cancers. *Nat. Med.* **21**, 938–945 (2015).

87. DeNardo, D. G. & Ruffell, B. Macrophages as regulators of tumour immunity and immunotherapy. *Nature Reviews Immunology* **19**, 369–382 (2019).

88. Wyckoff, J. B. *et al.* Direct visualization of macrophage-assisted tumor cell intravasation in mammary tumors. *Cancer Res.* **67**, 2649–2656 (2007).

89. Movahedi, K. *et al.* Different tumor microenvironments contain functionally distinct subsets of macrophages derived from Ly6C(high) monocytes. *Cancer Res.* **70**, 5728–5739 (2010).

90. Franklin, R. A. *et al.* The cellular and molecular origin of tumor-associated macrophages. *Science (80-.).* **344**, 921–925 (2014).

91. Qian, B.-Z. *et al.* CCL2 recruits inflammatory monocytes to facilitate breast-tumour metastasis. *Nature* **475**, 222–5 (2011).

92. Cortez-Retamozo, V. *et al.* Origins of tumor-associated macrophages and neutrophils. *Proc. Natl. Acad. Sci. U. S. A.* **109**, 2491–2496 (2012).

93. Sica, A. *et al.* Macrophage polarization in tumour progression. *Seminars in Cancer Biology* **18**, 349–355 (2008).

94. Yeo, E. J. *et al.* Myeloid wnt7b mediates the angiogenic switch and metastasis in breast cancer. *Cancer Res.* **74**, 2962–2973 (2014).

95. Du, R. *et al.* HIF1α Induces the Recruitment of Bone Marrow-Derived Vascular Modulatory Cells to Regulate Tumor Angiogenesis and Invasion. *Cancer Cell* **13**, 206–220 (2008).

96. Sangaletti, S. *et al.* Macrophage-derived SPARC bridges tumor cell-extracellular matrix interactions toward metastasis. *Cancer Res.* **68**, 9050–9059 (2008).

97. Bonde, A. K., Tischler, V., Kumar, S., Soltermann, A. & Schwendener, R. A. Intratumoral macrophages contribute to epithelial-mesenchymal transition in solid tumors. *BMC Cancer* **12**, (2012).

98. DeNardo, D. G. *et al.* Leukocyte complexity predicts breast cancer survival and functionally regulates response to chemotherapy. *Cancer Discov.* **1**, 54–67 (2011).

99. Kusmartsev, S. & Gabrilovich, D. I. STAT1 Signaling Regulates Tumor-Associated Macrophage-Mediated T Cell Deletion. *J. Immunol.* **174**, 4880–4891 (2005).

100. Geiger, R. *et al.* L-Arginine Modulates T Cell Metabolism and Enhances Survival and Anti-tumor Activity. *Cell* **167**, 829-842.e13 (2016).

101. Lin, H. *et al.* Host expression of PD-L1 determines efficacy of PD-L1 pathway blockade–mediated tumor regression. *J. Clin. Invest.* **128**, 805–815 (2018).

102. Ostrand-Rosenberg, S. & Sinha, P. Myeloid-Derived Suppressor Cells: Linking Inflammation and Cancer. *J. Immunol.* **182**, 4499–4506 (2009).

103. Gabrilovich, D. I., Velders, M. P., Sotomayor, E. M. & Kast, W. M. Mechanism of Immune Dysfunction in Cancer Mediated by Immature Gr-1 + Myeloid Cells. *J. Immunol.* **166**, 5398–5406 (2001).

104. Bronte, V. *et al.* Apoptotic death of CD8+ T lymphocytes after immunization: induction of a suppressive population of Mac-1+/Gr-1+ cells. *J. Immunol.* **161**, 5313–20 (1998).

105. Xu, X. C. *et al.* Progressive decreases in nuclear retinoid receptors during skin squamous carcinogenesis. *Cancer Res.* **61**, 4306–4310 (2001).

106. Sinha, P., Clements, V. K. & Ostrand-Rosenberg, S. Reduction of Myeloid-Derived Suppressor Cells and Induction of M1 Macrophages Facilitate the Rejection of Established Metastatic Disease. *J. Immunol.* **174**, 636–645 (2005).

107. Serafini, P., Mgebroff, S., Noonan, K. & Borrello, I. Myeloid-derived suppressor cells promote cross-tolerance in B-cell lymphoma by expanding regulatory T cells. *Cancer Res.* **68**, 5439–5449 (2008).

108. Huang, B. *et al.* Gr-1+CD115+ immature myeloid suppressor cells mediate the development of tumor-induced T regulatory cells and T-cell anergy in tumor-bearing host. *Cancer Res.* **66**, 1123–1131 (2006).

109. Kusmartsev, S., Nefedova, Y., Yoder, D. & Gabrilovich, D. I. Antigen-Specific Inhibition of CD8 + T Cell Response by Immature Myeloid Cells in Cancer Is Mediated by Reactive Oxygen Species. *J. Immunol.* **172**, 989–999 (2004).

110. Colegio, O. R. *et al.* Functional polarization of tumour-associated macrophages by tumour-derived lactic acid. *Nature* **513**, 559–563 (2014).

111. Mayadas, T. N., Cullere, X. & Lowell, C. A. The Multifaceted Functions of Neutrophils. *Annu. Rev. Pathol. Mech. Dis.* **9**, 181–218 (2014).

112. Bergers, G. *et al.* Matrix metalloproteinase-9 triggers the angiogenic switch during carcinogenesis. *Nat. Cell Biol.* **2**, 737–744 (2000).

113. Shojaei, F. *et al.* Bv8 regulates myeloid-cell-dependent tumour angiogenesis. *Nature* **450**, 825–831 (2007).

114. Houghton, A. M. G. *et al.* Neutrophil elastase-mediated degradation of IRS-1 accelerates lung tumor growth. *Nat. Med.* **16**, 219–223 (2010).

115. Gong, L. *et al.* Promoting effect of neutrophils on lung tumorigenesis is mediated by CXCR2 and neutrophil elastase. *Mol. Cancer* **12**, (2013).

116. Coffelt, S. B. *et al.* IL-17-producing γδ T cells and neutrophils conspire to promote breast cancer metastasis. *Nature* **522**, 345–348 (2015).

117. Wang, T. T. *et al.* Tumour-activated neutrophils in gastric cancer foster immune suppression and disease progression through GM-CSF-PD-L1 pathway. *Gut* **66**, 1900–1911 (2017).

118. Négrier, S. *et al.* Prognostic factors of survival and rapid progression in 782 patients with metastatic renal carcinomas treated by cytokines: A report from the Groupe Français d'Immunothérapie. *Ann. Oncol.* **13**, 1460–1468 (2002).

119. Jensen, T. O. *et al.* Intratumoral neutrophils and plasmacytoid dendritic cells indicate poor prognosis and are associated with pSTAT3 expression in AJCC stage I/II melanoma. *Cancer* **118**, 2476–2485 (2012).

120. Rao, H. L. *et al.* Increased intratumoral neutrophil in colorectal carcinomas correlates closely with malignant phenotype and predicts patients' adverse prognosis. *PLoS One* **7**, e30806 (2012).

121. Zhao, J. jing *et al.* The prognostic value of tumor-infiltrating neutrophils in gastric adenocarcinoma after resection. *PLoS One* **7**, e33655 (2012).

122. Ilie, M. *et al.* Predictive clinical outcome of the intratumoral CD66b-positive

neutrophil-to-CD8-positive T-cell ratio in patients with resectable nonsmall cell lung cancer. *Cancer* **118**, 1726–1737 (2012).

123. Tohme, S. *et al.* Neutrophil extracellular traps promote the development and progression of liver metastases after surgical stress. *Cancer Res.* **76**, 1367–1380 (2016).

124. Cools-Lartigue, J. *et al.* Neutrophil extracellular traps sequester circulating tumor cells and promote metastasis. *J. Clin. Invest.* **123**, 3446–3458 (2013).

125. Park, J. *et al.* Cancer cells induce metastasis-supporting neutrophil extracellular DNA traps. *Sci. Transl. Med.* **8**, 361ra138 (2016).

126. Governa, V. *et al.* The interplay between neutrophils and CD8+ T cells improves survival in human colorectal cancer. *Clin. Cancer Res.* **23**, 3847–3858 (2017).

127. Fridlender, Z. G. *et al.* Polarization of Tumor-Associated Neutrophil Phenotype by TGF-β: 'N1' versus 'N2' TAN. *Cancer Cell* **16**, 183–194 (2009).

128. Fu, C. & Jiang, A. Dendritic Cells and CD8 T Cell Immunity in Tumor Microenvironment. *Frontiers in immunology* **9**, 3059 (2018).

129. Dudziak, D. *et al.* Differential antigen processing by dendritic cell subsets in vivo. *Science (80-.).* **315**, 107–111 (2007).

130. Chiba, S. *et al.* Tumor-infiltrating DCs suppress nucleic acid-mediated innate immune responses through interactions between the receptor TIM-3 and the alarmin HMGB1. *Nat. Immunol.* **13**, 832–842 (2012).

131. Maurya, N. *et al.* Immunoregulation of Dendritic Cells by the Receptor T cell Ig and Mucin Protein-3 via Bruton's Tyrosine Kinase and c-Src. *J. Immunol.* **193**, 3417–3425 (2014).

132. Salmon, H. *et al.* Expansion and Activation of CD103+ Dendritic Cell Progenitors at the Tumor Site Enhances Tumor Responses to Therapeutic PD-L1 and BRAF Inhibition. *Immunity* **44**, 924–938 (2016).

133. Cerwenka, A. & Lanier, L. L. Natural killer cell memory in infection, inflammation and cancer. *Nature Reviews Immunology* **16**, 112–123 (2016).

134. Gasser, S., Orsulic, S., Brown, E. J. & Raulet, D. H. The DNA damage pathway regulates innate immune system ligands of the NKG2D receptor. *Nature* **436**, 1186–1190 (2005).

135. Liu, X. V, Ho, S. S. W., Tan, J. J., Kamran, N. & Gasser, S. Ras Activation Induces Expression of Raet1 Family NK Receptor Ligands. *J. Immunol.* **189**, 1826–1834 (2012).

136. Guerra, N. *et al.* NKG2D-Deficient Mice Are Defective in Tumor Surveillance in Models of Spontaneous Malignancy. *Immunity* **28**, 571–580 (2008).

137. Coca, S. *et al.* The prognostic significance of intratumoral natural killer cells in patients with colerectal carcinoma. *Cancer* **79**, 2320–2328 (1997).

138. Ishigami, S. *et al.* Prognostic value of intratumoral natural killer cells in gastric carcinoma. *Cancer* **88**, 577–583 (2000).

139. Paul, P. *et al.* HLA-G expression in melanoma: A way for tumor cells to escape from immunosurveillance. *Proc. Natl. Acad. Sci. U. S. A.* **95**, 4510–4515 (1998).

140. Bukur, J. *et al.* Functional role of human leukocyte antigen-G up-regulation in renal cell carcinoma. *Cancer Res.* **63**, 4107–4111 (2003).

141. Ashiru, O. *et al.* Natural killer cell cytotoxicity is suppressed by exposure to the human NKG2D ligand MICA*008 that is shed by tumor cells in exosomes. *Cancer Res.* **70**, 481–489 (2010).

142. Pardoll, D. M. The blockade of immune checkpoints in cancer immunotherapy. *Nat. Rev. Cancer* **12**, 252–64 (2012).

143. Hodi, F. S. *et al.* Abstract CT001: Durable, long-term survival in previously treated patients with advanced melanoma (MEL) who received nivolumab (NIVO) monotherapy in a phase I trial. in *Clinical Trials* **76**, CT001–CT001 (American Association for Cancer Research, 2016).

144. Hamid, O. *et al.* Five-year survival outcomes for patients with advanced melanoma treated with pembrolizumab in KEYNOTE-001. *Ann. Oncol.* **30**, 582–588 (2019).

145. Borghaei, H. *et al.* Nivolumab versus docetaxel in advanced nonsquamous non-small-cell lung cancer. *N. Engl. J. Med.* **373**, 1627–1639 (2015).

146. Fehrenbacher, L. *et al.* Atezolizumab versus docetaxel for patients with previously treated non-small-cell lung cancer (POPLAR): A multicentre, open-label, phase 2 randomised controlled trial. *Lancet* **387**, 1837–1846 (2016).

147. Brahmer, J. *et al.* Nivolumab versus docetaxel in advanced squamous-cell non-small-cell lung cancer. *N. Engl. J. Med.* **373**, 123–135 (2015).

148. Motzer, R. J. *et al.* Nivolumab versus everolimus in advanced renal-cell carcinoma. *N. Engl. J. Med.* **373**, 1803–1813 (2015).

149. Rosenberg, J. E. *et al.* Atezolizumab in patients with locally advanced and metastatic urothelial carcinoma who have progressed following treatment with platinum-based chemotherapy: A single-arm, multicentre, phase 2 trial. *Lancet* **387**, 1909–1920 (2016).

150. Seiwert, T. Y. *et al.* Safety and clinical activity of pembrolizumab for treatment of recurrent or metastatic squamous cell carcinoma of the head and neck (KEYNOTE-012): an open-label, multicentre, phase 1b trial. *Lancet Oncol.* **17**, 956–965 (2016).

151. Gide, T. N., Wilmott, J. S., Scolyer, R. A. & Long, G. V. Primary and acquired resistance to immune checkpoint inhibitors in metastatic melanoma. *Clin. Cancer Res.* **24**, 1260–1270 (2018).

152. Reuben, A. *et al.* Genomic and immune heterogeneity are associated with differential responses to therapy in melanoma. *npj Genomic Med.* **2**, 10 (2017).

153. Rizvi, N. A. *et al.* Mutational landscape determines sensitivity to PD-1 blockade in non-small cell lung cancer. *Science (80-.).* **348**, 124–128 (2015).

154. Rosenberg, J. E. *et al.* Atezolizumab in patients with locally advanced and metastatic urothelial carcinoma who have progressed following treatment with platinum-based chemotherapy: A single-arm, multicentre, phase 2 trial. *Lancet* **387**, 1909–1920 (2016).

155. Jiang, P. *et al.* Signatures of T cell dysfunction and exclusion predict cancer immunotherapy response. *Nat. Med.* **24**, 1550–1558 (2018).

156. Zheng, H. *et al.* HDAC inhibitors enhance T-cell chemokine expression and augment response to PD-1 immunotherapy in lung adenocarcinoma. *Clin. Cancer Res.* **22**, 4119–4132 (2016).

157. Restifo, N. P., Smyth, M. J. & Snyder, A. Acquired resistance to immunotherapy and future challenges. *Nature Reviews Cancer* **16**, 121–126 (2016).

158. Marshall, H. T. & Djamgoz, M. B. A. Immuno-oncology: Emerging targets and combination therapies. *Front. Oncol.* **8**, 1–29 (2018).

159. Gibney, G. T., Weiner, L. M. & Atkins, M. B. Predictive biomarkers for checkpoint inhibitor-based immunotherapy. *The Lancet Oncology* **17**, e542–e551 (2016).

160. Hida, K., Maishi, N., Annan, D. A. & Hida, Y. Contribution of tumor endothelial cells in cancer progression. *International Journal of Molecular Sciences* **19**, (2018).

161. Chang, Y. S. *et al.* Mosaic blood vessels in tumors: Frequency of cancer cells in contact with flowing blood. *Proc. Natl. Acad. Sci. U. S. A.* **97**, 14608–14613 (2000).

162. Senger, D. R. *et al.* Tumor cells secrete a vascular permeability factor that promotes accumulation of ascites fluid. *Science (80-.).* **219**, 983–985 (1983).

163. Tilki, D. *et al.* Zone-specific remodeling of tumor blood vessels affects tumor growth. *Cancer* **110**, 2347–2362 (2007).

164. Collins, T. *et al. Immune interferon activates multiple class II major histocompatibility complex genes and the associated invariant chain gene in human endothelial cells and dermal fibroblasts (mRNA induction/HLA-DR/HLA-DC/HLA-SB/monoclonal antibody)*. *Proc. Nati. Acad. Sci. USA* **81**, (1984).

165. Messadi, D. V, Pober, J. S. & Murphy, G. F. Effects of recombinant gamma-interferon on HLA-DR and DQ expression by skin cells in short-term organ culture. *Lab. Invest.* **58**, 61–7 (1988).

166. Pober, J. S. *et al.* Activation of cultured human endothelial cells by

recombinant lymphotoxin: comparison with tumor necrosis factor and interleukin 1 species. *J. Immunol.* **138**, 3319–24 (1987).

167. Pober, J. S. Cytokine-mediated activation of vascular endothelium. Physiology and Pathology. *Am. J. Pathol.* **133**, 426–433 (1988).

168. Boucher, Y., Baxter, L. T. & Jain, R. K. Interstitial Pressure Gradients in Tissue-isolated and Subcutaneous Tumors: Implications for Therapy. *Cancer Res.* **50**, 4478–4484 (1990).

169. Baxter, L. T. & Jain, R. K. Transport of fluid and macromolecules in tumors. II. Role of heterogeneous perfusion and lymphatics. *Microvasc. Res.* **40**, 246–263 (1990).

170. Klein, D. The tumor vascular endothelium as decision maker in cancer therapy. *Frontiers in Oncology* **8**, 367 (2018).

171. Griffioen, A. W., Damen, C. A., Martinotti, S., Blijham, G. H. & Groenewegen, G. Endothelial intercellular adhesion molecule-1 expression is suppressed in human malignancies: The role of angiogenic factors. *Cancer Res.* **56**, 1111–1117 (1996).

172. Piali, L., Fichtd, A., Terpe, H. J., Imhof, B. A. & Gisler, R. H. Endothelial vascular cell adhesion molecule 1 expression is suppressed by melanoma and carcinoma. *J. Exp. Med.* **181**, 811–816 (1995).

173. Griffioen, A. W. *et al.* Angiogenesis inhibitors overcome tumor induced endothelial cell anergy. *Int. J. Cancer* **80**, 315–319 (1999).

174. Farnsworth, R. H., Achen, M. G. & Stacker, S. A. The evolving role of lymphatics in cancer metastasis. *Current Opinion in Immunology* **53**, 64–73 (2018).

175. Swartz, M. A. & Lund, A. W. Lymphatic and interstitial flow in the tumour microenvironment: Linking mechanobiology with immunity. *Nature Reviews Cancer* **12**, 210–219 (2012).

176. Walker, C., Mojares, E. & Del Río Hernández, A. Role of extracellular matrix in development and cancer progression. *International Journal of Molecular Sciences* **19**, (2018).

177. Cammarota, F. & Laukkanen, M. O. Mesenchymal Stem/Stromal Cells in Stromal Evolution and Cancer Progression. *Stem Cells Int.* **2016**, 4824573 (2016).

178. Lu, P., Weaver, V. M. & Werb, Z. The extracellular matrix: A dynamic niche in cancer progression. *Journal of Cell Biology* **196**, 395–406 (2012).

179. Levental, K. R. *et al.* Matrix Crosslinking Forces Tumor Progression by Enhancing Integrin Signaling. *Cell* **139**, 891–906 (2009).

180. Kharaishvili, G. *et al.* The role of cancer-associated fibroblasts, solid stress and other microenvironmental factors in tumor progression and therapy resistance. *Cancer Cell Int.* **14**, 41 (2014).

181. Paszek, M. J. *et al.* Tensional homeostasis and the malignant phenotype. *Cancer Cell* **8**, 241–254 (2005).

182. Hartmann, N. *et al.* Prevailing role of contact guidance in intrastromal T-cell trapping in human pancreatic cancer. *Clin. Cancer Res.* **20**, 3422–3433 (2014).

183. Ohshio, Y. *et al.* Cancer-associated fibroblast-targeted strategy enhances antitumor immune responses in dendritic cell-based vaccine. *Cancer Sci.* **106**, 134–142 (2015).

184. Weathington, N. M. *et al.* A novel peptide CXCR ligand derived from extracellular matrix degradation during airway inflammation. *Nat. Med.* **12**, 317–323 (2006).

185. Houghton, A. M. G. *et al.* Elastin fragments drive disease progression in a murine model of emphysema. *J. Clin. Invest.* **116**, 753–759 (2006).

186. Midwood, K. *et al.* Tenascin-C is an endogenous activator of Toll-like receptor 4 that is essential for maintaining inflammation in arthritic joint disease. *Nat. Med.* **15**, 774–780 (2009).

187. Johnson, G. B., Brunn, G. J., Kodaira, Y. & Platt, J. L. Receptor-Mediated Monitoring of Tissue Well-Being Via Detection of Soluble Heparan Sulfate by Toll-Like Receptor 4. *J. Immunol.* **168**, 5233–5239 (2002).

188. Cirri, P. & Chiarugi, P. Cancer-associated-fibroblasts and tumour cells: A diabolic liaison driving cancer progression. *Cancer Metastasis Rev.* **31**, 195–208 (2012).

189. Ohlund, D., Elyada, E. & Tuveson, D. Fibroblast heterogeneity in the cancer wound. *J. Exp. Med.* **211**, 1503–1523 (2014).

190. Cortez, E., Roswall, P. & Pietras, K. Functional subsets of mesenchymal cell types in the tumor microenvironment. *Semin. Cancer Biol.* **25**, 3–9 (2014).

191. Augsten, M. Cancer-associated fibroblasts as another polarized cell type of the tumor microenvironment. *Front. Oncol.* **4**, 62 (2014).

192. Liu, Y. *et al.* Separation, cultivation and biological characteristics of oral carcinoma-associated fibroblasts. *Oral Dis.* **12**, 375–380 (2006).

193. Commandeur, S. *et al.* Functional characterization of cancer-associated fibroblasts of human cutaneous squamous cell carcinoma. *Exp. Dermatol.* **20**, 737–742 (2011).

194. Torres, S. *et al.* Proteome profiling of cancer-associated fibroblasts identifies novel proinflammatory signatures and prognostic markers for colorectal cancer. *Clin. Cancer Res.* **19**, 6006–19 (2013).

195. Jia, C. C. *et al.* Cancer-Associated Fibroblasts from Hepatocellular Carcinoma Promote Malignant Cell Proliferation by HGF Secretion. *PLoS One* **8**, 1–9 (2013).

196. Orimo, A. *et al.* Stromal fibroblasts present in invasive human breast carcinomas promote tumor growth and angiogenesis through elevated SDF-1/CXCL12 secretion. *Cell* **121**, 335–48 (2005).

197. Kalluri, R. & Zeisberg, M. Fibroblasts in cancer. *Nat. Rev. Cancer* **6**, 392–401 (2006).

198. Harper, J. & Sainson, R. C. a. Regulation of the anti-tumour immune response by cancer-associated fibroblasts. *Semin. Cancer Biol.* **25**, 69–77 (2014).

199. Erez, N., Truitt, M., Olson, P., Arron, S. T. & Hanahan, D. Cancer-Associated Fibroblasts Are Activated in Incipient Neoplasia to Orchestrate Tumor-

Promoting Inflammation in an NF-kappaB-Dependent Manner. *Cancer Cell* **17**, 135–47 (2010).

200. Cohen, N. *et al.* Fibroblasts drive an immunosuppressive and growth-promoting microenvironment in breast cancer via secretion of Chitinase 3-like 1. *Oncogene* **36**, 4457–4468 (2017).

201. Ren, G. *et al.* CCR2-dependent recruitment of macrophages by tumor-educated mesenchymal stromal cells promotes tumor development and is mimicked by TNFα. *Cell Stem Cell* **11**, 812–824 (2012).

202. Yang, X. *et al.* FAP Promotes immunosuppression by cancer-associated fibroblasts in the tumor microenvironment via STAT3-CCL2 Signaling. *Cancer Res.* **76**, 4124–4135 (2016).

203. Yu, P. F. *et al.* TNFα-activated mesenchymal stromal cells promote breast cancer metastasis by recruiting CXCR2+ neutrophils. *Oncogene* **36**, 482–490 (2017).

204. Ksiazkiewicz, M. *et al.* Importance of CCL2-CCR2A/2B signaling for monocyte migration into spheroids of breast cancer-derived fibroblasts. *Immunobiology* **215**, 737–747 (2010).

205. Jia, X. H. *et al.* Zoledronic acid prevents the tumor-promoting effects of mesenchymal stem cells via MCP-1 dependent recruitment of macrophages. *Oncotarget* **6**, 26018–26028 (2015).

206. Comito, G. *et al.* Cancer-associated fibroblasts and M2-polarized macrophages synergize during prostate carcinoma progression. *Oncogene* **33**, 2423–31 (2014).

207. Mace, T. A. *et al.* Pancreatic cancer-associated stellate cells promote differentiation of myeloid-derived suppressor cells in a StAT3-dependent manner. *Cancer Res.* **73**, 3007–3018 (2013).

208. Cheng, J. *et al.* Hepatic carcinoma-associated fibroblasts induce IDO-producing regulatory dendritic cells through IL-6-mediated STAT3 activation. *Oncogenesis* **5**, e198–e198 (2016).

209. Hsu, Y. L. *et al.* Lung cancer-derived galectin-1 contributes to cancer

associated fibroblast-mediated cancer progression and immune suppression through TDO2/kynurenine axis. *Oncotarget* **7**, 27584–27598 (2016).

210. Khalili, J. S. *et al.* Oncogenic BRAF(V600E) promotes stromal cell-mediated immunosuppression via induction of interleukin-1 in melanoma. *Clin. Cancer Res.* **18**, 5329–5340 (2012).

211. Gorchs, L. *et al.* Human pancreatic carcinoma-associated fibroblasts promote expression of co-inhibitory markers on CD4+ and CD8+ T-cells. *Front. Immunol.* **10**, 847 (2019).

212. Lee, S. K. *et al.* IFN-gamma regulates the expression of B7-H1 in dermal fibroblast cells. *J. Dermatol. Sci.* **40**, 95–103 (2005).

213. Davies, L. C., Heldring, N., Kadri, N. & Le Blanc, K. Mesenchymal Stromal Cell Secretion of Programmed Death-1 Ligands Regulates T Cell Mediated Immunosuppression. *Stem Cells* **35**, 766–776 (2017).

214. Costa, A. *et al.* Fibroblast Heterogeneity and Immunosuppressive Environment in Human Breast Cancer. *Cancer Cell* **33**, 463-479.e10 (2018).

215. Givel, A. M. *et al.* MiR200-regulated CXCL12β promotes fibroblast heterogeneity and immunosuppression in ovarian cancers. *Nat. Commun.* **9**, 1056 (2018).

216. Li, T. *et al.* Hepatocellular carcinoma-associated fibroblasts trigger NK cell dysfunction via PGE2 and IDO. *Cancer Lett.* **318**, 154–61 (2012).

217. Balsamo, M. *et al.* Melanoma-associated fibroblasts modulate NK cell phenotype and antitumor cytotoxicity. *Proc. Natl. Acad. Sci. U. S. A.* **106**, 20847–20852 (2009).

218. Ziani, L. *et al.* Melanoma-associated fibroblasts decrease tumor cell susceptibility to NK cell-mediated killing through matrix-metalloproteinases secretion. *Oncotarget* **8**, 19780–19794 (2017).

219. Davis-smyth, T. The Biology of Vascular Endothelial Growth Factor. *Endocr. Rev.* **18**, 4–25 (2016).

220. Hlatky, L., Tsionou, C., Hahnfeldt, P. & Coleman, C. N. Mammary fibroblasts

may influence breast tumor angiogenesis via hypoxia- induced vascular endothelial growth factor up-regulation and protein expression. *Cancer Res.* **54**, 6083–6086 (1994).

221. Guo, X., Oshima, H., Kitmura, T., Taketo, M. M. & Oshima, M. Stromal fibroblasts activated by tumor cells promote angiogenesis in mouse gastric cancer. *J. Biol. Chem.* **283**, 19864–71 (2008).

222. Fabris, V. T. *et al.* Inoculated mammary carcinoma-associated fibroblasts: contribution to hormone independent tumor growth. *BMC Cancer* **10**, 293 (2010).

223. Wandel, E., Grasshoff, A., Mittag, M., Haustein, U. F. & Saalbach, A. Fibroblasts surrounding melanoma express elevated levels of matrix metalloproteinase-1 (MMP-1) and intercellular adhesion molecule-1 (ICAM-1) in vitro. *Exp Dermatol.* **9**, 34–41 (2000).

224. Singer, C. F. *et al.* MMP-2 and MMP-9 expression in breast cancer-derived human fibroblasts is differentially regulated by stromal-epithelial interactions. *Breast Cancer Res. Treat.* **72**, 69–77 (2002).

225. Pickup, M. *et al.* Stromally Derived Lysyl Oxidase Promotes Metastasis of Transforming Growth Factor-β Deficient Mouse Mammary Carcinomas. *Cancer Res.* **148**, 825–832 (2008).

226. Thomasset, N. *et al.* Expression of autoactivated stromelysin-1 in mammary glands of transgenic mice leads to a reactive stroma during early development. *Am. J. Pathol.* **153**, 457–467 (1998).

227. Wandel, E., Graßhoff, A., Mittag, M., Haustein, U. F. & Saalbach, A. Fibroblasts surrounding melanoma express elevated levels of matrix metalloproteinase-1 (MMP-1) and intercellular adhesion molecule-1 (ICAM-1) in vitro. *Exp. Dermatol.* **9**, 34–41 (2000).

228. Poola, I. *et al.* Identification of MMP-1 as a putative breast cancer predictive marker by global gene expression analysis. *Nat. Med.* **11**, 481–483 (2005).

229. Noskova, V., Ahmadi, S., Åsander, E. & Casslén, B. Ovarian cancer cells stimulate uPA gene expression in fibroblastic stromal cells via multiple

paracrine and autocrine mechanisms. *Gynecol. Oncol.* **115**, 121–126 (2009).

230. Burridge, K. & Fath, K. Focal contacts: Transmembrane links between the extracellular matrix and the cytoskeleton. *BioEssays* **10**, 104–108 (1989).

231. Dumont, N. *et al.* Breast fibroblasts modulate early dissemination, tumorigenesis, and metastasis through alteration of extracellular matrix characteristics. *Neoplasia* **15**, 249–62 (2013).

232. Erdogan, B. *et al.* Cancer-associated fibroblasts promote directional cancer cell migration by aligning fibronectin. *J. Cell Biol.* **216**, 3799–3816 (2017).

233. Gaggioli, C. *et al.* Fibroblast-led collective invasion of carcinoma cells with differing roles for RhoGTPases in leading and following cells. *Nat. Cell Biol.* **9**, 1392–1400 (2007).

234. Calon, A. *et al.* Dependency of Colorectal Cancer on a TGF-β-Driven Program in Stromal Cells for Metastasis Initiation. *Cancer Cell* **22**, 571–584 (2012).

235. Bhowmick, N. A. *et al.* TGF-β Signaling in Fibroblasts Modulates the Oncogenic Potential of Adjacent Epithelia. *Science (80-.).* **303**, 848–851 (2004).

236. Lenos, K. J. *et al.* Stem cell functionality is microenvironmentally defined during tumour expansion and therapy response in colon cancer. *Nat. Cell Biol.* **20**, 1193–1202 (2018).

237. Sun, Y. *et al.* Cancer-associated fibroblasts secrete FGF-1 to promote ovarian proliferation, migration, and invasion through the activation of FGF-1/FGFR4 signaling. *Tumor Biol.* **39**, 1–10 (2017).

238. Wu, X. *et al.* IL-6 secreted by cancer-associated fibroblasts promotes epithelial-mesenchymal transition and metastasis of gastric cancer via JAK2/STAT3 signaling pathway. *Oncotarget* **8**, 20741–20750 (2017).

239. Orimo, A. & Weinberg, R. a. Heterogeneity of stromal fibroblasts in tumor. *Cancer Biol. Ther.* **6**, 618–619 (2014).

240. Luga, V. *et al.* Exosomes mediate stromal mobilization of autocrine Wnt-PCP signaling in breast cancer cell migration. *Cell* **151**, 1542–1556 (2012).

241. Zhang, D. *et al.* Tumor–Stroma IL1b-IRAK4 feedforward circuitry drives tumor fibrosis, chemoresistance, and poor prognosis in pancreatic cancer. *Cancer Res.* **78**, 1700–1712 (2018).

242. Qiao, Y. *et al.* IL6 derived from cancer-associated fibroblasts promotes chemoresistance via CXCR7 in esophageal squamous cell carcinoma. *Oncogene* **37**, 873–883 (2018).

243. Sun, Y. *et al.* Treatment-induced damage to the tumor microenvironment promotes prostate cancer therapy resistance through WNT16B. *Nat. Med.* **18**, 1359–1368 (2012).

244. Mueller, K. L. *et al.* Fibroblast-secreted hepatocyte growth factor mediates epidermal growth factor receptor tyrosine kinase inhibitor resistance in triple-negative breast cancers through paracrine activation of Met. *Breast Cancer Res.* **14**, R104 (2012).

245. Hirata, E. *et al.* Intravital imaging reveals how BRAF inhibition generates drug-tolerant microenvironments with high integrin β1/FAK signaling. *Cancer Cell* **27**, 574–88 (2015).

246. Comito, G. *et al.* Lactate modulates CD4 + T-cell polarization and induces an immunosuppressive environment, which sustains prostate carcinoma progression via TLR8/miR21 axis. *Oncogene* **38**, 3681–3695 (2019).

247. Tauriello, D. V. F. *et al.* TGFβ drives immune evasion in genetically reconstituted colon cancer metastasis. *Nature* **554**, 538–543 (2018).

248. Feig, C. *et al.* Targeting CXCL12 from FAP-expressing carcinoma-associated fibroblasts synergizes with anti-PD-L1 immunotherapy in pancreatic cancer. *Proc. Natl. Acad. Sci. U. S. A.* **110**, 20212–20217 (2013).

249. Gallagher, P. G. *et al.* Gene expression profiling reveals cross-talk between melanoma and fibroblasts: Implications for host-tumor interactions in metastasis. *Cancer Res.* **65**, 4134–4146 (2005).

250. Kojima, Y. *et al.* Autocrine TGF-beta and stromal cell-derived factor-1 (SDF-1) signaling drives the evolution of tumor-promoting mammary stromal myofibroblasts. *Proc. Natl. Acad. Sci.* **107**, 20009–20014 (2010).

251. Fukino, K. *et al.* Combined total genome loss of heterozygosity scan of breast cancer stroma and epithelium reveals multiplicity of stromal targets. *Cancer Res.* **64**, 7231–7236 (2004).

252. Kurose, K. *et al.* Frequent somatic mutations in PTEN and TP53 are mutually exclusive in the stroma of breast carcinomas. *Nat. Genet.* **32**, 355–7 (2002).

253. Walter, K., Omura, N., Hong, S. M., Griffith, M. & Goggins, M. Pancreatic cancer associated fibroblasts display normal allelotypes. *Cancer Biol. Ther.* **7**, 882–888 (2008).

254. Allinen, M. *et al.* Molecular characterization of the tumor microenvironment in breast cancer. *Cancer Cell* **6**, 17–32 (2004).

255. Aprelikova, O. *et al.* The role of miR-31 and its target gene SATB2 in cancer-associated fibroblasts. *Cell Cycle* **9**, 4387–4398 (2010).

256. Mitra, A. K. *et al.* MicroRNAs reprogram normal fibroblasts into cancer-associated fibroblasts in ovarian cancer. *Cancer Discov.* **2**, 1100–1108 (2012).

257. Shen, H. *et al.* Reprogramming of Normal Fibroblasts into Cancer-Associated Fibroblasts by miRNAs-Mediated CCL2/VEGFA Signaling. *PLoS Genet.* **12**, e1006244 (2016).

258. Wang, L. *et al.* Distinct miRNA profiles in normal and gastric cancer myofibroblasts and significance in Wnt signaling. *Am. J. Physiol. - Gastrointest. Liver Physiol.* **310**, G696–G704 (2016).

259. Doldi, V. *et al.* Integrated gene and miRNA expression analysis of prostate cancer associated fibroblasts supports a prominent role for interleukin-6 in fibroblast activation. *Oncotarget* **6**, 31441–31460 (2015).

260. Xiao, Q. *et al.* Cancer-associated fibroblasts in pancreatic cancer are reprogrammed by tumor-induced alterations in genomic DNA methylation. *Cancer Res.* **76**, 5395–5404 (2016).

261. Vizoso, M. *et al.* Aberrant DNA methylation in non-small cell lung cancer-associated fibroblasts. *Carcinogenesis* **36**, 1453–1463 (2015).

262. Zhao, L. *et al.* MiRNA expression analysis of cancer-associated fibroblasts and

normal fibroblasts in breast cancer. *Int. J. Biochem. Cell Biol.* **44**, 2051–2059 (2012).

263. Albrengues, J. *et al.* Epigenetic switch drives the conversion of fibroblasts into proinvasive cancer-associated fibroblasts. *Nat. Commun.* **6**, (2015).

264. Iwano, M. *et al.* Evidence that fibroblasts derive from epithelium during tissue fibrosis. *J. Clin. Invest.* **110**, 341–350 (2002).

265. Petersen, O. W. *et al.* Epithelial to mesenchymal transition in human breast cancer can provide a nonmalignant stroma. *Am. J. Pathol.* **162**, 391–402 (2003).

266. Potenta, S., Zeisberg, E. & Kalluri, R. The role of endothelial-to-mesenchymal transition in cancer progression. *Br. J. Cancer* **99**, 1375–1379 (2008).

267. Zeisberg, E. M. *et al.* Endothelial-to-mesenchymal transition contributes to cardiac fibrosis. *Nat. Med.* **13**, 952–61 (2007).

268. Zeisberg, E. M., Potenta, S., Xie, L., Zeisberg, M. & Kalluri, R. Discovery of endothelial to mesenchymal transition as a source for carcinoma-associated fibroblasts. *Cancer Res.* **67**, 10123–10128 (2007).

269. Yamazaki, T. & Mukouyama, Y. Tissue Specific Origin, Development, and Pathological Perspectives of Pericytes. *Front. Cardiovasc. Med.* **5**, 1–6 (2018).

270. Lin, S. L., Kisseleva, T., Brenner, D. A. & Duffield, J. S. Pericytes and perivascular fibroblasts are the primary source of collagen-producing cells in obstructive fibrosis of the kidney. *Am. J. Pathol.* **173**, 1617–1627 (2008).

271. Mederacke, I. *et al.* Fate tracing reveals hepatic stellate cells as dominant contributors to liver fibrosis independent of its aetiology. *Nat. Commun.* **4**, 2823 (2013).

272. Humphreys, B. D. *et al.* Fate tracing reveals the pericyte and not epithelial origin of myofibroblasts in kidney fibrosis. *Am. J. Pathol.* **176**, 85–97 (2010).

273. Hosaka, K. *et al.* Pericyte-fibroblast transition promotes tumor growth and metastasis. *Proc. Natl. Acad. Sci. U. S. A.* **113**, E5618–E5627 (2016).

274. Direkze, N. C. *et al.* Bone marrow contribution to tumor-associated

myofibroblasts and fibroblasts. *Cancer Res.* **64**, 8492–8495 (2004).

275. Ishii, G. *et al.* Bone-marrow-derived myofibroblasts contribute to the cancer-induced stromal reaction. *Biochem. Biophys. Res. Commun.* **309**, 232–240 (2003).

276. Bianco, P., Riminucci, M., Gronthos, S. & Robey, P. G. Bone Marrow Stromal Stem Cells: Nature, Biology, and Potential Applications. *Stem Cells* **19**, 180–192 (2001).

277. Klopp, A. H., Gupta, A., Spaeth, E., Andreeff, M. & Marini, F. Concise review: Dissecting a discrepancy in the literature: do mesenchymal stem cells support or suppress tumor growth? *Stem Cells* **29**, 11–9 (2011).

278. Quante, M. *et al.* bone marrow-derived myofibroblasts contribute to the growth MSC niche and promote tumour growth. *Cancer Cell* **19**, 257–272 (2012).

279. Ostermann, E. *et al.* Effective immunoconjugate therapy in cancer models targeting a serine protease of tumor fibroblasts. *Clin. Cancer Res.* **14**, 4584–4592 (2008).

280. Fang, J. *et al.* A potent immunotoxin targeting fibroblast activation protein for treatment of breast cancer in mice. *Int. J. Cancer* **138**, 1013–1023 (2016).

281. Duperret, E. K. *et al.* Alteration of the tumor stroma using a consensus DNA vaccine targeting Fibroblast Activation Protein (FAP) synergizes with antitumor vaccine therapy in Mice. *Clin. Cancer Res.* **24**, 1190–1201 (2018).

282. Loeffler, M., Krüger, J. A., Niethammer, A. G. & Reisfeld, R. A. Targeting tumor-associated fibroblasts improves cancer chemotherapy by increasing intratumoral drug uptake. *J. Clin. Invest.* **116**, 1955–1962 (2006).

283. Wang, L. C. S. *et al.* Targeting fibroblast activation protein in tumor stroma with chimeric antigen receptor T cells can inhibit tumor growth and augment host immunity without severe toxicity. *Cancer Immunol. Res.* **2**, 154–166 (2014).

284. Roberts, E. W. *et al.* Depletion of stromal cells expressing fibroblast activation protein-α from skeletal muscle and bone marrow results in cachexia and anemia. *J. Exp. Med.* **210**, 1137–1151 (2013).

285. Takai, K., Le, A., Weaver, V. M. & Werb, Z. Targeting the cancer-associated fibroblasts as a treatment in triple-negative breast cancer. *Oncotarget* **7**, 82889–82901 (2016).

286. Sherman, M. H. *et al.* Vitamin D receptor-mediated stromal reprogramming suppresses pancreatitis and enhances pancreatic cancer therapy. *Cell* **159**, 80–93 (2014).

287. Roswall, P. & Pietras, K. Of mice and men: a comparative study of cancer-associated fibroblasts in mammary carcinoma. *Ups. J. Med. Sci.* **117**, 196–201 (2012).

288. Fries, K. M. *et al.* Evidence of Fibroblast Heterogeneity and the Role of Fibroblast Subpopulations in Fibrosis. *Clin. Immunol. Immunopathol.* **72**, 283–292 (1994).

289. Chang, H. Y. *et al.* Diversity, topographic differentiation, and positional memory in human fibroblasts. *Proc. Natl. Acad. Sci. U. S. A.* **99**, 12877–82 (2002).

290. Rinn, J. L., Bondre, C., Gladstone, H. B., Brown, P. O. & Chang, H. Y. Anatomic demarcation by positional variation in fibroblast gene expression programs. *PLoS Genet.* **2**, e119 (2006).

291. Sriram, G., Bigliardi, P. L. & Bigliardi-Qi, M. Fibroblast heterogeneity and its implications for engineering organotypic skin models in vitro. *Eur. J. Cell Biol.* **94**, 483–512 (2015).

292. Azzarone, B. & Macieira-Coelho, A. Heterogeneity of the kinetics of proliferation within human skin fibroblastic cell populations. *J. Cell Sci.* **57**, 177–87 (1982).

293. Janson, D. G., Saintigny, G., van Adrichem, A., Mahé, C. & El Ghalbzouri, A. Different Gene Expression Patterns in Human Papillary and Reticular Fibroblasts. *J. Invest. Dermatol.* **132**, 2565–2572 (2012).

294. Sugimoto, H., Mundel, T. M., Kieran, M. W. & Kalluri, R. Identification of fibroblast heterogeneity in the tumor microenvironment. *Cancer Biol. Ther.* **5**, 1640–1646 (2006).

295. Öhlund, D. *et al.* Distinct populations of inflammatory fibroblasts and myofibroblasts in pancreatic cancer. *J. Exp. Med.* **214**, 579–596 (2017).

296. Su, S. *et al.* CD10+GPR77+ Cancer-Associated Fibroblasts Promote Cancer Formation and Chemoresistance by Sustaining Cancer Stemness. *Cell* **172**, 841-856.e16 (2018).

297. Brechbuhl, H. M. *et al.* Fibroblast subtypes regulate responsiveness of luminal breast cancer to estrogen. *Clin. Cancer Res.* **23**, 1710–1721 (2017).

298. Lambrechts, D. *et al.* Phenotype molding of stromal cells in the lung tumor microenvironment. *Nat. Med.* **24**, 1277–1289 (2018).

299. Bartoschek, M. *et al.* Spatially and functionally distinct subclasses of breast cancer-associated fibroblasts revealed by single cell RNA sequencing. *Nat. Commun.* **9**, 5150 (2018).

300. Puram, S. V. *et al.* Single-Cell Transcriptomic Analysis of Primary and Metastatic Tumor Ecosystems in Head and Neck Cancer. *Cell* **171**, 1611-1624.e24 (2017).

301. Elyada, E. *et al.* Cross-species single-cell analysis of pancreatic ductal adenocarcinoma reveals antigen-presenting cancer-associated fibroblasts. *Cancer Discovery* **9**, 1102–1123 (2019).

302. Raz, Y. *et al.* Bone marrow-derived fibroblasts are a functionally distinct stromal cell population in breast cancer. *J. Exp. Med.* **215**, 3075–3093 (2018).

303. Özdemir, B. C. *et al.* Depletion of carcinoma-associated fibroblasts and fibrosis induces immunosuppression and accelerates pancreas cancer with reduced survival. *Cancer Cell* **25**, 719–34 (2014).

304. Siegel, R. L., Miller, K. D. & Jemal, A. Cancer statistics, 2015. *CA. Cancer J. Clin.* **65**, 5–29 (2015).

305. Miller, K. D. *et al.* Cancer treatment and survivorship statistics, 2019. *CA. Cancer J. Clin.* **69**, 363–385 (2019).

306. Larue, L. & Beermann, F. Cutaneous melanoma in genetically modified animals. *Pigment Cell Research* **20**, 485–497 (2007).

307. Becker, J. C. *et al.* Mouse models for melanoma: A personal perspective. *Exp. Dermatol.* **19**, 157–164 (2010).

308. Bastian, B. C. The Molecular Pathology of Melanoma: An Integrated Taxonomy of Melanocytic Neoplasia. *Annu. Rev. Pathol. Mech. Dis.* **9**, 239–271 (2014).

309. Kim, C. *et al.* Long-Term Survival in Patients with Metastatic Melanoma Treated with DTIC or Temozolomide. *Oncologist* **15**, 765–771 (2010).

310. Domingues, B., Lopes, J., Soares, P. & Populo, H. Melanoma treatment in review. *ImmunoTargets Ther.* **Volume 7**, 35–49 (2018).

311. Soengas, M. S. & Lowe, S. W. Apoptosis and melanoma chemoresistance. *Oncogene* **22**, 3138–3151 (2003).

312. Kadla, S. & Malik, G. M. Risks of HIV infection in the health care setting. *JK Practitioner* **4**, 41–43 (1997).

313. Chapman, P. B. *et al.* Vemurafenib in patients with BRAFV600 mutation-positive metastatic melanoma: Final overall survival results of the randomized BRIM-3 study. *Ann. Oncol.* **28**, 2581–2587 (2017).

314. Rizos, H. *et al.* BRAF inhibitor resistance mechanisms in metastatic melanoma: Spectrum and clinical impact. *Clin. Cancer Res.* **20**, 1965–1977 (2014).

315. Robert, C. *et al.* Ipilimumab plus dacarbazine for previously untreated metastatic melanoma. *N. Engl. J. Med.* **364**, 2517–2526 (2011).

316. Hodi, F. S. *et al.* Nivolumab plus ipilimumab or nivolumab alone versus ipilimumab alone in advanced melanoma (CheckMate 067): 4-year outcomes of a multicentre, randomised, phase 3 trial. *Lancet Oncol.* **19**, 1480–1492 (2018).

317. Boon, T., Coulie, P. G., Eynde, B. J. Van den & Bruggen, P. van der. HUMAN T CELL RESPONSES AGAINST MELANOMA. *Annu. Rev. Immunol.* **24**, 175–208 (2006).

318. Straten, P. T. *et al.* In situ T cell responses against melanoma comprise high

numbers of locally expanded T cell clonotypes. *J. Immunol.* **163**, 443–447 (1999).

319. Speeckaert, R. *et al.* Immune reactions in benign and malignant melanocytic lesions: Lessons for immunotherapy. *Pigment Cell Melanoma Res.* **24**, 334–344 (2011).

320. Hino, R. *et al.* Tumor cell expression of programmed cell death-1 ligand 1 is a prognostic factor for malignant melanoma. *Cancer* **116**, 1757–1766 (2010).

321. Müller, R., Zheng, M. & Mrowietz, U. Significant reduction of human monocyte chemotactic response to monocyte-chemotactic protein 1 in patients with primary and metastatic malignant melanoma. *Exp. Dermatol.* **6**, 81–86 (1997).

322. Filipazzi, P. *et al.* Identification of a new subset of myeloid suppressor cells in peripheral blood of melanoma patients with modulation by a granulocyte-macrophage colony-stimulation factor-based antitumor vaccine. *J. Clin. Oncol.* **25**, 2546–2553 (2007).

323. Mourmouras, V. *et al.* Evaluation of tumour-infiltrating CD4+CD25+FOXP3+ regulatory T cells in human cutaneous benign and atypical naevi, melanomas and melanoma metastases. *Br. J. Dermatol.* **157**, 531–539 (2007).

324. Miracco, C. *et al.* Utility of tumour-infiltrating CD25+FOXP3+ regulatory T cell evaluation in predicting local recurrence in vertical growth phase cutaneous melanoma. *Oncol. Rep.* **18**, 1115–1122 (2007).

325. Filipazzi, P. *et al.* Identification of a new subset of myeloid suppressor cells in peripheral blood of melanoma patients with modulation by a granulocyte-macrophage colony-stimulation factor-based antitumor vaccine. *J. Clin. Oncol.* **25**, 2546–2553 (2007).

326. Gazzaniga, S. *et al.* Targeting tumor-associated macrophages and inhibition of MCP-1 reduce angiogenesis and tumor growth in a human melanoma xenograft. *J. Invest. Dermatol.* **127**, 2031–2041 (2007).

327. Varney, M. L. *et al.* Monocyte/macrophage recruitment, activation and differentiation modulate interleukin-8 production: A paracrine role of tumor-associated macrophages in tumor angiogenesis. *In Vivo (Brooklyn).* **16**, 471–

477 (2002).

328. Varney, M. L., Olsen, K. J., Mosley, R. L. & Singh, R. K. Paracrine regulation of vascular endothelial growth factor-A expression during macrophage-melanoma cell interaction: Role of monocyte chemotactic protein-1 and macrophage colony-stimulating factor. *J. Interf. Cytokine Res.* **25**, 674–683 (2005).

329. Borden, E. C. *et al.* Dual mechanistic function of MDSC subsets in melanoma resistance. *J. Clin. Oncol.* **28**, 8590–8590 (2010).

330. Cornil, I. *et al.* Fibroblast cell interactions with human melanoma cells affect tumor cell growth as a function of tumor progression. *Proc. Natl. Acad. Sci. U. S. A.* **88**, 6028–6032 (1991).

331. Zhou, L., Yang, K., Andl, T., Randall Wickett, R. & Zhang, Y. Perspective of targeting cancer-associated fibroblasts in melanoma. *Journal of Cancer* **6**, 717–726 (2015).

332. Tiago, M. *et al.* Fibroblasts protect melanoma cells from the cytotoxic effects of doxorubicin. *Tissue Eng. - Part A* **20**, 2412–2421 (2014).

333. Flach, E. H., Rebecca, V. W., Herlyn, M., Smalley, K. S. M. & Anderson, A. R. A. Fibroblasts contribute to melanoma tumor growth and drug resistance. *Mol. Pharm.* **8**, 2039–2049 (2011).

334. Kääriäinen, E. *et al.* Switch to an invasive growth phase in melanoma is associated with tenascin-C, fibronectin, and procollagen-I forming specific channel structures for invasion. *J. Pathol.* **210**, 181–191 (2006).

335. Massi, D., Franchi, A., Borgognoni, L., Reali, U. M. & Santucci, M. Osteonectin expression correlates with clinical outcome in thin cutaneous malignant melanomas. *Hum. Pathol.* **30**, 339–344 (1999).

336. Ledda, F. *et al.* The expression of the secreted protein acidic and rich in cysteine neoplastic progression of human melanoma. *J. Invest. Dermatol.* **108**, 210–214 (1997).

337. Rangel, J. *et al.* Osteopontin as a molecular prognostic marker for melanoma. *Cancer* **112**, 144–150 (2008).

338. Zhou, Y. *et al.* Osteopontin expression correlates with melanoma invasion. *J. Invest. Dermatol.* **124**, 1044–1052 (2005).

339. Ntayi, C., Hornebeck, W. & Bernard, P. Influence of cultured dermal fibroblasts on human melanoma cell proliferation, matrix metalloproteinase-2 (MMP-2) expression and invasion in vitro. *Arch. Dermatol. Res.* **295**, 236–241 (2003).

340. Wandel, E., Graßhoff, A., Mittag, M., Haustein, U. F. & Saalbach, A. Fibroblasts surrounding melanoma express elevated levels of matrix metalloproteinase-1 (MMP-1) and intercellular adhesion molecule-1 (ICAM-1) in vitro. *Exp. Dermatol.* **9**, 34–41 (2000).

341. Meierjohann, S. *et al.* MMP13 mediates cell cycle progression in melanocytes and melanoma cells: In vitro studies of migration and proliferation. *Mol. Cancer* **9**, (2010).

342. Straussman, R. *et al.* Tumour micro-environment elicits innate resistance to RAF inhibitors through HGF secretion. *Nature* **487**, 500–504 (2012).

343. Fidler, I. J. Selection of successive tumour lines for metastasis. *Nat. New Biol.* **242**, 148–149 (1973).

344. Nakamura, K. *et al.* Characterization of mouse melanoma cell lines by their mortal malignancy using an experimental metastatic model. *Life Sci.* **70**, 791–798 (2002).

345. Van Elsas, A., Hurwitz, A. A. & Allison, J. P. Combination immunotherapy of B16 melanoma using anti-cytotoxic T lymphocyte-associated antigen 4 (CTLA-4) and granulocyte/macrophage colony- stimulating factor (GM-CSF)-producing vaccines induces rejection of subcutaneous and metastatic tumors accompanied. *J. Exp. Med.* **190**, 355–366 (1999).

346. Curran, M. A., Montalvo, W., Yagita, H. & Allison, J. P. PD-1 and CTLA-4 combination blockade expands infiltrating T cells and reduces regulatory T and myeloid cells within B16 melanoma tumors. *Proc. Natl. Acad. Sci. U. S. A.* **107**, 4275–4280 (2010).

347. Lim, Y. S. *et al.* Augmentation of therapeutic antitumor immunity by B16F10 melanoma cells transfected by interferon-gamma and allogeneic MHC class I

cDNAs. *Mol. Cells* **8**, 629–636 (1998).

348. Merritt, R. E. *et al.* Augmenting major histocompatibility complex class I expression by murine tumors in vivo enhances antitumor immunity induced by an active immunotherapy strategy. *J. Thorac. Cardiovasc. Surg.* **127**, 355–364 (2004).

349. Steitz, J. *et al.* Genetic immunization of mice with human tyrosinase-related protein 2: Implications for the immunotherapy of melanoma. *Int. J. Cancer* **86**, 89–94 (2000).

350. Melnikova, V. O., Bolshakov, S. V., Walker, C. & Ananthaswamy, H. N. Genomic alterations in spontaneous and carcinogen-induced murine melanoma cell lines. *Oncogene* **23**, 2347–2356 (2004).

351. Dankort, D. *et al.* Braf(V600E) cooperates with Pten loss to induce metastatic melanoma. *Nat. Genet.* **41**, 544–52 (2009).

352. Haluska, F. G. *et al.* Genetic alterations in signaling pathways in melanoma. *Clinical Cancer Research* **12**, (2006).

353. Goel, V. K., Lazar, A. J. F., Warneke, C. L., Redston, M. S. & Haluska, F. G. Examination of mutations in BRAF, NRAS, and PTEN in primary cutaneous melanoma. *J. Invest. Dermatol.* **126**, 154–160 (2006).

354. Sensi, M. *et al.* Mutually exclusive NRASQ61R and BRAFV600E mutations at the single-cell level in the same human melanoma. *Oncogene* **25**, 3357–3364 (2006).

355. Zhang, T., Dutton-Regester, K., Brown, K. M. & Hayward, N. K. The genomic landscape of cutaneous melanoma. *Pigment Cell Melanoma Res.* **29**, 266–283 (2016).

356. Ackermann, J. *et al.* Metastasizing melanoma formation caused by expression of activated N-RasQ61K on an INK4a-deficient background. *Cancer Res.* **65**, 4005–4011 (2005).

357. Stott, F. J. *et al.* The alternative product from the human CDKN2A locus, p14(ARF), participates in a regulatory feedback loop with p53 and MDM2. *EMBO J.* **17**, 5001–5014 (1998).

358. Zhang, Y., Xiong, Y. & Yarbrough, W. G. ARF promotes MDM2 degradation and stabilizes p53: ARF-INK4a locus deletion impairs both the Rb and p53 tumor suppression pathways. *Cell* **92**, 725–734 (1998).

359. Hussussian, C. J. *et al.* Germline p16 mutations in familial melanoma. *Nat. Genet.* **8**, 15–21 (1994).

360. Damsky, W. *et al.* mTORC1 activation blocks brafV600E-induced growth arrest but is insufficient for melanoma formation. *Cancer Cell* **27**, 41–56 (2015).

361. Satija, R., Farrell, J. A., Gennert, D., Schier, A. F. & Regev, A. Spatial reconstruction of single-cell gene expression data. *Nat. Biotechnol.* **33**, 495–502 (2015).

362. Pérez-Guijarro, E., Day, C. P., Merlino, G. & Zaidi, M. R. Genetically engineered mouse models of melanoma. *Cancer* **123**, 2089–2103 (2017).

363. Zaidi, M. R., Day, C. P. & Merlino, G. From UVs to metastases: Modeling melanoma initiation and progression in the mouse. *Journal of Investigative Dermatology* **128**, 2381–2391 (2008).

364. Noonan, F. P. *et al.* Neonatal sunburn and melanoma in mice. *Nature* **413**, 271–272 (2001).

365. Otsuka, T. *et al.* c-Met autocrine activation induces development of malignant melanoma and acquisition of the metastatic phenotype. *Cancer Res.* **58**, 5157–5167 (1998).

366. Kuzu, O. F., Nguyen, F. D., Noory, M. A. & Sharma, A. Current State of Animal (Mouse) Modeling in Melanoma Research. *Cancer Growth Metastasis* **8s1**, CGM.S21214 (2015).

367. Einarsdottir, B. O. *et al.* Melanoma patient-derived xenografts accurately model the disease and develop fast enough to guide treatment decisions. *Oncotarget* **5**, B38–B38 (2014).

368. Ilie, M. *et al.* Setting up a wide panel of patient-derived tumor xenografts of non-small cell lung cancer by improving the preanalytical steps. *Cancer Med.* **4**, 201–211 (2015).

369. Flaberg, E. *et al.* High-throughput live-cell imaging reveals differential inhibition of tumor cell proliferation by human fibroblasts. *Int. J. Cancer* **128**, 2793–2802 (2011).

370. Qiu, P. *et al.* Extracting a cellular hierarchy from high-dimensional cytometry data with SPADE. *Nat. Biotechnol.* **29**, 886–91 (2011).

371. Anchang, B. *et al.* Visualization and cellular hierarchy inference of single-cell data using SPADE. *Nat. Protoc.* **11**, 1264–1279 (2016).

372. Picelli, S. *et al.* Full-length RNA-seq from single cells using Smart-seq2. *Nat. Protoc.* **9**, 171–81 (2014).

373. Scialdone, A. *et al.* Computational assignment of cell-cycle stage from single-cell transcriptome data. *Methods* **85**, 54–61 (2015).

374. Haghverdi, L., Buettner, F. & Theis, F. J. Diffusion maps for high-dimensional single-cell analysis of differentiation data. *Bioinformatics* **31**, 2989–2998 (2015).

375. Haghverdi, L., Büttner, M., Wolf, F. A., Buettner, F. & Theis, F. J. Diffusion pseudotime robustly reconstructs lineage branching. *Nat. Methods* **13**, 845–848 (2016).

376. Hooijkaas, A. I., Gadiot, J., Van Der Valk, M., Mooi, W. J. & Blank, C. U. Targeting BRAF V600E in an inducible murine model of melanoma. *Am. J. Pathol.* **181**, 785–794 (2012).

377. Denko, N. C. Hypoxia, HIF1 and glucose metabolism in the solid tumour. *Nat Rev Cancer* **8**, 705–713 (2008).

378. Zhong, H. *et al.* Modulation of Hypoxia-inducible Factor 1 α Expression by the Epidermal Growth Factor / Phosphatidylinositol 3-Kinase / PTEN / AKT / FRAP Pathway in Human Prostate Cancer Cells : Implications for Tumor Angiogenesis and Therapeutics Advances in Brief Prosta. *Cancer Res.* **60**, 1541–1545 (2000).

379. Laughner, E. *et al.* HER2 (neu) Signaling Increases the Rate of Synthesis : Novel Mechanism for HIF-1-Mediated Vascular Endothelial Growth Factor Expression HER2 (neu) Signaling Increases the Rate of Hypoxia-Inducible

Factor 1 ␣ (HIF-1 ␣) Synthesis : Novel Mechanism for. *Am. Soc. Microbiol.* **21**, 3995–4004 (2001).

380. Walter, K., Omura1, N., Hong1, S.-M., Griffith, M. & Goggins, M. Pancreatic cancer associated fibroblasts display normal allelotypes. *Cancer Biol. Ther.* **19**, 431–444 (2014).

381. Qiu, W. *et al.* No evidence of clonal somatic genetic alterations in cancer-associated fibroblasts from human breast and ovarian carcinomas. *Nat. Genet.* **40**, 650–5 (2008).

382. Buettner, F. *et al.* Computational analysis of cell-to-cell heterogeneity in single-cell RNA-sequencing data reveals hidden subpopulations of cells. *Nat. Biotechnol.* **33**, 155–60 (2015).

383. Martinez-Outschoorn, U. E. *et al.* Cancer cells metabolically 'fertilize' the tumor microenvironment with hydrogen peroxide, driving the Warburg effect: Implications for PET imaging of human tumors. *Cell Cycle* **10**, 2504–2520 (2011).

384. Martinez-Outschoorn, U. E. *et al.* Tumor cells induce the cancer associated fibroblast phenotype via caveolin-1 degradation: Implications for breast cancer and DCIS therapy with autophagy inhibitors. *Cell Cycle* **9**, 2423–2433 (2010).

385. Martinez-Outschoorn, U. E. *et al.* Oxidative stress in cancer associated fibroblasts drives tumor-stroma co-evolution: A new paradigm for understanding tumor metabolism, the field effect and genomic instability in cancer cells. *Cell Cycle* **9**, 3256–3276 (2010).

386. Martinez-Outschoorn, U. E. *et al.* Autophagy in cancer associated fibroblasts promotes tumor cell survival: Role of hypoxia, HIF1 induction and NF??B activation in the tumor stromal microenvironment. *Cell Cycle* **9**, 3515–3533 (2010).

387. Pavlides, S. *et al.* Warburg meets autophagy: cancer-associated fibroblasts accelerate tumor growth and metastasis via oxidative stress, mitophagy, and aerobic glycolysis. *Antioxid. Redox Signal.* **16**, 1264–84 (2012).

388. Toullec, A. *et al.* Oxidative stress promotes myofibroblast differentiation and

tumour spreading. *EMBO Mol. Med.* **2**, 211–230 (2010).

389. Izuishi, K., Kato, K., Ogura, T., Kinoshita, T. & Esumi, H. Remarkable tolerance of tumor cells to nutrient deprivation: Possible new biochemical target for cancer therapy. *Cancer Res.* **60**, 6201–6207 (2000).

390. Kauppila, S., Stenbäck, F., Risteli, J., Jukkola, A. & Risteli, L. Aberrant Type I and Type III Collagen Gene. *J. Pathol.* **186**, 262–268 (1998).

391. Zhu, G. -G *et al.* Immunohistochemical study of type I collagen and type I pN-collagen in benign and malignant ovarian neoplasms. *Cancer* **75**, 1010–1017 (1995).

392. Conklin, M. W. *et al.* Aligned collagen is a prognostic signature for survival in human breast carcinoma. *Am. J. Pathol.* **178**, 1221–1232 (2011).

393. Provenzano, P. P. *et al.* Collagen reorganization at the tumor-stromal interface facilitates local invasion. *BMC Med.* **4**, 38 (2006).

394. Riedel, A., Shorthouse, D., Haas, L., Hall, B. A. & Shields, J. Tumor-induced stromal reprogramming drives lymph node transformation. *Nat. Immunol.* **17**, 1118–1127 (2016).

395. Tegla, C. A. *et al.* Membrane attack by complement: The assembly and biology of terminal complement complexes. *Immunol. Res.* **51**, 45–60 (2011).

396. Reis, E. S., Mastellos, D. C., Ricklin, D., Mantovani, A. & Lambris, J. D. Complement in cancer: Untangling an intricate relationship. *Nature Reviews Immunology* **18**, 5–18 (2018).

397. Kalluri, R. Basement membranes: structure, assembly and role in tumour angiogenesis. *Nat. Rev. Cancer* **3**, 422–433 (2003).

398. Räsänen, K. & Vaheri, A. Activation of fibroblasts in cancer stroma. *Exp. Cell Res.* **316**, 2713–22 (2010).

399. Paulsson, J. & Micke, P. Prognostic relevance of cancer-associated fibroblasts in human cancer. *Semin. Cancer Biol.* **25**, 61–8 (2014).

400. Sawada, Y. *et al.* Force Sensing by Mechanical Extension of the Src Family Kinase Substrate p130Cas. *Cell* **127**, 1015–1026 (2006).

401. Paszek, M. J. *et al.* Tensional homeostasis and the malignant phenotype. *Cancer Cell* **8**, 241–254 (2005).

402. Miranti, C., Miranti, C. K. & Brugge, J. S. perspective on integrin signal transduction Sensing the environment : a historical perspective on integrin signal transduction. *Nat. Cell Biol.* **4**, (2015).

403. Yeung, T. *et al.* Effects of substrate stiffness on cell morphology, cytoskeletal structure, and adhesion. *Cell Motil. Cytoskeleton* **60**, 24–34 (2005).

404. Calvo, F. *et al.* Mechanotransduction and YAP-dependent matrix remodelling is required for the generation and maintenance of cancer-associated fibroblasts. *Nat Cell Biol* **15**, 637–646 (2013).

405. Huang, X. *et al.* Matrix stiffness-induced myofibroblast differentiation is mediated by intrinsic mechanotransduction. *Am. J. Respir. Cell Mol. Biol.* **47**, 340–348 (2012).

406. Olsen, A. L. *et al.* Hepatic stellate cells require a stiff environment for myofibroblastic differentiation. *Am. J. Physiol. Gastrointest. Liver Physiol.* **301**, G110–G118 (2011).

407. Galie, P. A., Westfall, M. V. & Stegemann, J. P. Reduced serum content and increased matrix stiffness promote the cardiac myofibroblast transition in 3D collagen matrices. *Cardiovasc. Pathol.* **20**, 325–333 (2011).

408. Salzer, M. C. *et al.* Identity Noise and Adipogenic Traits Characterize Dermal Fibroblast Aging. *Cell* **175**, 1575-1590.e22 (2018).

409. Kalluri, R. The biology and function of fibroblasts in cancer. *Nat. Rev. Cancer* **16**, 582–598 (2016).

410. Sorrell, J. M., Baber, M. A. & Caplan, A. I. Site-matched papillary and reticular human dermal fibroblasts differ in their release of specific growth factors/cytokines and in their interaction with keratinocytes. *J. Cell. Physiol.* **200**, 134–145 (2004).

411. Zheng, B. *et al.* CD146 attenuation in cancer-associated fibroblasts promotes pancreatic cancer progression. *Mol. Carcinog.* **55**, 1560–1572 (2016).

412. Chen, Y. T. *et al.* Platelet-derived growth factor receptor signaling activates pericyte-myofibroblast transition in obstructive and post-ischemic kidney fibrosis. *Kidney Int.* **80**, 1170–1181 (2011).

413. Bolm, L. *et al.* The Role of Fibroblasts in Pancreatic Cancer: Extracellular Matrix Versus Paracrine Factors. *Transl. Oncol.* **10**, 578–588 (2017).

414. Tirosh, I. *et al.* Dissecting the multicellular exosystem of metastatic melanoma by single-cell RNA-seq. *Science (80-.).* **352**, 189–196 (2016).

415. Li, H. *et al.* Reference component analysis of single-cell transcriptomes elucidates cellular heterogeneity in human colorectal tumors. *Nat. Genet.* **49**, 708–718 (2017).

416. Wherry, E. J. & Kurachi, M. Molecular and cellular insights into T cell exhaustion. *Nature Reviews Immunology* **15**, 486–499 (2015).

417. Kwan, W. hong, van der Touw, W., Paz-Artal, E., Li, M. O. & Heeger, P. S. Signaling through C5a receptor and C3a receptor diminishes function of murine natural regulatory T cells. *J. Exp. Med.* **210**, 257–268 (2013).

418. Strainic, M. G., Shevach, E. M., An, F., Lin, F. & Medof, M. E. Absence of signaling into CD4 + cells via C3aR and C5aR enables autoinductive TGF-β1 signaling and induction of Foxp3 + regulatory T cells. *Nat. Immunol.* **14**, 162–171 (2013).

419. van der Touw, W. *et al.* Cutting Edge: Receptors for C3a and C5a Modulate Stability of Alloantigen-Reactive Induced Regulatory T Cells. *J. Immunol.* **190**, 5921–5925 (2013).

420. Quell, K. M. *et al.* Monitoring C3aR Expression Using a Floxed tdTomato-C3aR Reporter Knock-in Mouse. *J. Immunol.* **199**, 688–706 (2017).

421. Martin, U. *et al.* The human C3a receptor is expressed on neutrophils and monocytes, but not on B or T lymphocytes. *J. Exp. Med.* **186**, 199–207 (1997).

422. Guy, C. T., Cardiff, R. D. & Muller, W. J. Induction of mammary tumors by expression of polyomavirus middle T oncogene: a transgenic mouse model for metastatic disease. *Mol. Cell. Biol.* **12**, 954–961 (1992).

423. Sugiura, K. & Stock, C. C. Studies in a tumor spectrum. I. Comparison of the action of methylbis(2-chloroethyl)amine and 3-bis(2-chloroethyl)aminomethyl-4-methoxymethyl-5-hydroxy-6-methylpyridine on the growth of a variety of mouse and rat tumors. *Cancer* **5**, 382–402 (1952).

424. Yang, Y. *et al.* Abstract 1846: Immunocompetent mouse allograft models for development of therapies to target breast cancer metastasis therapies to target breast cancer metastasis. in *Oncotarget* **8**, 1846–1846 (Impact Journals, 2017).

425. Miklos, A. C., Li, C., Sorrell, C. D., Lyon, L. A. & Pielak, G. J. An upper limit for macromolecular crowding effects. *BMC Biophys.* **4**, (2011).

426. Johnstone, C. N. *et al.* Functional and molecular characterisation of EO771.LMB tumours, a new C57BL/6-mouse-derived model of spontaneously metastatic mammary cancer. *DMM Dis. Model. Mech.* **8**, 237–251 (2015).

427. Shao, Z. M., Nguyen, M. & Barsky, S. H. Human breast carcinoma desmoplasia is PDGF initiated. *Oncogene* **19**, 4337–4345 (2000).

428. Hagood, J. S. Thy-1 as an Integrator of Diverse Extracellular Signals. *Front. Cell Dev. Biol.* **7**, 26 (2019).

429. Koyama, Y. *et al.* Mesothelin/mucin 16 signaling in activated portal fibroblasts regulates cholestatic liver fibrosis. *J. Clin. Invest.* **127**, 1254–1270 (2017).

430. Fiore, V. F. *et al.* Conformational coupling of integrin and Thy-1 regulates Fyn priming and fibroblast mechanotransduction. *J. Cell Biol.* **211**, 173–190 (2015).

431. Sanders, Y. Y. *et al.* Thy-1 promoter hypermethylation: A novel epigenetic pathogenic mechanism in pulmonary fibrosis. *Am. J. Respir. Cell Mol. Biol.* **39**, 610–618 (2008).

432. Hagood, J. S. *et al.* Loss of fibroblast Thy-1 expression correlates with lung fibrogenesis. *Am. J. Pathol.* **167**, 365–379 (2005).

433. Nazari, B. *et al.* Altered Dermal Fibroblasts in Systemic Sclerosis Display Podoplanin and CD90. *Am. J. Pathol.* **186**, 2650–2664 (2016).

434. Katsumata, L. W., Miyajima, A. & Itoh, T. Portal fibroblasts marked by the

surface antigen Thy1 contribute to fibrosis in mouse models of cholestatic liver injury. *Hepatol. Commun.* **1**, 198–214 (2017).

435. Sukowati, C. H. C. *et al.* The Expression of CD90/Thy-1 in Hepatocellular Carcinoma: An In Vivo and In Vitro Study. *PLoS One* **8**, e76830 (2013).

436. Driskell, R. R. *et al.* Distinct fibroblast lineages determine dermal architecture in skin development and repair. *Nature* **504**, 277–281 (2013).

437. Rinkevich, Y. *et al.* Identification and isolation of a dermal lineage with intrinsic fibrogenic potential. *Science (80-.).* **348**, (2015).

438. Ammirante, M., Shalapour, S., Kang, Y., Jamieson, C. A. M. & Karin, M. Tissue injury and hypoxia promote malignant progression of prostate cancer by inducing CXCL13 expression in tumor myofibroblasts. *Proc. Natl. Acad. Sci. U. S. A.* **111**, 14776–14781 (2014).

439. Galindo, M. *et al.* Hypoxia induces expression of the chemokines monocyte chemoattractant protein-1 (MCP-1) and IL-8 in human dermal fibroblasts. *Clin Exp Immunol* **123**, 36–41 (2001).

440. Kim, J. W. *et al.* Loss of fibroblast HIF-1α accelerates tumorigenesis. *Cancer Res.* **72**, 3187–3195 (2012).

441. Asgari, E. *et al.* C3a modulates IL-1β secretion in human monocytes by regulating ATP efflux and subsequent NLRP3 inflammasome activation. *Blood* **122**, 3473–3481 (2013).

442. Fischer, W. H., Jagels, M. A. & Hugli, T. E. Regulation of IL-6 synthesis in human peripheral blood mononuclear cells by C3a and C3a(desArg). *J. Immunol.* **162**, 453–9 (1999).

443. Zhang, C. *et al.* Complement C3a signaling facilitates skeletal muscle regeneration by regulating monocyte function and trafficking. *Nat. Commun.* **8**, (2017).

444. Nabizadeh, J. A. *et al.* The Complement C3a Receptor Contributes to Melanoma Tumorigenesis by Inhibiting Neutrophil and CD4 + T Cell Responses. *J. Immunol.* **196**, 4783–4792 (2016).

445. Nozaki, M. *et al.* Drusen complement components C3a and C5a promote choroidal neovascularization. *Proc. Natl. Acad. Sci. U. S. A.* **103**, 2328–2333 (2006).

446. Wang, Y. *et al.* Autocrine complement inhibits IL10-dependent T-cell-mediated antitumor immunity to promote tumor progression. *Cancer Discov.* **6**, 1022–1035 (2016).

447. Mathieu, M. C. *et al.* The C3a receptor antagonist SB 290157 has agonist activity. *Immunol. Lett.* **100**, 139–145 (2005).

448. Gunn, L. *et al.* Opposing Roles for Complement Component C5a in Tumor Progression and the Tumor Microenvironment. *J. Immunol.* **189**, 2985–2994 (2012).

449. Biffi, G. *et al.* Il1-induced Jak/STAT signaling is antagonized by TGFβ to shape CAF heterogeneity in pancreatic ductal adenocarcinoma. *Cancer Discov.* **9**, 282–301 (2019).

450. Stuart, T. *et al.* Comprehensive Integration of Single-Cell Data. *Cell* **177**, 1888-1902.e21 (2019).

451. Roberts, A. B. *et al.* Transforming growth factor type β: Rapid induction of fibrosis and angiogenesis in vivo and stimulation of collagen formation in vitro. *Proc. Natl. Acad. Sci. U. S. A.* **83**, 4167–4171 (1986).

452. Vaughan, M. B., Howard, E. W. & Tomasek, J. J. Transforming growth factor-β1 promotes the morphological and functional differentiation of the myofibroblast. *Exp. Cell Res.* **257**, 180–189 (2000).

453. Ignotz, R. a & Massague, J. Transforming growth factor-β stimulates the expression of fibronectin and collagen and their incorporation into the extracellular matrix. *J. Biol. Chem.* **261**, 4337–4345 (1986).

454. Varga, J., Rosenbloom, J. & Jimenez, S. A. Transforming growth factor beta (TGF beta) causes a persistent increase in steady-state amounts of type I and type III collagen and fibronectin mRNAs in normal human dermal fibroblasts. *Biochem. J.* **247**, 597–604 (1987).

455. Raghow, R., Postlethwaite, A. E., Keski-Oja, J., Moses, H. L. & Kang, A. H.

Transforming growth factor β increases steady state levels of type I procollagen and fibronectin messenger RNAs posttranscriptionally in cultured human dermal fibroblasts. *J. Clin. Invest.* **79**, 1285–1288 (1987).

456. Topalian, S. L. *et al.* Safety, Activity, and Immune Correlates of Anti–PD-1 Antibody in Cancer. *N. Engl. J. Med.* **366**, 2443–2454 (2012).

457. Hwang, R. F. *et al.* Inhibition of the hedgehog pathway targets the tumor-associated stroma in pancreatic cancer. *Mol. Cancer Res.* **10**, 1147–1157 (2012).

458. Walter, K. *et al.* Overexpression of smoothened activates the Sonic hedgehog signaling pathway in pancreatic cancer-associated fibroblasts. *Clin. Cancer Res.* **16**, 1781–1789 (2010).

459. Desmouliére, A. *et al.* α-Smooth muscle actin is expressed in a subpopulation of cultured and cloned fibroblasts and is modulated by γ-interferon. *Exp. Cell Res.* **201**, 64–73 (1992).

460. Avgustinova, A. *et al.* Tumour cell-derived Wnt7a recruits and activates fibroblasts to promote tumour aggressiveness. *Nat. Commun.* **7**, 10305 (2016).

461. Mueller, L. *et al.* Stromal fibroblasts in colorectal liver metastases originate from resident fibroblasts and generate an inflammatory microenvironment. *Am. J. Pathol.* **171**, 1608–1618 (2007).

462. Pasch, M. C., Van Den Bosch, N. H. A., Daha, M. R., Jan D, B. & Asghar, S. S. Synthesis of complement components C3 and factor B in human keratinocytes is differentially regulated by cytokines. *J. Invest. Dermatol.* **114**, 78–82 (2000).

463. Albrengues, J. *et al.* LIF mediates proinvasive activation of stromal fibroblasts in cancer. *Cell Rep.* **7**, 1664–1678 (2014).

464. Sanz-Moreno, V. *et al.* ROCK and JAK1 Signaling Cooperate to Control Actomyosin Contractility in Tumor Cells and Stroma. *Cancer Cell* **20**, 229–245 (2011).

465. Wang, J. H. C., Thampatty, B. P., Lin, J. S. & Im, H. J. Mechanoregulation of gene expression in fibroblasts. *Gene* **391**, 1–15 (2007).

466. Avery, D. *et al.* Extracellular matrix directs phenotypic heterogeneity of activated fibroblasts. *Matrix Biol.* **67**, 90–106 (2018).

467. Hinz, B., Mastrangelo, D., Iselin, C. E., Chaponnier, C. & Gabbiani, G. Mechanical tension controls granulation tissue contractile activity and myofibroblast differentiation. *Am. J. Pathol.* **159**, 1009–1020 (2001).

468. Mallo, M. & Alonso, C. R. The regulation of Hox gene expression during animal development. *Development (Cambridge)* **140**, 3951–3963 (2013).

469. Sahai, E. Illuminating the metastatic process. *Nat. Rev. Cancer* **7**, 737–49 (2007).

470. Vennin, C. *et al.* CAF hierarchy driven by pancreatic cancer cell p53-status creates a pro-metastatic and chemoresistant environment via perlecan. *Nat. Commun.* **10**, (2019).

471. Li, W. *et al.* Mechanism of Human Dermal Fibroblast Migration Driven by Type I Collagen and Platelet-derived Growth Factor-BB. *Mol. Biol. Cell* **15**, 294–309 (2004).

472. Ying, H. *et al.* PTEN is a major tumor suppressor in pancreatic ductal adenocarcinoma and regulates an NF-κB-cytokine network. *Cancer Discov.* **1**, 158–169 (2011).

473. Ancrile, B., Lim, K. H. & Counter, C. M. Oncogenic Ras-induced secretion of IL6 is required for tumorigenesis. *Genes Dev.* **21**, 1714–1719 (2007).

474. Sparmann, A. & Bar-Sagi, D. Ras-induced interleukin-8 expression plays a critical role in tumor growth and angiogenesis. *Cancer Cell* **6**, 447–458 (2004).

475. Burdelya, L. *et al.* Stat3 Activity in Melanoma Cells Affects Migration of Immune Effector Cells and Nitric Oxide-Mediated Antitumor Effects. *J. Immunol.* **174**, 3925–3931 (2005).

476. Wang, J., Dodd, C., Shankowsky, H. A., Scott, P. G. & Tredget, E. E. Deep dermal fibroblasts contribute to hypertrophic scarring. *Lab. Investig.* **88**, 1278–1290 (2008).

477. Honardoust, D., Varkey, M., Marcoux, Y., Shankowsky, H. A. & Tredget, E. E.

Reduced decorin, fibromodulin, and transforming growth factor-β3 in deep dermis leads to hypertrophic scarring. *J. Burn Care Res.* **33**, 218–227 (2012).

478. Dunkin, C. S. J. *et al.* Scarring occurs at a critical depth of skin injury: Precise measurement in a graduated dermal scratch in human volunteers. *Plast. Reconstr. Surg.* **119**, 1722–1732 (2007).

479. Canales, N. A. G. *et al.* A1BG and C3 are overexpressed in patients with cervical intraepithelial neoplasia III. *Oncol. Lett.* **8**, 939–947 (2014).

480. Habermann, J. K. *et al.* Increased Serum Levels of Complement C3a Anaphylatoxin Indicate the Presence of Colorectal Tumors. *Gastroenterology* **131**, 1020–1029 (2006).

481. Gast, M. C. W. *et al.* Serum protein profiling for diagnosis of breast cancer using SELDI-TOF MS. *Oncol. Rep.* **22**, 205–213 (2009).

482. Chen, J. *et al.* Profiling the potential tumor markers of pancreatic ductal adenocarcinoma using 2D-DIGE and MALDI-TOF-MS: Up-regulation of Complement C3 and alpha-2-HS-glycoprotein. *Pancreatology* **13**, 290–297 (2013).

483. Cho, M. S. *et al.* Autocrine effects of tumor-derived complement. *Cell Rep.* **6**, 1085–1095 (2014).

484. Markiewski, M. M. *et al.* Modulation of the antitumor immune response by complement. *Nat. Immunol.* **9**, 1225–1235 (2008).

485. GARRED, P., HETLAND, G., MOLLNES, T. E. & STOERVOLD, G. Synthesis of C3, C5, C6, C7, C8, and C9 by Human Fibroblasts. *Scand. J. Immunol.* **32**, 555–560 (1990).

486. Pavlides, S. *et al.* The reverse Warburg effect: Aerobic glycolysis in cancer associated fibroblasts and the tumor stroma. *Cell Cycle* **8**, 3984–4001 (2009).

487. Corrales, L. *et al.* Anaphylatoxin C5a Creates a Favorable Microenvironment for Lung Cancer Progression. *J. Immunol.* **189**, 4674–4683 (2012).

488. Ajona, D. *et al.* A combined PD-1/C5a blockade synergistically protects against lung cancer growth and metastasis. *Cancer Discov.* **7**, 694–703 (2017).

489. Harris, C. L. Expanding horizons in complement drug discovery: challenges and emerging strategies. *Seminars in Immunopathology* **40**, 125–140 (2018).

490. Mathern, D. R. & Heeger, P. S. Molecules great and small: The complement system. *Clin. J. Am. Soc. Nephrol.* **10**, 1636–1650 (2015).

491. Hillmen, P. *et al.* Long-term safety and efficacy of sustained eculizumab treatment in patients with paroxysmal nocturnal haemoglobinuria. *Br. J. Haematol.* **162**, 62–73 (2013).

492. Kinchen, J. *et al.* Structural Remodeling of the Human Colonic Mesenchyme in Inflammatory Bowel Disease. *Cell* **175**, 372-386.e17 (2018).

493. Croft, A. P. *et al.* Distinct fibroblast subsets drive inflammation and damage in arthritis. *Nature* **570**, 246–251 (2019).

494. McKenna, A. & Gagnon, J. A. Recording development with single cell dynamic lineage tracing. *Dev.* **146**, dev169730 (2019).